TABLE DES MATIÈRES

LISTE DES FIGURES

LISTE DES TABLEAUX

LISTE DES ABRÉVIATIONS, SIGLES ET ACRONYMES

AMD	Acid mine drainage
ARD	Acid rock drainage
BFS	Blast furnace slag
CO	Consommation d'oxygène
CPB	Cemented paste backfill
CV	Cendre volante
DMA	Drainage minier acide
DTA	Differential thermal analysis
DTG	Differential thermogravimetry
EDS	energy dispersive X-ray spectrometry
FA	Fly ash
FTIR	Fourier transform infrared spectroscopy
ICP	Induced coupled plasma
ICP-AES	Induced coupled plasma-atomic emission spectrometry
LHF	Laitier de haut-fourneau
MEB	Microscope electronique à balayage
MIP	Mercury intrusion porosimetry
MRTS	Most represented troat size
OC	Oxygen consumption
OPC	Ordinary Portland Cement (T10)
PSD	Pore size distribution
RCP	Remblai cimenté en pâte
SE	Secondary electron
SEM	Scanning electron microscopy
SEM-IA	Scanning electron microscopy and image analysis
SEM-XMAP	Technique d'évaluation minéralogique en utilisant les images rayon-X en mode point en provenance du microscope électronique à balayage

T10	Ciment de type 10 selon la norme CAN/CSA-A5-98
T10FA	Mélange T10 et cendre volante
T10SL	Mélange T10 et laitier de haut-fourneau
TD	Threshold diameter
TG/DSC	Thermogravimetry/Diferential scanning calorimetry
UCS	Uniaxial compressive strength
W0	Eau déionisée
W1	Eau d'une usine de remblai
W2	Eau d'une usine de remblai
w/c	Water to cement ratio
XRD	X-ray diffraction

LISTE DES SYMBOLES

A	Aire dans l'équation 2 du chapitre 5 (L^2)
A, B, C	Zones diverses sur l'histogramme des teintes de gris d'une image (-)
A_i	Aire totale de d_{pixi} (L^2)
A_{pixi}	Classe de dimension des pores (L^2)
BET	Surface spécifique selon la méthode Brunauer-Emmett-Teller (L^2/M)
C	Concentration d'oxygène au temps t (-)
C_0	Concentration atmosphérique en oxygène (-)
$(C_0)_n$	Résistance en compression uniaxiale (kPa)
$(C_0)_{nmin}$	Résistance en compression uniaxiale associée à n_{min}(kPa)
d	Diamètre déterminé au porosimètre au mercure (L)
D_0	Coefficient de diffusion moléculaire en absence d'obtacle (L^2/T)
D_{10}	Diamètre correspondant à 10 % volumique cumulé sur la distribution granulométrique (L)
D_{30}	Diamètre correspondant à 30 % volumique cumulé sur la distribution granulométrique (L)
D_{50}	Diamètre correspondant à 50 % volumique cumulé sur la distribution granulométrique (L)
D_{60}	Diamètre correspondant à 60 % volumique cumulé sur la distribution granulométrique (L)
D_a	Coefficient de diffusion moléculaire dans un matériau poreux (L^2/T)
D_e	Coefficient de diffusion effectif (L^2/T)
dL	Distance directe entre 2 TPJ (L)
d_{pixi}	Distance poreuse (L^2)
D_r	Densité des grains solides (M/L^3)
dx	Distance tortueuse entre 2 TPJ (L)
EhN	Potentiel d'oxydoréduction par rapport à l'électrode l'hydrogène (mV)
F	Facteur de formation (-)

FA_i	Fréquence relative d'apparition de A_{pixi} (-)
F_L	Flux d'oxygène $(M/L^2/T)$
GL_1	Teinte de gris au début de la zone A (-)
GL_2	Teinte de gris au début de la zone C (-)
Gs	Densité des grains solides (M/L^3)
IAP	Produit de l'acticité ionique (mol^x/L^x)
kPa	KiloPascal
K_r	Coeeficient de reaction du premier ordre (T^{-1})
K_{sat}	conductivité hydraulique saturée (L/T)
K_{sp}	Constante de produit de solubilité (mol^x/L^x)
μm	Micromètre (Micron)
m	Facteur de cimentation (-)
MPa	MegaPascal
n	Porosité (dans le cas de l'équation 2 du chapitre 2, n est la porosité totale mesurée au MIP) (-)
n_c	Porosité critique (-)
$n_{\geq d}$	Porosité MIP cumulative MIP ayant un diamètre $\geq$ à d (-)
$n_{<d}$	Porosité MIP cumulative MIP ayant un diamètre < à d (-)
n_{min}	Porosité minimum du RCP (-)
N_{pixi}	Nombre d'occurrences de d_{pixi} (-)
P	Pression appliquée au porosimètre au mercure (psi)
P_i	Proportion relative d'une classe de pores (-)
ppm	partie par million
psi	pound/square inch
R	Coeficient de corrélation (-)
R	Résolution d'une image (pixel/micron)
R^2	Coefficient de détermination (-)
$\mu S/cm$	MicroSiemens par cemtimètre
SI	Indice de saturation (-)
Sr	Degré de saturation (-)
T	Tortuosité (-)

T^2	Facteur de tortuosité (-)
TL	Teinte de gris seuil pour évaluer la porosité (-)
TPJ	Point de jonction triple
u	Coefficient de non-linéarité (-)
v	Coefficient de non-linéarité (-)
V	Volume (L^3)
% v/v	Pourcentage volumique (-)
% wt.	Pourcentage poids (-)
x_1	Coefficient de non-linéarité (-)
γ	Tension de surface au porosimètre au mercure (Force/L)
θ	Angle de contact au porosimètre au mercure (degré)
σ_{cn}	Résistance en compression uniaxiale (kPa)
σ_{nmin}	Résistance en compression uniaxiale associée à n_{min}(kPa)
⟨ ⟩	MacCauley brackets (⟨y⟩ = 0.5(y + |y|))

RÉSUMÉ

Les activités de concentration des minéraux métalliques et des métaux précieux produisent des quantités importantes de résidus miniers ayant un potentiel de génération de drainage minier acide (DMA). Un moyen de gestion des résidus miniers consiste à fabriquer un matériau appelé le remblai cimenté en pâte (RCP). Le RCP est un mélange de résidus miniers, de liant hydraulique et d'eau dont le pourcentage solide est compris entre 70 et 85%. Le RCP est acheminé sous terre afin de remplir les chantiers exploités et ainsi servir de soutènement pour l'extraction efficace du gisement. Cette activité permet aussi le retour sous terre d'une proportion importante de résidus miniers.

Historiquement, les travaux réalisés sur les RCP ont été principalement dédiés à l'optimisation des types et des proportions de ciment et d'eau afin d'améliorer la résistance mécanique. Étant donné l'impact important de la minéralogie des résidus miniers sur cette résistance, l'application des solutions proposées est souvent limitée à un site donné. Dans les dernières années, l'utilisation croissante du RCP, les modifications aux législations qui pointent à l'horizon et la mise sur pied de groupes de recherche voués aux problèmes associés à la gestion des résidus miniers ont cependant changé cette vision. En effet, les chercheurs ont commencé à s'intéresser à d'autres aspects des RCP tels que la minéralogie, l'évolution des propriétés hydriques et microstructurales et la capacité de stabilisation des contaminants pour n'en nommer que quelques uns.

Les travaux réalisés dans le cadre de cette thèse s'inscrivent à l'intérieur de ces efforts de la communauté scientifique pour la gestion intégrée des résidus miniers. Les objectifs de la thèse sont : i) une meilleure compréhension du RCP en étudiant les phénomènes fondamentaux à la base du gain de résistance mécanique, tel que l'évolution de la minéralogie et son impact sur la microstructure, et ii) établir des liens entre les aspects microstructuraux et minéralogiques préalablement étudiés et le comportement environnemental des remblais sulfureux potentiellement générateurs d'acide. Les chapitres de développement de la thèse sont au nombre de quatre. Les deux premiers mettent en lumière des travaux sur la structure des pores des RCP, le troisième traite de la minéralogie des RCP en lien avec les processus de cimentation et le dernier présente une étude sur la réactivité d'un RCP en chantier.

L'évolution de la porosité et de la structure des pores a été étudiée par porosimétrie au mercure (MIP) et par l'analyse d'images issues de la microscopie électronique à balayage en mode électrons rétrodiffusés (SEM-IA). Ces travaux ont été effectués sur des échantillons fabriqués à partir d'une poudre de silice ayant une granulométrie similaire aux résidus miniers. Pour tous les échantillons, trois liants

hydrauliques (ciment Portland de type 10 (T10), T10 additionné de 30% de cendre volante (CV) de type C et T10 additionné de 80% de laitier de haut-fourneau (LHF)) et trois types d'eau de gâchage (une eau pure et deux eaux en provenance des épaississeurs à résidus de deux mines) ont été utilisés. Les résultats obtenus avec la technique MIP ont montré une diminution de la dimension des pores avec le temps. Cependant, la porosité totale évaluée avec cette technique est demeurée pratiquement constante durant les 92 jours de cure. Les changements microstructuraux observés peuvent s'expliquer par l'hydratation des liants utilisés et la précipitation de sulfates. Ceci a occasionné une augmentation de la résistance en compression simple de tous les échantillons pendant la période d'essai. Une équation générale reliant la courbe de distribution des pores évaluée au MIP et la résistance en compression a été proposée. Les résultats SEM-IA ont permis de déceler une baisse de la porosité totale des échantillons dans le temps, ce qui est contraire aux résultats MIP. Dans le but d'estimer la taille des pores et la tortuosité des RCP, des algorithmes de traitement des images ont été développés. Ces analyses indiquent qu'un raffinement de la porosité s'opère dans le temps. Par ailleurs, le comportement du liant à base de LHF est atypique par rapport aux deux autres liants utilisés. Les échantillons fabriqués avec le mélange T10:LHF montre la porosité la plus fine et une résistance mécanique plus élevée. L'étude porosimétrie des RCP indique aussi une augmentation de résistance induite par les sulfates introduits dans les mélanges à partir des eaux de mine.

La phase solide du RCP (principalement du point de vue minéralogique) et son influence sur la structure du matériau ont été étudiées sur des échantillons similaires à ceux décrits ci-dessus. L'évolution des phases cimentaires a été suivie par thermogravimétrie et par mesure des flux de chaleur. Ces techniques ont aussi été appuyées par le développement d'un logiciel de cartographie minéralogique par traitement des images rayon X en mode point en provenance du MEB (SEM-XMAP). L'utilisation de SEM-XMAP dans le contexte des RCP (faible quantité de ciment et forte proportion d'eau) a favorisé la visualisation de la distribution des phases cimentaires dans un RCP. Les principaux résultats de l'étude montrent que les minéraux occasionnant la cimentation des RCP sont similaires à ceux retrouvés dans les matériaux tels que les pâtes de ciment et les mortiers. Un effet pouzzolanique est également noté dans les mélanges incluant des CV et des LHF. Ces résultats montrent aussi que malgré un rapport eau sur ciment élevé, une fraction des liants (principalement les CV et LHF) ne s'est pas hydratée même après 180 jours de cure. Par ailleurs, le gain de résistance mécanique semble avoir été favorisé par la précipitation de sulfates et par l'utilisation d'une eau sulfatée et acide qui a permis une meilleure dissolution et hydratation du ciment et des ajouts minéraux.

L'étude sur la réactivité d'un RCP sulfureux en chantier a révélé que la consommation d'oxygène a diminué rapidement et s'est stabilisée à environ 0,2 mol O_2/m^2/jour 14 jours après la mise en contact du remblai avec l'air. Cette diminution de consommation d'oxygène est attribuée à la création d'une couche protectrice d'oxydation de 200 à 400 µm d'épaisseur ayant une porosité plus faible que le RCP

non-oxydé en raison de la précipitation de minéraux secondaires. Cette baisse de réactivité est aussi attribuée à un degré de saturation élevé du RCP et à la formation d'une couche calcique autour des grains de pyrite de la couche d'oxydation qui réduit leur réactivité. Les techniques d'analyse minéralogique utilisées n'ont pas permis l'identification de sulfates secondaires dans le RCP de cette mine. Par contre, l'analyse de l'eau des pores obtenue par extraction sous presse a révélé de fortes concentrations en soufre et un pH supérieur à 9 tout au long de la période d'essai de 80 jours. Ainsi, malgré une proportion de sulfure inclus dans le RCP d'environ 53% et des conditions favorables à l'oxydation, le soufre n'a pas massivement précipité sous forme de sulfate.

Cette thèse a permis de mieux comprendre les mécanismes d'hydratation des liants dans les remblais cimentés en pâte et d'apprécier les changements microstructuraux associés. Considérant que les connaissances des propriétés microstructurales sont essentielles pour comprendre et prédire le comportement d'un matériau poreux, les méthodes originales développées et adaptées pour qualifier et quantifier l'évolution et la nature de la microstructure du matériau dans le temps favoriseront la compréhension des comportements mécaniques et environnementaux des RCP. Cette thèse a également permis d'établir que l'utilisation du RCP limite significativement la génération de DMA.

Mots clés : Remblai cimenté en pâte, Microstructure, Hydratation, Drainage minier acide, Résistance mécanique

CHAPITRE I

INTRODUCTION

1.1. Problématique générale

L'industrie minière génère, lors de ses activités de traitement du minerai, de grandes quantités de résidus de broyage, communément appelés « résidus miniers » ou « rejets de concentrateur ». Le broyage de la roche a pour objectif la libération des minéraux dits économiques afin de faciliter leur récupération. Ce faisant, des minéraux non-économiques sont aussi broyés. Lorsque ceux-ci sont entreposés dans des aires d'accumulation en surface, ils peuvent interagir avec l'environnement ambiant (l'eau, l'air). C'est le cas des sulfures de fer qui sont très souvent associés aux minéraux métalliques ou aux éléments ayant une valeur économique.

Les sulfures de fer, tels que la pyrite (FeS_2) et la pyrrhotite ($Fe_{1-x}S$, $0 \leq x \leq 0,125$), sont à l'origine du principal problème environnemental de l'industrie minière, soit le drainage minier acide (DMA). En effet, ces minéraux réagissent naturellement avec l'eau et l'air pour générer une solution acide ayant un contenu élevé en métaux et en sulfates. La plupart des sulfures ont un potentiel de génération d'acide mais comme la pyrite et la pyrrhotite sont généralement les plus abondants dans les résidus miniers, ceux-ci récoltent la plus grande attention. Les réactions d'oxydation directes (par l'oxygène) de ces minéraux peuvent être décrites de la façon suivante (p. ex. Kleinmann et al. 1981; Nicholson, 1994; Evangelou, 1995; Jambor, 2003) :

Pyrite : $FeS_2 + 7/2O_2 + H_2O \rightarrow Fe^{2+} + 2SO_4^{2-} + 2H^+$ (1)

Pyrrhotite (x=0.1) : $Fe_{0,9}S + 1,95O_2 + 0,1H_2O \rightarrow 0,9Fe^{2+} + SO_4^{2-} + 0,2H^+$ (2)
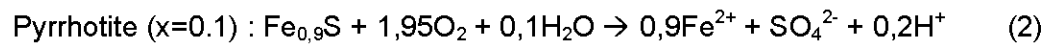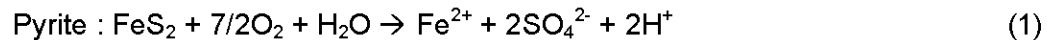
Lorsque le pH et les conditions d'oxydoréduction sont propices, des réactions dites indirectes peuvent aussi accélérer le processus de formation du DMA tel qu'il est possible de le voir pour la pyrite avec les équations (3) à (5) (Kleinmann et al. 1981).

$2Fe^{2+} + 1/2O_2 + 2H^+ \rightarrow 2Fe^{3+} + H_2O$ (3)

$Fe^{3+} + 3H_2O \rightarrow Fe(OH)_3 + 3H^+$ (4)

$FeS_2 + 14Fe^{3+} + 8H_2O \rightarrow 15 Fe^{2+} + 2SO_4^{2-} + 16 H^+$ (5)

Le Fe^{2+} généré par l'oxydation directe de la pyrite peut s'oxyder en fer ferrique (Fe^{3+}). Lorsque le pH est supérieur à environ 4,5, le Fe^{3+} précipite sous forme d'hydroxyde de fer $Fe(OH)_3$ tout en acidifiant davantage le milieu. À un pH inférieur à 4,5, le Fe^{3+} peut oxyder directement la pyrite. Dans ces conditions, chaque mole de pyrite produit 16 moles d'ions H^+. Certaines bactéries acidophiles peuvent également se développer dans le DMA et accroître le processus d'oxydation en catalysant l'équation (3) (Zagury et al., 2005).

De très nombreuses études ayant comme sujet de départ l'oxydation des sulfures existent. Elles sont de différents ordres, à savoir i) celles qui rapportent des observations réelles sur des sites existants et mettent en perspective l'importance du problème, ii) celles qui traitent des mécanismes de réaction et iii) celles qui ont pour objectif de contrôler les réactions d'oxydation afin de limiter les impacts environnementaux du DMA.

Le premier type d'études a mis en évidence les impacts environnementaux pouvant être causés par le DMA (voir les études récentes de Nordstrom et Alpers, 1999; Elberling et al., 2000; Frau, 2000; Nordstrom et al., 2000; Williams et Smith, 2000; Brake et al., 2001; Aubertin et al., 2002; Elberling et al., 2003; Lee, 2003; Moncur et al., 2003; Ptacek et Blowes, 2003; Tremblay et al. 2003; Verburg et al., 2003; Audry

et al., 2005; Sánchez España et al., 2005). Des chiffres éloquents sur la nature du DMA sont par exemple présentés dans Aubertin et al. (2002) et dans Ptacek et Blowes (2003); certains de ceux-ci se retrouvent au tableau 1.1.

Les coûts de restauration et de sécurisation des sites générateurs d'acide (incluant les empilements de roches et les parcs à résidus miniers), sont estimés entre 3 et 5 milliards de dollars ($CDN) au niveau des sites miniers canadiens et à plus de 100 milliards de dollars ($US) pour l'ensemble des sites répertoriés à l'échelle mondiale (Aubertin et al., 2002).

L'étude des mécanismes réactionnels de l'oxydation des sulfures est un champ de recherche qui est toujours en développement. Lowson (1982) a publié un article synthèse sur l'oxydation de la pyrite dans le contexte du DMA. De nombreuses autres études sur le sujet ont par la suite été publiées, notamment celles de Moses et al. (1987), Nicholson et al. (1988), Elberling et al. (1994), Nicholson (1994), Nicholson et Scharer (1994), Holmes et Crundwell (2000), Janzen et al. (2000), Rimstidt et Vaughan (2003) et Jerz et Rimstidt (2004). Ces études montrent que les mécanismes d'oxydation des sulfures sont forts complexes et impliquent de nombreux états intermédiaires entre le S^{2-} et le SO_4^{2-}. Malgré de nombreuses années de recherche sur ce sujet, ces mécanismes demeurent encore relativement mal compris (Rimstidt et Vaughan, 2003).

Tableau 1.1, Concentrations ioniques mesurées dans du DMA provenant de sites miniers (mg/l) (tiré de Ptacek et Blowes, 2003)

Site minier	SO_4	Fe	As	Cu	Zn
Richmond	> 700000	> 100000	> 300	> 4000	> 23000
Heath Steele	≤ 85000	≤ 48000	ns	≤ 70	≤ 3690
Sherridon	> 250000	> 80000	élevée	> 1500	> 50000
Brunswick	> 5000	> 7000	ns	ns	> 3000

ns : concentration non-spécifiée.

En parallèle avec ces travaux, d'autres études ont porté sur le développement de solutions pour contrôler et/ou limiter l'oxydation des sulfures et ainsi éviter la génération de DMA. La plupart de ces méthodes visent à limiter l'oxydation des sulfures en atténuant la migration des fluides (eau et/ou air) et ainsi empêcher la réaction d'oxydation directe (Équations (1) et (2)). Toute une panoplie de techniques ont été développées parmi lesquelles on retrouve l'ennoiement (p. ex. Atkins et al., 1997; Li et al., 1997; Aubertin et al., 2002) et la mise en place d'un recouvrement en sol avec ou sans géosynthétique (Aubertin et al. 1995; Aubertin et al., 2002; Bussière et al., 2004; Dagenais, 2005). Ces techniques de contrôle du DMA, bien qu'utilisées depuis les années 80, ont leurs limites et leurs inconvénients. Citons par exemple le maintien d'un niveau d'eau minimal pour l'ennoiement, ce qui implique un contrôle de la stabilité physique à long terme des digues de retenue (Aubertin et al., 2002; Bussière, 2006). La performance à long terme des recouvrements en sol et en matériau synthétique reste également à être établie. D'autres approches qualifiées d'émergentes ont aussi été proposées dans les dernières années, telles que la disposition des résidus épaissis en surface, la désulfuration environnementale et la co-disposition de résidus et de roches stériles (p. ex. Bussière, 2006). Ces approches visent essentiellement à améliorer la stabilité physique et chimique des résidus miniers sulfureux. Bien que ces nouveaux modes de gestion des résidus miniers sulfureux soient intéressants, leur application et leur efficacité ne sont pas encore démontrées.

Une méthode intéressante de gestion des rejets miniers sulfureux (résidus et stériles miniers) est le remblayage minier souterrain. Cette technique est de nos jours largement utilisée dans les exploitations souterraines canadiennes et à travers le monde afin d'optimiser la récupération du minerai et de réduire la quantité de rejets miniers à stocker en surface. Le remblayage souterrain est probablement presque aussi vieux que le minage lui-même (Potvin et Fourie, 2005), mais jusqu'à il y a seulement quelques années, les avantages environnementaux n'étaient pas perçus comme importants. L'essor du remblayage souterrain depuis les années 1980 et le besoin de mieux comprendre son comportement mécanique et environnemental ont

été les éléments déclencheurs de nombreux travaux de recherche au cours des dernières années (dont la présente thèse).

1.2. Types de remblais souterrains fabriqués à partir de résidus miniers

Deux types de remblayage souterrain constitués de résidus miniers sont généralement reconnus : le remblai hydraulique et le remblai cimenté en pâte (RCP). Le remblai hydraulique est fabriqué à partir des résidus miniers dont la granulométrie a été ajustée par hydrocyclonage et auxquels est ajouté un agent de cimentation. Le pourcentage solide du remblai hydraulique varie entre 60% et 70% en poids, ce qui permet de l'acheminer dans les chantiers minés par gravité via un réseau de transport de la pulpe (Hassani et Archibald, 1998). Quant au RCP, il est composé de résidus miniers épaissis (75 à 85% solide), auxquels sont ajoutés un liant et une eau de gâchage; cette dernière est ajoutée pour atteindre la consistance permettant le transport de la pâte jusqu'au chantier par gravité et/ou par pompage. La figure 1.1 illustre la séquence usuelle du remblayage souterrain, de la fabrication jusqu'à la déposition dans le chantier. Le tableau 1.2 présente les principales caractéristiques des deux types de remblai souterrain constitués de résidus miniers. Ce tableau met en évidence certains avantages du RCP. Parmi les plus importants, notons i) un pourcentage solide généralement situé entre 70 et 80%, ii) le maintien de l'eau à l'intérieur du RCP lors de sa déposition en chantier et iii) la possibilité d'utiliser le résidu minier total, i.e. sans ajustement granulométrique. Les caractéristiques du RCP favorisent un degré de saturation élevé de la pâte, qui à son tour permet d'augmenter la proportion en sulfure dans les résidus remblayés. En effet, en ayant un degré de saturation élevé, le RCP réduit de façon significative l'oxydation des sulfures (peu d'oxygène de disponible pour les réactions chimiques présentées aux équations 1 et 2), évitant ainsi les problèmes de combustion des chantiers que l'on retrouvait dans les chantiers remblayés par remblai hydraulique sulfureux (Thomas et al., 1979). Certains aspects techniques et monétaires associés à la gestion d'un
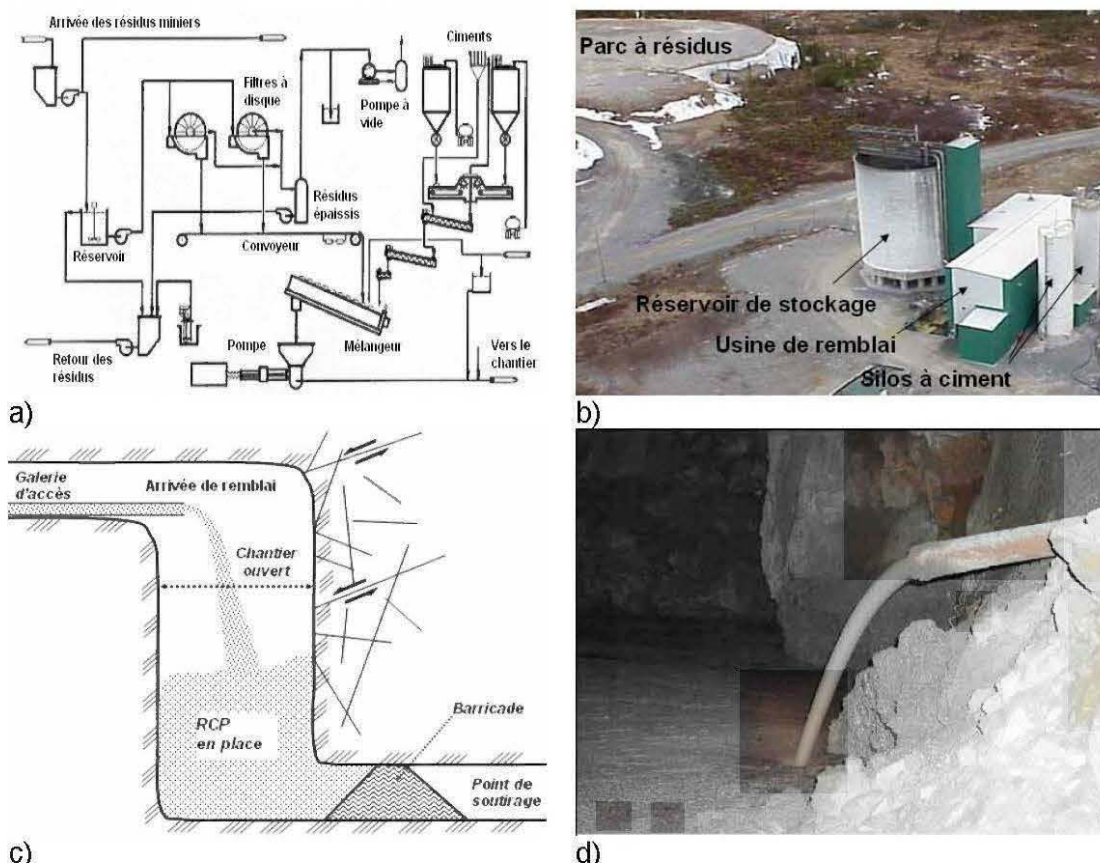
Figure 1.1, a) Schéma des étapes de préparation du RCP, b) Photo d'une usine de RCP, c) Schéma d'un chantier en cours de remblayage, d) Photo de la déposition du RCP dans un chantier; (figure adaptée d'images tirées de Paynter et Dodd, 1997 et de Belem et Benzaazoua, 2003).

Tableau 1.2, Principales caractéristiques des remblais souterrains (inspiré de Hassani et Archibald, 1998; Potvin et Fourie, 2005; Benzaazoua et al., 2005a)

Propriété	Hydraulique	Pâte
% solide initial approximatif	60% à 70%	70% à 80%
Ajustement granulométrique	Nécessaire	Non nécessaire
% de sulfures	Limité	Non limité
Consommation de liant	Élevée	Modérée-faible
Rapport eau/ciment	Élevé	Moyen à élevé (> 5)
Ségrégation (rhéologie)	Possible	Aucune
Gestion de l'excès d'eau	Élevée	Faible ou absente
Degré de saturation *in situ*	Moyen	Élevé
Dilution du chantier secondaire	Possible	Minimale
Coût en capital	Faible	Plus élevé que l'hydraulique
Coût d'opération	Faible	Moyen-faible

surplus d'eau (barricades et pompage) et à la séparation granulométrique sont aussi améliorés par l'utilisation du RCP sous terre (Potvin et Fourie, 2005). Un dernier avantage non négligeable pour les compagnies minières est certainement le gain de résistance mécanique plus rapide du RCP; cette caractéristique de stabilité améliore le temps de récupération et la quantité de minerai récupérée.

En partie pour les avantages évoqués ci-dessus, la quantité de résidus miniers retournée sous terre sous forme de RCP a augmenté depuis les 15 dernières années à travers le monde. La figure 1.2 met en relation les informations colligées à partir d'études sur les statistiques d'utilisation du RCP souterrain (Hassani et Bois, 1992; DeSouza et al., 2001; Gauthier, 2004; Benzaazoua et al., 2005a). Il est possible d'y observer que l'usage du RCP est en constante croissance depuis 1991. Ceci est particulièrement vrai au Québec où l'utilisation du RCP est passée de 5% à 63% entre 1991 et 2004. Cette augmentation est aussi constatée au niveau canadien, ce pourcentage passant alors de 24% en 2001 (DeSouza et al., 2001) à 44% en 2004 (Gauthier, 2004). En termes de quantité de RCP remblayé, l'étude de Gauthier (2004) montre que les mines interrogées en ont produit entre 150 kT et 1 MT en 2004, avec une proportion de 56% des mines ayant une production supérieure à 500 kT.

Les études à caractère économique dédiées à cette technologie ne sont pas nombreuses. Celles-ci laissent cependant voir que l'utilisation du RCP est moins dispendieuse que les autres techniques telles que le remblayage hydraulique et rocheux (Hassani et al., 1994; Benzaazoua et al., 2005a; Potvin et Fourie, 2005). Quant à savoir si le remblayage souterrain est plus économique que la disposition en surface des résidus, Hassani et al. (1994) abordent cette question délicate. L'adéquation entre les coûts et les gains doit entre autres prendre en compte les coûts associés aux infrastructures et à l'opération de même que les gains reliés à la récupération des chantiers secondaires et à la restauration des aires d'accumulation en surface. La nature des résidus miniers (générateur d'acide ou non) est également
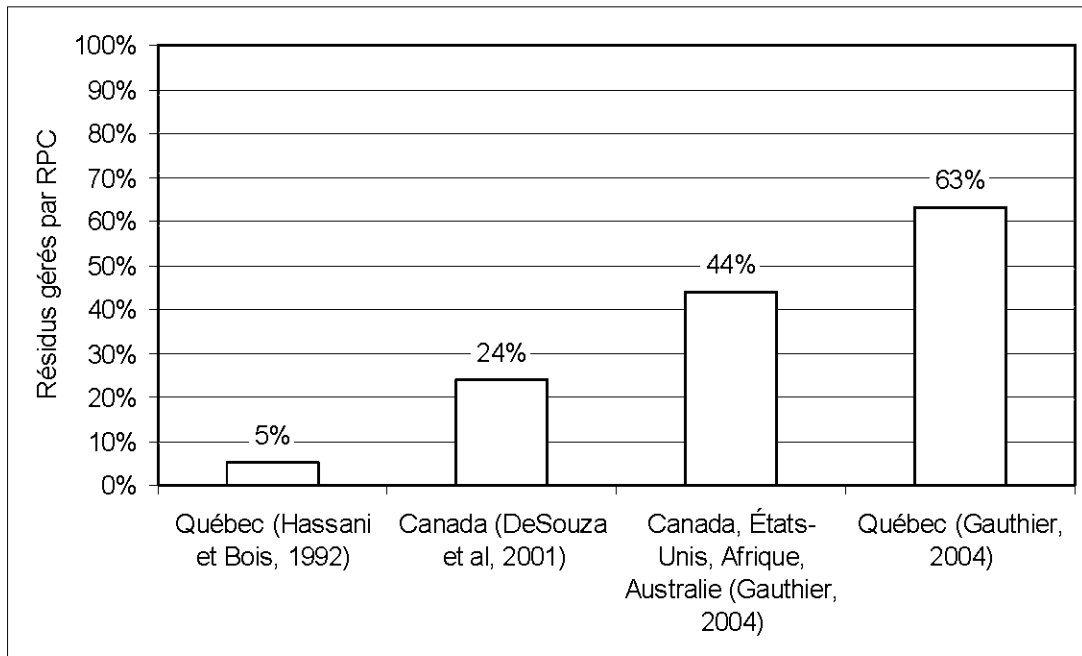
Figure 1.2, Histogramme illustrant l'évolution du pourcentage de résidus miniers entreposés sous forme de RCP entre 1991 et 2004.

importante et dans un cas où les résidus sont sulfureux, Hassani et al. (1994) montrent un scénario où le remblayage devient plus économique. Cependant, même si intuitivement on peut s'attendre à des avantages environnementaux et économiques en retournant sous-terre des résidus miniers sulfureux, il est difficile de quantifier ces bénéfices à l'aide de relations générales, chaque cas ayant ses propres caractéristiques.

Dans l'esprit des opérateurs miniers, la fonction première du RCP demeure toutefois la récupération optimale des réserves minières tout en assurant la stabilité mécanique des chantiers (Benzaazoua et al., 2005a). Les avantages environnementaux associés à la gestion des résidus par RCP constituent donc une valeur ajoutée pour les mines. La réduction de la quantité de résidus miniers sulfureux stockée en surface est certainement l'aspect le plus important. Dans les sections qui suivent, plus de détails sur le comportement mécanique et environnemental des RCP sont présentés.

1.3. Résistance mécanique des RCP

Puisque l'objectif du RCP est d'abord de répondre aux besoins opérationnels de la mine, les études réalisées sur ce matériau au cours des dernières décennies ont porté davantage sur la résistance mécanique que sur la performance environnementale (Benzaazoua et al., 2005b). Les paramètres qui influencent la résistance mécanique du RCP ont été étudiés par de nombreux chercheurs, ceci en mesurant principalement la résistance en compression uniaxiale (UCS, BNQ 2622-912) sur des échantillons fabriqués dans des conditions contrôlées au laboratoire. La résistance développée après 90 jours de cure est habituellement entre 500 et 3000 kPa (p. ex. Liping, 1997; Grice, 1998; Annor, 1999; Benzaazoua et al., 1999; 2000; 2002a; 2003a; 2004a; Kesimal et al., 2003; 2004; Cayouette, 2003; le Roux, 2004). En chantier, les conditions du milieu étant largement différentes, la résistance mécanique des échantillons prélevés en place est généralement supérieure à celle mesurée sur des échantillons préparés en laboratoire (Cayouette, 2003). Cependant, les conditions de mise en place du remblai en chantier limitent les possibilités d'intervention sur les facteurs qui régissent ce gain de résistance. La figure 1.3 illustre les principaux paramètres et variables d'influence du comportement mécanique des RCP. Du côté gauche de la figure 1.3, on retrouve la plupart des variables pouvant être ajustées par l'opérateur minier ou le laboratoire pour atteindre ses objectifs en termes de résistance du matériau. À droite, la majorité des paramètres de chantier du RCP ayant une incidence importante sur la qualité de la pâte sont présentés. Les paragraphes suivants discutent brièvement de l'impact sur la résistance mécanique des principaux facteurs présentés à la figure 1.3, soit la nature des résidus, les agents de cimentation et l'eau ajoutée ainsi que les conditions dans le chantier.
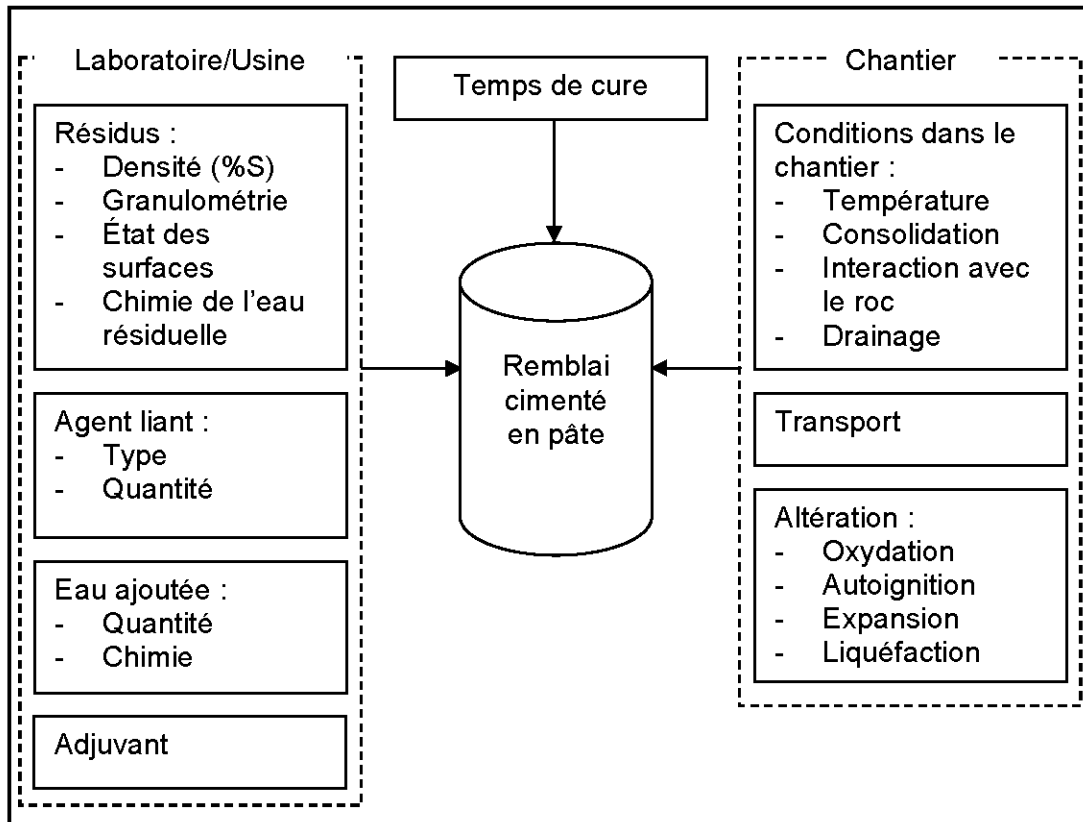
Figure 1.3, Identification des facteurs d'influence de la qualité du RCP.

1.3.1. L'influence des résidus miniers

L'influence des caractéristiques des résidus miniers sur la résistance mécanique du RCP est importante et de diverses natures (Thomas, 1983; Benzaazoua et al., 2003a). La densité des grains solides (D_r) joue un rôle de premier plan car la quantité de ciment ajoutée est traditionnellement calculée en poids et est donc proportionnelle à cette valeur; il en va de même pour la résistance mécanique (p. ex. Fall et Benzaazoua, 2003).

La granulométrie des résidus a également une influence significative sur la résistance mécanique (p. ex. Benzaazoua et al., 2003a; Cayouette, 2003; Kesimal et al., 2003; Fall et al., 2005a). Les études de Kesimal et al. (2003) et de Fall et al.

(2005a) montrent des augmentations significatives de la résistance mécanique associées à des diminutions de la teneur en eau du matériau lorsque les particules inférieures à 20 µm sont retirées des résidus. Une telle modification granulométrique est envisageable d'un point de vue théorique mais n'est pas applicable, à tout le moins pour des résidus sulfureux. En effet, il est recommandé d'avoir au moins 15% en poids de particules inférieures à 20µm dans les résidus miniers (Brackebusch, 1994; Landriault, 1995) pour maintenir un degré de saturation élevé et ainsi limiter l'oxydation des sulfures (voir section 1). Aussi, la présence des particules fines permet d'éviter la ségrégation de la pâte et favorise le transport du remblai dans les canalisations (Amaratunga et Yaschyshyn, 1997).

La minéralogie des résidus miniers peut également affecter le comportement mécanique des RCP, particulièrement lorsque ceux-ci contiennent des minéraux sulfureux qui s'oxydent au contact de l'eau et de l'oxygène. L'oxydation des minéraux sulfureux est un phénomène relativement rapide (à des niveaux variables selon le temps d'exposition et le type de résidu) qui se produit lors des étapes de préparation du RCP à l'usine de remblai (p. ex. Brookins et al., 1982; Thomson et al., 1986). L'eau interstitielle des résidus voit alors ses concentrations en ions sulfate et fer augmenter et son pH descendre (voir les équations 1 et 2). Dans la littérature, la principale conséquence rapportée de la présence de ces ions sur le comportement d'un RCP est une attaque sulfatique post-durcissement pouvant occasionner une perte de résistance lorsque des minéraux secondaires sulfatés (gypse, ettringite) précipitent (Bernier et al., 1999; Hassani et al., 2001; Benzaazoua et al., 2003b; 2004a; Fall et Benzaazoua, 2005). Il est par contre important de noter que la présence de sulfates peut aussi avoir un effet bénéfique sur la résistance mécanique dans certaines circonstances (Benzaazoua et al., 2003b; 2004a; 2004b; Belem et al., 2000; 2001; Ouellet et al., 2002).

1.3.2. L'influence du liant hydraulique

Une proportion de liant hydraulique comprise entre 3% et 7% en poids des résidus secs est normalement utilisée par les compagnies minières pour fabriquer le RCP. Les mines font majoritairement usage de ciment Portland standard (CAN/CSA-A5-98 type 10) alors que le ciment appauvri en gypse (type 50) est utilisé lorsque des problèmes de détérioration liés aux sulfates sont anticipés. Les cendres volantes (principalement de type C) et le laitier de haut-fourneau sont des additifs standardisés (ASTM C-618, ASTM C-989) employés couramment en remplacement de 50 à 90% du ciment Portland (Gauthier, 2004). Plusieurs auteurs ont montré que l'accroissement de la résistance mécanique est proportionnelle à la quantité de liant dans le RCP (Mitchell et Wong, 1982; Lamos et Clark, 1989; Belem et al., 2000; Benzaazoua et al., 2000; 2002a; 2003b; Hassani et al., 2001; Landriault et al., 2001; 2005; Kesimal et al., 2004). Ces études ont aussi montré l'effet du type de liant sur la résistance mécanique. De façon générale, on reconnaît qu'un liant n'a pas nécessairement le même comportement d'hydratation lorsqu'il est mélangé avec des résidus plus ou moins sulfureux. Par exemple, les résultats de résistance en compression sur des RCP sulfureux rapportés dans Benzaazoua et al. (2000; 2002a; 2003b) montrent qu'un mélange de ciment de type 10 et de laitier de haut-fourneau peut générer la résistance la plus élevée dans un cas et être pratiquement nulle dans un autre. Ceci démontre l'importance des essais préalables à une opération de remblayage.

1.3.3. L'influence de l'eau ajoutée

L'eau ajoutée au RCP permet son gâchage mais assure aussi une viscosité adéquate pour le transport de la pâte sous terre. Du point de vue du besoin en eau pour hydrater le ciment, l'eau est largement en excès avec un rapport eau sur ciment

généralement supérieur à 5 et pouvant aller jusqu'à 12 (Benzaazoua et al., 2003b). Le pourcentage solide du RCP a un impact direct sur la qualité de ce dernier. En effet, plusieurs études indiquent que la résistance mécanique est inversement proportionnelle à la quantité d'eau dans le mélange (Manca et al., 1983; Lamos et Clark, 1989; Amaratunga et Hein, 1997; Benzaazoua et al., 2003a; Kesimal et al., 2004; 2005). Le plus souvent, une eau potable est utilisée comme eau de gâchage des RCP, mais il peut arriver que l'eau de l'usine soit recirculée (Benzaazoua et al., 2002b). Celle-ci peut alors contenir des concentrations ioniques importantes, notamment en sulfates et les effets de ces ions s'ajoutent à ceux mentionnés sur l'oxydation des résidus (section 1.3.1). Certaines études montrent que la composition chimique de l'eau à un effet sur l'hydratation des différents types de liant et sur la résistance mécanique du remblai en pâte (p. ex. Benzaazoua et al., 2004b). Ces effets seront également approfondis au chapitre 4 de la thèse.

1.3.4. Les conditions dans le chantier

Les conditions dans le chantier influencent l'évolution du RCP et son comportement mécanique. Un premier facteur important est la température ambiante. Des mesures prisent à l'intérieur d'un RCP en place ont montré des températures supérieures à 35°C (Hassani et al., 1998). L'étude en laboratoire de Fall et al. (2005b) sur des échantillons de RCP à base de laitier de haut-fourneau maintenus à 0°C, 20°C, 35°C et 50°C indique que les échantillons muris à 35 et 50°C développent un UCS à 28 jours deux fois plus élevé que les échantillons curés à 0 et 20°C.

La consolidation et les interactions entre le remblai et les parois du chantier sont d'autres facteurs importants qui ont une incidence sur la résistance mécanique développée dans les chantiers remblayés par des RCP. Ces phénomènes peuvent faire varier verticalement la résistance mécanique à l'intérieur d'un chantier. Cayouette (2003) montre bien cet effet par des mesures de l'UCS sur des échantillons prélevés à différentes hauteurs dans un chantier; la résistance passe

d'approximativement 1,6 MPa au haut du chantier à 2,85 MPa au bas (sur une hauteur de 30 mètres). Les explications à ce phénomène peuvent être de diverses natures : pression des terres, drainage à la base et par les murs du chantier, pression de confinement exercée par les murs du chantier. Les mesures de pression interne obtenues par Belem et al. (2004) montrent que dans un chantier remblayé, la contrainte verticale est inférieure à la pression des terres et qu'un effet d'arche se développe (p. ex. Aubertin et al., 2003; Li et al., 2003; 2004; James et al., 2004; le Roux et al., 2005).

1.4. Comportement environnemental des RCP

Le comportement environnemental des RCP est un aspect important à connaître. En effet, la Directive 019 sur l'industrie minière (MDDEP, 2005) demande certaines informations concernant les aspects environnementaux du remblayage souterrain. Le paragraphe 3.2.8.6 de la Directive 019 se lit comme suit :

« En ce qui a trait au remblayage souterrain, le requérant doit fournir les éléments d'information suivants :

- *le type de remblayage prévu (hydraulique, en pâte, etc.);*
- *la composition des résidus et des additifs qui seront utilisés pour le remblayage souterrain, le cas échéant;*
- *la quantité de matériaux ou de résidus qui seront enfouis;*
- *l'évaluation des impacts sur les eaux souterraines et les eaux d'exhaure. »*

Outre l'évaluation de l'impact sur les eaux, il n'y a pas de directive précise qui limite les transferts de contaminants du remblai vers l'eau souterraine. Il faut cependant s'attendre à des modifications réglementaires en ce sens dans les prochaines années au Québec. En effet, une telle législation existe déjà depuis 1999 aux États-Unis (USEPA, 1999). Selon la législation fédérale américaine, le remblai en pâte est sous la juridiction du « Safe Drinking Water Act » et un propriétaire ou opérateur de puits d'injection ne peut effectuer d'activités de remblayage qui induisent des

mouvements de fluides contenant des contaminants à travers l'eau souterraine si la présence de ces contaminants peut amener le dépassement des normes ou nuire à la santé publique.

De façon générale, le remblai en pâte est considéré comme un matériau homogène et saturé (Benzaazoua et al., 2000; 2003a, 2004b; Ouellet et al., 2003) qui limite à un niveau jugé minimum la production de DMA en raison de l'accessibilité de l'oxygène qui est réduite à l'oxygène dissout dans l'eau interstitielle (Elberling et Damgaard, 2001). Levens et Boldt (1994) et Levens et al. (1996) ont réalisé des travaux sur des RCP souterrains et arrivent à quatre conclusions principales quant à l'addition du ciment aux résidus sulfureux : i) elle permet d'augmenter le potentiel de neutralisation, ii) elle réduit l'oxydation des sulfures en maintenant le matériau plus facilement saturé, iii) elle diminue la conductivité hydraulique ce qui favorise la rétention des métaux à l'intérieur du remblai et iv) elle augmente la résistance mécanique. Une conclusion intéressante du rapport de Levens et al. (1996) est l'identification de la distribution granulométrique des résidus comme un facteur important du contrôle des attaques chimiques liées à la neutralisation des acides.

Levens et al. (1996) commentent également le comportement des remblais suite à l'ennoiement de la mine. Ils prévoient que la zone de contact entre le remblai et le roc et les sections préalablement oxydées du remblai constitueront des voies d'écoulement préférentiel de l'eau. Par ailleurs, la diminution de la surface de contact des sulfures liée à l'addition du ciment et la précipitation de minéraux insolubles permettrait de compenser l'action de l'eau. D'autres chercheurs s'étaient aussi interrogés sur le comportement des RCP suite à la fermeture et à l'ennoiement d'une mine., une réduction de la réaction d'oxydation s'opèrerait alors (p. ex. Doepker et O'Conner, 1990a; 1990b; Doepker et Drake, 1990; 1991; Doepker, 1991a; 1991b).

Bien que la diminution de la conductivité hydraulique saturée (k_{sat}) des RCP est pressentie comme un facteur environnemental important, la quantification de cette

variation de k_{sat} est difficile à réaliser (Hassani et Archibald, 1998; Benzaazoua et al., 2005b). Contrairement à un sol, les changements microstructuraux occasionnés lors de la cure du RCP, l'interaction entre les liants et l'eau et les potentielles altérations chimiques induisent des variations de k_{sat} dans le temps. Belem et al. (2001) et Jones et al. (2001) ont mesuré des valeurs de k_{sat} de l'ordre de 10^{-8} cm/s après quelques semaines de cure. Godbout (2005) a mesuré l'évolution de k_{sat} à faibles temps de cure pour des RCP et ses mesures montrent la décroissance du k_{sat} avec le temps de cure et l'impact de l'addition du ciment. Une des conclusions importantes de cette étude demeure le fait que pour ce matériau, l'évolution de la microstructure ne peut expliquer à elle seule la diminution du k_{sat}; d'autres facteurs tels que les caractéristiques du fluide interstitielle et de la surface des grains solides contribueraient également à la diminution de k_{sat}. Godbout (2005) a également montré que les propriétés de rétention sont fortement affectées par l'ajout de liant. L'augmentation de cette capacité de rétention d'eau expliquerait pourquoi les chantiers remblayés avec du RCP demeurent saturés.

En ce qui concerne l'oxydation des sulfures dans les RCP, Ouellet et al. (2003) ont effectué une étude comparative au laboratoire entre cinq résidus sulfureux (4 à 74% de pyrite) sans ciment et des RCP préparés à partir des mêmes résidus miniers. Les résultats sur les résidus sans liant ont montré que lorsque le degré de saturation passait de 90 à 50%, la consommation d'oxygène augmentait de deux ordres de grandeur. Pour les RCP par contre, la consommation d'oxygène était significativement moindre et une couche d'oxydation d'environ un millimètre se développait en surface. Une telle couche d'oxydation a aussi été décrite par Chapman et al. (2003). La raison principale évoquée pour expliquer la consommation moindre des RCP est le maintien d'un degré de saturation supérieur à 85%. Néanmoins, Il est important de noter que des cas d'oxydation en chantier peuvent être retrouvés dans la littérature (Ouellet et al., 1998; Benzaazoua et al., 1999; Bernier et al., 1999). Quelques cas d'auto-ignition de RCP en chantier sont aussi discutés par Bernier et Li (2003).

Enfin, quelques études sur la stabilisation des résidus miniers additionnés d'un liant ont été présentées dans les dernières années (Benzaazoua, 1996; Doye et Duchesne, 2003; Benzaazoua et al. 2004c; 2006;). De façon générale, la présence d'un ciment ou d'un ajout minéral alcalin permet de stabiliser efficacement les minéraux métalliques. La présence de cendre volante ou de laitier de haut-fourneau améliore normalement la stabilisation chimique (p. ex. Duchesne et Reardon, 1999; Benzaazoua et al., 2005b; 2006). Certains de ces aspects seront également développés au chapitre 5 de la thèse.

1.5. Études à l'échelle microstructurale sur des RCP

Les travaux de recherche à caractère « fondamental » visent à comprendre les phénomènes intrinsèques qui influencent le comportement d'un matériau. Ils sont à l'opposé des études de cause à effet dites phénoménologiques. De manière générale, il faut en quelque sorte pouvoir s'insérer dans un univers microscopique afin d'observer la structure du vide ou la nature du solide. Ces travaux sont habituellement à la base de la compréhension de plusieurs mécanismes à caractère environnemental (p. ex. diffusion, mobilité de l'eau; Dullien, 1992) ou structural (p. ex. résistance mécanique; Rzhevsky et Novik, 1971).

Quelques chercheurs ont étudié divers aspects de la microstructure et de la structure des pores des RCP. La majorité de ces études ont utilisé soit la porosimétrie au mercure (MIP pour « Mercury Intrusion Porosimetry »), soit le microscope électronique à balayage (MEB). Les tests MIP sur le RCP permettent d'évaluer les effets de la cure, du type de liant, de la qualité de l'eau et de la distribution des grains (p. ex. Benzaazoua, 1996; Benzaazoua et al., 2000; Belem et al., 2001; Benzaazoua et al., 2003a; le Roux, 2004; Ouellet et al., 2004; Fall et al., 2005a; 2005b). La porosité totale ainsi mesurée se situe généralement entre 40% et 45%; ces valeurs sont assez similaires à celles obtenues sur des résidus miniers sans ciment agglomérés avec de l'eau (Belem et al., 2001). Fall et al. (2005a,

2005b) ont montré l'influence de la granulométrie des résidus et de la température de cure sur la distribution des pores mesurée au MIP. L'étude au MIP de Ouellet et al. (2004), comparant le RCP (eau/ciment = 7) et les pâtes de ciment (eau/ciment = 0,33) a permis de démontrer les différences microstructurales entre ces deux matériaux. Les résultats ont montré que le diamètre d'entrée au seuil (valeur généralement reconnue comme étant le diamètre le plus petit ayant une continuité géométrique à travers un échantillon; voir le chapitre 2) était de presque deux ordres de grandeur plus faible pour les pâtes de ciment que pour les RCP. D'autres travaux ont permis de faire la caractérisation de la microstructure et de la porosité des RCP (d'une façon qualitative) en utilisant le MEB (Benzaazoua et al., 1999; 2002; Belem et al., 2001; Ramlochan et al., 2004). Des observations sur des RCP fraîchement fracturés réalisées par Benzaazoua et al. (1999; 2002) et par Belem et al. (2001) ont montré la présence de précipités secondaires (sulfates) dans les pores qui semblaient participer à l'amélioration de la qualité du matériau. Ramlochan et al. (2004) ont aussi estimé par analyse d'images au MEB la porosité des RCP étudiés à environ 50%. Plus de détails sur ces aspects sont présentés dans les chapitres 2 et 3 de la thèse.

Les études sur la nature de la matrice solide dans les RCP ont touché principalement les minéraux primaires de la cimentation et les minéraux secondaires des RCP. Douglas et Malhotra (1989) de même que Lamos et Clark (1989) ont probablement été les premiers chercheurs à s'intéresser à l'hydratation des ciments mélangés avec des résidus miniers. Leurs études ont montré que l'addition de laitier de haut-fourneau améliorait la résistance mécanique du RCP. Une conclusion identique a été formulée par Amaratunga et Hein (1997) suite à l'utilisation de cendre volante de type C dans un RCP. Smart et al. (1993) ont identifié quelques phases cimentaires dans des remblais à l'aide du microscope électronique et remarquait que celles-ci amélioraient les contacts entre les résidus miniers. Bertrand et al. (2000) ont pu identifier au MEB des C-S-H (silicate de calcium hydraté), de la portlandite et de l'ettringite dans des RCP fabriqués à partir 6,2% en poids de ciment de type 10 (100%) et d'un mélange à 4,5% en poids de ciment de type 10 et de

laitier de haut-fourneau (20:80). Des sulfates secondaires ont aussi été observés mais seulement dans les échantillons mélangés avec le ciment de type 10. Ramlochan et al. (2004) ont investigué différents RCP ayant des proportions comprises entre 3,2% et 15% de ciment (ciment Portland de type 10 mélangé avec une cendre volante et un laitier de haut-fourneau) par diffraction X et au MEB. Le MEB a permis la reconnaissance de C-S-H et d'ettringite. Récemment, Benzaazoua et al. (2006) ont été à même d'identifier de la calcite, de l'ettringite, du gypse et de la portlandite par diffraction X dans des RCP sulfureux fabriqués à partir de 7% ciment en poids (ciment de type 10 et de type 50 à 50% :50% et ciment de type 10 et laitier de haut-fourneau à 20% :80%). Étant donné l'importance de la résistance mécanique pour les RCP, l'identification des phases secondaires expansives pouvant affecter la résistance mécanique à long terme a suscité l'intérêt de quelques chercheurs (p. ex. Ouellet et al., 1998; Benzaazoua et al., 1999; 2002; Bernier et al., 2001; Hassani et al., 2001). De façon générale, le gypse et l'ettringite sont observés dans les RCP sulfureux ayant subi une attaque sulfatique. Une revue de littérature plus complète sur la minéralogie des RCP est présentée dans l'article constituant le chapitre 4. L'appendice A présente aussi une brève introduction aux processus d'hydratation des ciments. Ces informations peuvent être utiles pour mieux comprendre certaines interprétations des résultats présentées dans la thèse.

1.6. Objectifs et contenu de la thèse

Les sections précédentes montrent que, même si des travaux intéressants (principalement de nature phénoménologique) ont été réalisés sur les RCP au cours des dernières années, il reste beaucoup à faire pour comprendre les mécanismes de base (à l'échelle du grain et du pore) qui régissent le comportement des RCP. Le principal objectif de la présente thèse est donc d'étudier le développement et l'organisation des deux phases d'un RCP, soit la porosité et le solide. Comme la porosité d'un matériau contrôle de nombreuses facettes de son comportement environnemental et mécanique, une partie importante de la thèse a porté sur l'étude

de cette propriété et de ses dérivées. La partie solide du RCP a été investiguée en portant une attention particulière au développement des phases cimentaires. Une étude sur le comportement environnemental d'un chantier remblayé avec un RCP sulfureux a complété la démarche expérimentale; cette étude a permis d'appliquer certaines connaissances acquises sur les aspects microstructuraux et minéralogiques à un cas réel.

La thèse est divisée en cinq chapitres principaux. Suite au chapitre 1, qui fait office d'introduction[1], les chapitres 2 à 5 présentent les travaux effectués sous forme d'articles scientifiques. Enfin, les principales conclusions et recommandations des travaux de recherche sont présentées.

De façon plus spécifique, le chapitre 2 est consacré à une étude sur la porosité et sur la dimension des pores des RCP en utilisant le porosimètre au mercure (MIP). Les courbes de distribution des pores obtenues par cette méthode sont analysées selon ce qui est normalement reconnu dans la littérature. Certains aspects particuliers sont discutés, tels que le séchage des échantillons et l'influence de l'essai lui-même sur la structure interne de l'échantillon de RCP. Le chapitre 2 introduit également une relation mathématique permettant de relier une courbe MIP à la résistance mécanique des RCP.

Le chapitre 3 poursuit l'étude de la structure des pores des RCP mais en utilisant cette fois-ci le microscope électronique à balayage (MEB) et l'analyse d'image. Ces méthodes ont permis d'estimer et de mesurer l'évolution de la porosité, de la distribution de la dimension des pores et de la tortuosité des RCP analysés. Afin de valider les approches développées, ces trois paramètres ont respectivement été comparés avec la réponse porosité versus résistance mécanique découlant du modèle de Li et Aubertin (2003), avec les dimensions des pores évaluées au MIP et avec des données en provenance de la littérature.

---

[1] Les références bibliographiques de l'introduction sont présentées à la section « RÉFÉRENCES » débutant à la page 279.

Le chapitre 4 présente une étude sur l'évolution des phases cimentaires des RCP. Les principales techniques utilisées pour réaliser cette étude sont la thermogravimétrie et la microscopie électronique à balayage (MEB). Cette partie du projet à permis de développer une technique de cartographie des phases cimentaires à partir des images élémentaires en rayon X du MEB (appelée SEM-XMAP). L'analyse combinée des résultats obtenus avec la thermogravimétrie et SEM-XMAP a permis de dégager des conclusions quant à la nature des précipités sulfatés et à l'hydratation des ciments dans les RCP. À noter que pour cette partie de l'étude (ainsi que pour le chapitre 3), une matrice mono-minérale constituée de silice a été utilisée. Ce choix a permis d'améliorer de façon significative la réponse de certains équipements utilisés (MEB, thermogravimétrie) en évitant les interférences des autres minéraux constituants les résidus miniers.

Le chapitre 5 est consacré à l'étude du comportement environnemental d'un RCP réel dans un chantier souterrain. Par le biais de divers essais (consommation d'oxygène, extraction de l'eau interstitielle sous presse, caractérisation minéralogique des phases secondaires et modélisations géochimiques), l'étude montre que dans la partie inférieure du chantier il y a une atténuation rapide de l'oxydation des sulfures inclus dans le RCP.

En terminant, le lecteur pourra remarquer que les matériaux, les méthodes et la littérature spécifique aux chapitres ne sont pas approfondis dans cette introduction. Ces aspects sont décrits dans chacun des chapitres et ils n'ont pas été répétés ici pour éviter les redondances.

Une série d'appendices peut également être retrouvée à la fin du document. Ces appendices visent à compléter l'information présentée dans les chapitres 2 à 5 de la thèse. L'appendice A propose une brève revue de littérature sur l'hydratation des ciments et des ajouts minéraux. Les appendices B et C présentent deux articles de conférence qui complètent certains aspects développés dans la thèse. L'appendice

B permet de mieux saisir les différences microstructurales entre les RCP et les pâtes de ciment en présentant une étude au MIP, et l'appendice C rapporte des travaux sur la consommation d'oxygène de résidus miniers sulfureux et de RCP en laboratoire. Les appendices D et E présentent des thermogrammes et des courbes MIP qui sont discutés dans les quatre chapitres de développement de la thèse. Enfin, l'appendice F montre deux essais de calibrage de la méthode de cartographie au MEB. Les résultats obtenus avec une pastille de calcite et avec une pastille de sphalérite (Mermillod-Blondin, 2006) peuvent être vus.

Les contributions scientifiques originales issues de ces travaux sont principalement liées à l'étude de la microstructure et de la structure des pores, ainsi que de la minéralogie des RCP. Comme il a été mentionné précédemment, les études antérieures sur les RCP étaient principalement de nature phénoménologique. Les travaux effectués dans le cadre de cette thèse ont permis de pousser plus loin l'interprétation des phénomènes observés par le biais d'une étude organisée autour d'équipements récents et technologiquement avancés. C'est ainsi que des méthodes originales et adaptées au RCP ont été développées pour qualifier et quantifier l'évolution et la nature du matériau dans le temps. Plus spécifiquement, les techniques d'analyse d'image présentées, qui permettent de quantifier la structure des pores des RCP et d'estimer la nature minérale et l'organisation microstructurale des phases cimentaires des RCP, sont des contributions majeures de la thèse. Dans chacun des trois premiers articles de la thèse, des efforts ont aussi été déployés pour relier la porosité et la minéralogie des RCP à la résistance en compression uniaxiale. Conscient que la résistance mécanique est une propriété importante du matériau et qu'elle peut être corrélée avec de nombreux autres paramètres de nature physique et économique, les efforts déployés sont vus par l'auteur comme un moyen de lier certains aspects fondamentaux de la thèse aux considérations pratiques du RCP en chantier. En terminant, une contribution originale importante de la thèse est certainement l'étude sur le comportement environnemental d'un RCP sulfureux en chantier. À la connaissance de l'auteur, c'est la première fois que de tels travaux sont effectués sous terre. Ceux-ci s'inscrivent dans l'optique où une

démonstration de stabilité chimique des RCP en chantier pourrait être exigée par les législateurs.

CHAPITRE II

MICROSTRUCTURAL EVOLUTION OF CEMENTED PASTE BACKFILL: MERCURY INTRUSION POROSIMETRY TEST RESULTS[2]

2. Résumé/Abstract

L'évolution microstructurale d'échantillons de remblai cimenté en pâte (RCP) fabriqués à partir d'une poudre de silice est évaluée par porosimétrie au mercure. L'influence de trois liants (Ciment Portland de type 10 (T10), T10 et cendre volante et T10 et laitier de haut-fourneau) et de trois types d'eau (une pure et deux sulfatées) est étudiée. L'analyse porosimétrique indique une évolution microstructurale des RCP associée principalement à une translation des pores grossiers vers des pores fins avec le temps de cure. Les résultats montrent également que la combinaison liant à base de laitier et eau de gâchage la plus sulfatée (7549 ppm) a permis d'atteindre la résistance en compression la plus élevée. Ce comportement est en partie attribué à la précipitation de phases sulfatées dans les pores. Sur la base des distributions de la taille des pores et des résultats de résistance mécanique, les auteurs proposent une relation générale applicable pour les RCP.

Mots clés : Remblai cimenté en pâte, Microstructure, Porosimétrie au mercure, Résistance en compression, Gestion des résidus miniers.

The microstructural evolution of different cemented paste backfill (CPB) samples made with ground silica was evaluated using mercury intrusion porosimetry (MIP). The influence of three binders (OPC, OPC with fly ash, and OPC with blast furnace slag) and of three types of water (one deionised and two sulphated) on the microstructure was studied over the curing time. Uniaxial compressive strength (UCS) tests were also performed to relate MIP results to the backfill mechanical

---

strength. Among other findings, the MIP analyses indicate that the slag based binder combined with a mixing water having a high sulphate content (of 7549 ppm) showed the highest percentage of fine pores and the highest strength. This behaviour is related to the potential precipitation of sulphate phases in pores, which may contribute to strength enhancement. Based on MIP pore size distributions and UCS results, the authors propose a general relationship applicable for CPB.

Keywords: Cemented paste backfill; Microstructure; Mercury porosimetry; Compressive strength; Mine wastes management.

2.1. Introduction

Mine tailings are generated by ore processing plants and consist of grounded rocks from which the valuable minerals have been extracted. The mining industry produces large volumes of tailings that have to be safely managed to avoid significant negative impact to the environment. In modern underground mines, it is a common practice to use an important fraction of the generated tailings as the main component of cemented paste backfill (CPB) material. CPB is usually prepared in surface installations and then transported underground in open stopes via boreholes and pipelines. The material is made by mixing filtered tailings (at a pulp density usually between 75 to 85%), binders (such as Portland cement, fly ash, blast furnace slag), and water. The amount of mixing water added is a function of the paste viscosity required to insure the delivery to underground stopes. CPB provides ground support to the rockmass around mine stopes and allows reducing the amount of tailings sent to surface facilities. Hence the use of CPB reduces environmental impacts and capital expenditures related to surface tailings disposal. Surveys conducted over the last few years (De Souza et al., 2001; Benzaazoua et al., 2005) indicate that CPB is increasingly used as a tailings management option around the world.

The properties of CPB are similar to those of a controlled low strength material (ACI, 1999): the water to cement ratio (w/c) is high (usually between 6 and 10); the

aggregates used in CPB (tailings) are mainly composed of silt size particles ($\approx$ 80% < 80μm); and the binder content is usually low at values between 2 to 7% by weight of dry tailings. The CPB strength developed after 92 days is usually between 0.5 to 3 MPa (e.g. Liping, 1997; Grice, 1998; Annor, 1999; Benzaazoua et al., 1999; 2000; 2002; 2003; 2004; Kesimal et al., 2003; 2004; Cayouette, 2003; le Roux, 2004). Depending on the ore processed at the mine, tailings can contain sulphide minerals (such as pyrite (FeS_2) and pyrrhotite (FeS)) in proportions that may reach up to 70% (e.g. Goulet and Blais, 2001; Benzaazoua et al., 2003; Cayouette, 2003; Kesimal et al., 2004). These minerals are known to react in the presence of water and oxygen generating acidity, metal hydroxides and sulphate ions (Evangelou, 1995; Aubertin et al., 2002). These reaction products can affect the behaviour and durability of CPB over the time (e.g. Benzaazoua et al., 1999). Another particularity of CPB is the chemistry of the interstitial water of the paste. Depending on the ore mineralogy and the mineral separation process, this water can contain high concentrations of sulphate and other ions (Benzaazoua et al., 2002) which can affect the hydration process of binders and precipitate in the paste as secondary minerals (Benzaazoua et al., 1999; 2002; 2004, Subauste and Odler, 2002).

In recent years, many papers and reports have been written on CPB characterization and behaviour (e.g. Benzaazoua et al., 2000; 2002; 2003; 2004; Fall et al., 2005; Kesimal et al., 2003; 2004; le Roux, 2004). Most of these studies relied on a phenomenological approach to develop correlations between mechanical strength and parameter(s) of the CPB recipe. To the authors knowledge, no detailed study has been reported on the understanding of the fundamental microstructural evolution of CPB during the curing period, and on the main influence factors affecting porosity and strength (such as water quality, type and percentage of binder, and curing time). Nevertheless, it is generally accepted in the mining community that a better understanding of the fundamental CPB behaviour would help to optimize CPB preparation and consequently to reduce operating costs.

The paper presents the results of a study on microstructural evolution during the curing of CPB using the mercury intrusion porosimetry (MIP) technique. The main objective of this paper is then to analyse the MIP porosity of CPB during curing and to relate this parameter with the material strength. After a brief overview of MIP tests performed on different geomaterials (cement pastes, natural soils, and CPB), the main results are presented. CPB samples were made from three binders commonly used and three types of mixing water containing typical sulphate concentrations. MIP test results are presented for three curing times: 14, 43 and 92 days. Uniaxial compressive strength (UCS) test results obtained at the same curing times are also presented. An equation relating porosity evolution and mechanical strength is proposed and discussed.

2.2. Mercury intrusion porosimetry

Mercury intrusion porosimetry (MIP) is based on the capillary law governing the penetration of a liquid into pores. The moisture-free sample to test is introduced into a chamber that is later filled by mercury. The pressure is gradually increased forcing mercury into the pores of the sample. By measuring the pressure applied and the mercury intrusion volume at each step of the test, it is possible to estimate the sample pore size distribution. For a non-wetting liquid like mercury and a material with cylindrical pores, the relationship between pore diameter and applied pressure is expressed by the Washburn (1921) equation:

$$d = -(1/P)\ 4\gamma\cos\theta \tag{1}$$

where d is pore diameter, P the applied pressure, γ the surface tension and θ the contact angle. Different factors may affect MIP test results but the main one is related to the inkbottle effect. According to Cook and Hover (1999), because mercury must access through the narrowest pores connecting the pore network, MIP tests may not provide a true pore size distribution. More details on limitations of the

technique can be found in Winslow and Diamond (1970), Olson et al. (1997), Diamond (2000), and Beaudoin and Marchand (2001). Nonetheless, based on the available literature, it can be said that when used on a comparative basis MIP is a reliable qualitative test to evaluate the microstructure of a material. The main limitations of the technique must however be taken into account in the interpretation of the results. Also, preparation of the samples must be done in a uniform (constant) manner for all tests.

MIP tests have been commonly used to evaluate the total porosity and the pore size distribution of different geomaterials such as concretes, mortars, cement pastes, CPB, and natural soils. MIP results are usually expressed as the total mercury volume intruded in a sample, giving the MIP total porosity, or by analysing the incremental volume intruded at each pressure step. From the latter representation, Winslow and Diamond (1970) named the pore width corresponding to the highest rate of mercury intrusion into the sample the "threshold diameter" (TD). This parameter is important since it can be seen as the smallest diameter of pores that are geometrically continuous throughout the sample. MIP results on cement paste show a decrease of the threshold diameter and of the total porosity with curing time (e.g. Feldman and Beaudoin, 1991; Cook and Hover, 1999). Most MIP tests on cemented materials such as cement paste and mortar were performed mainly to define the microstructure evolution during hardening and ultimately to relate microstructural evolution with mechanical strength (e.g. O'Farrell et al., 2001; Jiang and Guan, 1999).

On natural soils (silty and clayey soils), MIP measurements were mainly performed to relate the pore size distribution with hydraulic properties and the effect of compaction (e.g. Lapierre et al., 1990; Delage et al.; 1996; Simms and Yanful, 2001; 2004; Simms, 2003; Rahardjo et al., 2004; Cuisinier and Laloui, 2004; Dagenais, 2005). MIP tests on silty soils usually show a one mode intrusion behaviour in the 1-10 μm size range while silty-clayey soils typically show a bimodal intrusion behaviour, with a first peak associated with the silt fraction ranging between 1 and 10

µm and a second peak associated with clay fraction around 0.1 µm (Simms and Yanful, 2004; Dagenais, 2005). Lapierre et al. (1990) found a relatively good correlation between MIP test results and hydraulic conductivity of clayey soils. Delage et al. (1996) showed a decrease of the MIP pore size distribution with soil compaction and particularly when the water content is near the optimum Proctor value. The effect of compaction and of suction during water retention test on the fabric of fine-grained soils was also studied by Simms and Yanful (2001; 2004) and Cuisinier and Laloui (2004). Their results indicate that MIP test can be used to estimate pore volume changes due to suction or applied mechanical loading.

CPB is a cemented material having properties that are fairly similar to those of natural fine-grained soils, especially at an early curing age. Over the past few years, some authors have investigated the microstructure of CPB by MIP technique (Benzaazoua, 1996; Benzaazoua et al., 2000; Belem et al., 2001; Benzaazoua et al., 2003; le Roux, 2004; Ouellet et al., 2004; Fall et al., 2005). Their results show that the CPB total porosity is almost the same as that of tailings only agglomerated with water (between 40 and 45%). Belem et al. (2001) also showed that the addition of a mixture of blast furnace slag and Portland cement (80:20) modified tailings pore size distribution. A proportion of 5% wt. decreased the threshold diameter from 2 to 1 µm approximately. This refinement of the pore size reduces the saturated hydraulic conductivity and increases the water retention properties of the CPB (Godbout, 2005). Recently, Fall et al. (2005) used MIP to investigate the influence of tailings particle sizes on the microstructure of different CPB mixtures. This study showed that the amount of fine particles (<20 µm) strongly influenced MIP results. The increase in fine particle proportion leads to a decrease in the threshold diameter value (of approximately 1 micron when the proportion of <20 µm particles is increased from 40 to 55%), showing that pore size distribution is also influenced by the grain size distribution of the tailings used in the CPB mixture. Ouellet et al. (2004) presented a comparative MIP study between cement pastes (water to cement ratio w/c=0.33) and CPB (w/c=7) samples. Results show that the main mercury intrusion peak was almost two orders of magnitude lower for cement paste samples

than for CPB samples. This difference was anticipated due to the high w/c ratio of CPB. According to Powers et al. (1959), with a w/c ratio greater than 0.7, capillary pores should never become segmented.

2.3. Materials and methods

2.3.1. Binders

The three binders used in the CPB mixtures are: a 100% type 10 CAN/CSA-A5-98 ordinary Portland cement (OPC, named T10 in this study); a mix of 20% T10 and 80% ground granulated blast furnace slag (T10SL); and a mix of 70% T10 and 30% fly ash (T10FA). The Lafarge company provided these binders. The proportions are in the range used in the mining industry to produce CPB (e.g. Grice, 2001; Cayouette, 2003; Kesimal et al. 2004). Fly ash and slag are both by-products of industrial processes. The replacement of a fraction of the Portland cement by these mineral additives in the CPB mixture is often seen as an environmental value-added. Moreover, due to the lower cost of fly ash, its use can significantly reduce overall operational costs of a paste backfill plant (Ouellet et al., 2004; Benzaazoua et al., 2005).

The T10 cement shows a typical Bogue's composition of 64.4% for C_3S, 6.6% for C_2S, 8.7% for C_3A, and 7.4% for C_4AF. According to ASTM C618-00 standard, the fly ash can be classified as a class C with a cumulative value for SiO_2, Al_2O_3 and Fe_2O_3 of less than 70% and a SO_3 content of less than 5%. Blast furnace slag conforms to ASTM C989-99 and shows the highest BET specific surface among the studied binders with a value of 21 380 cm^2/g. The BET specific surfaces of the other two binder components are 12 764 and 8 697 cm^2/g for cement T10 and fly ash respectively.

2.3.2. Mixing water

CPB mixtures were made with three different types of water: the first one was deionised by filtration (named W0), while the other two mixing waters (named W1 and W2) were sampled at the tailings dewatering process of two mine backfill plants; the latter two contained 4613 ppm and 7549 ppm of SO_4^{2-} respectively. Alkali concentrations are high with 1266 ppm $Na_2O_{eq.}$ and 188 ppm $Na_2O_{eq.}$ for W1 and W2 respectively. One can also see in Table 2.1 that the calcium content of these waters is relatively high (803 and 1790 ppm for W1 and W2 respectively). Such high concentrations are mainly due to the ore processing techniques at the two mines that use lime to increase the pH. The pH and redox potential (Eh) were measured using the Benchtop pH/ISE Meter Orion model 920A with a coupling of different electrodes. An Orion Triode electrode was used for the pH and the Eh was measured with a Pt/Ag/AgCl combined electrode and then corrected for normal hydrogen electrode (EhN). The pH ranged for the three different waters between 4.57 and 9.62. Waters were filtered to remove suspended particles before analysis and mixing.

Table 2.1, Chemical composition of the waters used in this study (ICP analysis)

	W0 (ppm)	W1 (ppm)	W2 (ppm)
Al	0.03	1.06	0.29
Ca	0.02	803	1790
Cu	<0.01	0.59	0.21
Fe	0.05	0.04	1.01
K	0.14	41.40	48.00
Mg	0.01	1.00	1.71
Na	<0.2	915	111
Si	3.78	0.82	0.50
Zn	<0.02	0.08	0.53
SO_4^{2-}	0.36	4613	7549
pH	6.09	9.62	4.57
EhN	435.8	243.7	361.1
Cond. (µS/cm)	2	5950	3740

2.3.3. Tailings

For all CPB mixtures ground silica was used to simulate tailings. The silica contains 99.76% SiO_2 and has a grain size distribution (evaluated with a Malvern laser Mastersizer S) almost similar to the average of 11 mine tailings (as sampled from the province of Quebec and Ontario, Canada; see Figure 2.1). More than 50% of silica particles are smaller than 25 μm (D_{50}) and 10% smaller than 2 μm (D_{10}). The uniformity coefficient ($C_U = D_{60}/D_{10}$) and the coefficient of curvature ($C_C = D_{30}^2/D_{60}xD_{10}$) are respectively 16.5 and 1.5. According to the USCS classification (e.g. McCarthy, 2002), the silica material is a non plastic silt (ML), as are most of the tailings produced by hard rock mines (e.g. Vick, 1990; Aubertin et al., 2002). Ground silica (a mono-mineral non-reactive aggregate) was selected to focus the study on binder and water chemistry effects on CPB microstructure. Hence, the influence of sulphide minerals in CPB was not included in the present investigation.
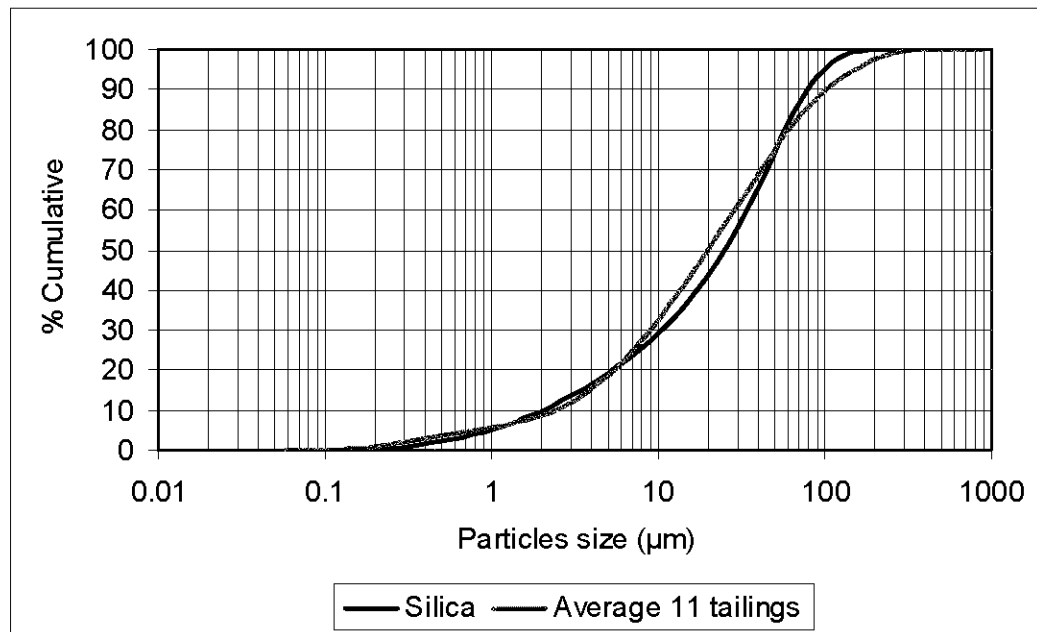
Figure 2.1, Volumetric cumulative particles size distribution of silica.

2.3.4. Sample preparation and curing

CPB mixtures were prepared in small batches in a 20-litres bucket and mixed for at least 5 minutes with a ½ inch electric drill using a paint mixer bit. A total of 54 CPB cylinders 10 cm long and 5 cm in diameter were cured at room temperature and at a relative humidity greater than 90%. The binder proportion for the CPB mixtures was 5% by weight of dry silica. Water to cement ratio (w/c) was 7 for all CPB mixtures (representing a water to solid ratio of 0.33); this is representative of values observed in the Canadian mining industry (Benzaazoua et al., 2002; 2003).

2.3.5. Drying

The drying method used before MIP tests consisted of a combination of freeze-drying and oven drying. The freeze-drying technique on CPB samples was not able to remove all the free water in a period of 24 hours. The authors noticed that freeze-drying was less effective for larger samples and for longer curing period. To accelerate the drying, a second drying period in an oven was introduced as proposed by Kjellsen (1996). More specifically, samples were first cut in small cubes of approximately 1 cm³ each and immersed for 5 minutes in liquid nitrogen. They were then dried for a period of 24 hours at 0.9 Pascal and -50°C in a Virtis Ultra 35 Super XL freeze dryer. After the first 24 hours, another period of 24 hours in an oven at 45°C completed the drying. CPB samples were then maintained in a desiccator to avoid rehydration.

2.3.6. MIP test procedures

Two cylindrical samples of each mixture were used to evaluate the uniaxial compressive strength (UCS) after 14, 43 and 92 curing days using a MTS 10/GL

press with a normal loading capacity of 50 kN and a displacement rate of 0.001 mm/min. The UCS corresponds to the maximum stress value (failure, peak) reached during the compression test. After the UCS test, the internal part of each cylinder was sampled and dried as described in the previous section. Samples were specifically selected outside the failure plane of cylinders; therefore no major influence of the strength testing on the microstructure is expected.

MIP tests were performed on CPB samples after each curing period. The equipment used is an Autopore III 9420 from Micromeritics that can generate a maximum pressure of 60 000 psi (414 MPa) and can evaluate a theoretical pore diameter of 0.003 µm. With this machine, the MIP test is performed in two steps: the low pressure step first evacuates gases, fills the sample holder with mercury and performs porosimetry from about 1 to 50 psi; the high pressure step reaches pressures between 50 and 60000 psi. Low and high pressure steps were always performed within a period of 8 hours. The contact angle and surface tension assumed for all tests were respectively 130° and 485 dynes/cm. All tests were performed to achieve the manufacturer recommendation of a mercury stem volume between 25% and 90%. Repeatability of MIP tests was not extensively investigated in this study since it is recognized as excellent in the literature (e.g. Winslow and Diamond, 1970; Beaudoin and Marchand, 2001; Simms and Yanful, 2004). Two repeatability tests (not presented) showed a difference of ±1% on the total MIP porosity, and the mercury intrusion behaviour (pore size distribution) was nearly the same.

2.3.7. Thermal and chemical analysis

Estimation of sulphate content in samples cured for 92 days was conducted using thermogravimetry/differential scanning calorimetry (TG/DSC) and chemical analysis. TG/DSC tests were performed with the SDT Q600 apparatus from TA Instruments which records simultaneously the weight loss and heat flow during thermal treatment

of the sample. Thermal behaviours of samples were registered in an inert nitrogen atmosphere at a rate of 20°C/min up to 1000°C. Approximately 35 mg of material, placed in a 90µl alumina cup and covered by an alumina lid, was used for each test. The chemical analysis technique followed the EPA 600/2-78-054 guidelines (Sobek et al., 1978) to determine the sulphate sulphur concentrations in each of the CPB samples. The Sobek method is mainly used to differentiate the sulphate sulphur and the sulphide sulphur in materials containing sulphide oxidation products by selective dissolution in HCl (40% v/v) and in $HNO_3/Br_2/HF$ acids. As CPB samples do not contain sulphide, only the HCl dissolution was performed and the extracted sulphur amount is assumed to be in precipitated sulphated phases. The resulting solutions were analysed by inductively coupled plasma-atomic emission spectrometry (ICP-AES). Sobek method was not specifically tested for sulfoaluminates, but based on the laboratory experience, only lead and barium sulphates are insoluble with this technique.

2.4. MIP porosity results

Figure 2.2 presents all the MIP pore size distribution curves. The caption indicates the type of water and binder, and the curing time (e.g. W0T1014d means that this CPB sample was made with W0 water and T10 binder, and that the UCS test was performed after 14 days of curing). In the following, results are analysed with respect to the evolution and the porosity refinement of these curves. In all cases, the MIP tests on CPB show a main intrusion peak at a pressure of about 1 MPa corresponding to an equivalent MIP pore diameter of 1.4 µm. This main peak intensity decreases with curing time while there is an increase in the volume of mercury intruded at higher pressure. The mean MIP total porosity for all samples is 44.6% with a standard deviation of 0.66%. Similar porosity results were obtained using the gravimetric technique (the porosity is measured by drying a sample of a known volume at 105°C and using the relative density of grains D_r evaluated by helium picnometry) with mean values of 45.4%, 45.3%, and 45.4% at 14 days, 43
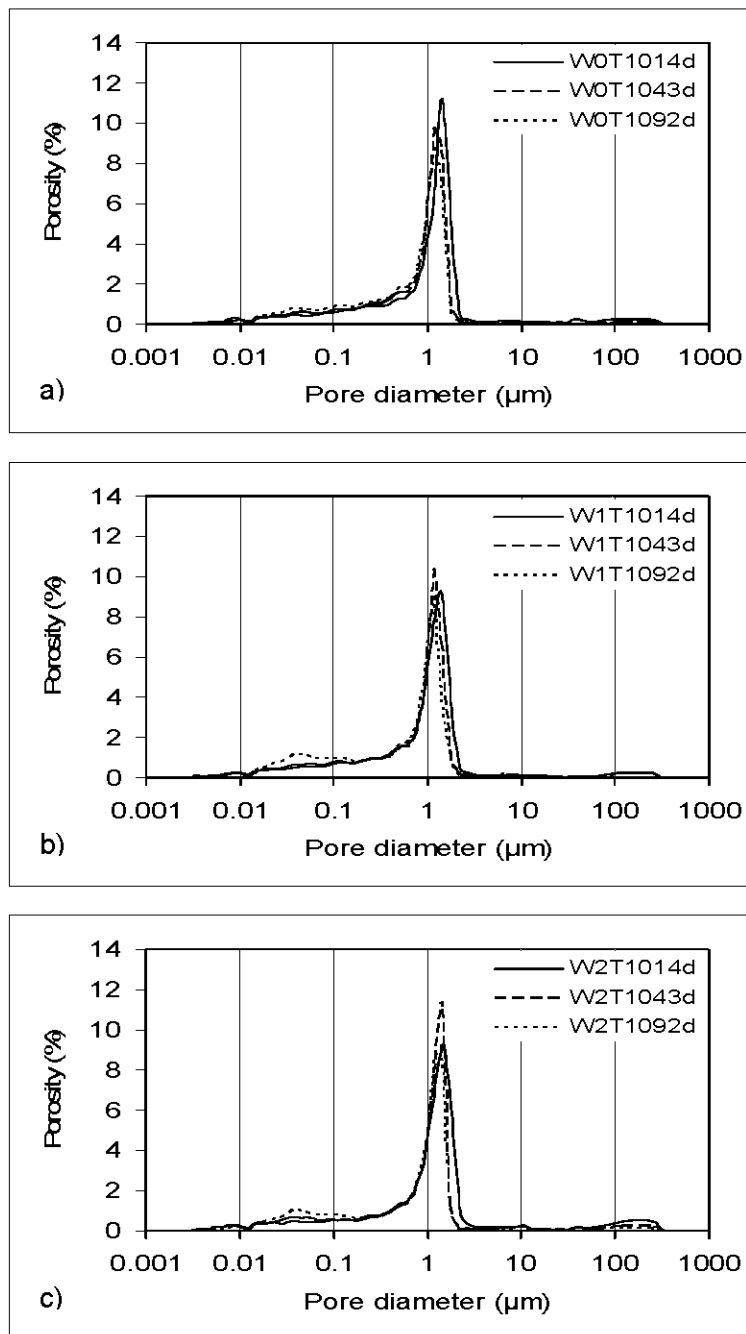
Figure 2.2, MIP pore size distributions of CPB samples: a) T10-W0, b) T10-W1, c) T10-W2.
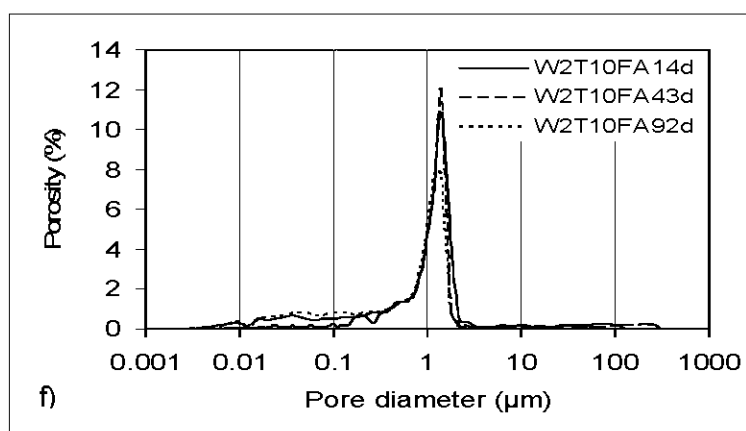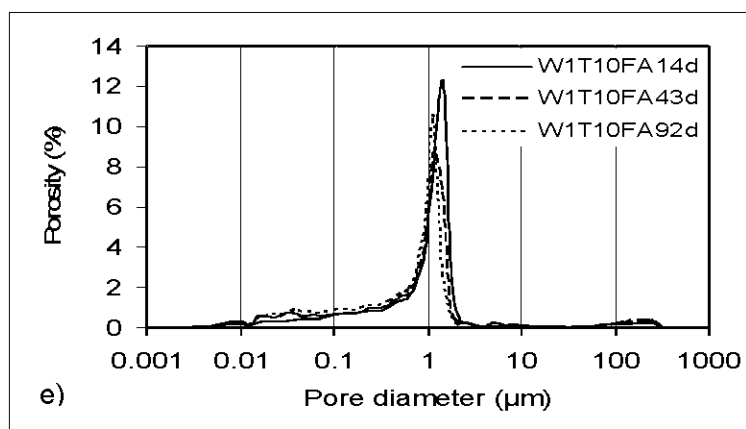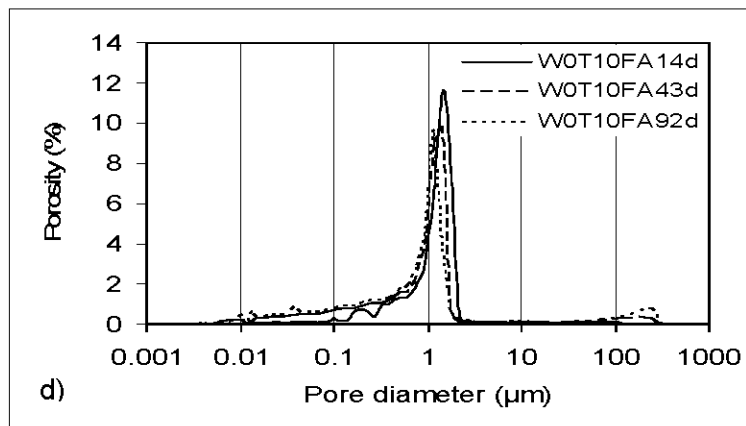
Figure 2.2, (continued), d) T10FA-W0, e) T10FA-W1, f) T10FA-W2.
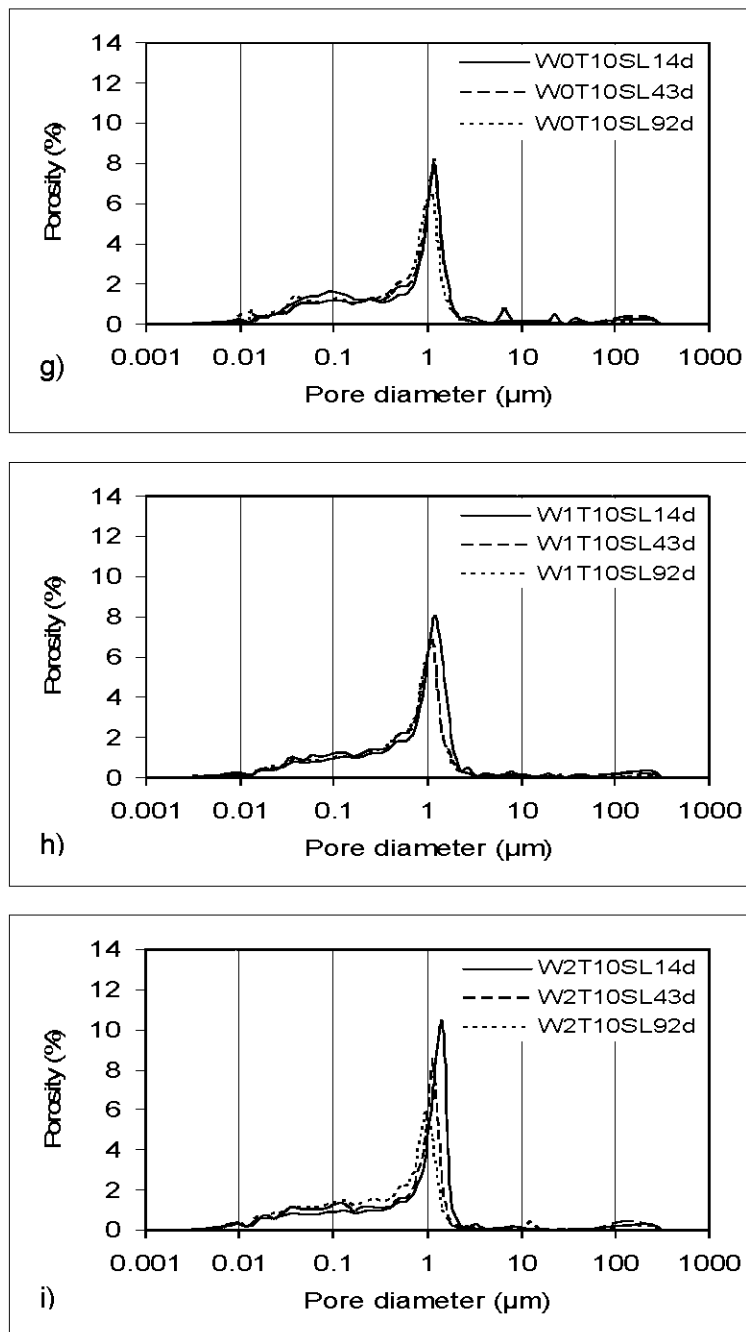
Figure 2.2, (continued), g) T10SL-W0, h) T10SL-W1, i) T10SL-W2.

days, and 92 days respectively; standard deviation for all these porosity values is 0.52%. Hence, there is no significant trend that would point towards a relationship between total porosity, curing time, and binder type.

2.4.1. Evolution of the threshold diameter

One way to appreciate the effect of curing and of the binder type is to look at the threshold diameter (TD) value. Figure 2.3 shows the histogram of the TD evolution for all binders at 14, 43 and 92 days. In general, there is a slight decrease of TD with curing time. For instance, in the case of the T10 and T10FA samples the TD moves from 1.43 µm at 14 days to 1.17 µm at 92 days. This indicates that as these samples cure, pores tend to become finer because the pressure needed for the mercury to significantly intrude the matrix increases. A somewhat different trend is observed for T10SL.
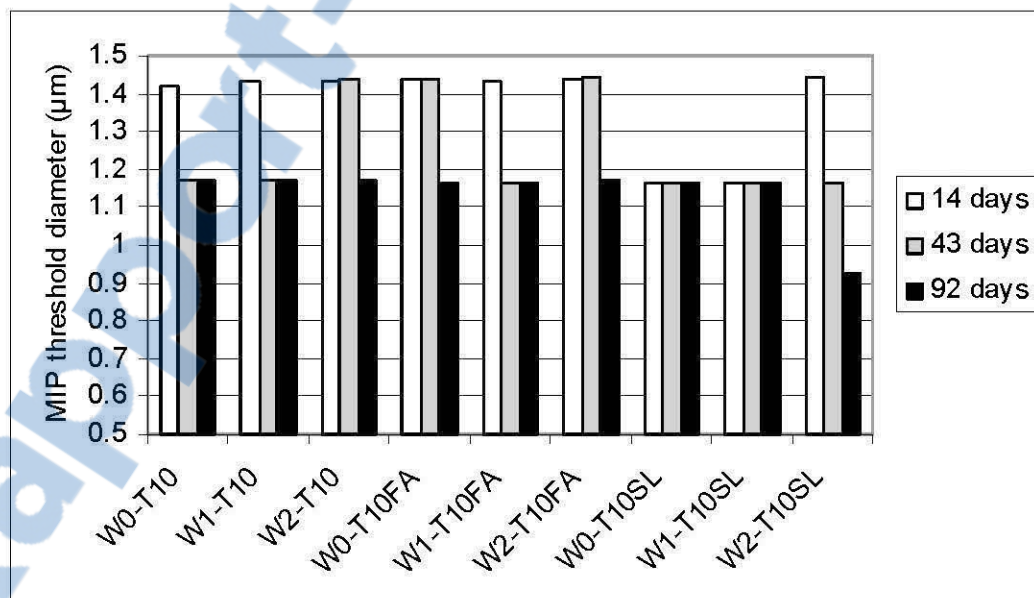
Figure 2.3, Evolution of the threshold diameter for the different studied CPB samples.

TD values for W0 and W1 waters remain constant at about 1.16 μm for the three curing period studied. Only the mixtures with T10SL and W2 water show a significant curing effect after 43 days; for this sample the TD values drop from 1.44 μm at 14 days to 0.93 μm at 92 days.

2.4.2. Evolution of the MIP curve

As proposed by few authors (O'Farrell et al., 2001; Jiang and Guan, 1999), the analysis of the area under the pore size distribution curve can also be used to represent the pore structure evolution. In the present study the pore size distribution is divided into two portions at a pressure of 4.4 MPa. The first portion includes the volume of pores having a MIP diameter greater than or equal to 0.3 μm, while the second portion corresponds to the volume of pores with a diameter less than 0.3 μm. According to the definition of the capillary pores (e.g. Powers, 1958) and of the threshold diameter, the first portion of the curve (pores $\geq$ 0.3 μm) corresponds to the main interconnected capillary porosity network. Values given in Figure 2.4 are indicative of a curing effect that is mainly due to a decrease in the TD height with time. The average porosity for the first portion of the curve for all samples is 34.0% at 14 days, 32.1% at 43 days and 30.3% at 92 days. Since the total porosity measured by the MIP tests remains practically unchanged after a curing time of 92 days, this indicated that pores of CPB samples become finer with curing time. The amount of pores $\geq$ 0.3 μm also shows the effect of the binder type. For all samples at all ages, average porosities are 33.5% for samples using T10 and T10FA binders and 29.4% for samples using T10SL binder. In light of these results, it appears that blast furnace slag seems to generate a finer microstructure in CPB.

Other authors have observed an increase in the proportion of small pores with curing time (Cook and Hover, 1999; Jiang and Guan, 1999). The evolution of these pores can be related to cement hydration products (Cook and Hover, 1999). Figure 2.5 shows the sum of MIP porosity values for pore sizes less than 0.3 μm.
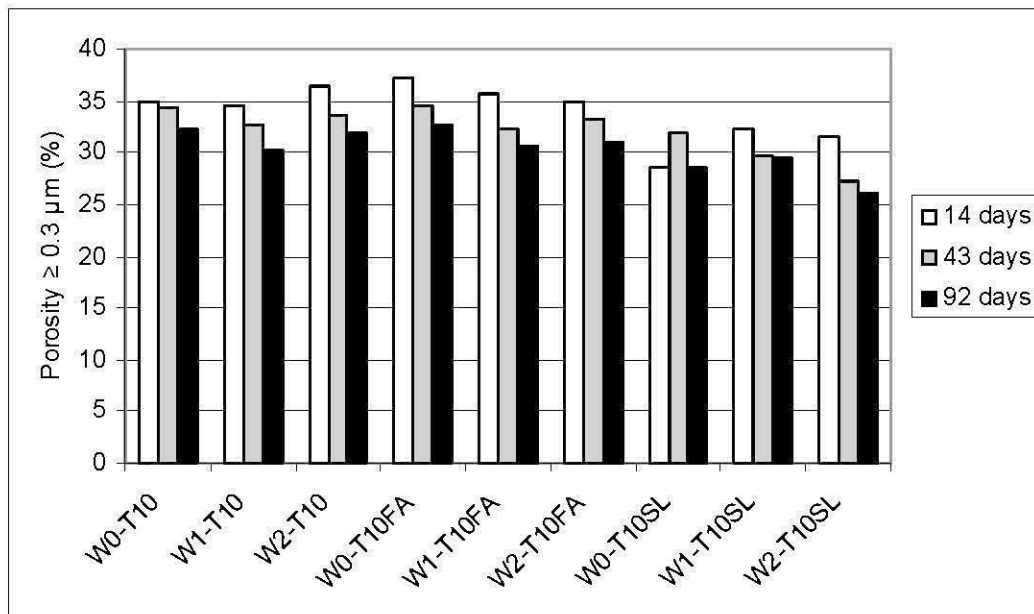
Figure 2.4, MIP Porosity occupied by pores having a MIP size ≥ 0.3 μm.
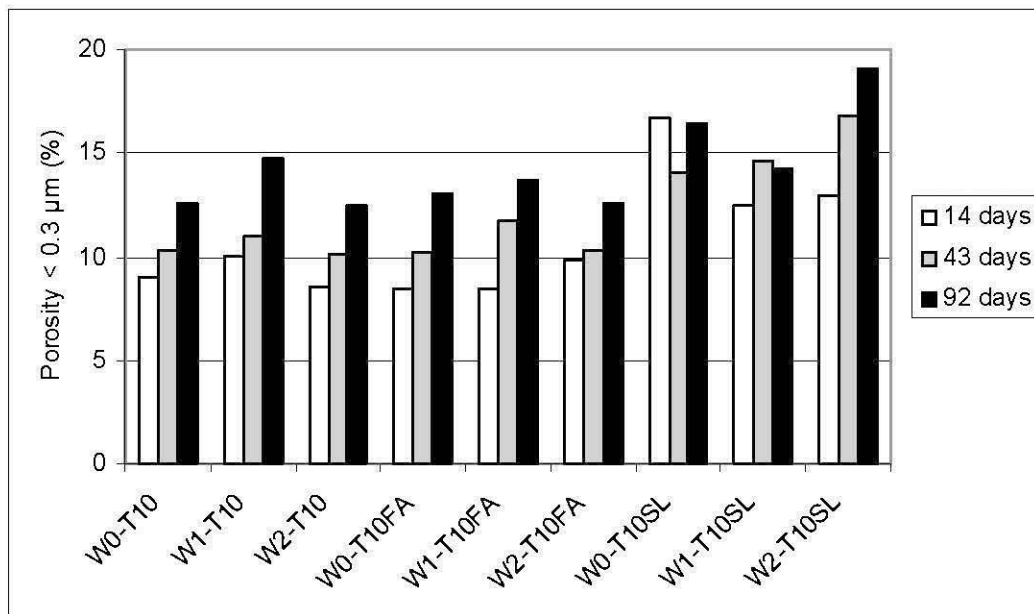
Figure 2.5, MIP Porosity occupied by pores having a MIP size < 0.3 μm.

An increase in the relative proportion in this size range is observed with the curing time for all samples except for T10SL using W0 water at 14 days. For all mixtures, the average MIP porosities below 0.3 μm are 10.7% at 14 days, 12.1% at 43 days,

and 14.3% at 92 days. These results also indicate that the binder T10SL gives the highest proportion of small pores for all curing times. Average porosities in the fine fraction are 11.0%, 10.9% and 15.3% at all curing times for T10, T10FA and T10SL binders respectively.

2.4.3. Influence of mixing water

When samples are sorted by water type, the influence of the water chemistry is not as clear as the binder effect. Average porosity values with a size below 0.3 μm (for all curing times and binder types) are 12.3%, 12.3% and 12.5% for W0, W1 and W2 waters respectively. This slight porosity difference is also accompanied by a slight influence of the water type in the pore fraction ≥ 0.3μm; average porosity values are 32.8%, 31.9% and 31.8% for W0, W1 and W2 waters respectively. However, the influence of water quality seems to be more significant for the smaller MIP pore sizes. For instance, when summing MIP porosity values for pore sizes less than 0.1 μm, the average values obtained are 7.2%, 7.5% and 8.2% for W0, W1 and W2 waters respectively.

Hence, for the CPB mixtures made with sulphated water, the precipitation of sulphate minerals in the voids could explain, at least in part, the refinement of the pore size. However, as the proportion of cement is low in CPB, spectroscopic mineral determination methods (e.g. XRD or FTIR) are not well adapted to validate this hypothesis. Chemical analysis (Sobek method) and TG/DSC were thus used on samples cured for 92 days to quantify the precipitated sulphated phases in CPB mixtures. TG weight loss results between 100°C and 250°C and between 100°C and 1000°C are presented in Figure 2.6; this figure shows also the measured sulphate sulphur concentrations in the samples. Based on these, the TG results between 100°C and 1000°C can be ordered as T10>T10FA>T10SL; this ranking follows the weight loss order for TG tests performed on unhydrated binders. The TG temperature zone between 100°C and 250°C can be related to C-S-H and to

sulphates such as ettringite ($Ca_6Al_2(SO_4)3(OH)_{12}\cdot26H_2O$), gypsum ($Ca(SO_4)\cdot2H_2O$) and, monosulphates (such as $3CaO\cdot Al_2O_3\cdot CaSO_4\cdot12H_2O$) (see Taylor, 1990; Ramachandran and Beaudoin, 2001). Except for the T10FA-W0 sample that lost more weight than the T10FA-W1 sample, all other results are in conformity with the hypothesis that more sulphate are precipitated in specimens having more SO_4^{2-} ions in the mixing water. Chemical analysis results are more explicit on the increasing presence of sulphates (in solid form) in samples made with water W1 and W2. Mean concentrations in the CPB samples are 0.06 % wt., 0.11 % wt. and, 0.18 % wt. for the samples mixed with the waters W0, W1 and, W2 respectively. Additionally, both methods show that amount of precipitated sulphates could be ranked as T10>T10FA>T10SL; the mineral additive replacement level could be responsible for these differences. However, it is worth mentioning that precipitated sulphates cannot explain all the mineralogical differences between the samples; mineralogical features of CPB are investigated in more detailed in Chapter 4.
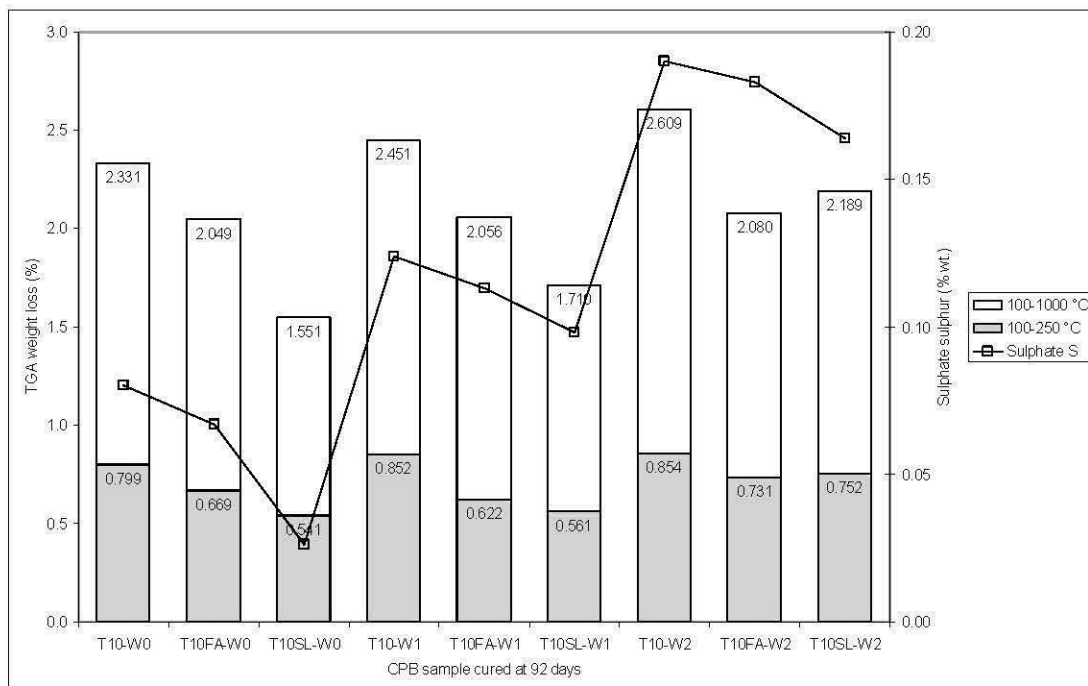
Figure 2.6, TGA and chemical analysis results on samples cured at 92 days.[3]

---

[3] Les thermogrammes sont présentés à l'appendice D

2.4.4. Influence of the slag

Results previously shown indicate also that slag specifically has a different behaviour than the other two binders. It is known that slag has a greater impact on pore refinement in cement pastes than other binders (Luo et al., 2003; Niu et al., 2002); which in turn affects the permeability coefficient (Malhotra, 2001; Taylor, 1990). The degree of reactivity of the slag particles is proportional to the specific surface, and depends on water availability (Escalante et al., 2001; Lumley et al., 1996). A particular aspect of slag is its interaction with water: more water is needed for mixture with ordinary Portland cement and slag to achieve the same viscosity (Malhotra, 2001). This phenomenon was also observed by Ouellet et al. (2004) on cement pastes (w/c = 0.33) made with the same binders and waters as the ones used in this study. Mini-slump tests on CPB with W0 water showed slump values of 7.5 cm, 11.5 cm and 5 cm for T10, T10FA and T10SL respectively. Even if CPB is significantly different from concrete or cement paste, results shown here confirm that the particular behaviour of slag observed is also seen with CPB mixtures having a high w/c ratio (w/c fixed to 7 in this study). This type of behaviour appears to have a positive (refinement) effect on the pore size distribution of the CPB.

2.4.5. Influence of MIP test on CPB microstructure

MIP results on CPB show an evolution and a refinement of the pore size over time. It is mainly due to the presence of hydrates and secondary minerals in the CPB matrix. These minerals precipitate in voids, filling them partially or completely (e.g. Benzaazoua et al., 2002; 2004; Fall and Benzaazoua, 2005). However, the MIP total porosity (or the volume of mercury that fills the samples) does not change significantly with the curing time. A possible explanation for this phenomenon was proposed by Feldman and Beaudoin (1991) and Cook and Hover (1999). Feldman and Beaudoin (1991) performed several mercury re-intrusion tests (Hg intrusion

followed by a drying step and then re-intrusion on the same sample) on cement pastes and noted that the second intrusion showed coarser MIP pore size distribution and a higher TD value than the first mercury intrusion. These authors raised the possibility that changes occurred in the pore structure during the first intrusion of mercury due to the breakage of pore walls at high pressure. Similar comments were made by Cook and Hover (1999) to explain the development of a rounded peak at a diameter of about 0.1 µm in cement pastes. They suggested that mercury crushed hydration products on its path when it filled the sample. According to this hypothesis, the peak developed near 0.1 µm was related to a crushing pressure rather than to the presence of true pores on the MIP distribution curve. Similar experiments to evaluate the influence of the mercury intrusion on the microstructure were performed by Lawrence (1978) on three fine-grained soils (with a clay fraction ranging from 15 to 60%). Contrary to cement pastes, damages to pore structure by the MIP test were not deemed significant.

To investigate the possible effect of mercury intrusion on the microstructure of CPB samples, mercury re-intrusion tests were performed on two samples. After a first test, samples were dried at 90°C and 1.5 kPa for 7 days to remove interstitial mercury. It was evaluated that 97% of the mercury was removed from the samples during this phase; using the differential weight between the sample before the first mercury intrusion and after the drying step, it was inferred that the residual mercury represented approximately 0.002 ml in each sample. The corresponding MIP curves are not presented here but they are quite similar to those shown in Figure 2.2[4]. The threshold diameter for all curves is the same (1.16 µm) and the total MIP porosity for the first and the second mercury intrusion are respectively 43.06% and 42.39% for the first sample and 43.05% and 42.02% for the second sample. These differences between the porosity values before and after the re-intrusion test could be explained in part by the residual mercury in the sample, which occupies a portion of the voids and could block access to some fine pores. Therefore, as observed by Lawrence (1978) on fine-grained soils, there is no clear evidence of modification to the internal

---

[4] Ces courbes de porosimétrie sont présentées à l'appendice E

structure of CPB by the MIP test. The absence of an effect from the mercury intrusion is probably due to the relatively coarse porosity of the CPB, which is offering little resistance to the mercury filling at each pressure step. Samples are thus expected to be completely filled at the end of each test; there is no MIP total porosity decrease observable over the curing time.

2.5. Relationship between MIP porosity and uniaxial compressive strength

It is generally accepted that the strength of cemented porous materials is a function of the form, quantity, and distribution of the voids within it (e.g. Neville, 1981; O'Farrell et al., 2001; Li and Aubertin, 2003). In general, an increase in total porosity induces a decrease in material strength. Nonetheless, when the voids are filled with precipitated phases, the strength can increase due to the refinement and segmentation of the porosity and to the nature of the precipitated phases. Figure 2.7 shows UCS results of the studied CPB samples; these curves show the mean UCS value, with the measured extreme values given as cross marks.

Once again, as for the MIP test results, mixtures using the T10 and the T10FA binders have similar behaviour. For these CPB samples, the UCS ranges from 288 kPa at 14 days to 1004 kPa at 92 days for the three water types. The strength of samples with T10SL binder is higher than that of the other two binders for all samples at all curing times. The highest UCS value measured is 1822 kPa with water W2 at 92 days, which is in concordance with MIP results that showed a finer porosity for this CPB mixture.
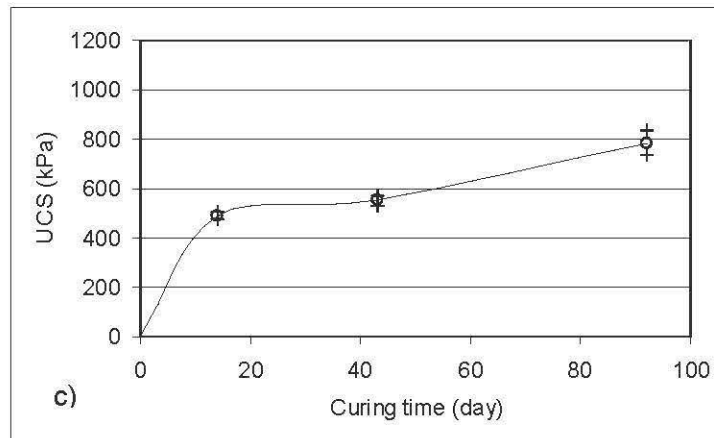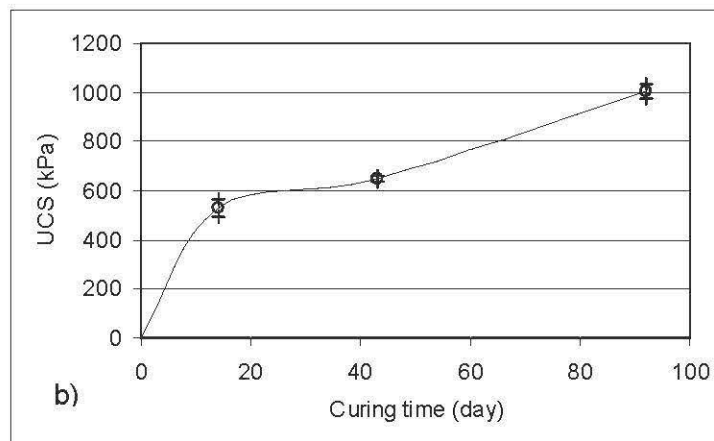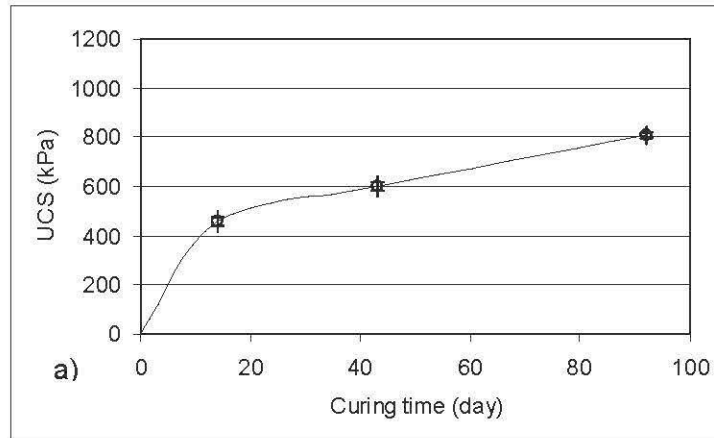
Figure 2.7, Mean UCS results for CPB samples: a) T10-W0, b) T10-W1, c) T10-W2 (cross marks show minimum and maximum UCS values).
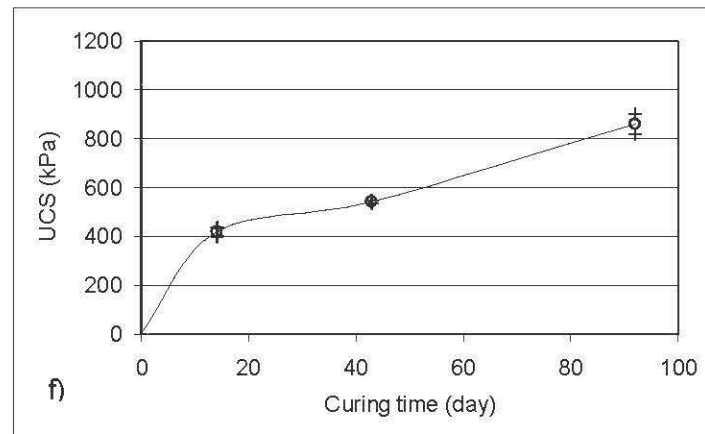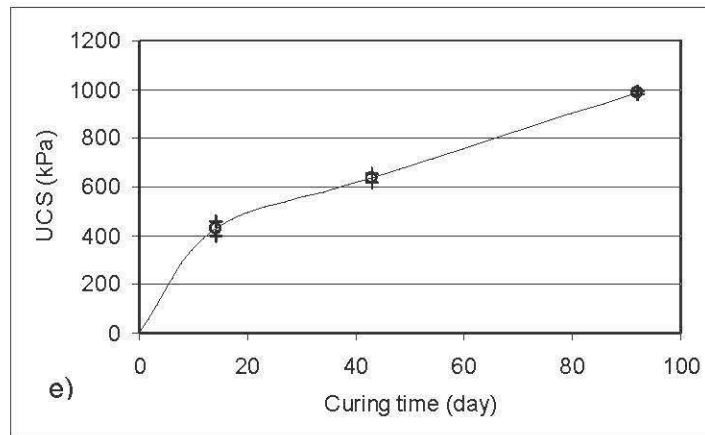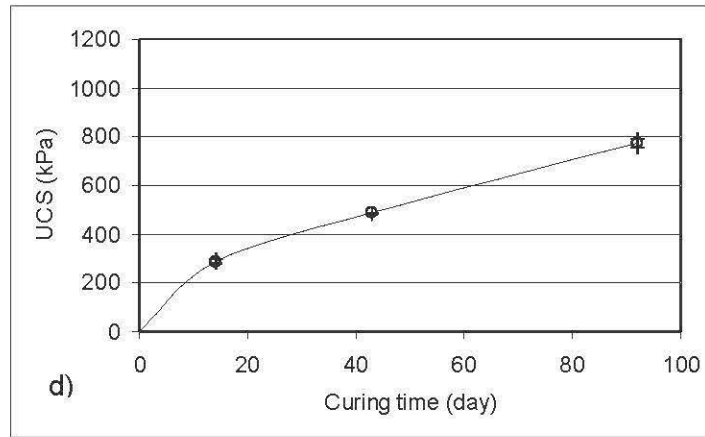
Figure 2.7, (continued), d) T10FA-W0, e) T10FA-W1, f) T10FA-W2.
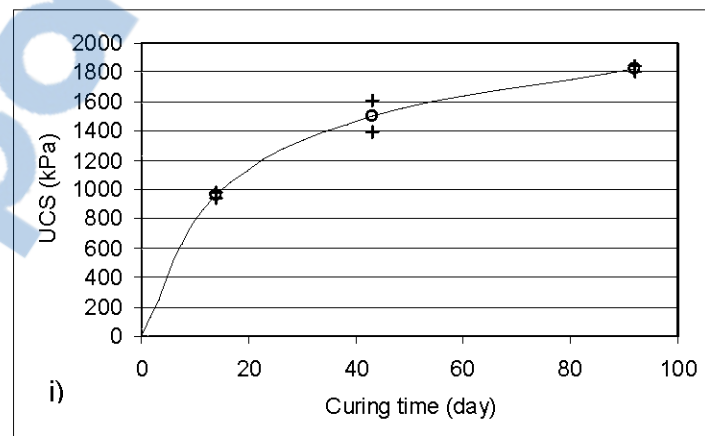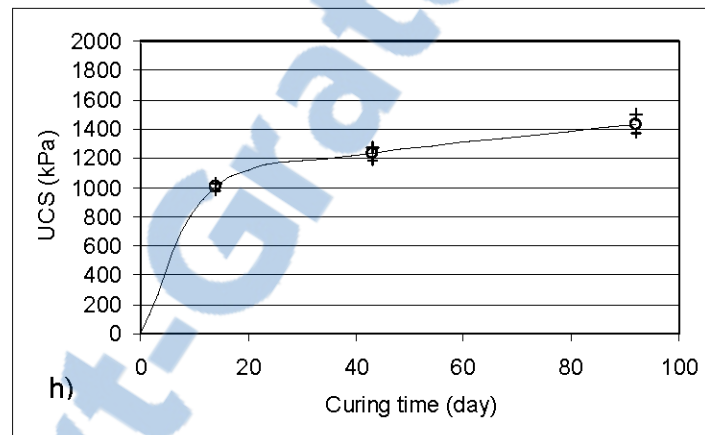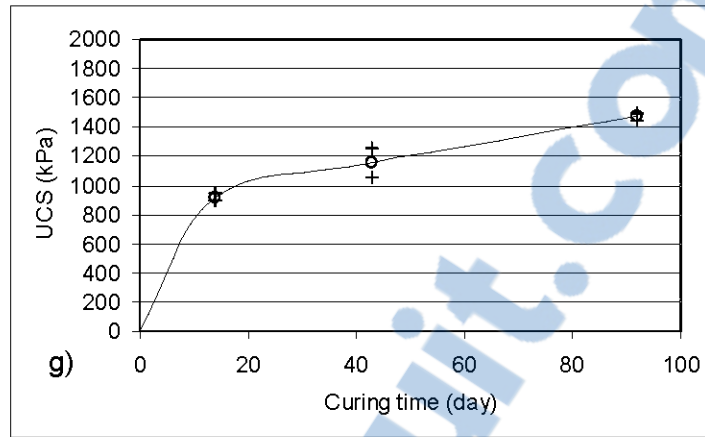
Figure 2.7, (continued), g) T10SL-W0, h) T10SL-W1, i) T10SL-W2.

Most of physically-based models relating strength and porosity use the total porosity value of the material as the key indicator (e.g. Li and Aubertin, 2003). As with other engineering materials, the total porosity of cement paste and concrete is typically inversely (and non linearly) proportional to the compressive strength. This dependency is also observed with the MIP porosity. The literature review of Beaudoin and Marchand (2001) presents many relationships between MIP porosity and strength; some of these use the total porosity (e.g. Poon et al., 1997) while others use different portions of the pore size distribution (e.g. Odler and Röbler, 1985; Jiang and Guan, 1999; O'Farrell et al., 2001). In the present study, a strength gain is usually not accompanied by a decrease of the MIP total porosity with time. Nevertheless, the pore size distribution does evolve with curing time, and this change in the microstructure can be related to strength evolution. The following equation is based on a generalized power law expression, which distinguish the contribution of the total porosity and of the size-dependent porosity. Equation (2) is proposed as a practical means to estimate the strength of CPB samples using the MIP pore size distribution.

$$\sigma_{cn} = \sigma_{nmin} \left[\frac{(1-n)}{(1-n_{min})} \right]^{u} \cdot \left[\frac{(1-n_{\geq d})}{(1-n_{<d})} \right]^{v} \tag{2}$$

where σ_{cn} is the compressive strength (UCS) for the CPB having a porosity n; σ_{nmin} is the reference strength at the minimum porosity of the material (n_{min}); n is the MIP total porosity; $n_{\geq d}$ is the cumulative MIP porosity for pores larger than diameter "d" (taken here as 0.3 μm); $n_{<d}$ is the cumulative MIP porosity for pores smaller than diameter "d" (= 0.3 μm); u and v, are the two exponents that control the non linearity of the two porosity terms on the right hand site of Equation (2). This relationship can be viewed an extension of the existing power law functions that relate strength and porosity (e.g. Rzhevsky and Novik, 1971; Neville, 1981; Odler and Röbler, 1985; Li and Aubertin, 2003). Equation (2) includes two terms to define the porosity dependency: one for the total n value (first bracket on the right hand side of Equation

(2), and one for the fractional size (second bracket). The minimum porosity value (n_{min}) associated with the maximum strength (σ_{nmin}) of the material is introduced explicitly in Equation (2) as a reference state. For the materials tested, the minimum porosity n_{min} is estimated at 0.25, based on various test results taken from the literature (as reported by Bussière, 1993). For instance, in the case of tailings samples (without binder), Aubertin et al. (1996) reported a minimum porosity value of approximately 0.32 at the optimum modified Proctor density, while Mabes et al. (1977) reported a value of 0.31 at the end of long term consolidation tests. A minimum porosity value of 0.25 is retained here, considering that an additional porosity reduction (of about 0.06 to 0.07) would appear due to the precipitation of cementitious phases in the CPB (see Chapters 4 and 5). The minimum n value is associated to the maximum strength, which is estimated to be σ_{nmin} = 4080 kPa, based on the available results on CPB.

In the proposed equation, the relative contribution of the two fractional size distributions (fine and coarse pore size, based on diameter "d") is used to represent the effect of microstructural evolution. The limiting size "d" (MIP diameter that distinguishes the fine and coarse pore fractions) was fixed at 0.3 µm in this study, based on MIP observations; however, the value of d may be different for other CPBs, as this size-dependency may vary with the material studied. The porosity dependent terms (inside the two brackets of Eq. 2) are related to strength by a geometric (power law) function, with exponents u and v used to define the non-linearity of the dependency. The value of these parameters was evaluated with a regression (best fit) analysis, giving: u = 1 and, v = 5.2.

Before arriving at Equation (2), various mechanistic and empirical approaches based on existing formulations were investigated. None of the other expressions were correlated as well to the authors' results, while maintaining a range of application that covers the theoretical value for the porosity variables (which can range from 0 to 1). Equation (2) includes a term for the total porosity, which is typical of many power law relationships. This term is coupled to a correction factor (second bracket on the

right side) that represents the relative contribution of the two fractional porosities. This last term may increase or decrease the uniaxial strength, depending on how the pore size distribution evolves. It can thus be seen as a secondary internal state variable component in the proposed model.

Figure 2.8 (a) shows how the total porosity influences the mechanical strength of CPB (represented by the ratio $\sigma_{cn}/\sigma_{n\ min}$) for different proportions of fine and coarse pores, expressed from the ratio $(1-n_{\geq 0.3})/(1-n_{<0.3})$. When the latter ratio is fixed, the relationship between $\sigma_{cn}/\sigma_{nmin}$ and the total porosity n appears to be linear (with u = 1), at least over a certain range (n from 0.25 to 0.60 approximately). Observations on other materials indicate however that the linear dependency may not extend to a larger range of porosity (e.g. Li and Aubertin, 2003), but more data would be required to evaluate this aspect of the model response. At the same time as the material strength increases when the total porosity decreases, it can also become larger when the ratio $(1-n_{\geq 0.3})/(1-n_{<0.3})$ increases. This is because of a rise in the relative number of small pores (at a fixed porosity) has a positive effect on strength. The contrary applies when the proportion of larger pores is increased. Figure 2.8 (b) shows how the ratio of fine to coarse pores influences the material relative strength (i.e. $\sigma_{cn}/\sigma_{n\ min}$) for three typical CPB porosities (0.3, 0.4, and 0.5), according to Equation (2). As can be seen on this figure, the UCS becomes larger when the ratio $(1-n_{\geq 0.3})/(1-n_{<0.3})$ increases (i.e. with a higher proportion of small pores).
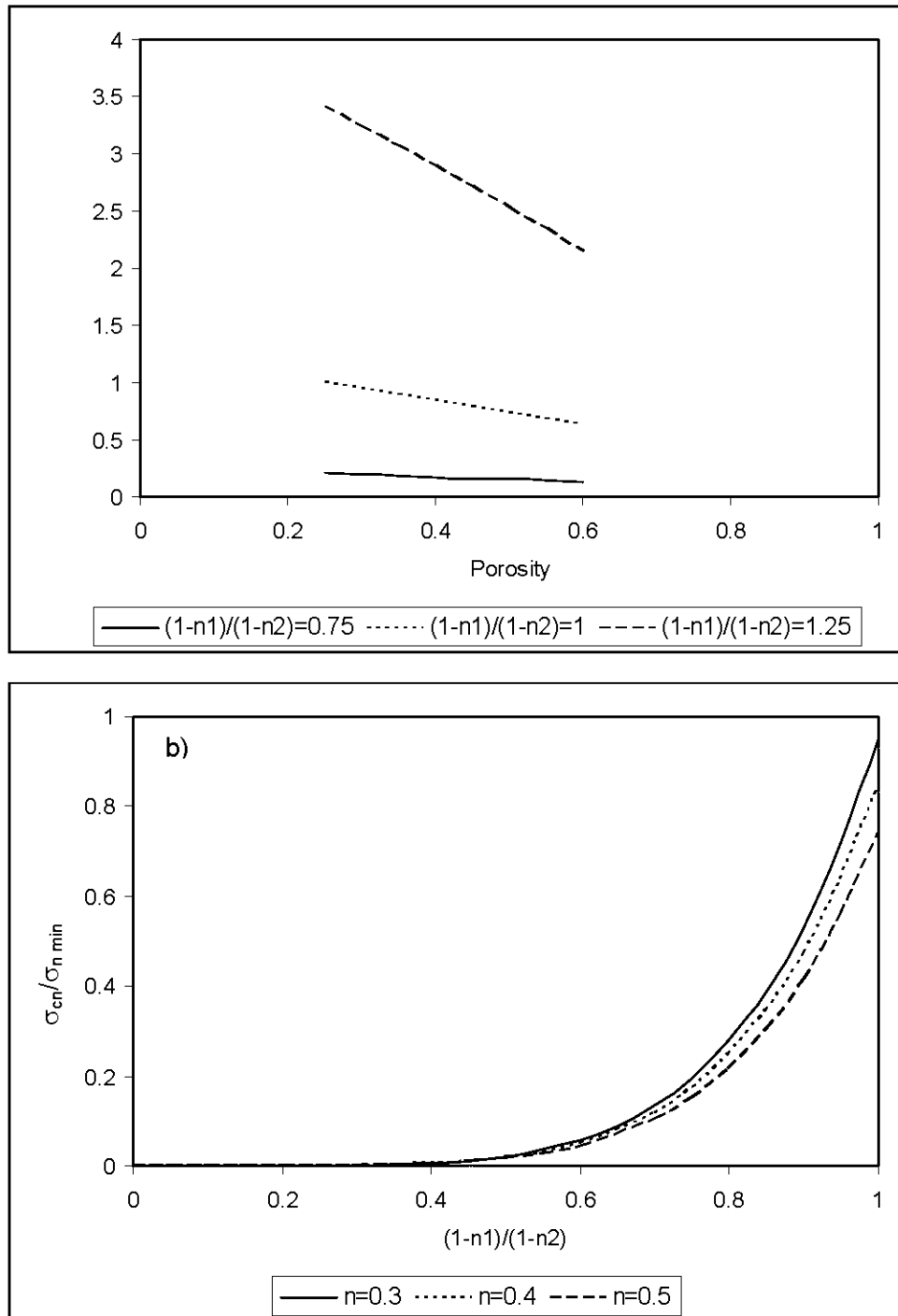
Figure 2.8, Graphical representation of Eq. (2) for the relative uniaxial compressive strength: (a) influence of the ratio $(1-n_{\geq 0.3})/(1-n_{<0.3})$ and of the total porosity (for a range between 0.25 and 0.6); (b) influence of the MIP total porosity (n1 = $n_{\geq 0.3}$ and n2 = $n_{<0.3}$).

Figure 2.9 shows the measured UCS versus the calculated UCS values based on the application of Equation (2). The coefficient of determination (R^2) between the experimental data presented here and Equation (2) is relatively high, at 0.83. Higher correlation coefficients could be obtained by including other variables in the model, such as mixture parameters (especially the binder type), but a more global approach is retained here to arrive at a simple relationship based only on porosity terms. It is interesting to note also that Figure 2.9 shows some data not included in the database used to develop the model and to perform the initial analysis; these were taken from two independent studies (Benzaazoua et al., 2000, 2003). Even if these 31 additional results were obtained with different types of tailings (some samples were made of fine tailings and others with coarser tailings), with another sample preparation procedure, and using different MIP pressure steps; a similar trend between MIP porosity and strength is observed.
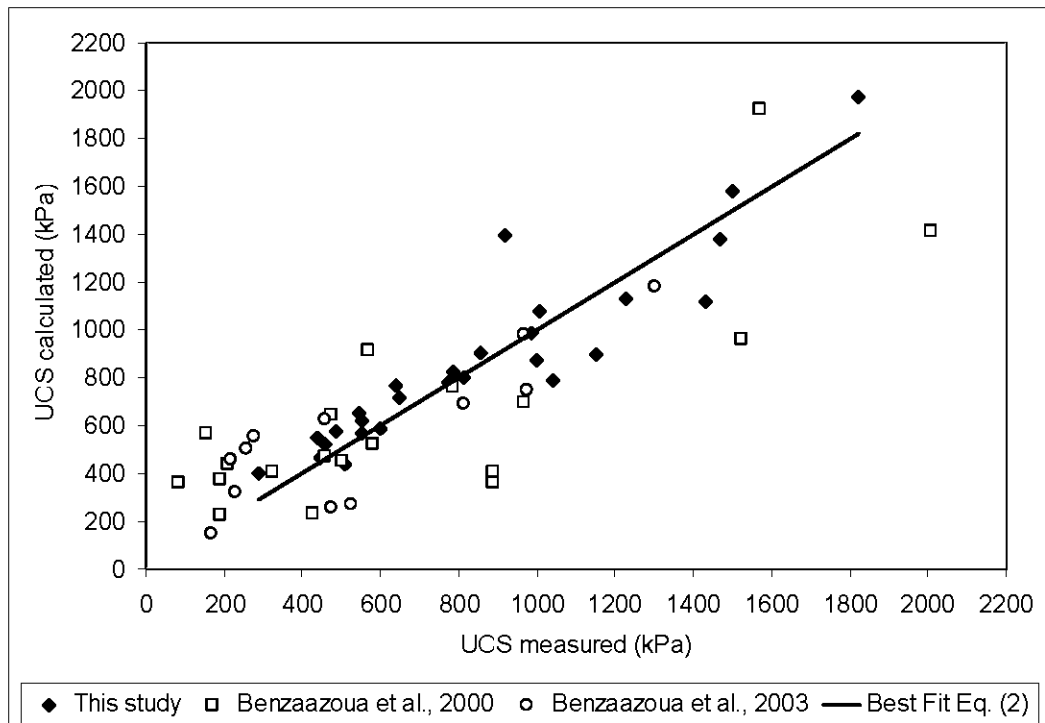
Figure 2.9, UCS calculated with Eq. (2) versus UCS measured. Linear fit is applied only on data coming from this study.

The coefficient of determination (R^2) between measured UCS and calculated UCS for all points included in Figure 2.9 is 0.66 when forcing the linear regression to go through the origin (i.e. 0,0 coordinates). Considering the numerous influence factors involved in the mixing, testing, and basic nature of the various CPB, this tend to indicate that the same trend would apply to various types of CPB. Of course, additional data are required to confirm this preliminary assumption.

As *in situ* sampling is expensive, Equation (2) could provide a useful means to estimate the strength of CPB when only small pieces of material are available. After a few tests, this relationship could also be calibrated on a given site to provide the variations of CPB strength in a mine where the conditions are expected to vary from one stope to the other (and even within a given stope). However, more work will have to be performed to validate the proposed equation for a wider range of conditions, including different types of CPB. It is worth emphasizing that the proposed estimation method does not eliminate the need for a detailed mechanical characterization of CPB samples with traditional approaches (UCS and triaxial tests).

2.6. Summary and conclusion

Microstructural evolution of different cement paste backfill (CPB) samples made with ground silica was measured by mercury intrusion porosimetry (MIP). Three binders were used at 5% by weight of dry silica: a type 10 Portland cement alone (T10), a mix 20:80 of T10 and blast furnace slag (T10SL) and a mix 70:30 of T10 and fly ash (T10FA). Three different types of water were used in the preparation of the mixtures: a deionised water and two waters sampled from two mine backfill plants and containing 4613 and 7549 ppm SO_4^{2-}. These waters are representative of a true interstitial water of highly sulphidic tailings. Uniaxial compressive strength (UCS) tests were also performed on the different CPB mixtures to investigate the link between pore size distribution and mechanical strength. Based on the results obtained, the following conclusions can be drawn:

1. MIP test is sufficiently sensitive to detect differences between porosity evolutions of different CPB mixtures containing 5% by weight of binder.

2. The threshold diameter (TD) decreases with curing time for all mixtures, indicating a decrease in pore size in the main pore network. The quantity of pores below the main intrusion peak increases with curing time for all mixtures, showing a porosity refinement due to the hydration process.

3. For the curing period and for the types of water used, the CPB samples made with sulphated waters usually showed a higher UCS value, with a smaller TD size. There was also a slight increase in the relative proportion of smaller pores. Precipitation of sulphated minerals in voids could explain this observation.

4. CPB samples made of binder T10SL showed the highest percentage of fine pores and the highest UCS values. The fineness of the slag particles induced a more effective water to binder cementitious effect than that of the other two binders studied.

5. CPB mixtures with fly ash showed a similar pore size distribution and strength evolution as CPB mixtures with ordinary Portland cement (OPC) alone. Since fly ash is cheaper than OPC and it contributes to reduce CO_2 emission, a partial replacement (30%) in the CPB mixture can be seen as an environmental and economical opportunity.

6. For all samples at all curing times, MIP total porosity remained at approximately 44%. Mercury re-intrusion tests performed on CPB samples showed that the test did not significantly affect the internal structure of the material. This would indicate that because of the high w/c ratio and the low binder percentages, the hydration/precipitation phenomena do not significantly affect the total porosity of CPB.

7. In spite of a constant MIP total porosity, the MIP pore size distribution is affected by different factors such as curing time, binder type and proportion, and, to a smaller extent, water quality. The pore size distribution curve of CPB samples was divided into two fractional sizes (<0.3 μm; ≥ 0.3 μm), and

these were related to the UCS evolution. A simple equation is proposed to represent the pore-size dependency of the strength.

CPB is a particular material that has a unique evolutive microstructure. This study has led to a better understanding of the influence of some important factors, including binder type, curing time, and water quality, on the microstructural evolution of CPB. The authors were also able to correlate this evolution with the mechanical strength of the material. Despite the promising results, more work is needed to evaluate other types of CPB and to assess the influence of other parameters on CPB microstructure. In this regard, work is ongoing to study the effect cement proportion, tailings grain size distribution and mineralogy.

2.7. Acknowledgments

2.8. References

ACI Committee 229 (1999). Controlled Low-strength Materials (CLSM), ACI 229R-99, American Concrete Institute, 15 p.

Annor, A.B. (1999). A study of the characteristics and behaviour of composite backfill material, Ph. D. Thesis, McGill University, Montreal, Canada, 394 p.

Aubertin, M., Bussière, B. and Chapuis, R.P. (1996). Hydraulic conductivity of homogenized tailings from hard rock mines, Can. Geotech. J., 33, 470-482.

Aubertin, M., Bussière, B. and Bernier, L. (2002). Environnement et gestion des rejets miniers, CD-ROM manual, Presses Internationales Polytechnique.

Beaudoin, J.J. and Marchand, J. (2001). Pore Structure. Chapter 14 in Handbook of Analytical Techniques in Concrete Science And Technology, Ramachandran, V.S. and Beaudoin, J.J. Eds., National Research Council of Canada, Noyes Publications, 528-628.

Belem, T., Bussière, B. and Benzaazoua, M. (2001). The effect of microstructural evolution on the physical properties of paste backfill, Proceedings of Tailings and Mine Waste '01, Balkema, Rotterdam, ISBN 90 5809 182 1, 365-374.

Benzaazoua, M., (1996). Caractérisation physico-chimique et minéralogique de produits miniers sulfurés en vue de la réduction de leur toxicité et de leur valorisation. PH. D. Thesis, Institut National Polytechnique de Lorraine, Nancy, France, 267 p.

Benzaazoua M., Ouellet, J., Servat, S., Newman, P. and Verburg, R. (1999). Cementitious backfill with high sulfur content: physical, chemical and mineralogical characterization. Cement and Concrete Research, 29, 719-725.

Benzaazoua, M., Belem, T. and Jolette, D. (2000). Investigation de la stabilité chimique et son impact sur la qualité des remblais miniers cimentés, IRSST Report R-260, ISBN 2-551-20431-3, 158 p. (in French).

Benzaazoua, M., Belem, T. and Bussière, B. (2002). Chemical factors that influence the performance of mine sulphidic paste backfill, Cement and Concrete Research, 32, 7, 1133-1144.

Benzaazoua, M., Fall. M., Ouellet, S. (2003). Étude pluridisciplinaire visant à mettre au point un outil expert pour la prédiction du comportement des remblais en pâte. IRSST Research Project 099-085, Final Report, 187 p. (in French).

Benzaazoua, M., Fall, M. and Belem, T. (2004). A contribution to understanding the hardening process of cemented pastefill, Minerals Engineering, 17, 2, 141-152.

Benzaazoua, M., Bois, D., Belem, T., Gauthier, P., Ouellet, S., Fall, M. and St-Onge, J.F. (2005). Remblais souterrains, évolution des connaissances et de la pratique. 20th Colloque Contrôle de terrains, Association Minière du Québec, Val d'Or, Quebec, Canada, march 2005, 23 p.

Bussière, B. (1993). Évaluation des propriétés hydrogéologiques des résidus miniers utilisés comme barrières de recouvrement, M. Sc. A. Thesis, École Polytechnique de Montréal, Montréal, Canada.

Cayouette, J. (2003). Optimization of the paste backfill plant at Louvicourt mine, CIM Bulletin, Canadian Institute of Mining, November/December, 51-57.

Cook, R.A. and Hover, K.C. (1999). Mercury porosimetry of hardened cement pastes, Cement and Concrete Research, 29, 6, 933-943.

Cuisinier, O. and Laloui, L. (2004). Fabric evolution during hydromechanical loading of a compacted silt, International Journal for Numerical and Analytical Methods in Geomechanics, 28, 483-499.

Dagenais, A.-M. (2005). Techniques de contrôle du DMA basées sur les effets capillaires, Ph. D. Thesis, École Polytechnique de Montréal, Montréal, Canada, 394 p.

Delage, P., Audiguier, M., Cui, Y-J., and Howatt, M.D. (1996). Microstructure of a compacted silt. Canadian Geotechnical Journal, 33,150-158.

De Souza E., DeGagné D., Archibald J.F., (2001). Minefill applications, practices and trends in Canadian mines. Proceedings of the 7th International Symposium on Mining with Backfill, Society for Mining, Metallurgy, and Exploration, 311-319.

Diamond, S. (2000). Mercury porosimetry: An inappropriate method for the measurement of pore size distributions in cement-based materials, Cement and Concrete Research, 30, 10, 1517-1525.

Escalante, J.I., Gomez, L.Y., Johal, K.K., Mendoza, G., Mancha, H., Mendez, J. (2001). Reactivity of blast-furnace slag in Portland cement blends hydrated under different conditions, Cement and Concrete Research, 31, 1403-1409.

Evangelou, V.P. (1995). Pyrite Oxidation and Its Control. CRC Press. 285p.

Fall, M., Benzaazoua, M. and Ouellet., S. (2005). Experimental characterization of the influence of tailings fineness and density on the quality of cemented paste backfill, Minerals Engineering, 18, 1, 41-44.

Fall, M. and Benzaazoua, M. (2005). Modeling the effect of sulphate on strength development of paste backfill and binder mixture optimization, Cement and Concrete Research, 35, 301–314.

Feldman, R.F. and Beaudoin, J.J. (1991). Pretreatment of hardened hydrated cement pastes for mercury intrusion measurements, Cement and Concrete Research, 21, 2-3, 297-308.

Godbout, J. (2005). Évolution des propriétés hydriques des remblais miniers cimentés en pâte durant le curage, M. Sc. A. Thesis, École Polytechnique de Montréal, Montréal, Canada. 190 p.

Goulet, C. and Blais, S. (2001). Utilisation du remblai en pâte à la mine Bouchard-Hébert, 16e Colloque en contrôle de terrain, Association minière du Québec, Val d'Or, Québec, Canada, march 2001, 21 p. (in French).

Grice, A. (1998). Underground mining with backfill, The 2nd Annual Summit – Mine Tailings Disposal Systems, Brisbane, Australia, 6 p.

Grice, T. (2001). Recent Minefill Developments in Australia, Proceedings of the 7th international symposium on mining with backfill, Seattle, Washington, 5 p.

Jiang, L. and Guan, Y. (1999). Pore structure and its effect on strength of high-volume fly ash paste, Cement and concrete Research, 29, 631-633.

Kesimal, A., Ercikdi, B. and Yilmaz, E. (2003). The effect of desliming by sedimentation on paste backfill performance, Minerals Engineering, 16, 10, 1009-1011.

Kesimal, A., Yilmaz, E. and Ercikdi, B., (2004) Evaluation of paste backfill mixtures consisting of sulphide-rich mill tailings and varying cement contents, Cement and Concrete Research, 34, 10, 1817-1822.

Kjellsen, K.O. (1996). Heat curing and post-heat curing regimes of high-performance concrete: Influence on microstructure and C-S-H composition, Cement and Concrete Research, 26, 2, 295-307.

Lapierre, C., Leroueil, S. and Locat, J. (1990). Mercury intrusion and permeability of Louiseville clay, Can. Geotech. J., 27, 761-773.

Lawrence, G. P. (1978). Stability of soil pores during mercury intrusion porosimetry. J. Soil Sci., 29, 299-304.

le Roux, K-A (2004). In situ properties and liquefaction potential of cemented paste backfill, Ph. D. thesis, University of Toronto, 271 p.

Li, L. and Aubertin , M. (2003). A general relationship between porosity and uniaxial strength of engineering materials, Can. J. Civ. Eng., 30, 4, 644-658.

Liping, L. (1997). Solidification and strengthening of mine tailings using a high-water rapid-setting cement, Master Thesis, Technical University of Nova-Scotia, Halifax, Canada, 148 p.

Lumley, J.S., Gollop, R.S., Moir, G.K., Taylor, H.F.W. (1996). Degrees of reaction of slag in some blends with Portland cements, Cement and Concrete Research, 26, 139-151.

Luo, R., Cai, Y., Wang, C., Huang, X. (2003). Study of chloride binding and diffusion in GGBS concrete, Cement and concrete research, 33, 1-7.

Mabes, D.L., James, H.H., Williams, R.E. (1977). Physical properties of Pb-Zn mine-process wastes, Proceedings of Conference on Geotechnical Practice for Disposal of Solid Waste Materials, American Society of Civil Engineers, p. 103-117.

Malhotra, V. M. (2001). High performance, high volume fly ash concrete for sustainability, P.-C. Aïtcin Symposium on the Evolution of Concrete Technology, Tagnit-Hamou, A., Khayat, K.H. and Gagné, R. Eds., American Concrete Institute, Quebec and Eastern Ontario Chapter, 19-74.

McCarthy, D.F. (2002). Essentials of Soil Mechanics and Foundations, Prentice Hall, 6th Edition, ISBN: 0-13030-383-6, 788 p.

Neville, A.M. (1981). Properties of concrete, third edition, 779 p.

Niu, Q., Feng, N., Yang, J., Zheng, X. (2002). Effect of superfine slag powder on cement properties, Cement and Concrete Research, 32, 615-621.

Odler, I. and Röbler, M. (1985). Investigations on the relationship between porosity, structure and strength of hydrated Portland cement pastes. II. Effect of pore structure and of degree of hydration, Cement and Concrete Research, 15, 3, 401-410.

O'Farrell, M. Wild, S. and Sabir, B.B. (2001). Pore size distribution and compressive strength of waste clay brick mortar, Cement & Concrete Composites, 23, 81-91.

Olson, R.A., Neubauer, C.M. and Jennings, H.M. (1997). Damage to the pore structure of hardened Portland cement paste by mercury intrusion, J. Am. Ceram. Soc., 80, 9, 2454-2458.

Ouellet, S., Bussière, B., Benzaazoua, M., Aubertin, M., Belem, T. (2004) Effect of binder type and mixing water chemistry on microstructural evolution of cemented paste backfill, Proceedings of the 57th Annual Canadian Geotechnical Conference and 5th joint IAH-CNC/CGS Conference, Quebec, Quebec, Canada, October 23rd to 27th, 8 p.

Ouellet, S., Bussière, B., Mbonimpa, M., Benzaazoua, M., Aubertin, M. (2006). Reactivity of an underground mine sulphidic cemented paste backfill, Minerals Engineering, 19, 407-419.

Poon, C.S., Wong, Y.L., Lam, L. (1997). The influence of different curing conditions on the pore structure and related properties of fly-ash cement pastes and mortars, Construction and Building Materials, 11, 7-8, 383-393.

Powers, T.C. (1958). The physical structure and engineering properties of concrete, Research and Development Laboratories of the Portland Cement Association, Bulletin 90, 28 p.

Powers, T.C., Copeland, L.E. and Mann, H.M. (1959). Capillary continuity or discontinuity in cement pastes, J. Port. Cem. Assoc. Research and Development Laboratories, 1, 2, 38-48.

Rahardjo, H., Aung, K.K., Leong, E.C. and Rezaur, R.B. (2004). Characteristics of residual soils in Singapore as formed by weathering, Engineering Geology, 73, 157-169.

Ramachandran, V.S., Beaudoin, J.J. (2001). Handbook of Analytical Techniques in Concrete Science and Technology, National Research Council of Canada, Noyes Publications, 985 p.

Rzhevsky, V., Novik, G. (1971). The physics of rocks. MIR Publisher, Moscow.

Simms P.H. and Yanful E.K. (2001). Measurement and estimation of pore shrinkage and pore distribution in a clayey till during soil-water characteristic curve tests, Canadian Geotechnical Journal, 38, 741-754.

Simms, P.H. (2003). A Fundamental Study of Unsaturated Flow in Compacted Clayey Soil, Ph. D. Thesis, University of Western Ontario, 336 p.

Simms P.H. and Yanful E.K. (2004). A discussion of the application of mercury intrusion porosimetry for the investigation of soils, including an evaluation of its use to estimate volume change in compacted clayey soils, Géotechnique, 54, 6, 421-426.

Sobek, A.A., Schuller, W.A. Freeman, J.R., Smith, R.M. (1978), Field and laboratory methods applicable to overburden and minesoils, EPA 600/2-78-054, 203 p.

Subauste, J.C. and Odler, I. (2002). Stresses generated in expansive reactions of cementitious systems, Cement and Concrete Research, 32, 1, 117-122.

Taylor, H.F.W. (1990). Cement Chemistry, Academic Press, 475 p.

Vick, S.G. (1990). Planning, Design, and Analysis of Tailings Dams, Bitech, Vancouver, 369 p.

Washburn, E.W. (1921). Note on a method of determining the distribution of pore sizes in a porous material, Proceedings, National Academy of Sciences, 7, 115-116.

Winslow, D.N. and Diamond, S. (1970). A mercury porosimetry study of the evolution of porosity in portland cement. Journal of Materials, 5, 3, 564-585.

CHAPITRE III

SCANNING ELECTRON MICROSCOPY AND IMAGE ANALYSIS APPLIED TO THE PORE STRUCTURE CHARACTERIZATION OF CEMENTED PASTE BACKFILL[5]

3. Résumé/Abstract

Cet article présente une étude de la structure des pores d'échantillons de remblai cimenté en pâte (RCP) par microscopie électronique et analyse d'image (SEM-IA). L'approche proposée permet d'étudier la porosité totale (n), la distribution de la taille des pores (DTP) et la tortuosité (T). L'influence de trois liants (Ciment Portland de type 10 (T10), T10 et cendre volante et T10 et laitier de haut-fourneau) et de trois types d'eau (une pure et deux sulfatées) est étudiée à 14 et 92 jours. L'évaluation de n révèle une porosité du même ordre de grandeur que celle mesurée par porosimétrie au mercure. Cependant, contrairement à cette technique les analyses SEM-IA montrent une baisse de n avec la cure. Comme dans la littérature, les DTP évaluées par SEM-IA sont différentes de celles mesurées par porosimétrie au mercure, mais pas autant que pour les pâtes de ciment. La dimension des gorges poreuses la plus fréquemment mesurée est passée de 6.7 µm à 5.7 µm en moyenne de 14 à 92 jours. De façon similaire, la technique d'évaluation de T a montré une augmentation de ce paramètre avec le temps. Les résultats ont aussi montré que le liant à base de laitier et que l'eau sulfatée ont induit des diminutions de la taille des pores et des augmentations de tortuosité. Les résultats de résistance en compression sont en corcordance avec ces changements microstructuraux.

Mots clés: Remblai cimenté en pâte, Microscopie électronique, Analyse d'image, Distribution de la taille des pores, Tortuosité

---

[5] Ouellet, S., Bussière, B., Aubertin, M., Benzaazouaa, M. (2006). Scanning electron microscopy and image analysis applied to the pore structure characterization of cemented paste backfill, à soumettre.

This paper presents a pore structure study on cemented paste backfill (CPB) using scanning electron microscopy and image analysis (SEM-IA). SEM-IA approaches were adapted and developed to estimate three pore structure parameters: the porosity (n), the pore size distribution (PSD), and the tortuosity (T). The influence of three binders (OPC, OPC with fly ash, and OPC with blast furnace slag) and three types of water (one deionised and two sulphated) were studied at 14 and 92 days of curing. The evaluation of n by SEM-IA gave results that are in the same range as those obtained by mercury intrusion porosimetry (MIP), but contrary to MIP results, n decreased slightly with curing time. As observed in the literature, the PSD evaluated by IA and by MIP were different, but not as much as for cement paste. The CPB throat size most frequently encountered in images decreased with curing time, from an average of 6.7 µm at 14 days to 5.7 µm at 92 days. Similarly, the measurement technique of T based on skeletonized images showed an increase in this parameter over time. The results also showed that OPC with slag admixture induced the most pronounced pore refinement among binder used, and that sulphated mixing waters contributed to a reduction of the pore size and an increase of the tortuosity (compared to control samples mixed with pure water). Mechanical strength measurements are in accordance with pore structure parameters: the highest strength values were observed on samples made of sulphated water and with the OPC-slag binder that induced a smaller and a finer porosity.

Keywords: Cemented Paste Backfill; SEM; Image Analysis; Pore Size Distribution; Tortuosity

3.1. Introduction

Pore sizes, shapes, and distributions are key microstructural characteristics that control or strongly influence many geotechnical and hydrogeological properties (Mitchell, 1993). For instance, some predictive models of mechanical strength are based on the total porosity (n) (e.g. Bal'shin, 1949; Rzhevsky and Novik, 1971), and occasionally on the pore size distribution (PSD) (e.g. Odler and Röbler, 1985; Poon et al., 1997; Jiang and Guan, 1999). Other models use pore structure parameters such as n and tortuosity (T) (e.g. Aubertin et al., 1996) or PSD (e.g. Kosugi, 1999) to predict the saturated hydraulic conductivity of porous media.

The porous structure of a material can be characterized by many parameters (see Dullien, 1992). In this study, three parameters related to the pore space are investigated. The first one is n, which is the fraction of the bulk volume occupied by the voids. The second parameter is the PSD defined as the representation of the pore sizes in term of density distribution (Dullien, 1992). The representation given by Dullien (1992, p. 29) for pores and pore throats apply well to the studied material and is retained here. The third parameter investigated is T, which is defined as the ratio of the length of a true flow path over the straight-line distance between inflow and outflow in a porous medium. (e.g. Scheidegger, 1974; Bear, 1988; Epstein, 1989; Dullien, 1992).

These pore structure parameters (particularly total porosity and pore size) can be quantified with different approaches such as simple drying and weighting of a known volume, mercury intrusion porosimetry, gas adsorption, or by image analysis (e.g. Washburn, 1921; Gregg and Sing, 1982; Russ, 1990; Ramachandran and Beaudoin, 2001). Each of these methods has advantages and disadvantages, i.e. each needs special treatment of the samples, covers a different pore size range, and gives a particular representation of the void volume often based on theoretical mathematical relationships. Among these approaches, the combination of scanning electron microscopy and image analysis (SEM-IA) allows a direct investigation of the pore structure of a material. As reported by Scrivener (2004), the main advantages of this technique include the wide range of magnification that can be used to observe features of interest, the quantification possibilities by image analysis, and the possibility to combine images with other signal detected by SEM. Another important advantage of SEM is that the material microstructure becomes directly visible; the challenge is then the quantification of what is observed. On the other hand, the main limitation is certainly that the third dimension is not apparent. This implies that two dimensional observations have to be validated for accuracy, especially when trying to study connected structures.

In this paper, the authors focus on a mining geomaterial called cemented paste backfill (CPB) that can be classified as a controlled low strength material (ACI, 1994). CPB is a particular geomaterial which consists of a mixture of thickened mine tailings, binder (between 2% to 7% of Portland cement usually mixed with mineral additives), and water. CPB is placed in underground mine stopes (Hassani and Archibald, 1998; Benzaazoua et al., 1999) via boreholes and pipelines, where it provides ground support to the rockmass around stopes and allows recovering secondary pillars. Moreover, when mine operators use this tailings management technique, the environmental impact and capital expenditures related to surface tailings disposal are reduced. General information on the use of CPB in the mining industry can be found in Hassani and Archibald (1998) and Potvin et al. (2005).

Few studies dealing with the microstructure of cemented paste backfill (CPB) are reported in the literature. Most investigations involved the mercury intrusion porosimetry (MIP) technique (Benzaazoua, 1996; 2000; 2003; Belem et al., 2001; le Roux, 2004; Ouellet et al., 2004; Fall et al., 2005). MIP tests performed on CPB material have shown the influence of curing time, binder type, water quality, and grain size distribution of tailings on the PSD. The MIP total porosity of the CPB remained nearly constant during curing, probably because the porosity of this material is too coarse and it does not impede complete filling of its pores by mercury under pressure (see chapter 2). Other investigations included a qualitative characterization of the microstructure of CPB using SEM (Benzaazoua et al., 1999; 2002; Belem et al., 2001; Ramlochan et al., 2004; Ouellet et al., 2006). For instance, Benzaazoua et al. (1999) showed photos of rough surfaces which revealed the presence of secondary minerals (gypsum: $Ca(SO_4) \cdot 2H_2O$) in CPB pores; they obtained a porosity of about 50% for an in situ paste backfill sample. Similar observations were made by Belem et al. (2001) and Benzaazoua et al. (2002) on a sulphidic CPB mixed in the laboratory. These SEM observations showed precipitated secondary minerals that reduced the porosity of CPB with curing time, indicating that these minerals appear to participate to the strengthening process. Ramlochan et al. (2004) examined epoxy impregnated flat-polished CPB samples by SEM. They

found no evidence of a cemented matrix bridging between tailings particles; rather they observed hydrated minerals sparsely filling the spaces separating the tailings particles. According to these authors, their observations result from the high water content used in CPB. They also evaluated the total porosity of one CPB sample by image analysis and obtained a value of n close to 50%. To the authors knowledge, no attempt to further characterize the pore structure of CPB has been reported in the literature.

This paper presents a quantitative analysis of the pore structure evolution of CPB samples using SEM-IA. As pore structure parameters can be related to mechanical, hydraulic, and environmental behaviours of porous materials (e.g. Vervoort and Cattle, 2003; Ouellet et al. 2006), the main objective of the paper is to establish a technical and practical basis for determining relevant pore structure parameters in CPB by SEM-IA. The studied CPB samples were made from ground silica. Three binders (ordinary Portland cement (OPC), OPC mixed with fly ash type C and OPC mixed with blast furnace slag) were used to make the different mixtures as well as three types of mixing water containing different sulphate (and other ions) concentrations. SEM-IA results are presented for samples cured for 14 and 92 days. The pore structure was characterized by evaluating the total porosity (n), pore size distribution (PSD), and tortuosity (T). The mechanical strength of the different CPB mixtures was also evaluated using uniaxial compressive strength. Different evaluation strategies were used to validate the obtained results: the n values estimated by image analysis were compared to those evaluated using the porosity versus uniaxial compressive strength model proposed by Li and Aubertin (2003); the SEM-IA PSD were compared to MIP PSD performed on the same samples; and T values were compared with data reported in the literature. Since it is often difficult and expensive to directly measure some CPB properties such as the saturated hydraulic conductivity, water retention curve, and effective diffusion coefficient due to the evolution of the material caused by the binder hydration (e.g. Belem et al., 2001; Godbout, 2005), the SEM-IA can be seen as a promising approach for estimation purposes.

3.2. Materials and samples preparation

Materials used in the present study are briefly described in the next paragraphs; more details are presented in Chapter 2.

The three binders used in the CPB mixtures are: a 100% type 10 CAN/CSA-A5-98 Portland cement (named T10); a mix of 20% T10 and 80% ground granulated blast furnace slag (T10SL); and a mix of 70% T10 and 30% fly ash (T10FA). Cement and admixtures were provided by Lafarge Canada. CPB mixtures were prepared with three different types of water: a deionised water (named W0) and two mine waters (W1 and W2) sampled at the tailings dewatering system of two backfill plants dealing with highly sulphidic tailings. The water W1 contains a sulphate concentration of 4613 ppm, while the water W2 has a sulphate concentration of 7549 ppm. Other major ions in W1 and W2 mixing waters are respectively calcium with 803 ppm and 1790 ppm, sodium with 915 ppm and 111 ppm and, potassium with 41 ppm and 48 ppm. The pH values for W0, W1 and W2 waters are 6.09, 9.62, and 4.57 respectively. Mine waters were filtered to remove suspended particles before analysis and mixing.

For all CPB mixtures, ground silica was used to simulate tailings. The silica contains 99.68% SiO_2 and has a grain size distribution (evaluated with a Malvern laser Mastersizer S) similar to the average grain size of 11 mine tailings (coming from the province of Quebec and northern Ontario, Canada). This mono-mineral non-reactive aggregate, having a typical tailings grain size curve, was selected (instead of real tailings) to eliminate the effect of tailings mineralogy on the geochemistry of CPB. Hence, the study presented here focuses on the binder and water effects on the pore structure of CPB.

CPB mixtures were prepared in small batches in a 20 litres bucket and mixed for at least 5 minutes with a ½ inch electric drill using a paint mixer bit. CPB cylinders of 10

cm long and 5 cm in diameter were cured at room temperature and at relative humidity above 90%. The binder proportion for the CPB was 5% by weight of dry silica. Water to cement ratio was 7 for all CPB mixtures and water/solid ratio equalled 0.33. After measuring the uniaxial compressive strength (UCS) on two cylindrical samples, the internal part of one cylinder was sampled and dried by a combination of freeze drying and oven drying. The 18 samples studied were first cut in small cubes of approximately 1 cm³ each and immersed for more than 5 minutes in liquid nitrogen. They were then freeze dried for a period of 24 hours at 0.9 Pascal and -50°C in a Virtis Ultra 35 Super XL freeze dryer. After this first 24 hours, another period of 24 hours in an oven at 45°C completed the drying. After the drying steps, the samples were epoxy impregnated using the Struers Epovac vacuum apparatus and a low viscosity, low shrinkage epoxy. Prior to impregnation, the resin (but not the hardener) was heated at 40°C for a period of one hour. Impregnated specimens were then cured over night before polishing (final polish with a 0.25 µm diamond compound). Flat-polished specimens were then maintained in a desiccator afterward to avoid rehydration. Tests performed on some specimens showed that the epoxy intruded about 3-5 mm all around, inside the CPB sample.

3.3. Methods used to evaluate the pore structure parameters

3.3.1. Capture and treatment of BSE images

SEM observations were done on a Hitachi S-3200-N microscope in BSE mode at accelerating voltage of 20 keV, with an emission current of 100 µA, and at a focal distance of 15 mm. All acquired images were at 800x magnification and had a dimension of 512 x 368 pixels representing an area of 19178.25 µm² at 3.1344 pixels per micron. The study of a porous material by IA, and particularly the determination of n, is mainly based on the discrimination of grey levels in BSE images with an image processing software. In BSE mode, the grey level is directly proportional to

the backscatter coefficient, which is related to the atomic number of chemical elements (Goldstein et al., 1992). With 256 grey levels, the mineral phases presenting the highest average atomic numbers are the brightest in the image. Because epoxy resin (used as pore filling material) mainly contains carbon (Z=6), the backscatter coefficient of pores is low and pixels representing the voids in BSE images are dark. This allows separating the porosity from the solid grains by IA.

It is well known that the IA threshold evaluation is critical for a good microstructural analysis of cemented materials (Bartoli et al., 2005; Coster and Chermant, 2001), since this step is at the base of subsequent processing stages. This is particularly the case in this investigation, as binary images are used for more than one purpose (i.e. evaluation of n, PSD, and T). CPB are known to have a high porosity, often above 40% (e.g. Benzaazoua et al., 1999; 2002; Belem et al., 2001; Ramlochan et al., 2004). Under this condition, the evaluation of a threshold value related to the porosity in a histogram of grey levels is relatively straight forward. Figure 3.1 shows a BSE image of a CPB sample, and the corresponding histogram of tones is presented in Figure 3.2. For such CPB, the typical grey level histogram is always bimodal, with one mode related exclusively to the solid phase (zone "C" in Figure 3.2), and the second mode partly related to the voids and partly related to the solid (zones "A" and "B"). The grey levels in zone "A" are only associated with the epoxy resin while the zone "B" is mainly seen as a transition zone showing the epoxy containing less or more solids interlaced. A few other authors have previously observed such transition zone in cement paste (Scrivener et al., 1987; Darwin, 2001; Scrivener, 2004) and in CPB (Ramlochan et al., 2004).

In the present study, the threshold is determined as the average between the darker grey values occupying the highest proportion of the image (GL_1 value in Figure 3.2) and the lowest value of the valley between the two main family peaks (GL_2 value). The implementation of an unambiguous, objective, and repeatable procedure to evaluate the threshold value is a key aspect to be able to recognize and compare the evolution of the pore structure parameters over time.
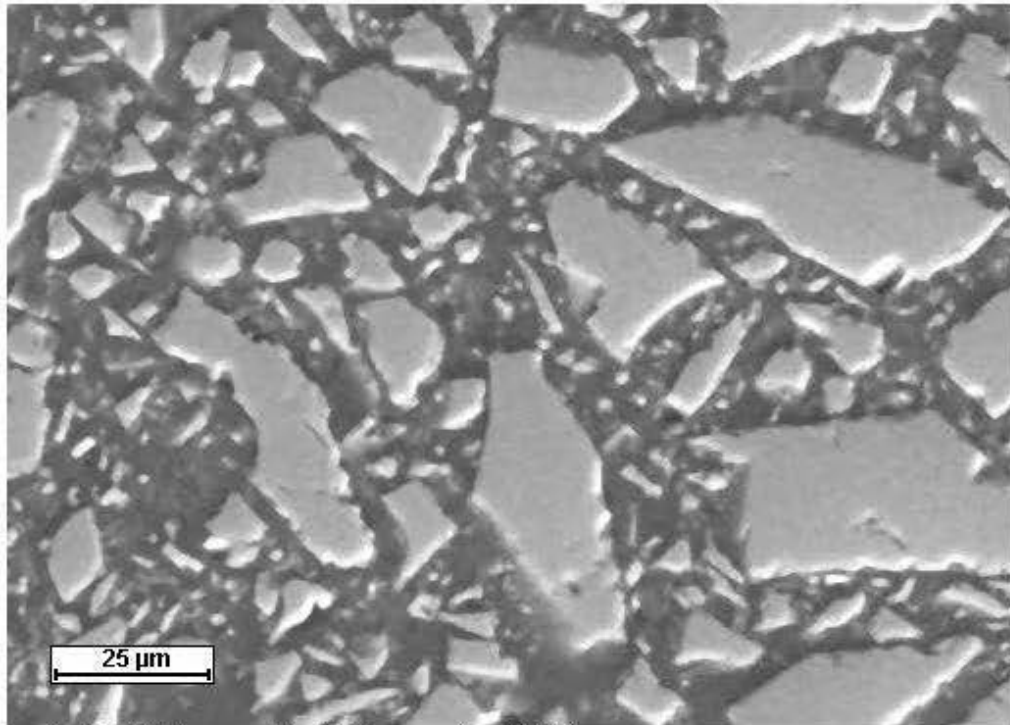
Figure 3.1, BSE image of a CPB sample at 800x.
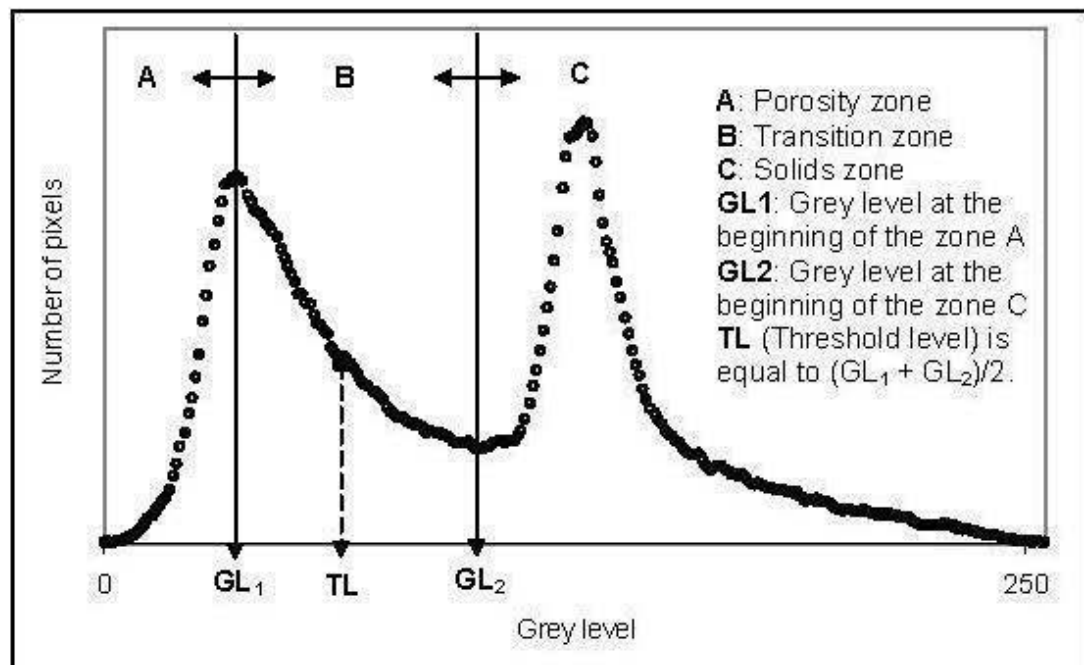
Figure 3.2, Grey level distribution obtained from the image shown in Figure 3.1. The values GL_1 and GL_2 are used to determine the threshold level TL.

3.3.2. Total porosity

After the threshold determination, the conversion into binary patterns, and the application of a 1 pixel radius median filter, the value of n is evaluated according to the ratio of the covered areas by black pixels (pores) over the total area for each captured image. Figure 3.3 shows the content of Figure 3.1 after the thresholding and filtering stages.
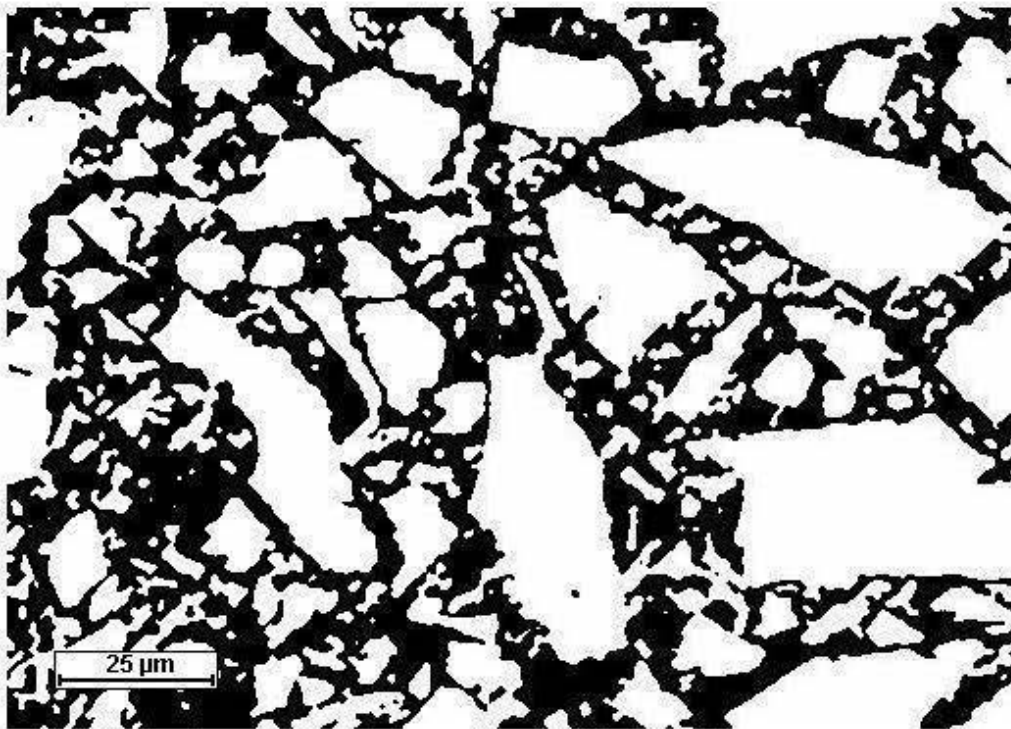
Figure 3.3, Binary image of the image shown in Figure 3.1.

A first capturing run of 16 images was performed on all CPB specimens using the Oxford LINK ISIS program and n was evaluated for each image. Mean n values, standard deviations, and statistical errors were then calculated for each set of images. The objective was to obtain a representative mean n value with a tolerated statistical error of less than 2% for a confidence level of 95%. If the first set of 16 images did not meet this tolerance, more images would be captured until a representative value of n is obtained. Depending on the specimen, up to 80 images were captured; in this study the calculated error level on n was between 0.86% and 1.93%.

3.3.3. Pore size distribution

3.3.3.1. Description of the measurement method

A standard IA program cannot discriminate any individual structure in binary images taken from a CPB sample. A look at Figure 3.3 reveals that the material does not present isolated pores; rather the material presents a connected porosity made of voids and throats with various widths. Thus, the PSD cannot be evaluated using approaches applied to cement paste in which the pores are clearly isolated. Instead, the PSD is evaluated with a method similar to the intercept method (Launeau and Robin, 1996) that allows scanning throat width in four directions (0, 45, 90 and 135°) (e.g. Vervoort and Cattle, 2003). At least 400 000 sizes were measured for each set of binary images to evaluate the PSD; all widths are then sorted and grouped by size. The PSD of a sample is calculated according to the following expressions.

The pixel area of each pore size class (A_{pixi}) is equal to:

$$A_{pixi} = d_{pixi} \times N_{pixi} \tag{1}$$

where d_{pixi} is the size in pixel and N_{pixi} is the number of time d_{pixi} is measured in a given image. The relative appearance frequency FA_i of d_{pixi} is then:

$$FA_i = \frac{A_{pixi}}{\sum A_{pixi}} \tag{2}$$

The actual area A_i of a pore is defined as:

$$A_i = \frac{d_{pixi}}{R} \times \frac{1}{R} \tag{3}$$

where R is the image resolution in pixel/micron. The relative proportion of each size class interval P_i, adjusted according to the previously measured total porosity (n), is equal to:

$$P_i = \frac{n \times FA_i \times A_i}{\sum FA_i \times A_i} \tag{4}$$

3.3.3.2. Assessment of the method

Prior to the measurement of the PSD of CPB samples, tests were performed on a cement paste sample to assess the validity of the approach proposed here. More specifically, the evaluation was made by comparing: i) the SEM-IA approach proposed with the one using the diameter of a circle having the equivalent area as observed pores, ii) the MIP PSD with SEM-IA PSD evaluated using both SEM-IA

techniques, and iii) the PSD evaluated in this study using SEM-IA with the PSD evaluated by Diamond and Leeman (1995).

Diamond and Leeman (1995) presented side by side the mercury intrusion porosimetry (MIP) cumulative curve and the SEM-IA cumulative curve for an OPC paste samples having a w/c of 0.4 and cured for 28 days. These authors evaluated the SEM-IA PSD using the diameter of a circle having the area equivalent area to that of the observed pore. In the present study, the processing of the images to evaluate the PSD with this approach was performed with the program ImageJ (Rasband, W., National Institute of Health, USA, http://rsb.info.nih.gov/ij/).

The cement paste sample tested here was cured for 14 days and made from a mixture of T10 and W2 water at a w/c ratio of 0.33 (more details are presented in Ouellet et al., 2004). Figure 3.4 shows five cumulative PSD; two of these curves compare MIP results and the other three compare the SEM-IA results. The MIP curve and the SEM-IA curves presented in the Figure 3.4 are in the same range as those presented by Diamond and Leeman (1995), with a MIP PSD curve that is approximately two orders of magnitude smaller than the IA PSD curves. When SEM-IA curves obtained here are compared with the SEM-IA curve of Diamond and Leeman (1995), it seems that these curves are different. However, the difference is accentuated in Figure 3.4 due to the cumulative presentation of the results. In fact, the frequency distribution of the pore size measured is fairly similar; the sizes having the highest individual proportion are all close to 2 µm. Moreover, the PSD obtained by the intercept method (see section 3.3.1) is similar to the one obtained with the program ImageJ. In light of these results, it can be considered that the proposed approach gives realistic PSD.
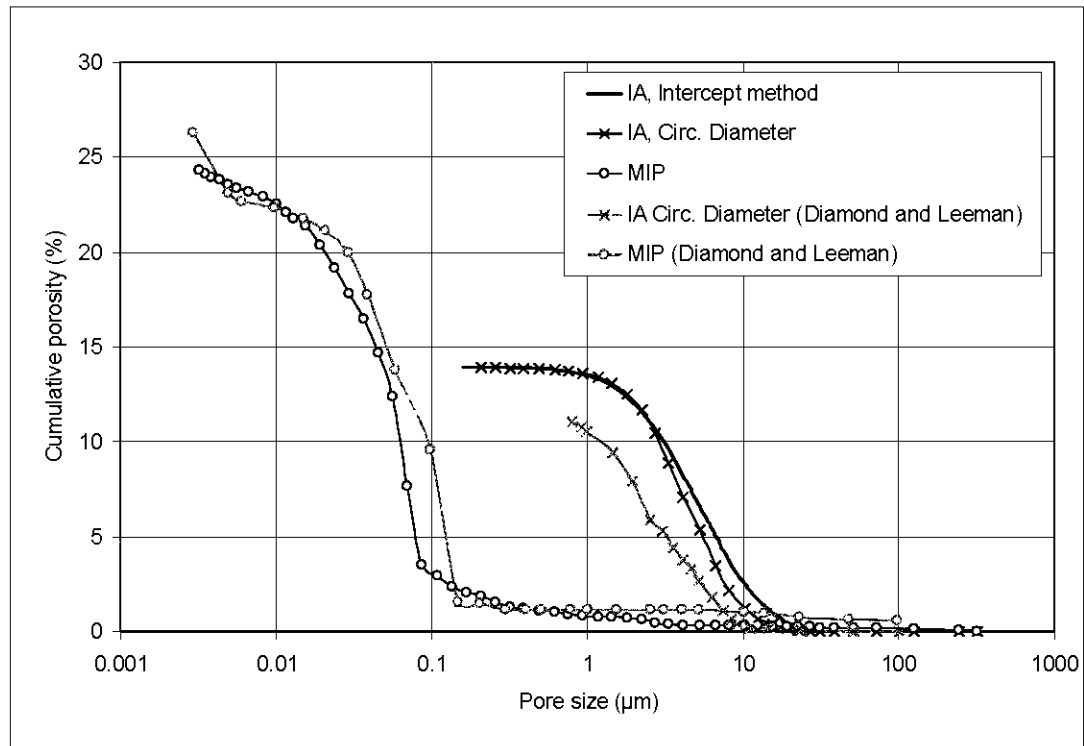
Figure 3.4, Cumulative pore size distributions (PSD) of a cement paste sample (w/c 0.33 at 14 days) evaluated by the SEM-IA technique developed in this study (Intercept method), by image analysis assuming a circular diameter for pores area, and by mercury intrusion porosimetry (MIP). This figure also shows the results obtained by Diamond and Leeman (1995) on a cement paste (w/c 0.4 at 28 days); values were digitized and converted to fraction assuming a specific gravity of 2.2 for cement paste.

3.3.4. Tortuosity

3.3.4.1.   Definition and previous studies

The tortuosity (T) is a parameter associated with fluid flow, solute and gas transport (e.g. Bear, 1988; Aubertin et al., 1996; Moldrup et al., 2001; Aachib et al. 2004). Definition of T can be expressed as the ratio of the incremental distance "dL" that an ion must travel to cover a direct distance "dx" in the flow direction (Carman, 1937; Berner, 1980), i.e., $dL/dx \geq 1$. This definition is used by many authors (Maerki et al.,

2004; Cousin et al., 1999; Moldrup et al., 2001; Boudreau, 1996; Epstein, 1989). Other authors (Bear, 1988; Millington and Shearer, 1971; Collin and Rasmuson, 1988; Aachib et al., 2004) use the opposite definition, i.e. dx/dL and the ratio is < 1. T can be considered a fundamental property of the flow that is closely related to the porosity and the relative difficulty for a fluid to percolate through a porous medium. Because this parameter is usually difficult to measure directly, T is often deduced from the ratio between the diffusion coefficient in free air and the diffusion coefficient in the porous media (e.g. Berner, 1980; Cousin et al., 1999), or by using a mathematical relationship that relates T, n, and the formation resistivity factor (F) (e.g. Berner, 1980; Ullman and Aller, 1982).

Two dimensional approaches have been applied several times to analyse fluid flow and to select parameters related to fluid flow such as T (e.g. Ruzyla, 1986; Spangenberg et al., 1998; Mota et al., 1999; Solymar and Fabricius, 1999; Sammartino et al., 1999; Sardini et al, 1999; Schaap and Lebron, 2001; Vervoort and Cattle, 2003). For example, Mota et al. (1999) performed 2D simulations of packed beds formed with binary and ternary particle mixtures and evaluated parameters such as n and T. T was determined from the ratio of the estimated tortuous path through the bed to the height of the layer. Spangenberg et al. (1998) used IA to estimate the PSD of porous rock salt samples and to calculate the constrictivity of the pore network. The evaluated constrictivity was well correlated with n, F and the permeability. Sardini et al. (1999) evaluated the fluid pathway and T of a magmatic rock by determining the contact line (or microcrack) between mineral grains and estimated the geometry of the percolation path.

3.3.4.2. Skeletonization approach

The proposed method to evaluate the tortuosity of CPB combines different aspects of the papers previously cited. The method is mainly based on the IA skeletonize function (see Coster and Chermant, 2001; Russ, 1990). Few papers deal with the

application of the skeletonization technique to characterize the pore structure of porous materials. Among these, one can mention Delerue et al. (1999) who used the skeletonize function to evaluate the PSD in vertisol. Ringot and Bascoul (2001) and Ammouche et al. (2001) used also this function to evaluate the microcracking in concrete.

In this application of the technique, all thresholded images are first independently skeletonized using the batch processing option included in the ImageJ software. Figure 3.5 presents an example of skeletonization with the image presented in Figure 3.3. When applied to CPB images, skeletonize function has the ability to reduce a pore to one line at the mid point between all other structures. A programmed algorithm is then used to find all triple points junction (TPJ) (the three pixels circled in the inserted image of Figure 3.5) in the resulting network and to evaluate the distance between two consecutive TPJ by the skeletonized path (dL) and by the direct path (dx; straight line in the box of Figure 3.5). The ratio between both values gives T using the definition T = dL/dx. Depending on the image set, the number of measurements ranged from 6750 to 62560. The resulting T is the arithmetic average of measurements performed on a set of at least 16 images. To allow a comparison with the available literature data, results are presented as the tortuosity factor:

$$T^2 = (dL/dx)^2 \tag{5}$$

It is worth mentioning here that the proposed technique to evaluate T^2 of CPB is not applicable to all porous materials. For instance, it would not be recommended for materials presenting low and disconnected porosity. Due to the interconnected character of the CPB porosity and because individual values of T are measured over a short distance (between two consecutive TPJ), the evaluated path can be considered as a probable fluid flow path in 2D. Since CPB is a material that evolves with time, and that hydrated phases precipitate in throats, it is expected that the path
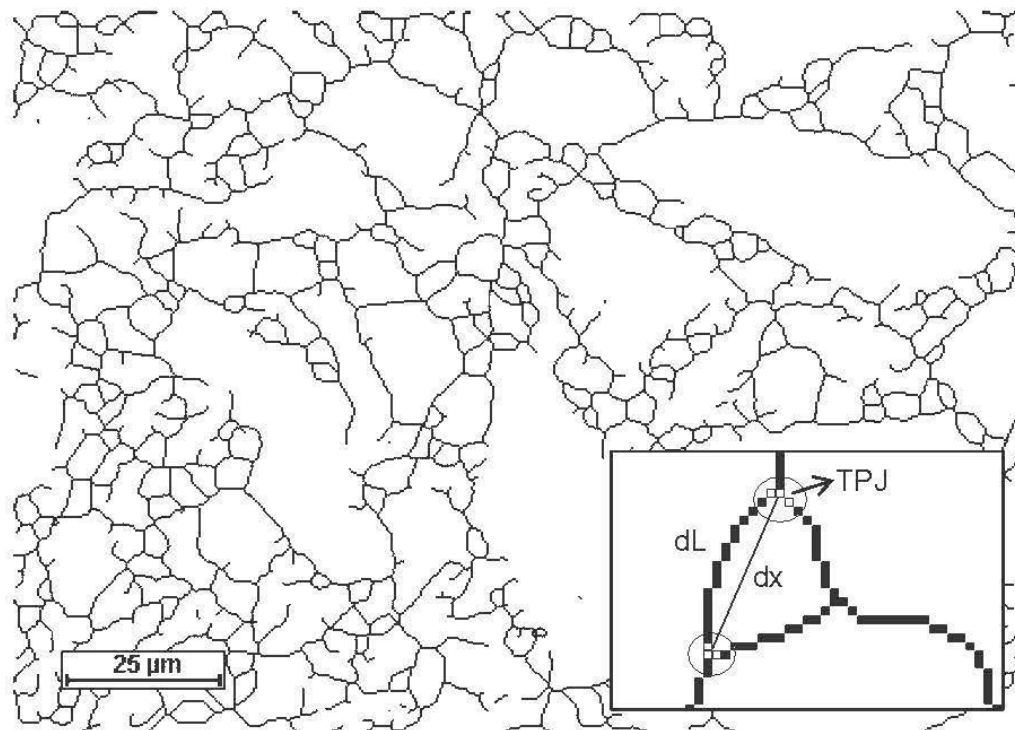
Figure 3.5, Treatment of the Figure 3.3 after the skeletonization. The inserted image shows details at the pixel scale, the selected triple points junction (TPJ), the tortuous distance (dL), and the direct distance (dx).

between two consecutive TPJ progressively becomes longer and then more tortuous.

3.4. Results

3.4.1. Total porosity

Figure 3.6 shows the SEM-IA results at 14 and 92 days of curing and the difference between n values at 14 and 92 days of curing. The SEM-IA porosity decreases from 14 days to 92 days. Mean n values for all samples are 44.7% at 14 days and 40.0% at 92 days. SEM-IA porosity values also show an influence of the binder type and water type; mean values of the n differences between data at 14 days and 92 days

are 4.7%, 2.9% and 6.3% for T10, T10FA, and T10SL binders respectively and 2.9%, 4.6%, and 6.5% for W0, W1, and W2 waters respectively. According to these values, the blast furnace slag additive has the greatest impact on porosity refinement over time. This finding is in agreement with the behaviour of slag reported in the literature (e.g. Lamos and Clark, 1989; Luo et al., 2003; Niu et al., 2002). Additionally, the mixing water with the highest sulphate ions content induces the largest porosity decrease. Precipitation of sulphates in CPB samples can explain, at least in part, the decrease of n with W1 and W2. According to sulphur differentiation chemical analysis results (see Sobek et al., 1978) and thermogravimetry results obtained on the 92 days cured samples (not presented here), the amount of sulphates in samples mixed with W1 and W2 waters was significantly higher than with W0 water (see Chapter 2 for details).

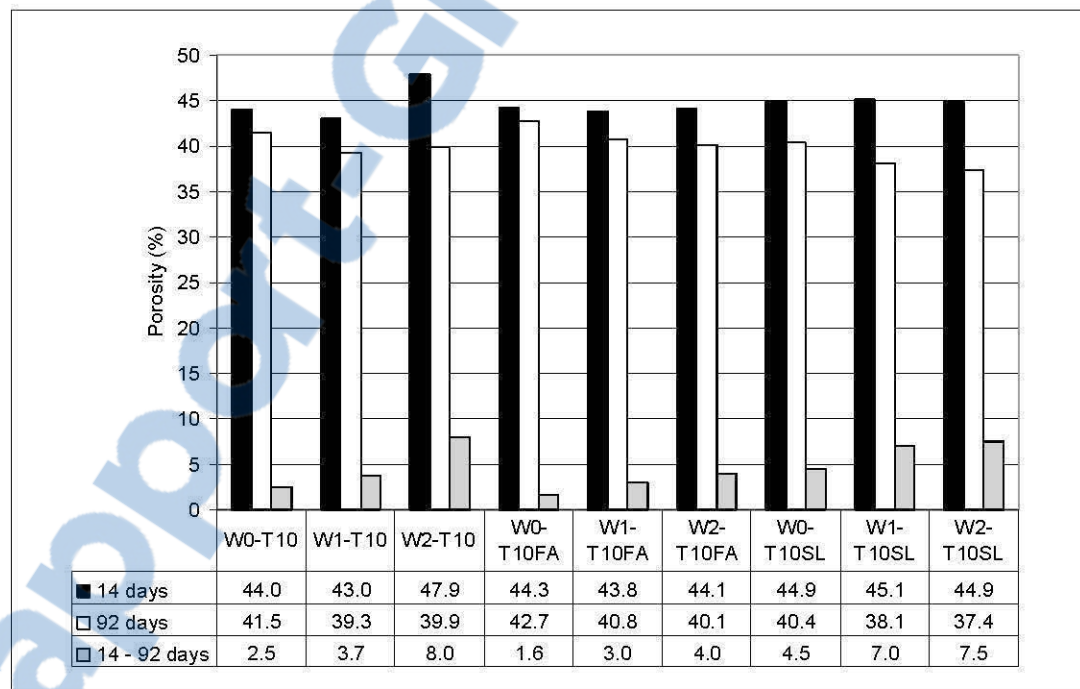|	W0-T10	W1-T10	W2-T10	W0-T10FA	W1-T10FA	W2-T10FA	W0-T10SL	W1-T10SL	W2-T10SL
■ 14 days	44.0	43.0	47.9	44.3	43.8	44.1	44.9	45.1	44.9
□ 92 days	41.5	39.3	39.9	42.7	40.8	40.1	40.4	38.1	37.4
□ 14 - 92 days	2.5	3.7	8.0	1.6	3.0	4.0	4.5	7.0	7.5

Figure 3.6, Total porosity results by SEM-IA.

However, since mixing waters contain significant concentrations of different ions, it is worth mentioning that precipitated sulphates do not explain all the mineralogical differences observed between the samples; mineralogical aspects of CPB are investigated in more details in the Chapter 4.

3.4.2. Pore size distribution

Figure 3.7 shows the PSD obtained by SEM-IA and by MIP for all samples studied (MIP PSD will be discussed in the section 3.5.2). One can observe that a curing effect is usually visible. All curves are slightly shifted to the left when curing time increases, which signifies that voids become smaller due to a constriction of the pores. The results can also be analysed using the most represented throat size (MRTS) in the distribution. The MRTS is defined as the pore size that is measured the most frequently in each section; MRTS is considered as a microstructural variable representative of the CPB evolution. Figure 3.8 shows the evolution of the MRTS at 14 and 92 days. Mean MRTS for all samples at 14 days is 6.7 µm while this value is 5.3 µm at 92 days. A possible effect of the mixing water seems to appear. Mean MRTS values of 6.2 µm, 6.1 µm, and 5.8 µm are obtained for W0, W1 and W2 waters respectively. The type of cement also affects the PSD of CPB samples. The MRTS means at 14 days are 6.8 µm, 6.4 µm, and 7.0 µm for T10, T10FA, and T10SL respectively; however at 92 days, T10SL generates a finer porosity with a MRTS of 5.1 µm, compared to 5.4 and 5.5 µm for T10 and T10FA respectively. Therefore, as observed for the total porosity measurements, it seems that the T10SL cement has the most significant impact on the pore size of CPB, particularly for a long curing period (92 days). The last noticeable effect is the height of the SEM-IA distribution. For most PSD, the peak height of the distribution increased with the curing time. This observation indicates that since the total porosity of CPB samples decreases with the curing time, their PSD becomes less outspread and more narrowly centered around the MRTS value.
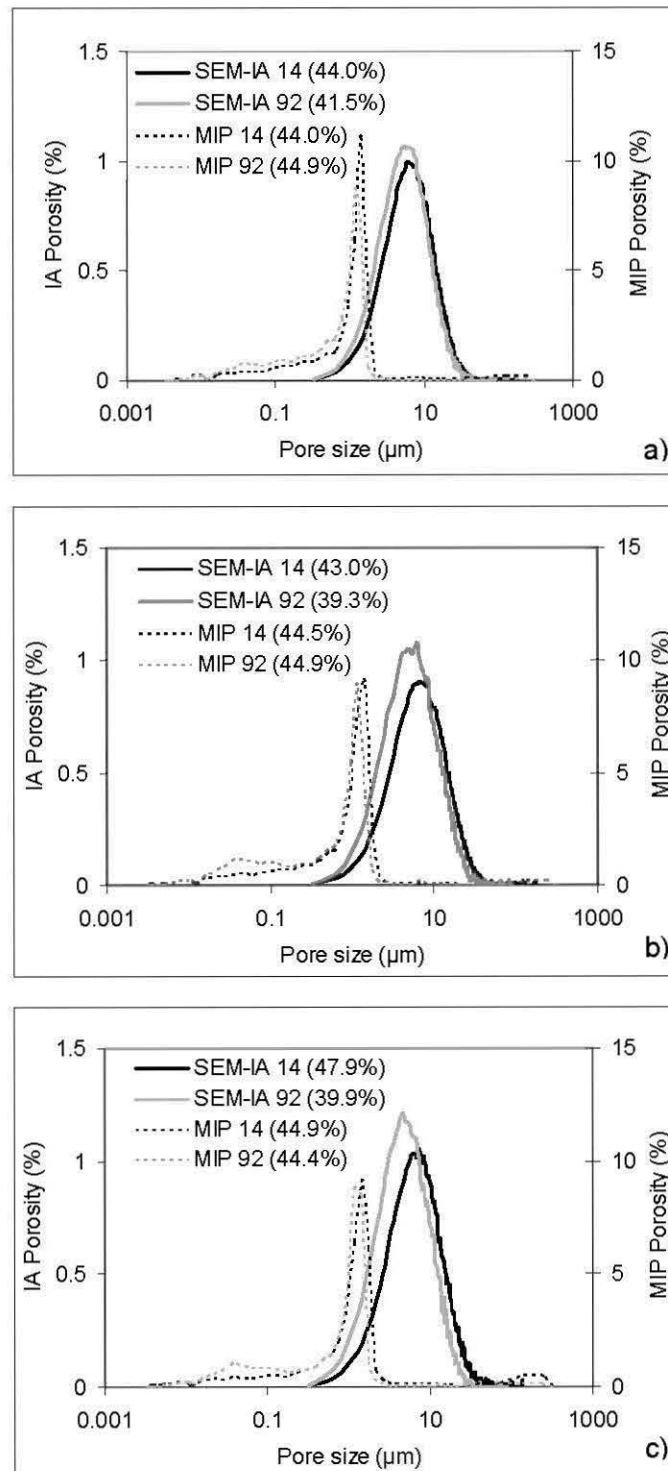
Figure 3.7, Pore size distributions of CPB samples evaluated by IA and by MIP: a) T10-W0, b) T10-W1, c) T10-W2 (data in parenthesis is the total porosity).
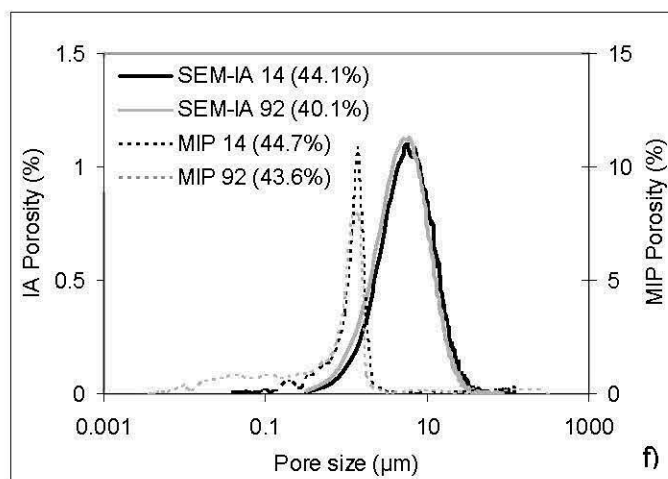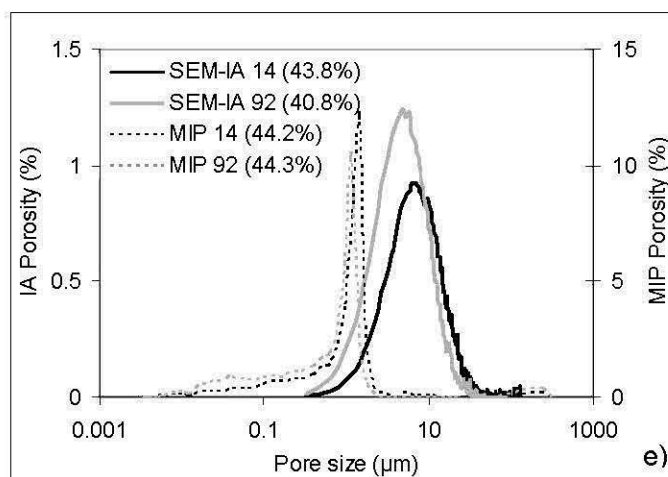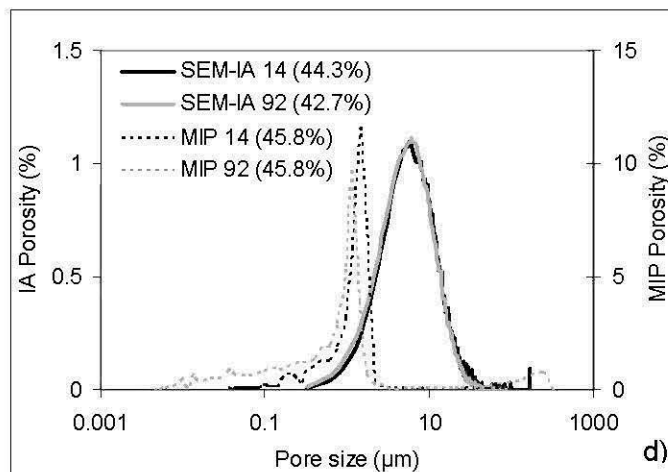
Figure 3.7 (continued), d) T10FA-W0, e) T10FA-W1, f) T10FA-W2.

Figure 3.7 (continued), g) T10SL-W0, h) T10SL-W1, i) T10SL-W2.

	WO-T10	W1-T10	W2-T10	WO-T10FA	W1-T10FA	W2-T10FA	WO-T10SL	W1-T10SL	W2-T10SL
■ 14 days	6.58	6.82	6.91	6.14	6.99	6.04	7.24	7.24	6.54
□ 92 days	5.78	5.38	4.97	5.95	5.01	5.48	5.36	5.16	4.79
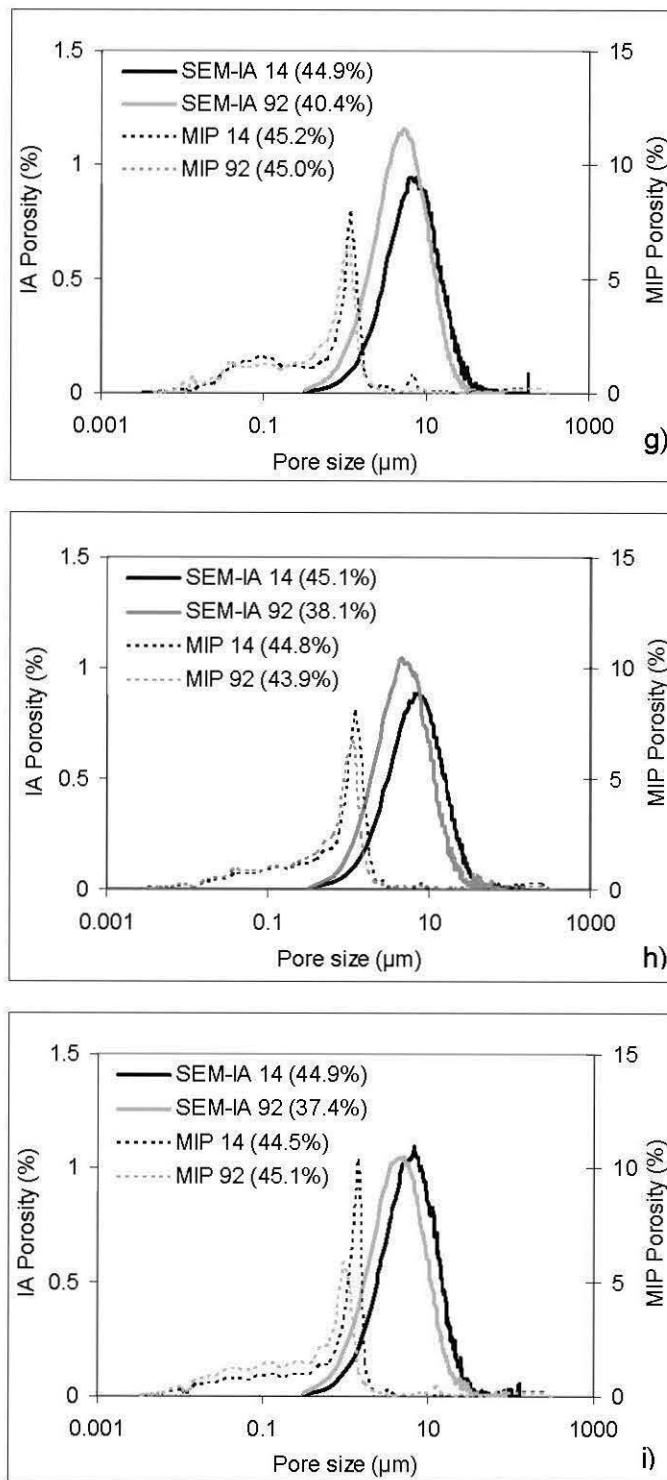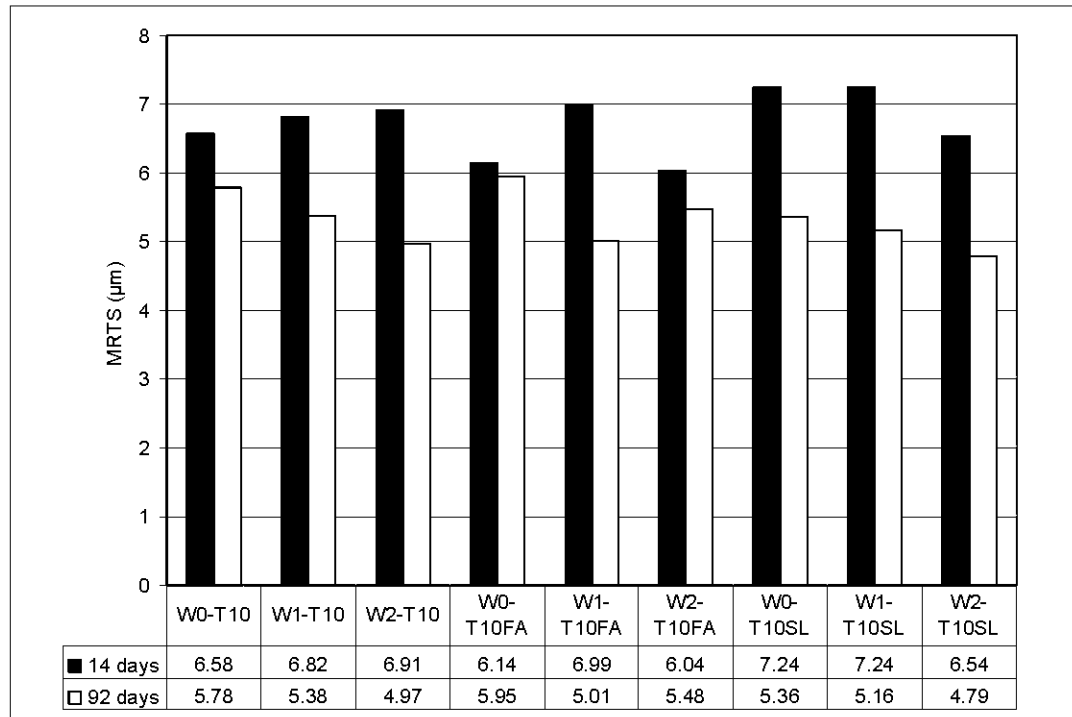
Figure 3.8, Histogram of the most represented throat size (MRTS) for all samples at 14 and 92 days.

3.4.3. Tortuosity

Figure 3.9 presents the tortuosity factors (T^2) evaluated with Eq. (5) for all samples. The values show an increase with the curing time; the mean T^2 for all samples at 14 and 92 days are respectively 1.68 and 1.94. These values are in accordance with the fact that the path between two consecutive TPJ in the image skeleton tend to increase with time, and that tortuosity is inversely proportional to the porosity (see models presented in Boudreau, 1996). A small difference is also noticeable when T^2 values are sorted by binder type: mean values for T10, T10FA and T10SL are 1.75, 1.79 and 1.89 respectively. The binder containing the slag additive (T10SL) has a greater impact on T^2, which is in concordance with results presented in the two previous sections. When results are sorted by mixing water type, the sulphate waters seem to generate a more tortuous pore structure; the average value T^2 is 1.72 for all

	W0-T10	W1-T10	W2-T10	W0-T10FA	W1-T10FA	W2-T10FA	W0-T10SL	W1-T10SL	W2-T10SL
■ 14 days	1.71	1.77	1.60	1.60	1.63	1.68	1.72	1.76	1.65
□ 92 days	1.74	1.92	1.77	1.80	1.97	2.05	1.76	2.34	2.14
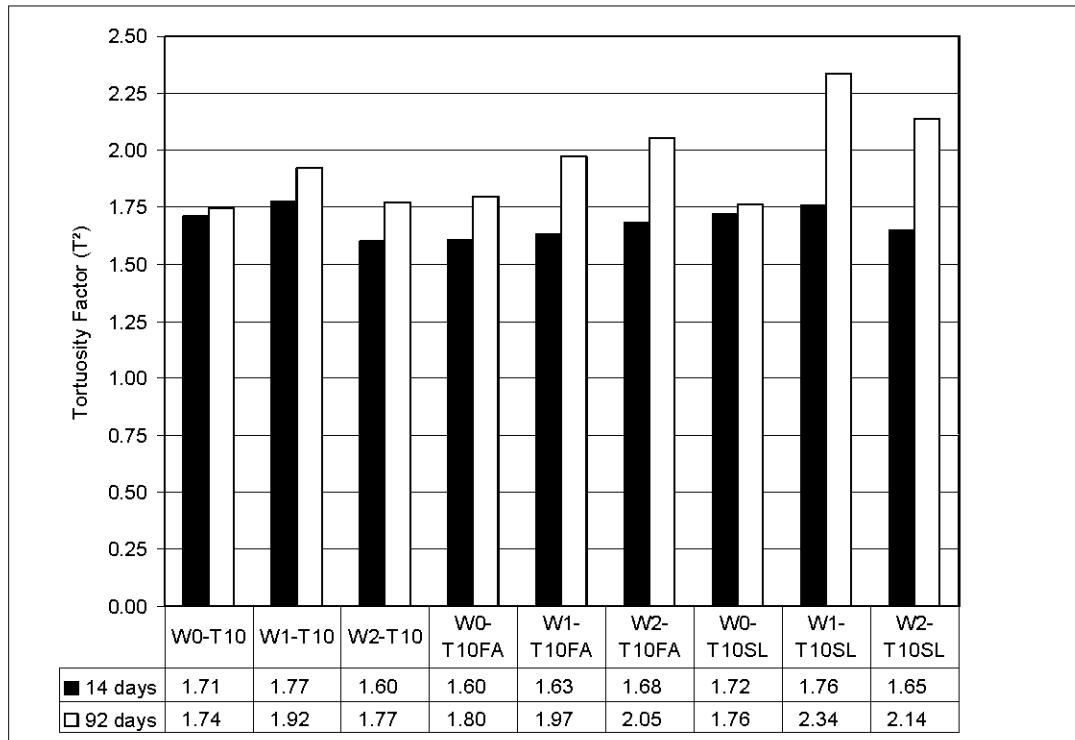
Figure 3.9, Tortuosity factors evaluated by SEM-IA.

samples mixed with pure water (W0), while it is 1.90 and 1.81 for W1 and W2 respectively.

3.4.4. Uniaxial compressive strength

Two cylindrical samples of each mixture were used to measure the uniaxial compressive strength (UCS, BNQ 2622-912) after 14, 43 and 92 curing days using a MTS 10/GL press with a normal loading capacity of 50 kN and a displacement rate of 0.001 mm/min. The UCS corresponds to the maximum peak stress value reached during the compression test. Since SEM observations were performed at 14 and 92 days, only the corresponding UCS values are presented in Figure 3.10 (see Chapter 2 for a more detailed description of the UCS results). The standard deviation on mean UCS results is between 10 kPa and 90 kPa for all samples. UCS results show

a similar behaviour for CPB prepared with the T10 and the T10FA binders. For these CPB samples, the UCS values range from 288 kPa at 14 days to 1004 kPa at 92 days for the three water types. The strength of samples made with T10SL binder is higher than that of the other samples with the two binders. The highest UCS value measured is 1822 kPa with the T10SL binder and the water W2 at 92 days, which is in concordance with pore structure results that showed a lower total porosity, a finer PSD, and a higher T^2 value for this CPB mixture.

	W0-T10	W1-T10	W2-T10	W0-T10FA	W1-T10FA	W2-T10FA	W0-T10SL	W1-T10SL	W2-T10SL
■ 14 days	456	551	510	288	445	436	920	1040	997
□ 92 days	810	1004	784	772	985	857	1468	1433	1822

Figure 3.10, UCS results measured at 14 and 92 days.

3.5. Discussion

In this section, CPB pore structure characterization results obtained by SEM-IA are compared with results from other direct or indirect approaches to validate the methods adopted here. First, total porosity values are assessed using a theoretical model that relates porosity and mechanical strength of geomaterials. Second, the
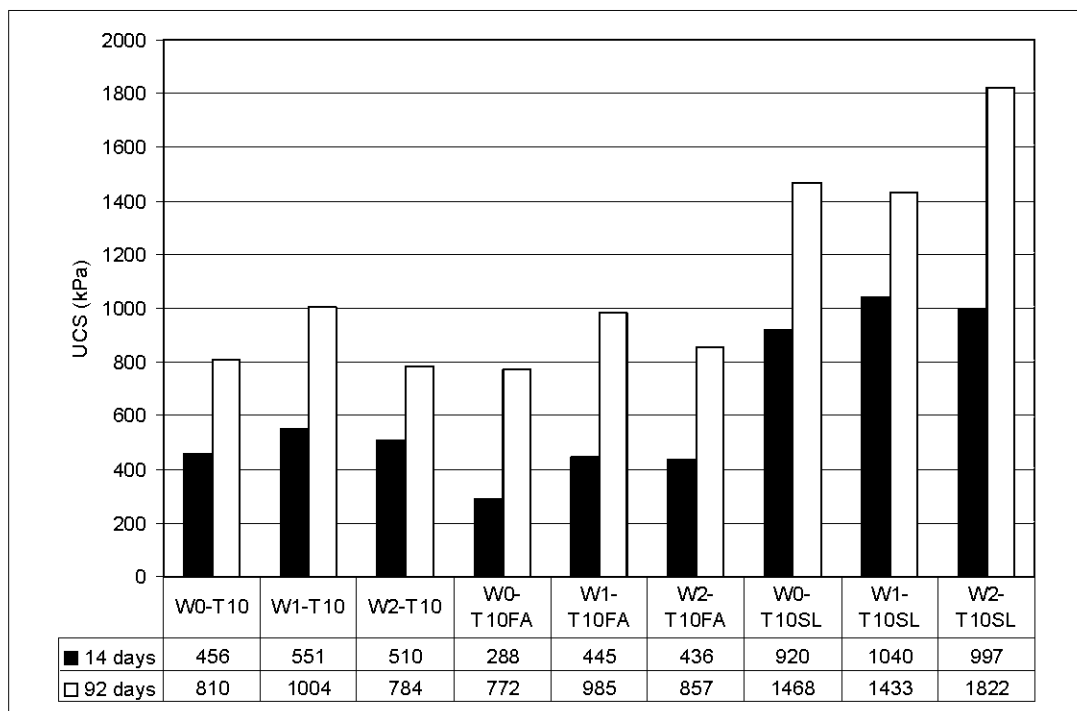
PSD obtained by SEM-IA are compared with those obtained by MIP on the same samples. Finally, the tortuosity factors estimated by the skeletonization technique are confronted with typical values found in the literature on different geomaterials.

3.5.1. Relationship between porosity and uniaxial compressive strength

In Chapter 2, the mean MIP total porosity n evaluated for the same samples as those tested at 14 days and 92 days of curing times was 44.7% and 44.6% respectively. Hence, there was no significant trend that would point towards a relationship between total porosity and UCS. However, as mentioned previously, this is not the case with the n values obtained with the SEM-IA approach that evolves with curing time. To evaluate the significance of porosity results measured with the IA technique, the n and UCS values were compared with strength versus porosity analysis performed using a modified version of the model of Li and Aubertin (2003) for geomaterials. The latter model is a unified equation that can be applied to uniaxial compressive strength and uniaxial tensile strength. The relationship was tested on a wide variety of materials (rocks, soils, metals, ceramics, and concrete) and for a large range of porosity values. For compressive strength, this model can be adapted in the following manner:

$$\frac{(C_0)_n}{(C_0)_{n\,min}} = 1 - \sin^{X_1}\left(\frac{\pi}{2}\frac{\langle n - n_{min}\rangle}{n_c - n_{min}}\right) \tag{6}$$

$(C_0)_n$ is the evaluated uniaxial strength for porosity n, n_c is the material critical porosity when the strength becomes almost nil, and $(C_0)_{nmin}$ corresponds to strength at the minimum porosity n_{min} that can be attained. The minimum porosity n_{min} is estimated at 0.25, based on various test results on similar materials taken from the literature (as reported by Bussière, 1993). For instance, in the case of tailings samples (without binder), Aubertin et al. (1996) reported a minimum porosity value of

approximately 0.32 at the optimum modified Proctor density, while Mabes et al. (1977) reported a value of 0.31 at the end of long term consolidation tests. A minimum porosity value of 0.25 is retained here, considering that an additional porosity reduction (of about 0.06 to 0.07) would appear due to the precipitation of cementitious phases in the CPB (e.g. Ouellet et al., 2006). The minimum n value is associated to the maximum strength, which is estimated to be $(C_0)_{nmin}$ = 4080 kPa, based on the available results on CPB. Exponent x_1 is fitting material parameter that controls the nonlinearity of the strength porosity relationship; and $\langle \rangle$ are MacCauley brackets ($\langle y \rangle$ = 0.5(y + |y|)). Figure 3.11 presents the comparison between the calculated and the measured values. The fitted parameters for this evaluation are x_1 = 0.72 and n_c = 58.5%. The correlation coefficient (R) between these two set of data is 0.71. These results indicate that the observed trend between the SEM-IA porosity and the UCS follows the one depicted by the Li and Aubertin (2003) model.
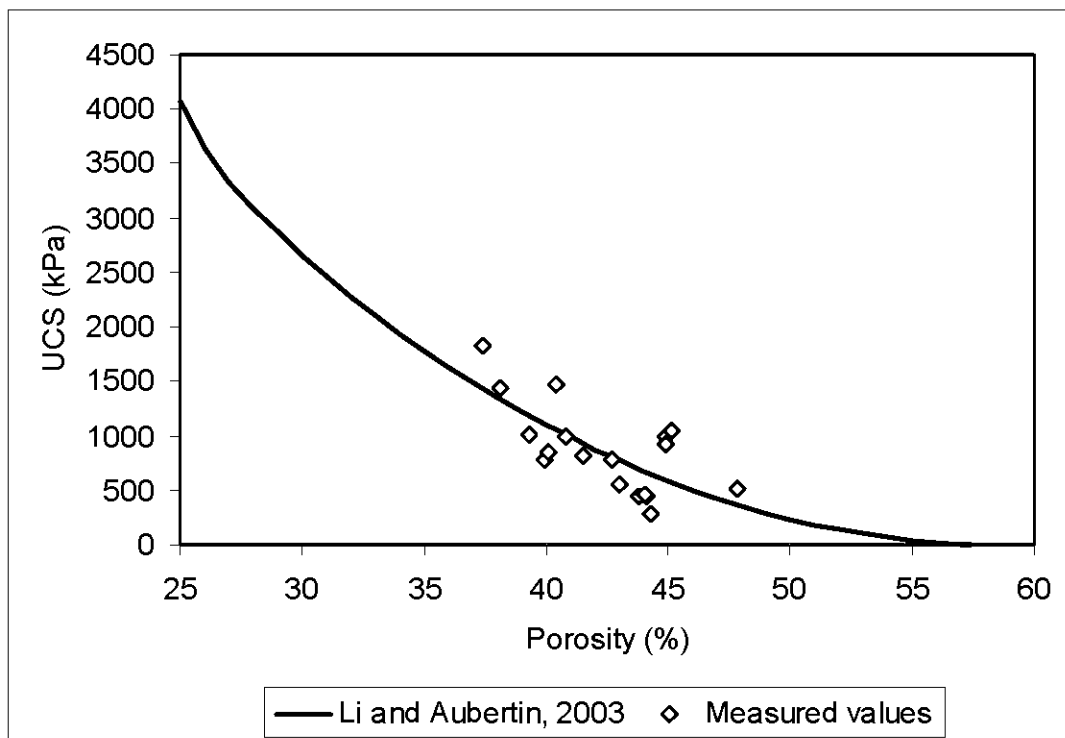

Figure 3.11, Conformity of SEM-IA porosity with Li and Aubertin (2003) model.

3.5.2. Relationship between IA and MIP

The mercury intrusion porosimetry (MIP) technique was also used to investigate the pore structure of the same CPB samples. Detailed analyses of these results are presented in Chapter 2. The samples used to perform MIP analysis came from the same CPB cylinders as those used to perform SEM observations, and were prepared with the same approach. By measuring the pressure applied by the MIP apparatus and the mercury volume intruded in a sample, it is possible to estimate the sample pore size distribution according to the Washburn (1921) equation. More details about the MIP technique can be found in Winslow and Diamond (1970) and Cook and Hover (1999).

As mentioned previously (see Figure 3.4), differences between MIP PSD and SEM-IA PSD can be important for cement paste. Pore sizes measured with MIP are typically almost 2 orders of magnitude lower than the ones evaluated by SEM-IA (Lange et al., 1994; Diamond and Leeman, 1995). Nonetheless, with natural geomaterials such as silty and clayey soils, PSD obtained by SEM-IA are relatively similar to those obtained by MIP (Simms, 2003). Hence, the nature of the material may be the source of significant differences between the two techniques.

Results on the studied CPB samples show that SEM-IA gives PSD with larger pore sizes than MIP (see Figure 3.7). However, the difference does not appear to be as significant as for cement paste. For instance, one can compare the pore size of the class intervals that show the maximum frequency of CPB in both PSD (i.e. a comparison between the MIP threshold diameter and the MRTS) at 14 days and 92 days. The mean results for all samples are respectively 1.43 µm and 1.17 µm for MIP tests and 6.7 µm and 5.3 µm for the SEM-IA method. A noticeable difference between PSD of cement paste and CPB using MIP and SEM-IA techniques is the total volume of pores monitored. For cement pastes, the IA method seems to identify approximately half of the porosity accessed by MIP (e.g. Diamond and Leeman, 1995). For CPB, the total porosity evaluated with both methods is approximately the

same (see values in the graph legends of Figure 3.7), but SEM-IA evaluation shows a slight decrease with the curing time, a phenomenon that is not observed by MIP. PSD evaluated by MIP and by IA are less different for CPB than for cement paste, mainly because the pores in CPB are larger than in cement paste and more accessible by the SEM-IA technique. The "ink-bottle" shape of voids is largely mentioned to explain the particular mercury intrusion behaviour in cement paste (Diamond, 2000). The mercury must access internal pores by narrow paths so a threshold pressure is needed to get a significant mercury volume intrusion at this size. The difference between the SEM-IA and the MIP for CPB can also be explained, at least in part, by this phenomenon.

Despite the recognized ink bottle effect problem for MIP tests, this technique can access fine pores that could not be measured by IA (for a given resolution). One can then argue that the lower porosity value observed at 92 days (for all samples) is the consequence of a lack of resolution of the IA method. To the authors' opinion, the lack of resolution is not the main factor for the porosity drop because: i) the IA total porosities are well correlated with the mechanical strength (see section 3.5.1) and ii) according to BSE images resolution used here (1 pixel = 0.32 µm), the minimum measured MRTS have a length of 15 pixels and the end of the curve shows no sign of missed pore families (% of IA porosity near zero at the lowest resolution). It is possible however that a portion of the porosity related to the grain porosity of hydrated and precipitated phases is missed by the IA approach.

Another difference between PSD of CPB evaluated by SEM-IA and MIP techniques is the pore size frequencies that are approximately one order of magnitude less for the SEM-IA approach. This difference could also be due to the "ink-bottle" effect that causes a significant mercury volume intrusion when the threshold pressure is reached. However, in light of the results obtained in this study, it appears that the PSD evaluation of CPB samples by MIP technique is less affected by the "ink-bottle" effect than for cement paste.

3.5.3. Comparison of SEM-IA tortuosity with values taken from the literature

Figure 3.12 shows tortuosity factor (T^2) values taken from the literature, all presented values were obtained by electrical or diffusive means. Some values were directly collected in papers, but most of them were calculated using the formula relating the formation resistivity factor (F), porosity (n) and T^2 (Berner, 1980; Ullman and Aller, 1982):

$$T^2 = F \cdot n \tag{6}$$

Others were obtained using the relation between the molecular diffusion coefficient in the absence of obstacle (D_0) and the molecular diffusion coefficient in the porous material (D_a) (Berner, 1980):

$$T^2 = D_0/D_a \tag{7}$$

Numerous relationships have been proposed to relate porosity to the tortuosity factor (see Boudreau, 1996; Aachib et al., 2004). Most of them are based on results obtained on natural fine soils and fail to fit adequately reported T^2 values for porosities below 0.3. Among these relationships, the general equation of Archie (1942) seems to give reliable results for a wide range of n. The equation is written as:

$$T^2 = n^{1-m} \tag{8}$$

where m is a best fit constant. For the data presented in Figure 3.12, Equation (8) gives a correlation coefficient (R) of 0.78 when m is equal to 2.3. When Equation 8 is specifically applied to T^2 values measured with the SEM-IA approach on the studied CPB (as shown in the upper box of the Figure 3.12 for the porosity range 0.25-0.6), the best fit constant m takes a value of 1.7 and R becomes 0.83. This m value is in

the range of literature values: Archie (1942) determined m between 1.3 and 2 for sands and sandstones; values of 1.90 and 1.81 were obtained by Iversen and Jorgensen (1993) and Maerki et al. (2004) respectively for clay-silt sediments. The meaning of m is reported to be the cementation factor or the void-distribution coefficient of a material (Jones and Buford, 1951). It is worth mentioning here that the value of m is not reported to be constant in the literature (see Jones and Buford, 1951; Salem and Chilingarian, 1999); it depends on different factors such as the range of porosity and the nature of the material studied. T^2 values calculated for CPB are in the mid-range of other reported values for uncemented materials, between those of sand samples studied by Jones and Buford (1951) and the silt and clay samples studied by Manheim and Waterman (1974) and by Sweerts et al. (1991). Hence, the solution proposed to evaluate the tortuosity (skeletonization of the captured images) can be considered effective for CPB.
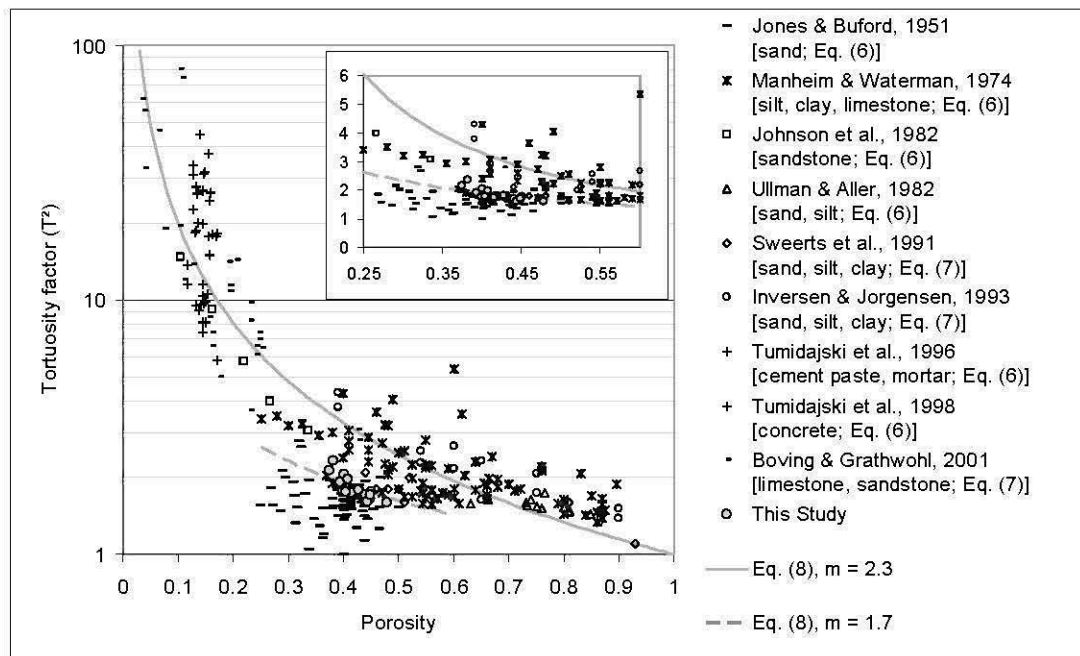

Figure 3.12, Graph of the relation between the tortuosity factor and the porosity. Values in the box are in the range of CPB porosities.

3.6. Conclusion

This paper addresses the evolution of pore structure parameters of CPB samples evaluated by SEM and IA. New approaches using SEM-IA were adapted and/or developed to estimate the total porosity (n), pore size distribution (PSD), and tortuosity (T). The CPB samples were made with three different binders: a type 10 Portland cement alone (T10), a mix 20:80 of type 10 Portland cement and blast furnace slag (T10SL), and a mix 70:30 of type 10 Portland cement and fly ash (T10FA). Three different types of water were used in the preparation of the mixtures: deionised water and two waters coming from two mine backfill plants.

The evaluation of n by SEM-IA is in the same range as MIP total porosity at short curing times. However, while the MIP technique does not detect any decrease of n over curing time, SEM-IA shows a slight reduction in n for the CPB samples studied (decrease of 4.6% in average). The SEM-IA measurements show a higher porosity decrease for the T10SL binder and for the mixing water containing sulphates. The SEM-IA porosity versus strength evaluation using a modified version of the Li and Aubertin's (2003) equation reveals that the evaluated porosities are in concordance with expected results.

SEM-IA PSD shows a slight curing effect that is mainly represented, in this study, by an evolution of the most represented throat size (MRTS) parameter. This parameter decreases with time and reaches a difference of between 4 and 5 μm with the MIP threshold diameter. This observation is interesting for future application of the MIP technique on CPB material; CPB seems less affected by the so-called inkbottle effect than other stronger cemented material containing more binder agent. Also, the PSD obtained by SEM-IA becomes less outspread with curing and more centered on the MRTS value.

The tortuosity factor T^2 values evaluated with the skeletonization approach are in the expected range for materials having such porosities. Moreover, T^2 presents a curing

effect with mean values of 1.68 and 1.94 at 14 and 92 days respectively. Higher tortuosity values were obtained with the T10SL binder and with mixing waters W1 and W2. These results are in concordance with n and PSD results; the lower n values and finer PSD correspond to the highest T^2 values.

The evaluation of the pore structure of CPB by the SEM-IA technique shows mainly that samples using T10SL binder present a more effective pore refinement over the curing time. Additionally, when sulphated waters were used in the mixtures, the CPB samples presented a higher decrease of the total porosity with the curing time, a more pronounced refinement of the pore size, and a higher tortuosity than the control samples mixed with pure water. The highest mechanical strength was observed on samples having the lower n, the finer PSD, and the higher tortuosity, confirming the impact of pore structure refinement on the mechanical behaviour of porous materials.

CPB is a cemented material widely used in the mining industry. Results shown here and in related studies indicate that CPB is structurally different from other cementitious materials. To the knowledge of the authors, no specific image analysis strategy was developed prior to this work to investigate the microstructure and pore distribution of CPB. More work is underway to use these pore structure parameters to predict hydro-geotechnical, mechanical, and environmental behaviours of CPB.

3.7. Acknowledgments

3.8. References

ACI. (1994). Controlled low-strength materials, SP-150, W.S. Adaska ed., 113 p.

Aachib, M., Mbonimpa, M., Aubertin, M. (2004). Measurement and prediction of the oxygen diffusion coefficient in unsaturated media, with applications to soil covers, Water, Air, and Soil Pollution, 156: 163–193.

Ammouche, A., Riss, J., Breysse, D., Marchand, J. (2001). Image analysis for the automated study of microcracks in concrete, Cement and Concrete Composites, 23, 267-278.

Archie, G.E. (1942). The electrical resistivity log as an aid in determining some reservoir characteristics, Petrol. Tech., 1, 55-62.

Aubertin, M., Bussière, B., Chapuis, R.P. (1996). Hydraulic conductivity of homogenized tailings from hard rock mines, Canadian Geotechnical Journal, 33, 3, 470-482.

Bal'shin, M.Y. (1949). Relation of mechanical properties of powder metals and their porosity and the ultimate properties of porous metal-ceramic materials. Doklady Akademii Nauk SSSR, 67, 5, 831–834.

Bartoli, F., Genevois-Gomendy, V., Royer, J.J., Niquet, S., Vivier, H., Grayson, R. (2005). A multiscale study of silty soil structure, European Journal of Soil Science, 56, 2, 207-223.

Bear, J. (1988). Dynamics of fluids in porous media, Dover Edition, 764 p.

Belem T., Bussière B., Benzaazoua M. (2001). The effect of microstructural evolution on the physical properties of paste backfill. Tailings and Mine Waste'01, January 16-19, Fort Collins, Colorado, Balkema : Rotterdam, 365-374.

Benzaazoua, M., (1996). Caractérisation physico-chimique et minéralogique de produits miniers sulfurés en vue de la réduction de leur toxicité et de leur valorisation. PH. D. Thesis, Institut National Polytechnique de Lorraine, Nancy, France, 267 p.

Benzaazoua, M., Ouellet, J., Servant, S., Newman, P., Verburg, R. (1999). Cementitious backfill with high sulfur content Physical, chemical, and mineralogical characterization, Cement and Concrete Research, 29, 5, 719-725.

Benzaazoua, M., Belem, T., Jolette, D. (2000). Investigation de la stabilité chimique et son impact sur la qualité des remblais miniers cimentés, IRSST Report R-260, ISBN 2-551-20431-3, 158 p. (in French).

Benzaazoua, M., Belem, T., Bussière, B. (2002). Chemical factors that influence the performance of mine sulphidic paste backfill, Cement and Concrete Research, 32, 7, 1133-1144.

Benzaazoua, M., Fall. M., Ouellet, S. (2003). Étude pluridisciplinaire visant à mettre au point un outil expert pour la prédiction du comportement des remblais en pâte. IRSST Research Project 099-085, Final Report, 187 p. (in French).

Berner, R.A. (1980). Early Diagenesis: A Theoretical Approach, Princeton University Press, 241 p.

Boudreau, B.P. (1996). The diffusive tortuosity of fine-grained unlithified sediments, Geochimica et Cosmochimica Acta, 60, 16, 3139-3142.

Boving, T.B., Grathwohl, P. (2001). Tracer diffusion coefficients in sedimentary rocks: correlation to porosity and hydraulic conductivity, Journal of Contaminant Hydrology, 53, 1-2, 85-100.

Bussière, B. (1993). Évaluation des propriétés hydrogéologiques des résidus miniers utilisés comme barrières de recouvrement, M. Sc. A. Thesis, École Polytechnique de Montréal, Montréal, Canada.

Carman, P.C. (1937). Fluid flow through a granular bed, Trans. Inst. Chem. Eng., 15, 150-156.

Collin, M., Rasmuson, A. (1988). A comparison of gas diffusivity models for unsaturated porous media, Soil Science Society of America Journal, 52, 1559–1565.

Cook, R.A., Hover, K.C. (1999). Mercury porosimetry of hardened cement pastes, Cement and Concrete Research, 29, 6, 933-943.

Coster, M., Chermant, J.-L. (2001). Image analysis and mathematical morphology for civil engineering materials, Cement and Concrete Composites, 23, 2-3, 133-151.

Cousin, I., Porion, P., Renault, P., Levitz, P. (1999). Gas diffusion in silty-clay soil: experimental study on an unsaturated soil core and simulation in its three dimensional reconstruction, European Journal of Soil Science, 50, 249-259.

Darwin, D. (2001). Image Analysis, Chapter 19 in Handbook of Analytical Techniques in Concrete Science And Technology, Ramachandran, V.S. and Beaudoin, J.J. Eds. National Research Council of Canada, Noyes Publications, 985 p.

Delerue, J.-F., Perrier, E., Yu, Z.Y., Velde, B. (1999). New algorithms in 3D image analysis and their application to the measurement of a spatialized pore size distribution in soils. Journal of Physics and Chemistry of the Earth, 24, 7, 639-644.

Diamond, S., Leeman, M.E. (1995). Pore size distributions in hardened cement paste by SEM image analysis, Materials Research Society Symposium Proceedings, 370, 217-226.

Diamond, S. (2000). Mercury porosimetry: An inappropriate method for the measurement of pore size distributions in cement-based materials, Cement and Concrete Research, 30, 10, 1517-1525.

Dullien, F.A.L. (1992). Porous media: Fluid transport and pore structure, 2nd ed., Academic Press, 574 p.

Epstein, N. (1989). On tortuosity and the tortuosity factor in flow and diffusion through porous media, Chemical Engineering Science, 44, 3, 777-779.

Fall, M., Benzaazoua, M., Ouellet., S. (2005). Experimental characterization of the influence of tailings fineness and density on the quality of cemented paste backfill, Minerals Engineering, 18, 1, 41-44.

Godbout, J. (2005). Évolution des propriétés hydriques des remblais miniers cimentés en pâte durant le curage, M. Sc. A. Thesis, École Polytchnique de Montréal, 190 p.

Goldstein, J.I., Romig, A.D., Newbury, D.E., Lyman, C.E., Echlin, P., Fiori, C., Joy, D.C., Lifshin, E. (1992). Scanning Electron Microscopy and X-Ray Microanalysis, 2nd ed., Plenum, New York, 820 p.

Gregg, S.J., Sing, K.S.W. (1982). Adsorption, Surface Area and Porosity, Academic Press, 303 p.

Hassani, F., Archibald, J. (1998). Mine Backfill, CD-ROM, Canadian Institute of Mining, 263p.

Iversen N., Jorgensen B. B. (1993). Diffusion coefficients of sulfate and methane in marine sediments: Influence of porosity, Geochimica Cosmochimica Acta, 57, 571-578.

Johnson, D.L., Plona, T.J., Scala, C., Pasierb, F., Kojima, H. (1982). Tortuosity and acoustic slow waves, Physical Review Letters, 49, 25, 1840-1844.

Jones, P.H., Buford, T.B. (1951). Electric logging applied to ground-water exploration, Geophysics, 16, 1, 115-139.

Jiang, L. and Guan, Y. (1999). Pore structure and its effect on strength of high-volume fly ash paste, Cement and Concrete Research, 29, 631-633.

Kosugi, K. (1999). General model for unsaturated hydraulic conductivity for soils with lognormal pore-size distribution, Soil Science Society of America Journal, 63, 270-277.

Lamos, A.W., Clark, I.H. (1989). The influence of material composition and sample geometry on the strength, Innovation in Mining backfill technology, Hassani et al. eds., Rotterdam, ISBN 9061919851, 89-94.

Lange, D.A., Jennings, H.M., Shah, S.P. (1994). Image analysis techniques for characterization of pore structure of cement-based materials, Cement and Concrete Research, 24, 5, 841-853.

Launeau, P., Robin, P.-Y.F. (1996). Fabric analysis using the intercept method, Tectonophysics, 267, 1-4, 91-119.

le Roux, K-A (2004). In situ properties and liquefaction potential of cemented paste backfill, Ph. D. Thesis, University of Toronto, 271 p.

Li, L. and Aubertin , M. (2003). A general relationship between porosity and uniaxial strength of engineering materials, Canadian Journal of Civil Engineering, 30, 4, 644-658.

Luo, R., Cai, Y., Wang, C., Huang, X. (2003). Study of chloride binding and diffusion in GGBS concrete, Cement and concrete research, 33, 1-7.

Mabes, D.L., James, H.H., Williams, R.E. (1977). Physical properties of Pb-Zn mine-process wastes, Proceedings of Conference on Geotechnical Practice for Disposal of Solid Waste Materials, American Society of Civil Engineers, p. 103-117.

Maerki, M., Wehrli, B., Dinkel, C., Müller, B. (2004). The influence of tortuosity on molecular diffusion in freshwater sediments of high porosity, Geochimica et Cosmochimica Acta, 68, 7, 1519–1528.

Manheim F. T., Waterman L. S. (1974). Diffusimetry (diffusion constant estimation) on sediment cores by resistivity probe. In Initial Reports of the Deep Sea Drilling Project (ed. C. C. von der Borch and G. C. Sclater), 22, 663-670.

Millington, R.J., Shearer, R.C. (1971). Diffusion in aggregated porous media, Soil Science, 111, 372–378.

Mitchell, J.K. (1993). Fundamentals of Soil Behaviour, 2nd Edition, 437 p.

Moldrup, P., Olesen, T., Komatsu, T., Schjønning, P., Rolston, D. E. (2001). Tortuosity, Diffusivity, and Permeability in the Soil Liquid and Gaseous Phases, Soil Science Society of America Journal, 65, 613–623.

Mota, M., Teixeira, J.A., Yelshin, A. (1999). Image analysis of packed beds of spherical particles of different sizes, Separation and Purification Technology, 15, 59-68.

Niu, Q., Feng, N., Yang, J., Zheng, X. (2002). Effect of superfine slag powder on cement properties, Cement and Concrete Research, 32, 615-621.

Odler, I., Röbler, M. (1985). Investigations on the relationship between porosity, structure and strength of hydrated Portland cement pastes. II. Effect of pore structure and of degree of hydration, Cement and Concrete Research, 15, 3, 401-410.

Ouellet, S., Bussière, B., Benzaazoua, M., Aubertin, M., Belem, T. (2004) Effect of binder type and mixing water chemistry on microstructural evolution of cemented paste backfill, Proceedings of the 57th Annual Canadian Geotechnical Conference and 5th joint IAH-CNC/CGS Conference, Quebec, Quebec, Canada, October 23rd to 27th, 8 p.

Ouellet, S., Bussière, B., Mbonimpa, M., Benzaazoua, M., Aubertin, M. (2006). Reactivity of an underground mine sulphidic cemented paste backfill, Minerals Engineering, 19, 5, 407-419.

Poon, C.S., Wong, Y.L., Lam, L. (1997). The influence of different curing conditions on the pore structure and related properties of fly-ash cement pastes and mortars, Construction and Building Materials, 11, 7-8, 383-393.

Potvin, Y., Fourie, A. (2005). Paste fill in Australia, Symposium 2005 Mines and the Environment, Rouyn-Noranda, Canada, May 15-18, 16 p.

Ramachandran, V.S., Beaudoin, J.J. (2001). Handbook of Analytical Techniques in Concrete Science And Technology, National Research Council of Canada, Noyes Publications, 985 p.

Ramlochan, T., Grabinsky, M.W., Hooton, R.D. (2004). Microstructural and chemical investigations of cemented paste backfills, Tailings and Mine Waste '04, October 10-13, 2004, Vail, Colorado, 293-304.

Ringot, E., Bascoul, A. (2001). About the analysis of microcracking in concrete, Cement and Concrete Composites, 23, 261-266.

Russ, J.C. (1990). Computer-Assisted Microscopy: The Measurement and Analysis of Images, Plenum Press, 453 p.

Ruzyla, K. (1986). Characterization of pore space by quantitative image analysis, SPE Formation Evaluation, August, p.389-398.

Rzhevsky, V., Novik, G. (1971). The physics of rocks. MIR Publisher, Moscow.

Salem, H.S., Chilingarian, G.V. (1999). The cementation factor of Archie's equation for shaly sandstone reservoirs, Journal of Petroleum Science and Engineering, 23, 2, 83-93.

Sammartino, S., Partier, P., Sardini, P., Meunier, A., Tevissen, E. (1999). Evolution of fluid pathways of Charroux-Civary tonalite (part I): Alteration effects – an analytical approach, Physics and Chemistry of the Earth, Part A: Solid Earth and Geodesy, 24, 7, 601-606.

Sardini, P., Sammartino, S., Meunier, A., Tevissen, E. (1999). Evolution of fluid pathways of Charroux-Civray tonalite (part II): Numerical study of microcracks networks, Physics and Chemistry of the Earth, Part A: Solid Earth and Geodesy, 24, 7, 621-625.

Schaap, M.G., Lebron, I. (2001). Using microscope observations of thin sections to estimate soil permeability with the Kozeny-Carman equation, Journal of Hydrology, 251, 186-201.

Scheidegger, A.E. (1974). The physics of flow through porous media, 3rd ed., University of Toronto Press, 353 p.

Scrivener, K.L. (2004). Backscattered electron imaging of cementitious microstructures: Understanding and quantification, Cement and Concrete Composites, 26, 935-945.

Scrivener, K.L., Patel, H.H., Pratt, P.L., Parrott, L.J. (1987). Analysis of phases in cement paste using backscattered electron images, methanol adsorption and thermogravimetric analysis, Mat. Res. Soc. Symp. Proceedings, 85, 67-76.

Simms, P.H. (2003). A fundamental study of unsaturated flow in compacted clayey soil, Ph. D. Thesis, University of Western Ontario, 336 p.

Sobek, A.A., Schuller, W.A. Freeman, J.R., Smith, R.M. (1978), Field and laboratory methods applicable to overburden and minesoils, EPA 600/2-78-054, 203 p.

Solymar, M., Fabricius, I.L. (1999). Image analysis and estimation of porosity and permeability of Arnager greensand, Upper Cretaceous, Denmark, Physics and Chemistry of the Earth, Part A: Solid Earth and Geodesy, 24, 7, 587-591.

Spangenberg, E., Spangenberg, U., Heindorf, C. (1998). An experimental study of transport properties of porous rock salt, Physics and Chemistry of the Earth, 23, 3, 367-371.

Sweerts, J.-P. R.A., Kelly, C.A., Rudd, J.W.M., Hesslein, R., Cappenberg, T.E. (1991). Similarity of whole-sediment molecular diffusion coefficients in freshwater sediments of low and high porosity, Limnology and Oceanography, 36, 2, 335-342.

Tumidajski, P.J., Schumaker, A.S., Perron, S., Gu, P., Beaudoin, J.J. (1996). On the relationship between porosity and electrical resistivity in cementitious systems, Cement and Concrete Research, 26, 4, 539-544.

Tumidajski, P.J., Lin, B. (1998). On the validity of the Katz-Thompson equation for permeabilities in concrete, Cement and Concrete Research, 28, 5, 643-647.

Ullman, W.J., Aller, R.C. (1982). Diffusion coefficients in near shore marine sediments, Limnology and Oceanography, 27, 552-556.

Vervoort, R.W., Cattle, S.R. (2003). Linking hydraulic conductivity and tortuosity parameters to pore space geometry and pore-size distribution, Journal of Hydrology, 272, 1-4, 36-49.

Washburn, E.W. (1921). Note on a method of determining the distribution of pore sizes in a porous material, Proceedings, National Academy of Sciences, 7, 115-116.

Winslow, D.N., Diamond, S. (1970). A mercury porosimetry study of the evolution of porosity in Portland cement. Journal of Materials, 5, 3, 564-585.

CHAPITRE IV

MINERALOGICAL CHARACTERIZATION OF CEMENTED PASTE BACKFILL: EFFECT OF WATER CHEMISTRY, BINDER TYPE, AND CURING TIME[6]

4. Résumé/Abstract

Cet article présente l'étude des phases cimentaires d'échantillons de remblai cimenté en pâte (RCP) fabriqués à partir d'une poudre de silice, de trois liants (Ciment Portland de type 10 (T10), T10 et cendre volante et T10 et laitier de haut-fourneau) et de deux types d'eau (une pure « W0 » et une contenant environ 22000 ppm SO_4^{2-} « W1 »). Les méthodes de caractérisation utilisées sont la microscopie électronique à balayage (MEB) et la thermogravimétrie/mesure des flux de chaleur. Un programme qui combine des routines d'analyse d'image, des images en rayon X en mode point et les analyses spectrométriques du MEB a été créé pour générer des images minéralogiques (SEM-XMAP). L'utilisation de ces techniques de caractérisation a permis l'identification des phases cimentaires principales des RCP étudiés et de visualiser l'organisation de ces phases dans la matrice de cimentation. Les résultats montrent aussi l'influence de la qualité de l'eau, la proportion de sulfates mesurée étant plus importante dans les échantillons mélangés avec l'eau W1. D'autre part, la quantité d'ajout minéral non hydraté est supérieure dans les échantillons mélangés avec l'eau W0. La nature acide de l'eau W1 semble avoir favorisé la dissolution des liants, ce qui a occasionné une augmentation de la résistance en compression pour les échantillons à base de laitier. L'étude a aussi montré par thermogravimétrie que la perte de masse associée aux C-S-H et aux sulfates peut être corrélée avec la résistance en compression.

Mots clés : Remblai cimenté en pâte, Microscopie électronique, Image rayon X en mode point, Analyse d'image, Analyse thermique.

---

[6] Ouellet, S., Benzaazouaa, M., Bussière, B., Aubertin, M. (2006). Mineralogical characterization of cemented paste backfill: effect of water chemistry, binder type, and curing time, à soumettre.

The cementitious phases within cemented paste backfill (CPB) samples made with three binders (ordinary Portland cement, fly ash (FA) and blast furnace slag (BFS)) and two types of mixing water (deionised water W0 and water W1 containing about 22000 ppm SO_4^{2-}) are characterized using scanning electron microscopy (SEM) equipped with an energy dispersive spectrometry (EDS) detector and thermogravimetry/differential scanning calorimetry (TG/DSC). A program that combines image analysis routines, X-ray dot mapping images, and EDS analysis was developed to create mineralogical images (SEM-XMAP). The combination of these three techniques (SEM-EDS, SEM-XMAP, and TG/DSC) allows an identification of the main minerals associated to the cementitious phases in CPB (mainly C-S-H, sulphated minerals, portlandite, carbonates). The organisation of these phases in the matrix can also be visualized. The mineralogical characterization highlights the influence of mixing water quality and of binder type. The proportion of sulphated minerals is more important in samples mixed with water W1. Similarly, the amount of unhydrated FA and BFS particles is found to be higher in samples made with W0 than in mixtures made with W1 water. The lower pH of W1 seems to favour the dissolution of binders which, in the case of BFS samples, appears to be beneficial for mechanical strength development. Finally, the study showed that for a given CPB recipe, UCS results can be correlated to the weight loss in the temperature zone of C-S-H and sulphated minerals (100-250°C), evaluated by TG/DSC.

Keywords: Cemented paste backfill; Scanning electron microscope; X-ray dot mapping; Image Analysis; Thermal analysis

4.1. Introduction

Cemented paste backfill (CPB) has gained increasing popularity as a mine backfilling method. CPB offers practical, mechanical and environmental advantages compared to other backfilling techniques that use hydraulic and cemented rock fill, CPB is usually made with the whole tailings (including the fine particles), and no excess water is used in the preparation. The final product has a relatively viscous consistency, but is still transportable by gravity and/or by positive displacement pumps. Furthermore, the fine-grained tailings combined with a small percentage of binders (typically between 3 to 7 %) eliminate the need for the construction of complex barricades. The lower water to cement (w/c) ratio of CPB (compared to

hydraulic fill) also leads to a higher mechanical strength for a similar percentage of binder. On an operational side, CPB can be placed more rapidly in stopes and it requires less underground preparation than the other types of backfill (Hassani and Archibald, 1998). To evaluate the optimal CPB recipe for a given mine, the general practice consists of determining the strength properties (usually, Uniaxial Compressive Strength test results are used for that purpose) with different mixtures made of different binder types and percentages, prepared in a controlled laboratory environment. The goal is then to find the recipe that gives the desired strength for the lower cost.

Such phenomenological approach has been used by researchers to evaluate the impact of the different CPB components on mechanical strength (e.g. Benzaazoua et al., 2003; Cayouette, 2003; Fall and Benzaazoua, 2003; Kesimal et al., 2003; Fall et al., 2005a). Other studies have shown that the type and amount of sulphide in the tailings have an impact on the strength of CPB since some binders seem to be influenced by these minerals (e.g. Benzaazoua et al., 2002). Another significant advantage of CPB, from an environemental point of view, is its ability to maintain a high degree of saturation. This high degree of saturation (S_r usually greater than 90 %; Benzaazoua et al., 2000, 2002, 2004; Belem et al., 2002; Ouellet et al., 2003) limits the interaction between sulphide minerals contained in the tailings and the oxygen, which may reduce sulphide oxidation (e.g. Ouellet et al. 2006), acid generation (Levens and Boldt, 1994; Levens et al., 1996) and the possibility of spontaneous combustion inside stopes (Bernier and Li, 2003; Wu and Li, 2005).

Despite of these advantages and its relatively wide application, many aspects related to the behaviour of CPB are still not well understood. One of them is the impact of water quality on strength development in CPB. Indeed, even when there is a low acid generation rate in CPB, high concentration of sulphates and other ions can be found in the interstitial water. Values as high as 207000 ppm SO_4^{2-} (stoichiometric conversion assuming all S in its SO_4^{2-} form) have been measured in pore water of sulphidic CPB (Ouellet et al., 2006). Such high concentration of sulphates can come

from the previous oxidation of sulphide minerals during ore treatment and/or from a cyanide destruction process that uses SO_2 as reagent. Under these conditions, sulphate attack problems could appear and the long term stability of the CPB might be affected (Benzaazoua et al., 1999; 2002; 2004; Bernier et al., 1999; Hassani et al., 2001; Fall and Benzaazoua, 2005; Kesimal et al., 2005).

Most studies performed on the influence of water quality on CPB were conducted to assess the impact on UCS strength. These phenomenological studies were useful to identify key influence factors, but did not lead to a clear understanding of the main mechanisms behind the observed behaviour. Hence, additional studies have been recently performed to better understand the internal structure evolution of different CPB mixtures made with different mixing water. This aspect is important for both mechanical and environmental behaviour of CPB. The focus of these more fundamental studies was mainly on the pore size evolution during curing using different approaches such as the mercury intrusion porosimetry and SEM image analysis (e.g. Belem et al., 2001; Benzaazoua et al., 2003; Ouellet et al., 2004; 2006; Ramlochan et al., 2004; Fall et al., 2005a; 2005b). More details on these investigations can be found in Chapters 2 and 3. Another important basic aspect recently studied is the mineralogy of CPB and its evolution during curing. The mineralogy of common cemented materials such as paste cement and mortar is relatively well known, but because of the differences between these materials and CPB (in terms of % binder, w/c ratio, aggregate mineralogy and grain size distribution), the knowledge cannot be applied directly to the latter. Therefore, complementary studies have been undertaken to characterize CPB mineralogy (Smart et al., 1993; Benzaazoua et al., 1996; 2002; 2004; 2006; Hassani et al., 2001; Ramlochan et al., 2004; Ouellet et al., 2006). Most of these studies were mainly qualitative, focussing on the presence and on the nature of the cemented phases observed in CPB.

The main objective of this paper is to characterize more extensively the cementitious phases of CPB. Mixtures made with a silica powder, three types of binder (ordinary

Portland cement (OPC), OPC mixed with a type C fly ash (FA) and OPC mixed with a blast furnace slag (BFS)) and two types of water (deionised and sulphated) are studied at w/c = 7 (a typical ratio for CPB). The effects of water quality and binder type on CPB mineralogy and strength are investigated over 180 days of curing time by thermogravimetry/differential scanning calorimetry (TG/DSC), and by scanning electron microscopy (SEM). A mono-mineral aggregate (silica powder) was used to facilitate the identification of the cementitious phases appearing in the CPB mixtures. The interference of actual tailings mineralogy on characterization results is then significantly minimized. A computer software and image analysis routines were developed to construct images of the CPB cemented matrix from SEM X-ray dot mapping. The resulting colour images allow visualizing the microstructure of the different CPB samples and also give a qualitative representation of the CPB mineralogy. It is worth mentioning that other techniques such as X-ray diffraction (XRD) and Fourier transform infrared (FTIR) spectroscopy have been tested to characterize the mineralogy of the CPB samples. Because the ensuing results do not bring additional information, they are not presented here.

4.2. Related research

To the authors knowledge, the hydration of binders and the characterization of precipitated cementitious phases in CPB are issues that have not been specifically addressed in the literature. Most papers found on this subject focussed on the identification of cementitious phases in a given CPB and on the link with the observed mechanical behaviour. In the following, a brief summary of the main studies that provide mineralogical observations on CPB samples is presented.

A pionneering paper dealing with observations of cement hydration products in CPB was published by Smart et al. (1993). These authors noticed that X-Ray diffraction (XRD) was ineffective to identify cementitious phases in CPB due to the low binder content and the overlapping of cementitious phases XRD peaks with those of tailings

minerals. They also performed SEM observations and energy dispersive X-ray spectrometry (EDS) on fractured surfaces. They observed that tailings particles acted as nucleation sites for cementitious phases, and mentioned the potential presence of calcium-silicate-hydrate (C-S-H), gehlenite ($Ca_2Al_2SiO_7$), and ettringite ($Ca_6Al_2(SO_4)3(OH)_{12} \cdot 26H_2O$) in a CPB containing BFS as binder. Smart et al. (1993) also mentioned that these phases increase solid contacts between tailings particles which increase the CPB strength.

Ouellet et al. (1998) and Benzaazoua et al. (1999) investigated a sulphidic CPB field sample (17%wt. sulphur) containing 4.5%wt. of a 60:40 mix of OPC and FA. This CPB showed durability problems (presence of cracks and strength decrease) due to sulphide oxidation (and decrease of the pore solution pH) and precipitation of expansive sulphate. SEM-EDS analysis revealed an important decalcification of primary hydrated phases and the presence of gypsum ($Ca(SO_4) \cdot 2(H_2O)$) as well as ferrous, silicon and aluminium hydroxides in cracks.

The same research team observed secondary gypsum in bubbles and in intergranular voids by SEM in sulphidic CPB (in two mixtures having approximately 30%wt. and 10%wt. of pyrite (FeS_2)) mixed with OPC and FA, or with OPC and BFS (Benzaazoua et al., 2002). Observations on a fractured surface showed C-S-H gels, but portlandite ($Ca(OH)_2$) was not identified. The results indicated that the sulphate content in the pore water had a great impact on the hydration of cement (by slowing the process). Nevertheless, under certain circumstances, the precipitation of secondary sulphated minerals increased the cohesion and the strength of the CPB (see also Benzaazoua et al., 2003b; 2004; Belem et al., 2000; 2001; Ouellet et al., 2002; Ouellet et al., 2006).

Benzaazoua and collaborators also investigated the mineralogy of CPB made from sulphidic tailings (40%wt. pyrite), 7%wt. of binder (OPC:sulphate resisting PC at 50:50, OPC:BFS at 20:80), and 0.15%wt. to 0.3%wt. of sludge or red mud coming respectively from high density sludge lime treatment and aluminium processing

(Benzaazoua et al. 2006). Contrary to other studies, the XRD results (using the Rietveld method) presented in their paper showed significant amount of phases such as calcite ($CaCO_3$), ettringite, gypsum, and portlandite. However, the EDS characterization performed on an unpolished CPB surface was not successful in identifying mineralogical and microstructural differences between samples. The interference of tailings grains and the drying of samples were the reasons mentioned by the authors to explain these difficulties.

Bernier et al. (1999) tried to identify secondary minerals in CPB made with highly sulphidic tailings (over 50% wt. of sulphides) and various binders (OPC, sulphate resisting PC, OPC and BFS, OPC and FA) at 5%wt. XRD and thermogravimetry methods were ineffective for a material containing such a low proportion of binder. A strength lost associated with an internal sulphate attack was observed after 180 days, but no ettringite was directly observed by SEM.

Bertrand et al. (2000) were able to identify, using SEM, cementitious phases in CPB made with sulphidic tailings (> 35%wt. of pyrite) and two different binders (6.2%wt. OPC and 4.5%wt. OPC:BFS at 20:80). Portlandite, C-S-H, and ettringite, as well as secondary sulphates (ettringite, gypsum) were identified in the CPB containing OPC, but these latter minerals were not observed in the mixture made with the OPC:BFS binder.

Ramlochan et al. (2004) performed different tests on CPB made of tailings having a low sulphide content and various amounts of binder (3.2% to 15%wt. of OPC:FA at 50:50 and OPC:BFS at 10:90). XRD was not successful in identifying cementitious phases (portlandite, ettringite or C-S-H) in CPB. Better results were obtained by SEM on epoxy impregnated and polished samples where small amounts of C-S-H (having a fibrillar morphology) were observed, appearing probably as an artefact of drying. EDS analysis on the sample containing 15%wt. of OPC:FA revealed a Ca/Si ratio in C-S-H of approximately 1 and the spectra contained significant amount of Mg and Na. Ettringite was also identified, but observations did not distinguish portlandite

crystals. The authors mentioned that the presence of C-S-H in the sample containing only 5%wt of OPC:FA was difficult to confirm. However ettringite crystals were seen sparsely throughout the void space. The CPB made with the OPC:BFS binder showed C-S-H in the void space and at the surface of the tailings and BFS particles.

In summary, informations gathered from the literature indicate that only few studies were performed on the mineralogy of CPB. Most papers pointed to some difficulties on identifying with confidence the main minerals that create the CPB cohesion. The low binder content combined with the high water to cement ratio create a relatively loose material where cementitious phases are sparsely precipitated. SEM combined with EDS is the main tool used to investigate the mineralogy of CPB. XRD and thermogravimetry techniques have been used with limited success, mainly because of the interference of the tailings grains.

4.3. Materials and methods

4.3.1. CPB components and sample preparation

The three binders used in this investigation are: a 100% type 10 (CAN/CSA-A5-98) ordinary Portland cement (T10); a mix of 20% T10 and 80% blast furnace slag (T10SL); and a mix of 70% T10 and 30% class C fly ash (T10FA). Table 4.1 shows ICP-AES analysis results for the three binders that were provided by Lafarge Company. Ground silica was used for all mixtures as aggregate instead of mine tailings. The ground silica contains 99.68% SiO_2; this value was determined by difference with other oxides since the silicon proportion was too high to be chemically measured accurately. The grain size distribution of the ground silica is similar to typical hard rock mine tailings (see details in Ouellet et al. 2003) and can be classified as non plastic silt (ML) according to the USCS classification (e.g. McCarthy, 2002).

CPB samples were prepared by mixing the binders and the dry silica with two types of water. The first mixing water was pure (deionised by filtration and named hereinafter W0) and had a near neutral pH of 6.09. The second mixing water (named W1), which was in contact with highly sulphidic mine tailings (containing pyrite and pyrrhotite), was sampled directly at the dewatering system of a mine backfill plant; the pH of this water was 3.32. Assuming all sulphur in W1 water in the SO_4^{2-} form, the concentration of sulphate was 21690 ppm. The calcium content of the mine water was relatively high at 1760 ppm (lime was added during flotation and dewatering processes). Before analysis and mixing, W1 was filtered to remove solids in suspension. 48 cylinders (10 cm long and 5 cm in diameter) coming from six batches of CPB were prepared, capped and poured at room temperature and at a relative humidity greater than 90%. The binder proportion for all CPB mixtures was 5% by weight of dry silica and the water to cement ratio (w/c) was 7; this high w/c is representative of values observed in the Canadian mining industry (Benzazoua et al., 2002; 2003b).

Table 4.1, Analysis results for binders, silica and mine water

(%wt.)	T10	FA	BFS	Silica	(ppm)	W1 water
Al_2O_3	4.82	17.67	10.28	0.11	Al	0.12
B_2O_3	0.02	0.57	0.42	0.00	Ba	0.04
BaO	0.01	0.95	0.09	0.00	Ca	1760
CaO	60.59	15.39	31.34	0.02	Cu	0.43
CuO	0.01	0.01	0.00	0.00	Fe	0.08
Fe_2O_3	2.42	6.09	0.51	0.05	K	53
K_2O	0.81	0.65	0.48	0.00	Mg	1.38
MgO	2.19	2.95	11.18	0.01	Mn	0.01
MnO	0.05	0.04	0.91	0.00	Mo	0.03
Na_2O	2.10	7.41	2.01	0.03	Na	108
SO_3	3.92	1.90	3.20	0.05	Ni	0.01
ZnO	0.04	0.00	0.00	0.04	S	7240
SiO_2	19.25	44.93	36.37	99.68	Si	0.30
Total	96.22	98.55	96.79	100.00	Zn	0.09
BET (m²/g)	1.28	0.87	2.14	0.74		-

After UCS testing (BNQ 2622-912), many pieces (approximately two cm³ of CPB) were dried in a vacuum oven for 24 hours at 35°C and approximately 3 kPa. CPB samples were then maintained in a desiccator to avoid rehydration and/or carbonation prior to the different investigations performed to identify the main cementitious phases in the CPB. For SEM analyses, after the drying step, samples were vacuum impregnated with low viscosity epoxy, polished (final polish with a 0.25 µm diamond compound), and carbon coated.

4.3.2. Compressive strength evaluation

Two cylinders of each mixture were tested to evaluate the uniaxial compressive strength (UCS) after 14, 28, 90, and 180 curing days using a MTS 10/GL press with a normal loading capacity of 50 kN and a displacement rate of 0.001 mm/min. The UCS corresponds to the maximum stress value (failure peak) reached during the compression test.

4.3.3. Thermogravimetry and differential scanning calorimetry

TG and DSC were performed on dried samples using a SDT Q600 apparatus from TA Instruments. This equipment allows simultaneous registry of weight loss and heat flow along thermal treatment of an unsealed sample. Thermal behaviours were registered in an inert nitrogen atmosphere at a rate of 10°C/min from ambient temperature up to 1000°C. Tests were performed with approximately 35 mg of material placed in a 90 µl alumina cup and covered by an alumina lid. Temperature calibrations of the apparatus following the recommendation of the manufacturer were performed once a month using indium and zinc, having their melting point at 156.6 °C and 419.5°C respectively. More information on this technique can be found in Todor (1976).

4.3.4. Scanning electron microscopy

SEM observations were performed with a Hitachi S-3500N variable pressure microscope equipped with an EDS detector with micro analyser from Oxford Instrument LINK ISIS (programmable for automatic acquisition of images and energy dispersive spectrums). Images were acquired in the backscattered electron (BSE) mode at low pressure (< 0.1 Pa), using a primary voltage of 20 keV, a current emission of 120 µA, and a working distance of 15 mm. Twelve images in BSE were acquired and twelve others in X-ray dot mapping mode (Na, Mg, Al, Si, S, K, Ca, Fe) were captured over 50 frames for each image and for each specimen. 800x magnification was used giving a resolution of 1.57 pixel/µm. Each set of images gave a rectangular area of 490 µm x 470 µm. In addition, for all twelve beam positions, an X-ray EDS spectrum was registered for about 2 minutes with a deadtime between 30 and 40%. The spectra were corrected using the ZAF technique (e.g. Goldstein et al., 1992) and the weight percentages of the elements were evaluated respecting the oxide stoichiometry and normalized to 100%. Since the spectra were acquired over the entire region covered by the electron beam, they give the mean chemical composition of each image. More information on SEM can be found in Goldstein et al. (1992). For all specimens, some special features (precipitate in pores, unhydrated binders, cemented matrix, and sulphated phases) were also observed at 1500x magnification, and EDS spectra were acquired to define the chemistry of phases.

4.3.5. Sulphate content

The sulphate sulphur concentrations in CPB samples cured for 180 days were evaluated using the EPA 600/2-78-054 guidelines (Sobek et al., 1978). The Sobek method is mainly used to differentiate the sulphate sulphur and the sulphide sulphur

in materials containing sulphide oxidation products. The procedure involves two dissolutions using two acids: HCl (40% v/v) and $HNO_3/Br_2/HF$. Sobek method was not specifically tested for sulfoaluminates, but based on the laboratory experience, only lead and barium sulphates are insoluble with this technique. In the present study, as CPB samples do not contain sulphide minerals, only the HCl dissolution was performed and the extracted sulphur amount is assumed to come from precipitated sulphated phases. The resulting solutions were analysed by inductively coupled plasma-atomic emission spectrometry (ICP-AES).

4.3.6. SEM-XMAP processing

As mentioned previously, twelve images in X-ray dot mapping mode were captured for 8 elements over 50 frames for each image and for each sample. The X-ray dot-mapping technique allows observing the position of chemical elements in a sample. Under favorable conditions, the resulting maps are sufficiently contrasted to distinguish of the relative proportion of elements. This technique is widely used to evaluate local variation of the chemistry of a specimen, but not necessarily to perform mineralogical characterization. Nevertheless, the combination of SEM-XMAP and image analysis techniques to characterize different geomaterials has reported in the literature. Such mineralogical characterization was performed on rocks by Petruk (1987) and Kahn et al. (2002), on fine grained soils by Knight et al. (2002), on ore concentrate by Gu (2003), and on mine tailings by Mermillod-Blondin (2006). For cement and cemented materials, some studies showed how X-ray dot mapping and image analysis can be combined to identify cementitious phases (Bentz and Stutzman, 1994; Bentz et al., 1999; Stutzman, 2004).

The image processing technique developed for this project is mainly inspired from the works of Bentz and collaborators cited above. However, there are important differences between the two approaches, mainly because the studied CPB samples are made with low binder content. Hence, the processing algorithm has to deal with

low elemental concentrations in the X-ray images. Since this study investigates the cemented matrix within CPB, routines and processing steps are applied especially to increase the response of this matrix. Figure 4.1 summarizes the processing of X-ray maps and the image analysis routines used to produce a final coloured mineralogical image (called in this paper SEM-XMAP).

The following paragraphs explain the nine stages. Stages 1, 4, and 8 are performed using the existing program ImageJ (Rasband, W., National Institutes of Health, USA, http://rsb.info.nih.gov/ij/) while all other stages are performed with a software program written specifically for this study.

4.3.6.1. Filtering

All acquired X-ray images are filtered with a 4x4 Gaussian and a Median 5x5 filter. A Gaussian filter was selected for the smoothing procedure because edge definition is not a critical issue in the case of X dot mapping. The application of the Gaussian filter also improves the accuracy of the grey tone selection for the following image treatment steps. A Median filter is applied to remove the residual noise. More details on image analysis filters can be found in Russ (1999).

1) Filtering:
Gaussian (4x4)
Median (5x5)

2) Normalizing

5) Edition of grey tones of X-images:
Zone A: = black (0)
Zone B: = value adjusted according to EDS wt. %
Zone C: = white (255)

3) Merging

4) Evaluation of the porosity in BSE image and production of the thresholded image

6) X-ray images processing

7) Production of the coloured image

8) Addition of images

9) Final image
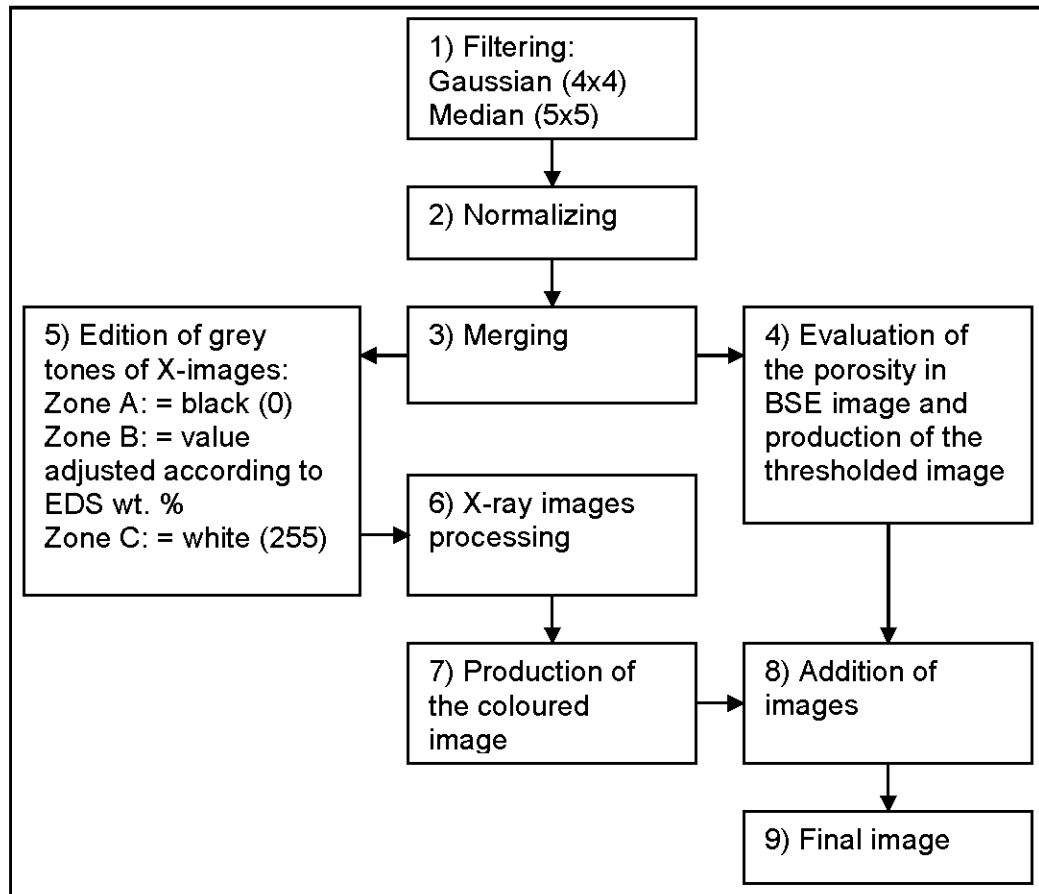
Figure 4.1, Block diagram of the SEM-XMAP image processing techniques.

4.3.6.2. Normalizing X-ray images

Because X-ray images of a given mosaic (twelve images of the same element) can have different brightness due to little current variations of the SEM or to a high concentration point in the image, it is necessary to apply a grey tone normalization procedure. An example of this normalization is illustrated in Figure 4.2 where two calcium images from the same set are presented (images "c" and "e" are the same). Figure 4.2a shows Ca (in light grey) and the silica grains (in dark grey or black). Although the concentration of Ca is relatively low, the presence of this element in the analyzed zone is clearly visible.

a)

b)

c)

d)

e)

f)
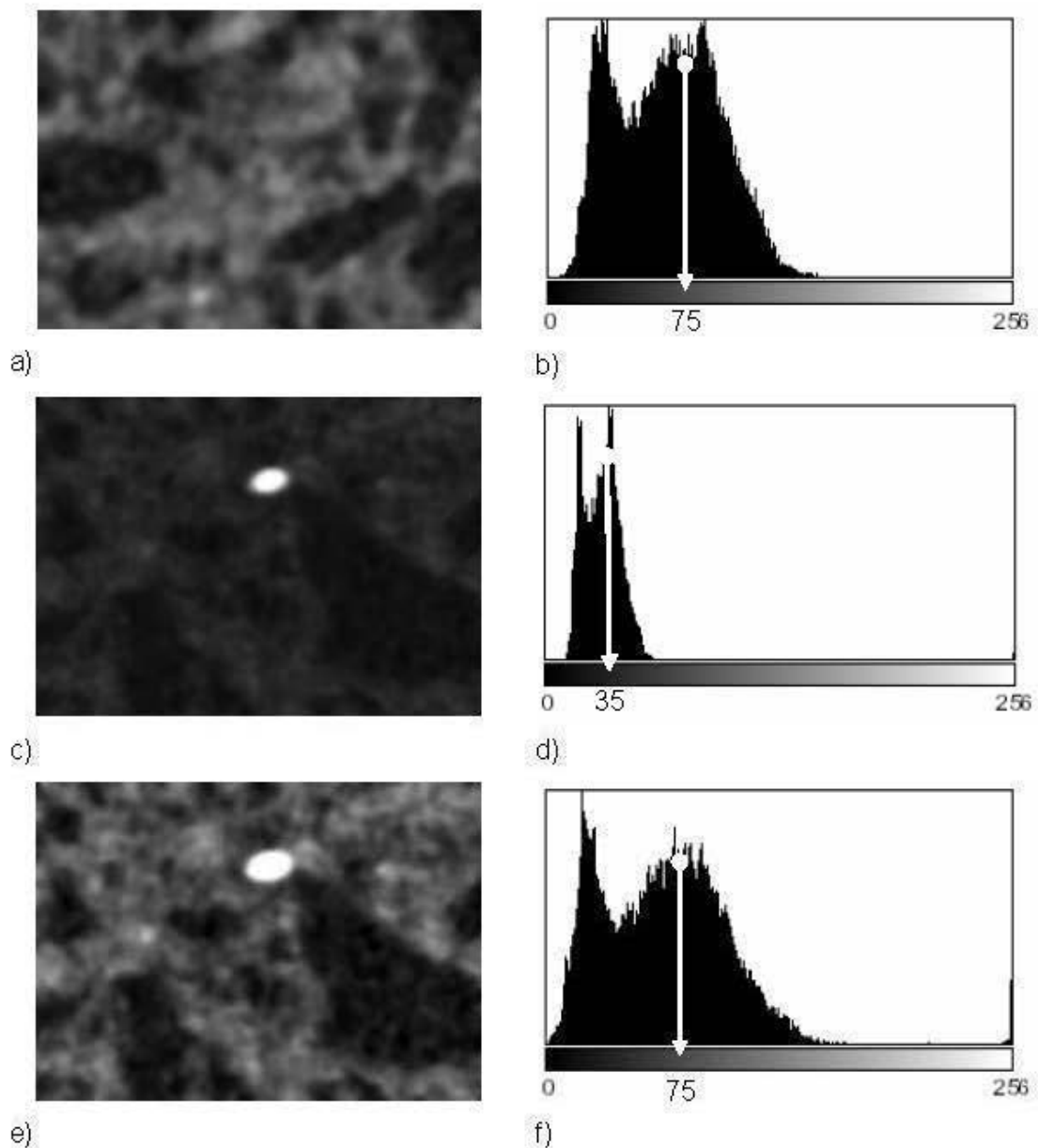
Figure 4.2, Example of the normalizing process (image width = 163 μm) using calcium images (see text for details).

Figure 4.2c shows a darker Ca background than Figure 4.2a due to the presence of a grain much more concentrated in Ca. In order to compare all X-ray images of a same chemical element, pixel values of each digital image are multiplied by the ratio of the grey tones at the mid width of the main peak of the greyscale histogram; the numerator being always the highest grey tone value observed in the samples (all

images). For instance, the image in the Figure 4.2c is multiplied by 2.14 (75/35, see Figure 4.2b, 4.2d, and 4.2f) to produce, according to all other Ca images in the set, the normalized image "e". The main disadvantage of this method is that it increases the brightness of grain edges with a high concentration. This deviation is considered acceptable since this study focuses on the cemented matrix; this will also be partially corrected during stage 6. The normalizing operation is performed for all X-ray images except for Si, as a silica powder is used as aggregate this correction is not required. Figure 4.3 shows a set of eight normalized images (Al, Ca, Fe, K, Mg, Na, Si, and S). The brightness of these images was increased to facilitate features distinction. Three concentration levels are clearly seen for Ca image: almost zero in silica grains, low for the cemented matrix and relatively high in some spots. Contrary to Ca, low concentrations in Al, Mg, and Na are observable in silica grains; some more concentrated spots in the latter elements are also distinguishable. Except for some spots in Fe, Na and S, images related to these elements reveal almost only a coloured background that will be ignored in next processing steps.

4.3.6.3. Merging images

As the BSE and the X-ray images were captured on a 3x4 images grid, each set of 12 images was merged together at this stage to make a mosaic of images. This operation facilitates the further processing stages and allows a better global definition of the elemental images.

4.3.6.4. Evaluation of the porosity

Figure 4.4 presents a BSE image of a CPB specimen and its corresponding greyscale histogram. All BSE images acquired on epoxy impregnated and polished CPB samples show a similar greyscale distribution: a zone "C" that can be related to
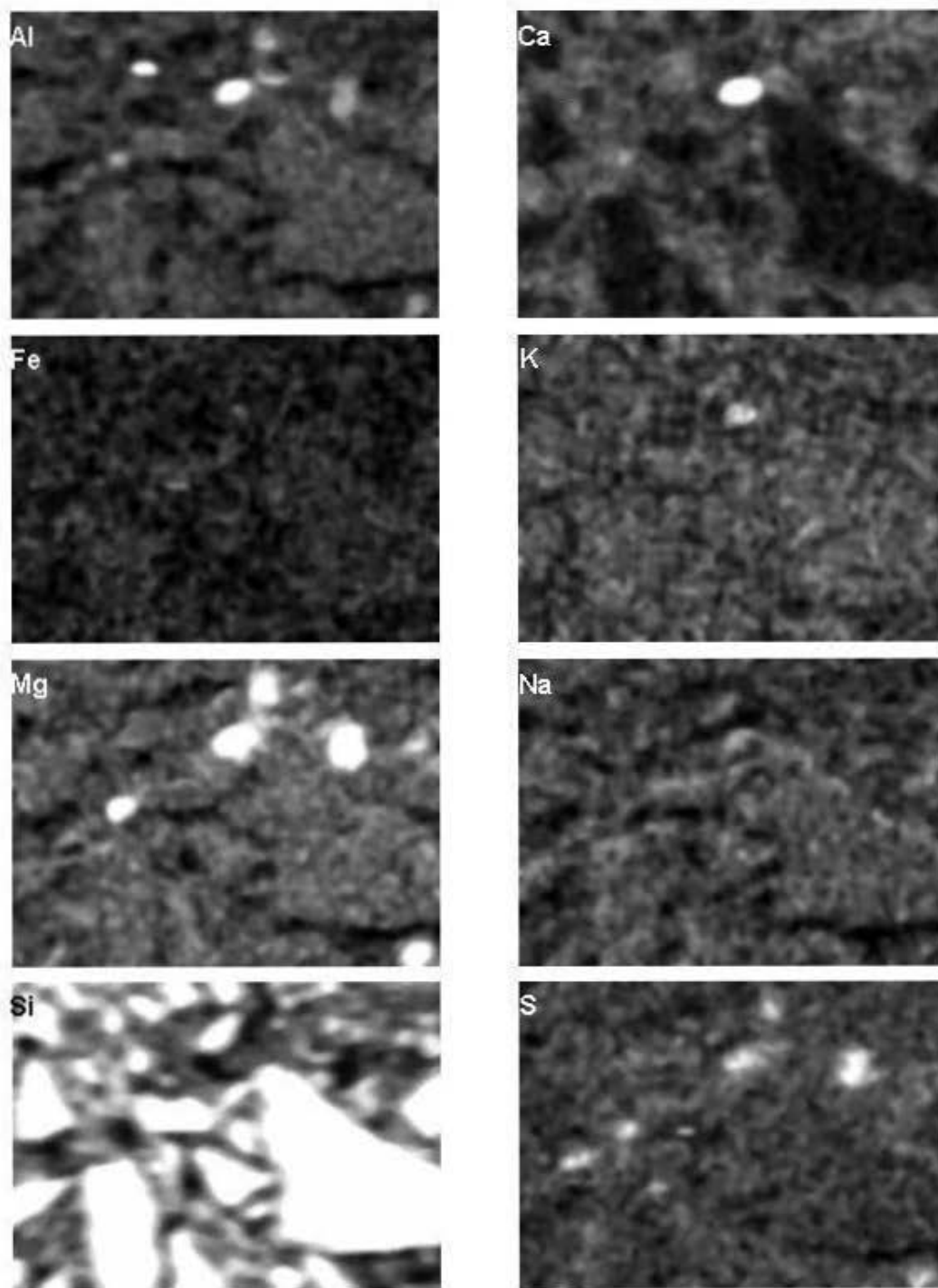
Figure 4.3, A set of eight normalized X-ray images (after steps 1 and 2) acquired at one electron beam position (Al, Ca, Fe, K, Mg, Na, Si, and S; field width = 163 μm).
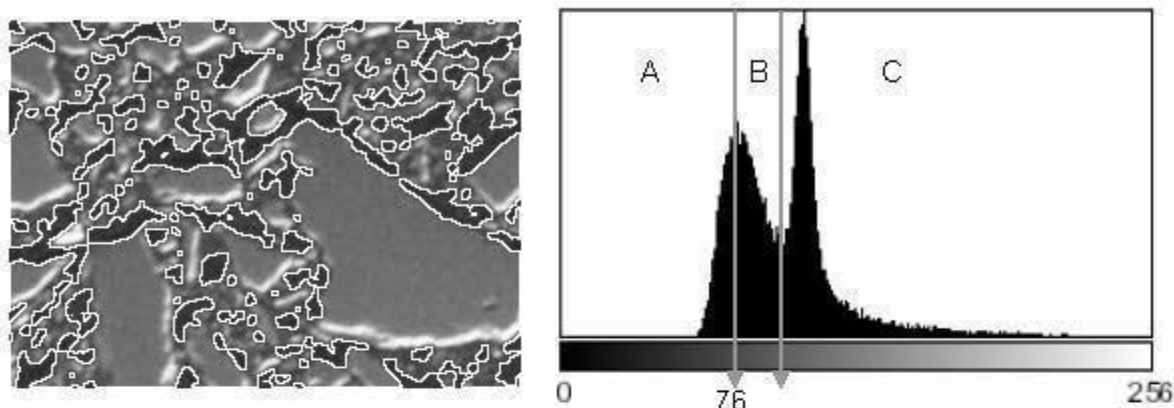
Figure 4.4, Example of the evaluation of the porosity in one BSE image, white contours indicate the selected porosity regions (image width = 163 μm).

silica grains, a zone "B" defined as the transition zone between silica grains and the epoxy, and a zone "A" corresponding to the epoxy (porosity). More details about the determination procedure for these zones and the processing method can be found in Chapter 3. In the present study, only the zone "A" is considered. The threshold value (that separates the zone A and B) corresponds to the highest value of the first histogram peak (76 in the case of the Figure 4.4). The resulting thresholded image will be used in stage 9 to remove colours assigned in porosity zones.

4.3.6.5. Edition of grey tones in X-ray images

From a quantitative point of view, the energy-dispersive spectrometry dot mapping is not very accurate with a reported limit of detection of approximately 2-5 wt. % (Goldstein et al., 1992). Also, with the equipment used in this study, the X-Ray count rate is lost in the recording process which reduces further the accuracy of the method (Goldstein et al., 1992). Under optimal conditions, the relative accuracy for quantifying the concentration of an element is approximately 2% for concentrations greater than 50% and decreases to approximately 20% when the concentration is only 1 wt. % (Stutzman, 2004). In practice, although elemental concentrations cannot be established with accuracy, the X-ray dot mapping can distinguish low elemental

concentration values and can represent them as a contrast in the greyscale of images. This can be seen in Figure 4.3 where X-ray maps show the presence of Al, Na, and Mg at the silica grains positions, as revealed by the chemical analysis of the silica powder (Table 4.1).

As mentionned earlier for calcium, three zones or levels of elemental concentrations can be established in X-ray images: the zones clearly having a high concentration shown as a brighter colour than the matrix, the cemented matrix, and the background representing the area where the presence of the element is not sure. Another problematic aspect is the relative chemical proportion between all mapped elements. For low elemental concentrations, as in the case of cementitious phases of CPB, it is impossible to establish which element is more concentrated than another only on the basis of the greyscale contrast of X-ray images. To solve this problem, the X-ray images have been filtered one more time according to the average of EDS analyses performed on the twelve captured images. The new X-ray image then contains only three grey levels selected as follow (see Figure 4.5):

1. A grey tone of 0 (black) is attributed to pixels in zone A;
2. A grey tone proportional to mean EDS analyses is attributed to pixels in zone B;
3. A grey tone of 255 (white) is attributed to pixels in zone C.

Figure 4.6 shows the resulting images presented in Figure 4.3 after the edition of grey tones (step 5).
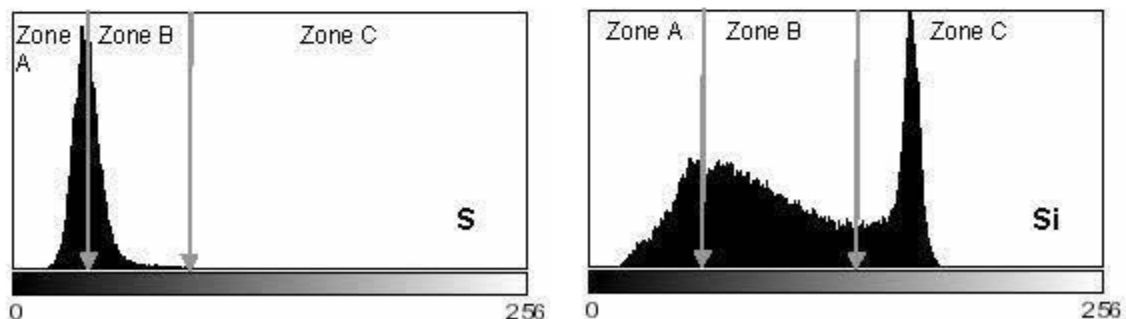
Figure 4.5, Example of grey levels selection for S and Si images.
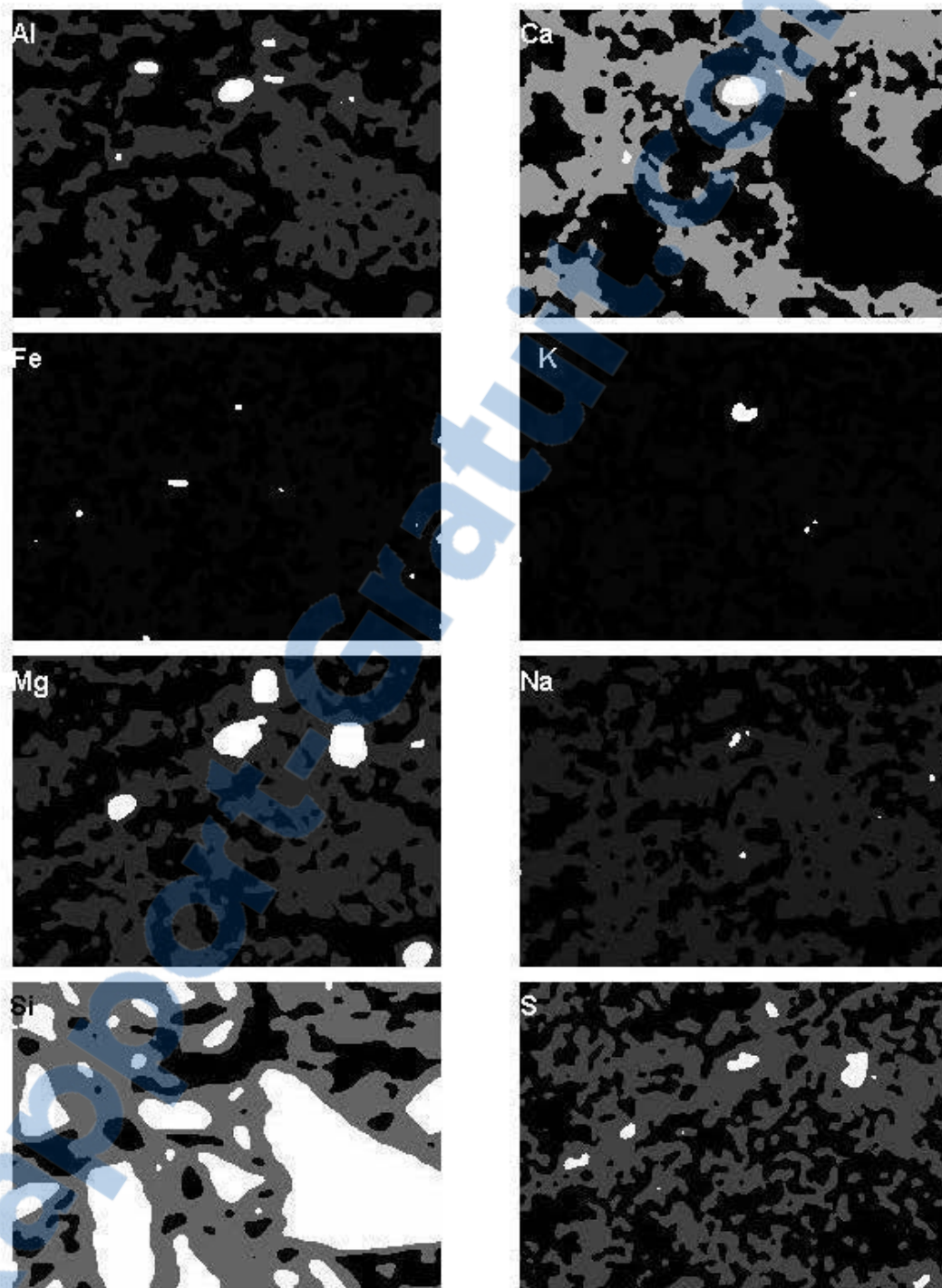
Figure 4.6, X-ray images of Al, Ca, Fe, K, Mg, Na, Si, and S after the greyscale edition (see text for processing details; field width = 163 µm).

One can see that the calcium is removed from silica grain zones and the grey tone in low Ca regions (zone B) of the image is now uniform and more representative of the mean proportion of this element in the specimen. Similar results are noticeable for all other chemical elements except silicon. The edition of silicon image is effectively more complex because the used aggregate for the CPB mixtures is ground silica; an important proportion of grey tones is then present in the zone C. It is impossible for Si to know with certainty if the X-rays signal comes from the cemented matrix or a silica grain, due to the interaction volume of the analysis. Consequently, the processing algorithm has to deal with the presence of Si in almost all pixel positions and the selection of a phase that does not contain Si is limited to regions in black in silicon images.

4.3.6.6.   X-ray image processing and final image creation

Table 4.2 summarizes the main cementitious phases identified for cement and mortar with their simplified chemical formula. Most of these phases are stoichiometrically variable and only the generic name is used. More information on mineral and cement phase formulas can be found in Taylor (1990).

Studies performed on cement paste and mortar showed that the hydration of OPC alone or mixed with mineral additives involves relatively complex reactions that produce mainly calcium silicate hydrates (C-S-H), portlandite and sulphoaluminates (ettringite, monosulphate: $3CaO \cdot Al_2O_3 \cdot CaSO_4 \cdot 12H_2O$); other phases such as hydrogarnet ($3CaO \cdot Al_2O_3 \cdot 6H_2O$), hydrotalcite ($Mg_6Al_2CO_3(OH)_{16} \cdot 4H_2O$) and calcite can also be found (Taylor, 1990). Gypsum can be present since it is added to cement to regulate its hydration, or it can be found with ettringite if the CPB suffers from sulphate attack (Tian and Cohen, 2000; Benzaazoua, 1996; Fall and Benzaazoua, 2005). Hydration products of FA and BFS are basically the same as those produced by OPC (Taylor, 1990). However, these additives mixed with OPC lead to a pozzolanic reaction with portlandite and the formation of additional C-S-H

gel. Stratlingite or gehlenite hydrate ($[Ca_2Al(OH)_6][AlSiO_3(OH)_2 \cdot 4H_2O]$) and hydrogarnet are phases that can be encountered in small amount when high-calcium FA is used (Taylor, 1990). For BFS, the hydrotalcite can be found as a hydration product when the MgO content is high (Taylor, 1990). Brew and Glasser (2005) report the formation of magnesium silicate hydrate (M-S-H gel) in BFS paste.

The developed program allows formulating different chemical combinations and the selection of the X-ray files (Figure 4.7). Nine elements can be selected; these elements can lead to the formulation of a maximum of fifty minerals. The program records at each pixel position the grey tones of selected X-ray files, sorts it in descending order, compares the result to the available mineralogy, and assigns the preset colour. Due to the sorting of grey tones, only the most bright pixels (pixels reflecting the highest concentrations) are used to create a mineral.

Table 4.2, Phases investigated in X-ray images and chemical elements arrangement considered to generate the final image

Mineral phases*	Mineral formulas used in the program
C-S-H, Portlandite, Calcite, uCS	Ca, CaSi
Hydrogarnet, uCA, uCAF	Al, CaAl, Fe, CaFe, CaAlFe
Alkalis, Fly ash	K, Na, AlNa, AlK
C-A-S-H, hydrogarnet	CaAlSi
Silica	Si, KSi, AlSi, NaSi, FeSi
Gypsum, Ettringite, Monosulphate	S, CaS, CaAlS
Brucite, Mg Sulphates, BFS, Fly ash	Mg, CaMg, CaMgSi, MgS, MgCaS, SAl, SFe
Hydrotalcite	MgAl
M-S-H, M-A-S-H	MgSi, MgAlSi

*: C-S-H: calcium silicate hydrate; uCS: unhydrated silicated clinker phases; uCA: unhydrated aluminate clinker phase; uCAF: unhydrated ferrite clinker phase; C-A-S-H: calcium silicate aluminate hydrate; BFS: blast furnace slag; M-S-H and M-A-S-H: Sepiolite like gel; C: CaO; S: SiO_2; H: H_2O; A: Al_2O_3; F: Fe_2O_3; M: MgO.
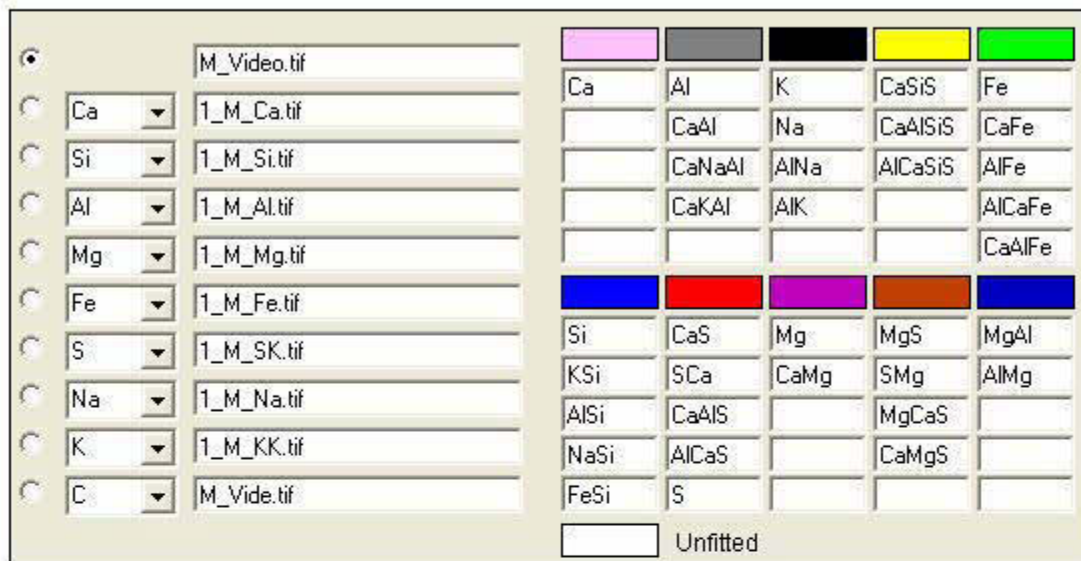
Figure 4.7, Chemical composition program window. Acquired chemical elements and related X-ray images are showed at the left; right part of the figure shows selected combinations for the T10FA-W0 sample.

During the last step, the binary image of the porosity (stage 4) is added to the resulting image and coloured porosity zones are removed. The final result produced is a coloured map where each color represents one mineral or one family of cementitious phases. The final image is then scanned and the percentage of the image area covered by each colour (corresponding to one of the phases) in the CPB sample is given by the software. It is worth mentioning here that the image produced should be considered as a qualitative representation of the micro-organization (microstructure) of the mineralogy of the studied CPB sample and not as a quantitative result of the amount of cementitious phases observed in the samples. Because the amount of cementitious phases in CPB is low and that elemental concentrations are usually lower than the quantitative accuracy limit of the SEM for X-ray dot mapping, the produced image should be considered only as an indication of the presence of a mineral or a phase group.

4.4. Characterization results

This section presents the mineralogical characterization results obtained from the TGA/DSC, the SEM images in BSE and SE, and the SEM-XMAP imaging method. Since the precipitation of sulphates can induce stress and strength loss in cemented material, the UCS was measured on samples over all the testing period and results are also presented in this section.

4.4.1. TGA/DSC

4.4.1.1. Thermal behaviour of cementitious phases

The thermal methods such as thermogravimetry (TG) and differential scanning calorimetry (DSC) are often applied to characterize several phases in cementitious materials (e.g. Ramachandran, 1969). During a continuous temperature increase, the TG technique measures the weight loss while the DSC monitors the heat flux related to events such as evaporation, melting, and crystallization. These thermal behaviours can be due to the dehydration of C-S-H gels, portlandite, or sulphated phases, the CO_2 release by carbonate minerals, or the transformation of low quartz (SiO_2) into high quartz. The accurate identification of a mineral is however complex with TG and DSC as many factors (such as the heating rate, the initial sample weight, the purge gas type and rate) can affect the temperature yield of a thermal peak (TA Instruments, 2004a; 2004b). The literature is abundant for most cementitious phases encountered in cemented materials. However, no standard data base exists to interpret TGA/DSC results, so the user must interpret the thermal behaviours based on data from various sources such as the one presented in Table 4.3.

Table 4.3, Minimum and maximum peak temperature gathered from
the literature for different cementitious phases*

Phase	Minimum observed (°C)	Maximum observed (°C)	Median (°C)	References**
Interlayer water, C-S-H	50	300	124	1, 2, 4, 5, 9-18, 20-23, 27-32, 34, 35
Ettringite	80	300	125	1-3, 5, 9, 10, 15, 18, 19, 23-27, 29-34
Gypsum	98	220	140	5, 7-10, 18, 19, 23, 26, 30, 33, 36
Monosulphate	130	250	187	1, 9, 10, 12, 13, 15, 18, 19, 21, 23, 27, 30, 31, 34
Hemihydrate	150	230	165	7, 8, 19, 27, 36
Carboaluminate $(Ca_4[Al(OH)_6]2CO_3 \cdot 5H_2O)$	165	230	180	18, 23, 34, 35
Stratlingite	170	180	175	6, 76
$Ca_7Al_2O_7 \cdot 13H_2O$	175	300	230	1, 6, 13, 15, 23, 27, 31, 34
Hydrogarnet	250	400	325	10, 16, 20, 24, 28
Hydrotalcite	330	400	365	12
Portlandite	370	580	475	1, 2, 5, 10, 13-16, 18, 20, 21, 23, 26, 27, 29-32, 34, 35
Complex Carbonate	500	850	700	1, 2, 5, 13, 15, 17, 18, 21, 23, 28-32, 34, 35
C-S-H(I) (Tobermorite)	600	900	750	14, 16, 20, 27
Calcite	800	828	800	5, 8, 16, 17
Wallastonite from C-S-H (exo)	840	1160	870	8, 11, 14, 16, 17, 22, 28
Devitrification of Slag (exo)	845	950	915	1, 2, 27
Al-tobermorite (exo)	903	903	903	16
Anorthite from Hydrogarnet (exo)	940	985	962	11, 16

*: The main techniques used are differential thermal analysis (DTA), derivative thermogravimetry (DTG), and DSC; the temperatures given correspond to the summit of a DTG peak or of a DSC and DTA endothermic peak, "exo" means exotherm from DTA or DSC.

**: See section 8 for the legend of the references

As it can be seen in Table 4.3, some significant thermal stage variations exist between studies for a given mineral. However, some trends can be identified for each mineral. The temperature range for weight loss associated with C-S-H is usually below 100° for relatively fresh samples (low curing time). In mature cement

paste (at long curing time), the main observed peak for C-S-H is usually close to 120°C. Temperature range for TGA/DSC peaks of the main sulphated minerals encountered in cemented pastes is relatively large (100 to 300°C), probably because weight losses happen in two or three stages. Most authors report weight loss for ettringite at approximately 120°C; tests on synthesized ettringite show that the main loss occurs at 115°C (Perkins and Palmer, 1999). Dehydration of gypsum occurs in two stages: it is first transformed into hemihydrate ($CaSO_4 \cdot 0.5H_2O$) and then to anhydrite ($CaSO_4$). These two stages release water that can be monitored clearly by DSC using a hermetic pan (TA Instruments, 2004b). Otherwise, if an unsealed pan is used (as is the case here), the DSC shows a broad endothermic peak that includes the two water release stages at 140°C. Weight loss for monosulphates are usually reported between 130°C and 250°C with a median temperature observed at 187°C. The dehydroxilation of Portlandite occurs between 370°C and 580°C; this mineral is usually easy to identify using TG because no other mineral loses weight in this temperature zone. The CO_2 release by calcite is reported at 800°C while the same event for non crystalline or complex carbonate occupies a wide region, between 500 and 850°C. Weight loss and endothermic effect related to C-S-H(I) (tobermorite: $\approx Ca_5(Si_6O_{18}H_2) \cdot 8H_2O$) are also reported in the same temperature zone (Georgescu and Bananoiu, 1997; Singh and Garg, 2002); the weight loss generally increasing with curing time and DTA peaking at approximately 750°C in mature paste.

4.4.1.2. Main TGA/DSC results

Although the average weight loss was relatively low during the tests (between 1% and 2% of the initial sample weights), the accuracy of this thermal technique and the use of silica as the only aggregate were advantageous to identify cementitious phases. Indeed, since the only DCS effect of quartz is a unique structural inversion at 573°C, with a weight loss of about 0.2%, almost all monitored changes can be related to the mineralogical phases associated to the cementation process.

The effect of curing time can be seen in Figure 4.8 where the weight loss in different temperature zones for the 24 CPB samples tested is presented. Figure 4.8a shows TG results between 100 and 250°C and indicates that the weight loss increases with curing time in almost all cases. Since this temperature zone is usually related to C-S-H gels, sulphates, and sulphoaluminates (see Table 4.3), the increase in weight loss can be partly related to these phases.

The effect of binder on TG results can be seen on Figure 4.8b. Almost all weight losses in the different temperature zones selected can be ranked as T10>T10FA>T10SL. TG tests performed on unhydrated and unmixed cement and mineral additives particles (results not shown here) revealed the same ordering (i.e. T10>FA>BFS). Thus, two reasons can explain this weight loss order observed for studied CPB samples: i) since the mineral additive replacement level is 30% and 80% for T10FA and T10SL samples respectively, a significant amount of unhydrated FA and BFS particles is present in mixtures at all testing times and/or ii) since TG removes volatile molecules associated to cementitious phases, the ranking can be related to a greater amount of these phases in CPB samples (which does not seem to be the case as it will be shown later).
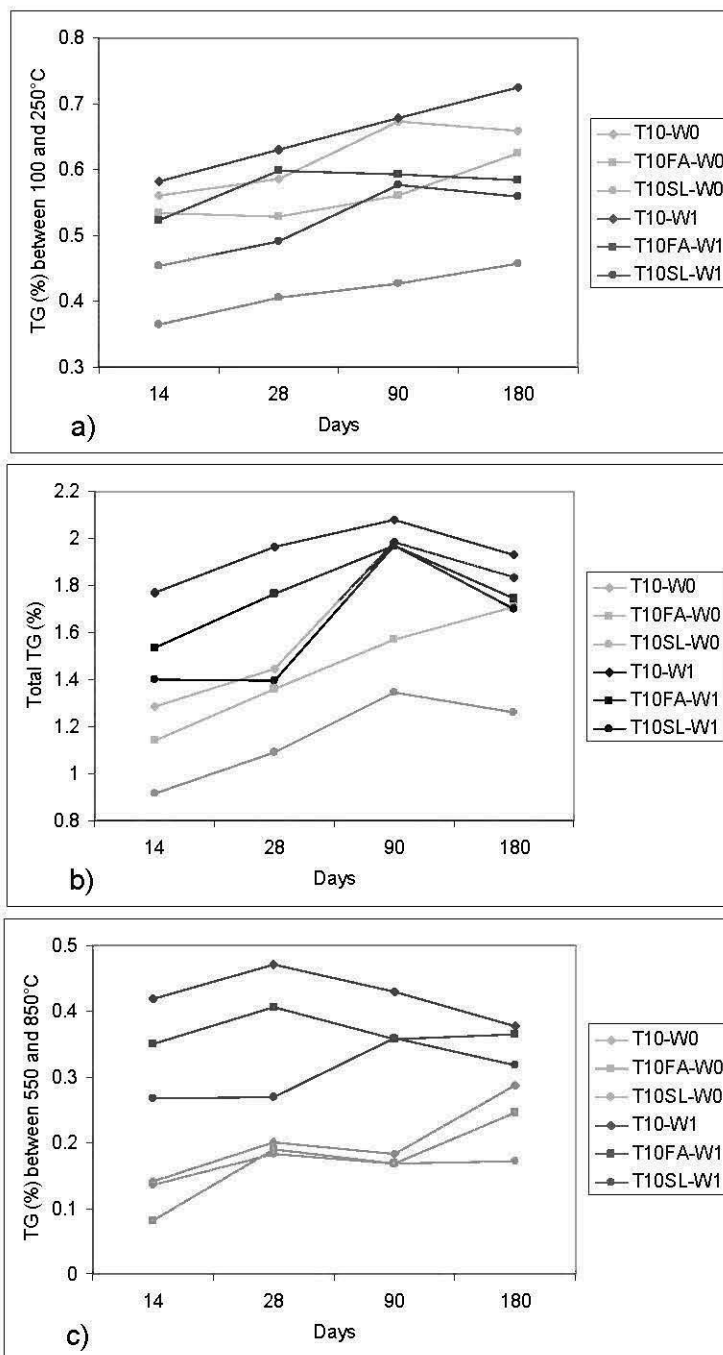
Figure 4.8, TG (weight loss) results at 14, 28, 90, and 180 days: a), TG between 100 and 250°C b) Total TG, and c) TG between 550 and 850°C.

The influence of water quality on TG results can be clearly identified for the studied samples. First, TG curves presented in Figure 4.8 show that weight losses are higher for samples mixed with W1. For instance, mean TG differences between W1 and W0 samples over the 100°C-1000°C temperature zone are 0.30%, 0.31%, and 0.46% for T10, T10FA, and T10SL respectively, indicating that CPB samples mixed with W1 seem to contain a more important amount of hydrated phases than those mixed with W0. Results also indicate that despite the fact that T10SL loses less weight than the other two binders, its TG loss is proportionally more important when combined with the W1 water. This behaviour is also observed in the 100°C-250°C region where the mean weight loss differences between W1 and W0 samples is 0.1% for T10SL specimens and approximately 0.03% for the other two binders. Thus, the T10SL-W1 samples have a greater amount of C-S-H gel and/or sulphates/sulphoaluminates, also meaning that the amount of unhydrated binder could explain, at least in part, the ranking presented above for the effect of binders. Another important difference between samples with W0 and W1 is observed in the 550°C-850°C range , which is usually associated with the occurrence of carbonated minerals and/or C-S-H(I). Figure 4.8c shows that the average weight losses in this zone are 0.18% and 0.37% for samples mixed with W0 and W1 respectively.

Figures 4.9 to 4.14 show the DTG curves of the studied samples with the interpretation of the results based on the literature data presented in Table 4.3. Observations on all samples suggest the presence of C-S-H (B) and monosulphoaluminates (D) at approximately 120°C and 180°C respectively. As observed in the literature, the C-S-H peak seems to shift to a higher temperature with curing time. Gypsum is also identified by DTG at 140°C in T10-W0 and T10FA-W0 only, but DSC showed a slight endotherm in all samples at this temperature. The weight loss between 350 and 400°C (E) is assumed to be related to hydrogarnet in T10 and T10FA mixtures and to hydrotalcite in T10SL samples. Portlandite (F) is present in specimens prepared with T10 at early ages, but the mineral disappears with curing time (as indicated by the absence of a portlandite peak at 90 and 180 days). This absence is surprising since T10 samples are not expected to become

carbonated during curing. Nevertheless, Bénézet and Benhassaine (2001) reported that the finest silica grains can act as a pozzolanic material in the presence of portlandite and form C-S-H after portlandite consumption. Since fine silica powder was used as unique aggregate in CPB, this hypothesis seems reasonable to explain the absence of the portlandite peak at 90 and 180 days in T10 samples. Portlandite is also observed in T10FA and T10SL-W0 samples at early curing time. For these samples, the pozzolanic effect with the FA and the BFS can be added to the silica effect to explain the relatively fast disappearing of the calcium hydroxide. Portlandite is not observed in T10SL-W1 sample.

The interpretation of the DTG results above 500°C is much more complex. First, all samples lose a slight amount of weight at 600°C; this is generally related to complex or amorphous carbonates. Second, as showed by TG results, the samples have a DTG peak at approximately 800°C. The intensity of this peak is more important for CPB mixed with W1. In the case of T10-W1 and T10FA-W1, the latter peak is followed by a second peak at 850°C that seems to decrease in intensity with curing time. This decrease in weight loss at 850°C explains why the sum of TG response between 550°C and 850°C is less important for samples mixed with W1 in the Figures 4.8 b) and c). The peak at 800°C is generally attributed to calcite, but C-S-H(I) (tobermorite) can also lose weight in this temperature zone (e.g. Georgescu and Badanoiu, 1997; Singh and Garg, 2002). The peak at 850°C is not clearly identified and is assumed here to be a part of the wide hump corresponding to calcite and/or tobermorite. If weight loss in the 800°C region can effectively be related to C-S-H this means that W1 allowed a better hydration of silicated clinkers than W0. More works will be needed to clearly identify phases and the influence of water in this temperature zone.
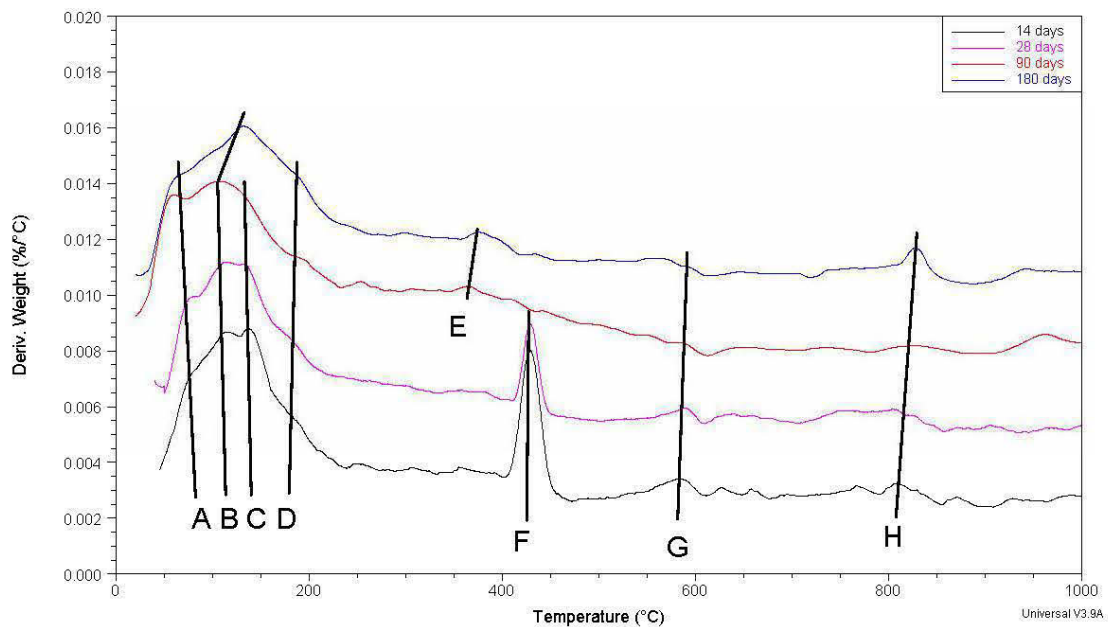
Figure 4.9, DTG curves for T10-W0 samples; A: Adsorbed water, B: C-S-H, C: Gypsum, D: Monosulphate, E: Hydrogarnet, F: Portlandite, G complex carbonate, H: Calcite/C-S-H.
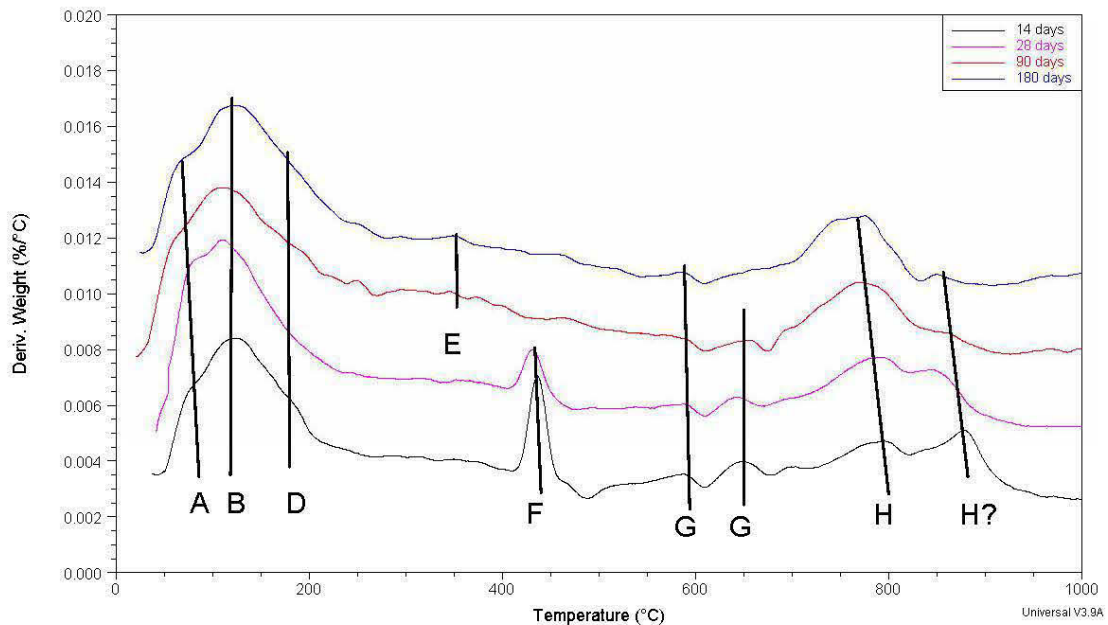
Figure 4.10, DTG curves on T10-W1 samples; A: Adsorbed water, B: C-S-H, D: Monosulphate, E: Hydrogarnet, F: Portlandite, G complex carbonate, H: Calcite/C-S-H.
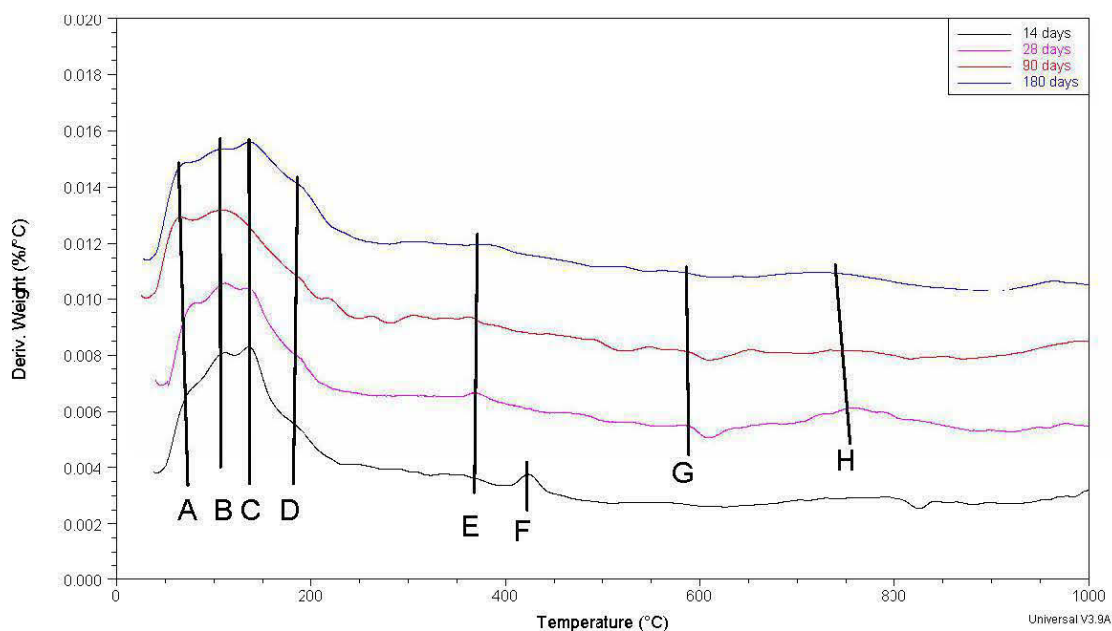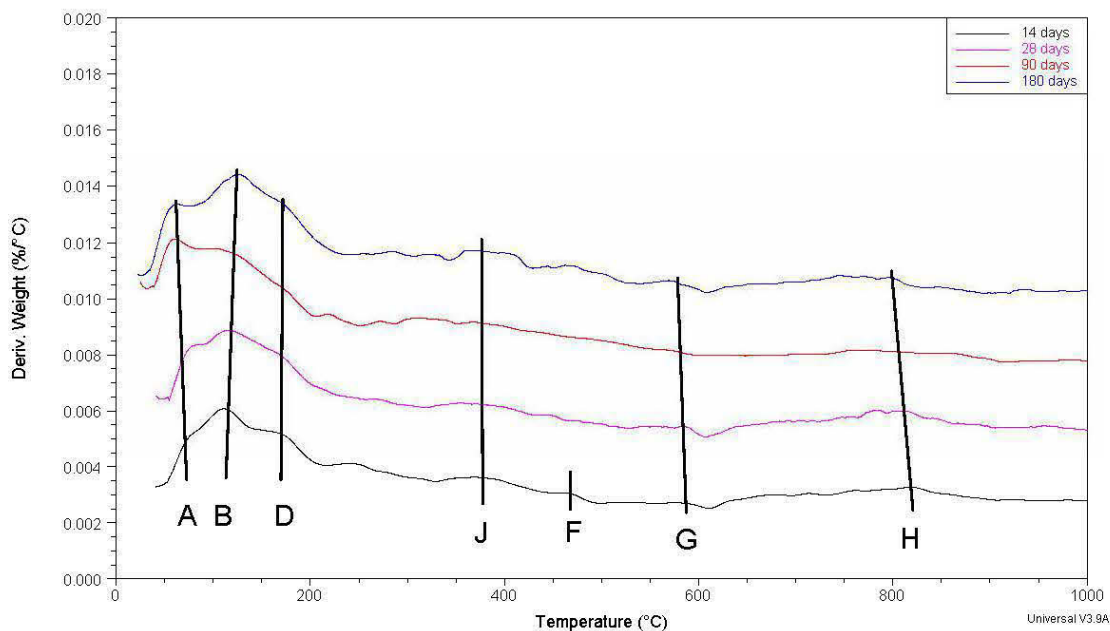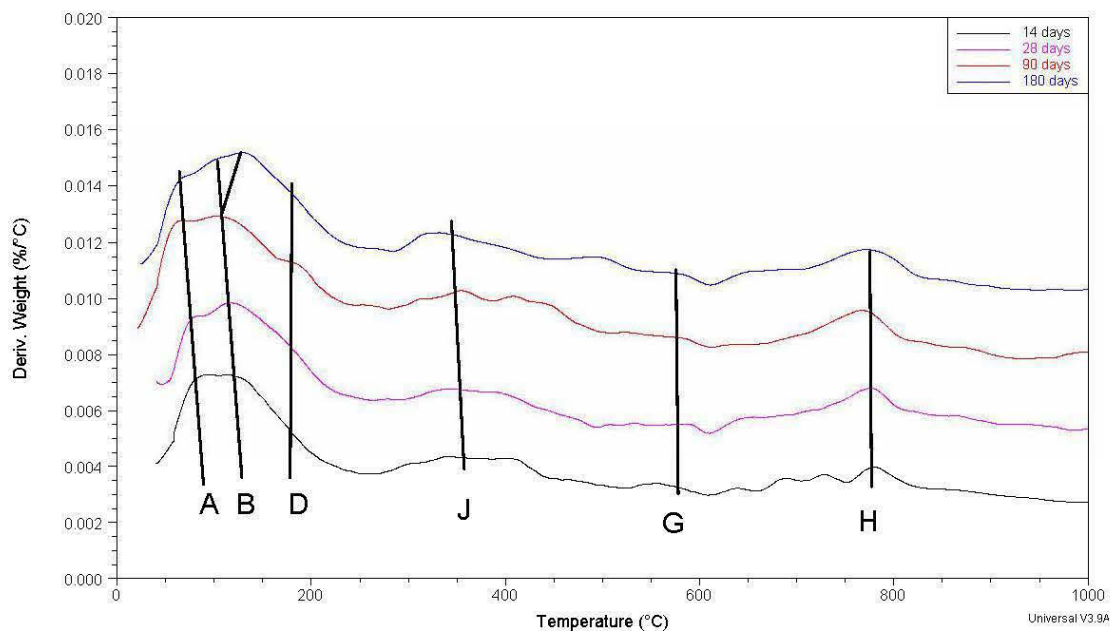
Figure 4.11, DTG curves on T10FA-W0 samples; A: Adsorbed water, B: C-S-H, C: Gypsum, D: Monosulphate, E: Hydrogarnet, F: Portlandite, G complex carbonate, H: Calcite/C-S-H.
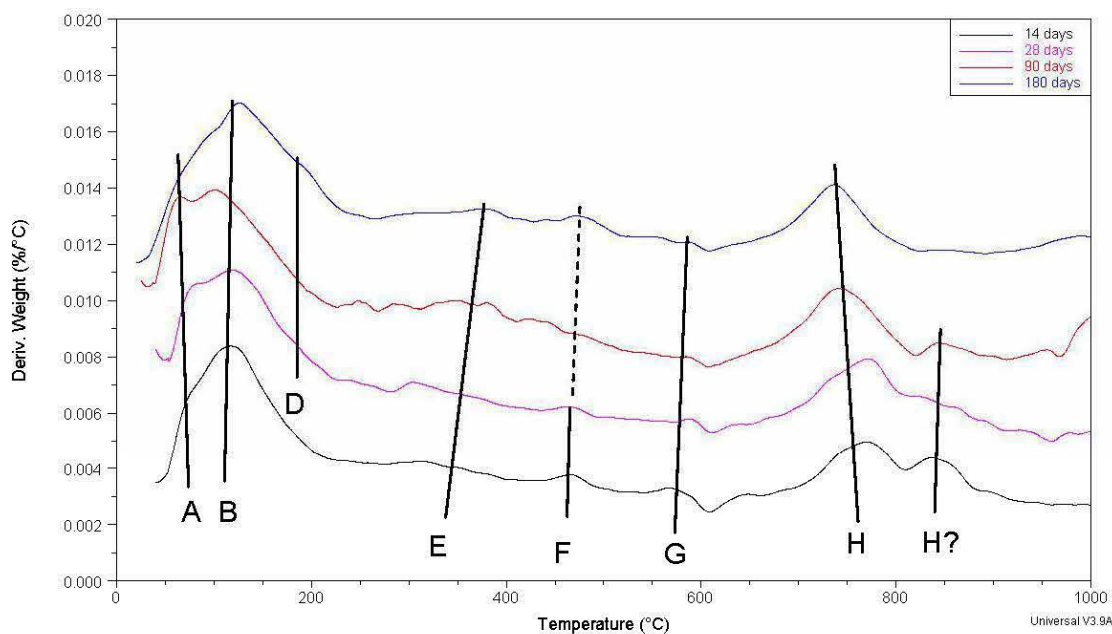
Figure 4.12, DTG curves on T10FA-W1 samples; A: Adsorbed water, B: C-S-H, D: Monosulphate, E: Hydrogarnet, F: Portlandite, G complex carbonate, H: Calcite/C-S-H.

Figure 4.13, DTG curves on T10SL-W0 samples; A: Adsorbed water, B: C-S-H, D: Monosulphate, J: Hydrotalcite, F: Portlandite, G complex carbonate, H: Calcite/C-S-H.

Figure 4.14, DTG curves on T10SL-W1 samples; A: Adsorbed water, B: C-S-H, D: Monosulphate, J: Hydrotalcite, G complex carbonate, H: Calcite/C-S-H.

4.4.2. Scanning electron microscopy

4.4.2.1. BSE and SE images

Figure 4.15 shows two BSE images captured on rough surface fracture of samples T10FA-W1 and T10SL-W1; BSE observations on CPB samples mixed with T10 cement are quite similar (not shown here). The images in Figure 4.15 include mainly coarse and fine silica particles with voids partially filled by cementitious phases. The loose microstructure of samples is similar to observations made on CPB composed of sulphidic mine tailings (e.g. Benzaazoua et al., 1999; 2002; Ramlochan et al., 2004). Except for fly ash particles that are identified due to their spherical form (see Figure 4.15a), other unhydrated binders can not be distinguished. No well crystallized cementitious phases such as ettringite needle or gypsum are visible. However, since the aggregate used is silica, chemical element such as calcium and sulphur can be associated with the cemented matrix and/or water influence. EDS analysis and X-ray dot mapping, although they are not accurate on rough surface, reveal the presence of a background in all elements analysed (Al, Ca, Fe, K, Mg, Na, and S) with some main zones having an increased concentration in calcium, magnesium, and sulphur.
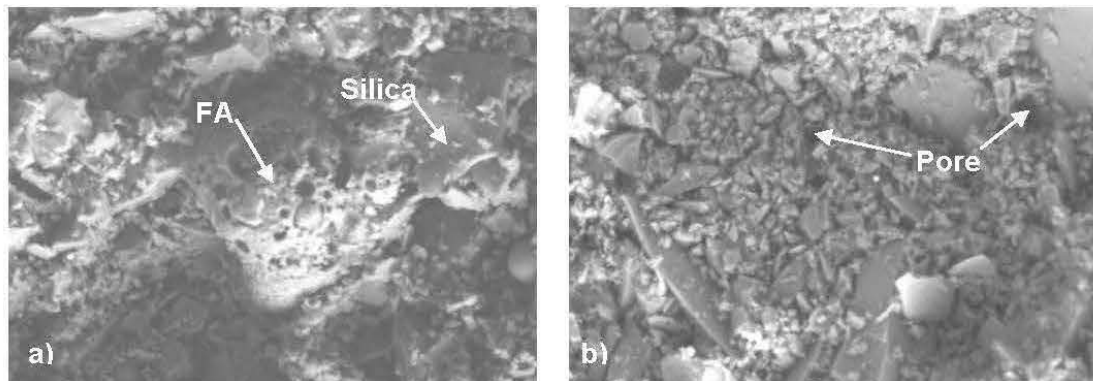
Figure 4.15, BSE images on fractured surface, a) T10FA-W1 and b) T10SL-W1 (field width = 163 μm).

SEM observations on polished surface give further information on the mineralogy and the microstructure of the CPB samples. Figure 4.16 shows a secondary electron (SE) image of the T10FA-W1 sample captured at 1800x of magnitude and 5.5 KeV. CPB appears in this image as a porous material (porosity estimation is 35% by thresholding this image; see Section 3.6.4) with silica grains having Feret diameters from about 20 µm to less than 1 µm. Cracks (probably due to the drying process) can be observed in the darker zones of the image. Cementitious phases appear around silica grains creating solid bridges between some of the closest particles. This figure also shows a big pore filled with epoxy at the centre of the image. This zone reveals an increase in the proportion of Ca, Mg, and S around the pore; this could be seen as a drying residue.
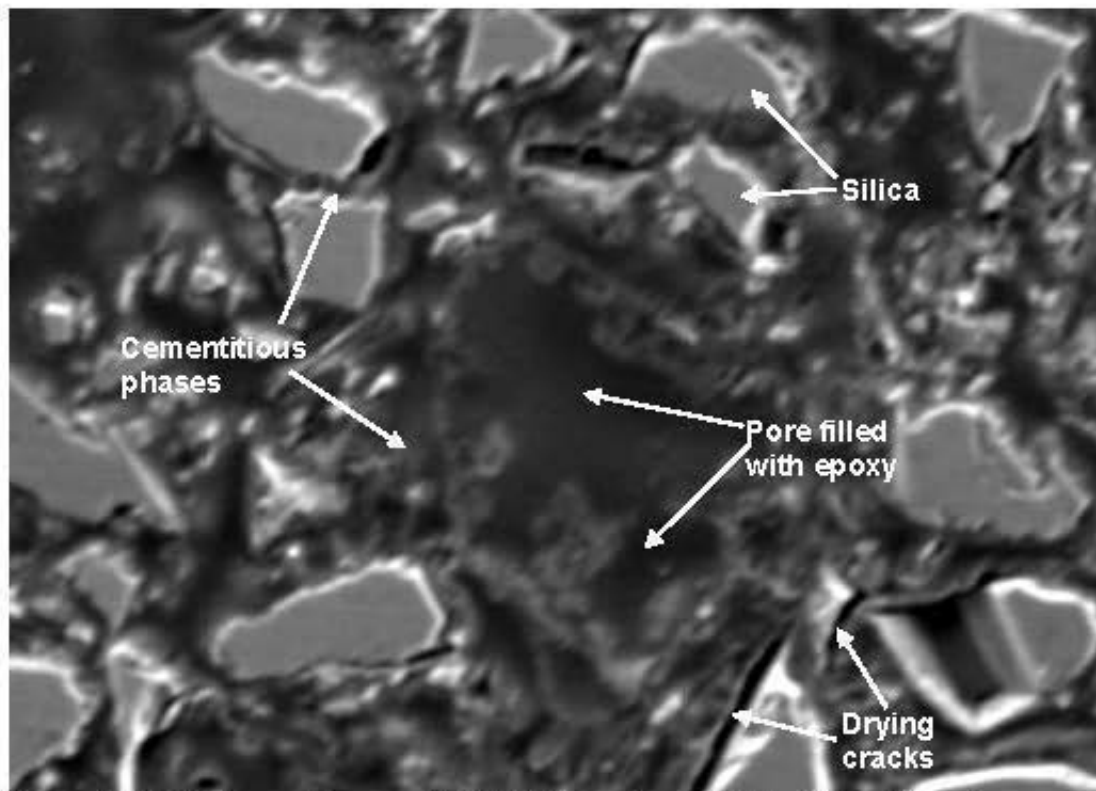
Figure 4.16, SE image taken on T10FA-W1 specimen (field width = 73 µm).

4.4.2.2. SEM-XMAP images

The six CPB mixtures studied were X-ray mapped after 180 days of curing. The results were interpreted using the image analysis procedure presented in section 3.6. Figures 4.17 to 4.22 show the processed coloured images and Tables 4.4 to 4.9 present the corresponding mineral phases, the colour legends, and the measured area of each colour for the six samples (the resulting percentages are rounded to 1/10 of one percent and sums may not be 100%). The images show silica grains (in blue) surrounded by a calcitic matrix (in light pink) where few other minerals such as sulphoaluminates/sulphates or unhydrated cement phases are sparsely found. Based on the measured area, the proportion occupied by the silica is between 40 and 50%. This range is in accordance with the amount of silica used in mixtures and usual porosity for CPB. Assuming all remaining minerals as the cementitious phases and unhydrated binders, their areas are between 30.9% and 39.4%. Sulphated phases (in red, brown and dark blue) are present in various proportions in the samples; the areas covered by these colours are between 4.4% (W0) and 9.4% (W1). All samples show minerals containing sulphur in their porosity zones and they often cover the pore surfaces. This is particularly the case with the T10-W1 image (Figure 4.18). These phases have probably precipitated from the pore water during the drying step. Therefore, it is difficult to establish with certainty if the observed sulphates are original minerals that participate to the strength gain of the CPB or a drying residue.

Based on SEM-XMAP area measurements, some observed binder effects on the cementitious phases can be mentioned. CPB samples prepared with T10 and T10FA have similar area value representing C-S-H (21 to 23%). This value seems to be slightly higher for T10SL with an average percentage of 24.6% for both samples. T10FA and T10SL images show unhydrated or partly unhydrated FA and BFS particles (also observed by Ramlochan et al., 2004). This observation is based on the form and/or the chemistry of these additives that are different than those of the cementitious phases. The presence of unhydrated or partly hydrated BFS particles in

the T10SL samples was surprising because of the high specific surface area of the BFS and the elevated w/c ratio of the CPB. No unhydrated cement phase was identified with certitude in CPB samples mixed with T10. In terms of particular cementitious phases related to a given binder, only the T10SL CPB samples show chemical associations such as MgAl and MgSi; these associations are assumed to be hydrotalcite and M-S-H gel respectively and are found in both samples in low proportion (0.5% of the images). These phases are usually located around or close to BFS particles. All other cementitious phases are observed in the six specimens studied.

The effect of water chemistry on the samples mineralogy is mainly noticeable by the presence of minerals containing sulphur. Total surfaces of these minerals are slightly higher in W1 specimens than in W0 specimens. The measured areas are 4.4%, 6.5%, 6.2%, 7.7%, 4.4%, and 9.4% for T10-W0, T10-W1, T10FA-W0, T10FA-W1, T10SL-W0, and T10SL-W1 respectively. T10SL-W1 sample shows the greatest area of sulphated phases among samples. Again, it is difficult to discriminate between phases before the drying process from these chemical elements precipitated due to the drying process. The amount of unhydrated FA is higher in the W0 sample than in the W1 sample ($\approx$ 1.4% against 0.4%). The same observation can be made for hydrogarnet minerals, C-A-S-H and/or, unhydrated aluminate and ferrite. The areas of these phases are 3.5%, 2.3%, 7.6%, and 3.2% for T10-W0, T10-W1, T10FA-W0, and T10FA-W1 respectively. As mentioned above, unhydrated BFS grains are found in T10SL samples; an area of 5.3% is measured for W0 while this area is significantly lower in T10SL-W1 with 0.5%. Finally, the association between Mg and S covers between 0.7 to 2.9% of the images and is mainly located around or within pores; this association could also be the result of a drying artefact.
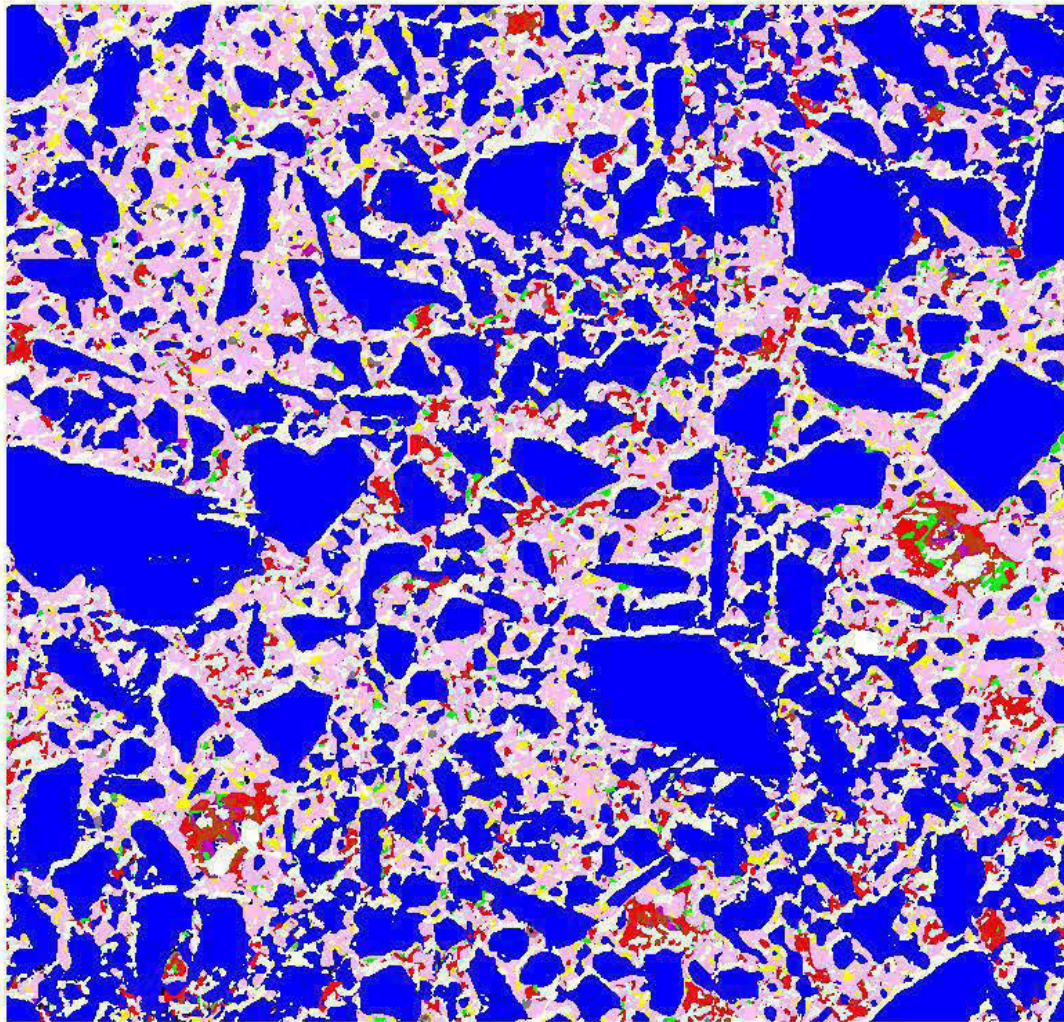
Figure 4.17, Resulting mineralogical image for T10-W0 specimen (colours legend is presented at Table 4.4; image width = 490 µm).

Table 4.4, Mineral phases and areas of the T10-W0 sample (see Figure 4.17)

Mineral phases	Colour legend	Area (%)
1- C-S-H, Portlandite, Calcite, uCS		23.0
2- Hydrogarnet, uCA		0.2
3- Hydrogarnet with Fe, uCAF		0.8
4- Alkalis		0.1
5- C-A-S-H, hydrogarnet		2.5
6- Silica		50.4
7- Gypsum, Ettringite, Monosulphate		3.7
8- Brucite, Mg minerals		0.6
9- Mg minerals with sulphur		0.7
10- Phases with sulphur and Fe or Al		<0.1
11- Void space		18.0
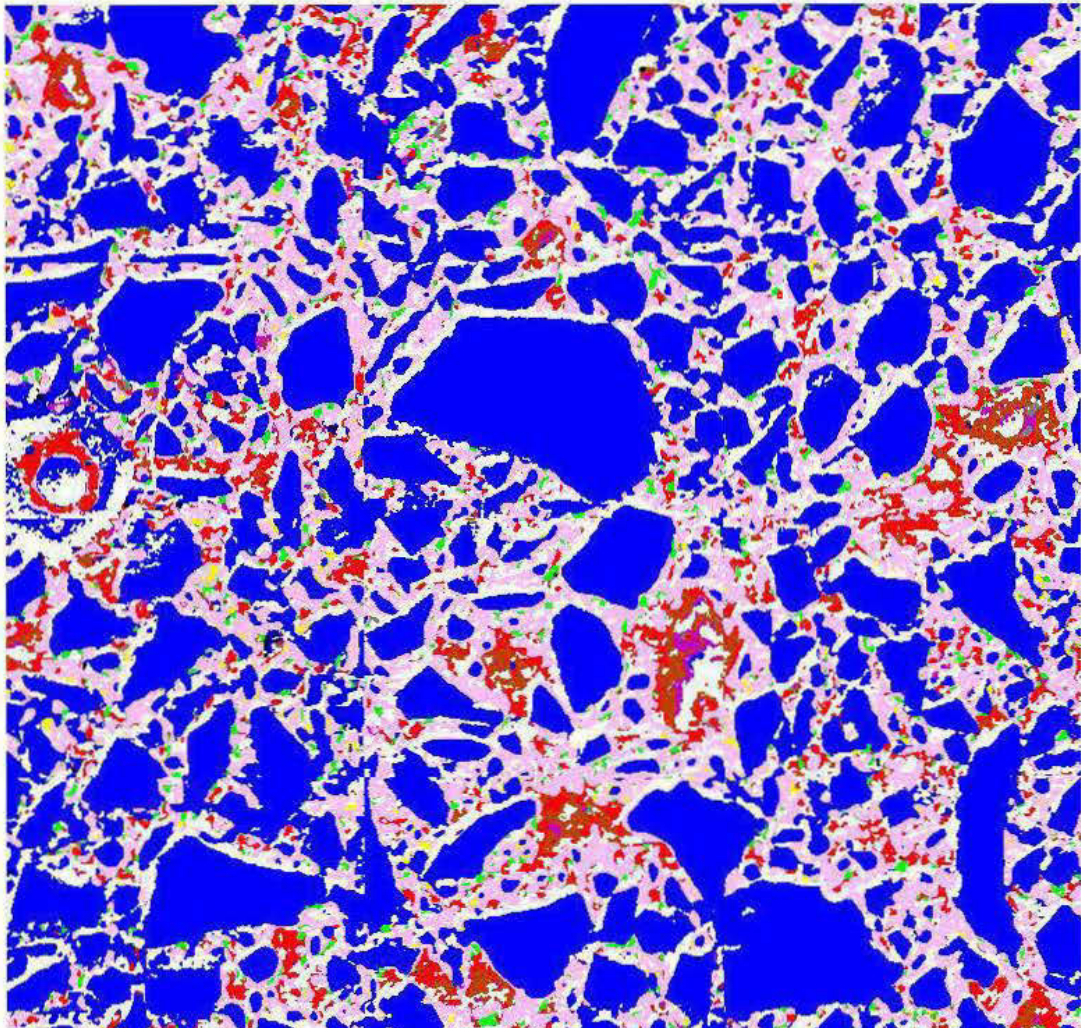
Figure 4.18, Resulting mineralogical image for T10-W1 specimen (colours legend is presented at Table 4.5; image width = 490 µm).

Table 4.5, Mineral phases and areas of the T10-W1 sample (see Figure 4.18)

Mineral phases	Colour legend	Area (%)
1- C-S-H, Portlandite, Calcite, uCS		21.5
2- Hydrogarnet, uCA		0.2
3- Hydrogarnet with Fe, uCAF		1.6
4- Alkalis		0.1
5- C-A-S-H, hydrogarnet		0.5
6- Silica		50.0
7- Gypsum, Ettringite, Monosulphate		4.8
8- Brucite, Mg minerals		0.5
9- Mg minerals with sulphur		1.6
10- Phases with sulphur and Fe or Al		0.1
11- Void space		19.2
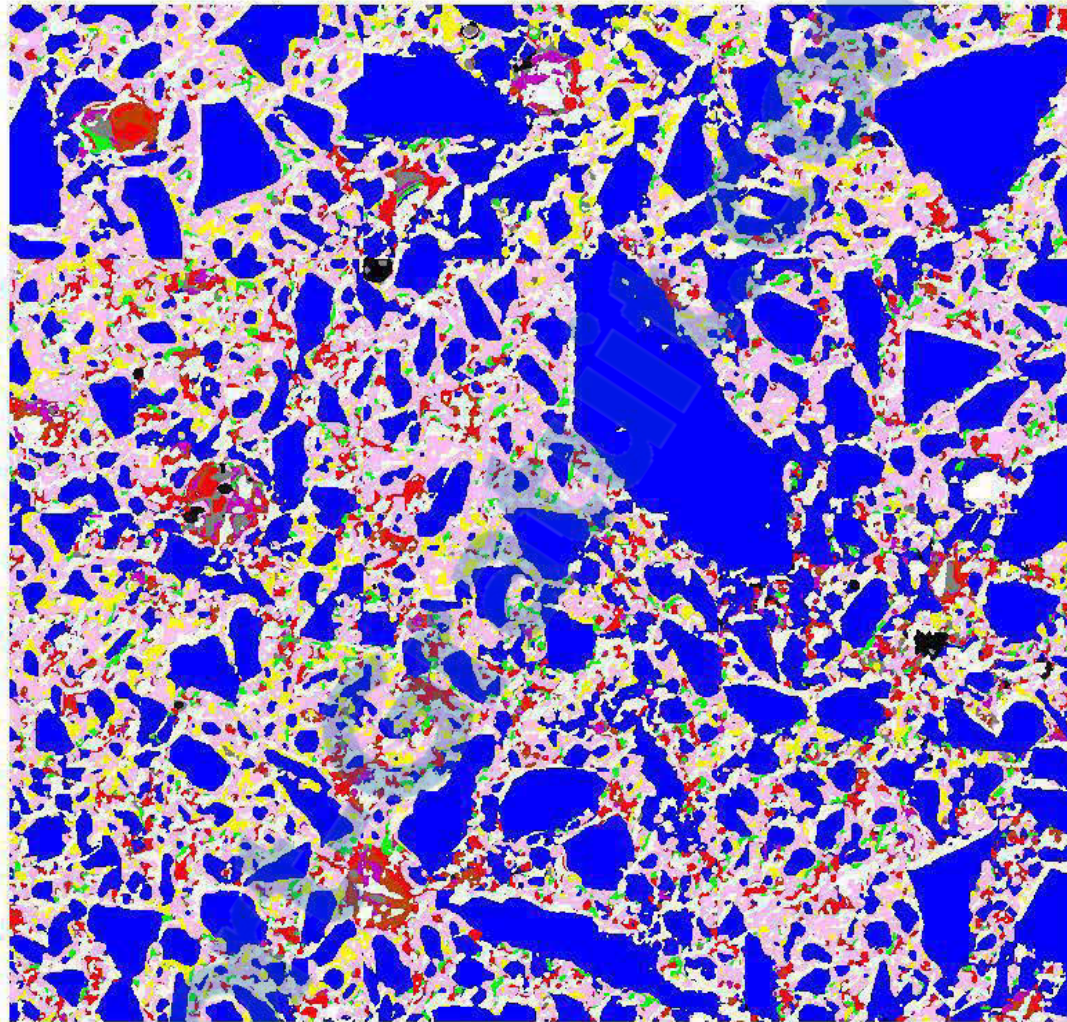
Figure 4.19, Resulting mineralogical image for T10FA-W0 specimen (colours legend is presented at Table 4.6; image width = 490 μm).

Table 4.6, Mineral phases and areas of the T10FA-W0 sample (see Figure 4.19)

Mineral phases	Colour legend	Area (%)
1- C-S-H, Portlandite, Calcite, uCS		22.6
2- Hydrogarnet, Fly ash, uCA		0.9
3- Hydrogarnet with Fe, uCAF		2.1
4- Alkalis, Fly ash		0.4
5- C-A-S-H, hydrogarnet		4.6
6- Silica		43.6
7- Gypsum, Ettringite, Monosulphate		4.8
8- Brucite, Mg minerals		1.0
9- Mg minerals with sulphur		1.2
10- Phases with sulphur and Fe or Al		0.2
11- Void space		18.7
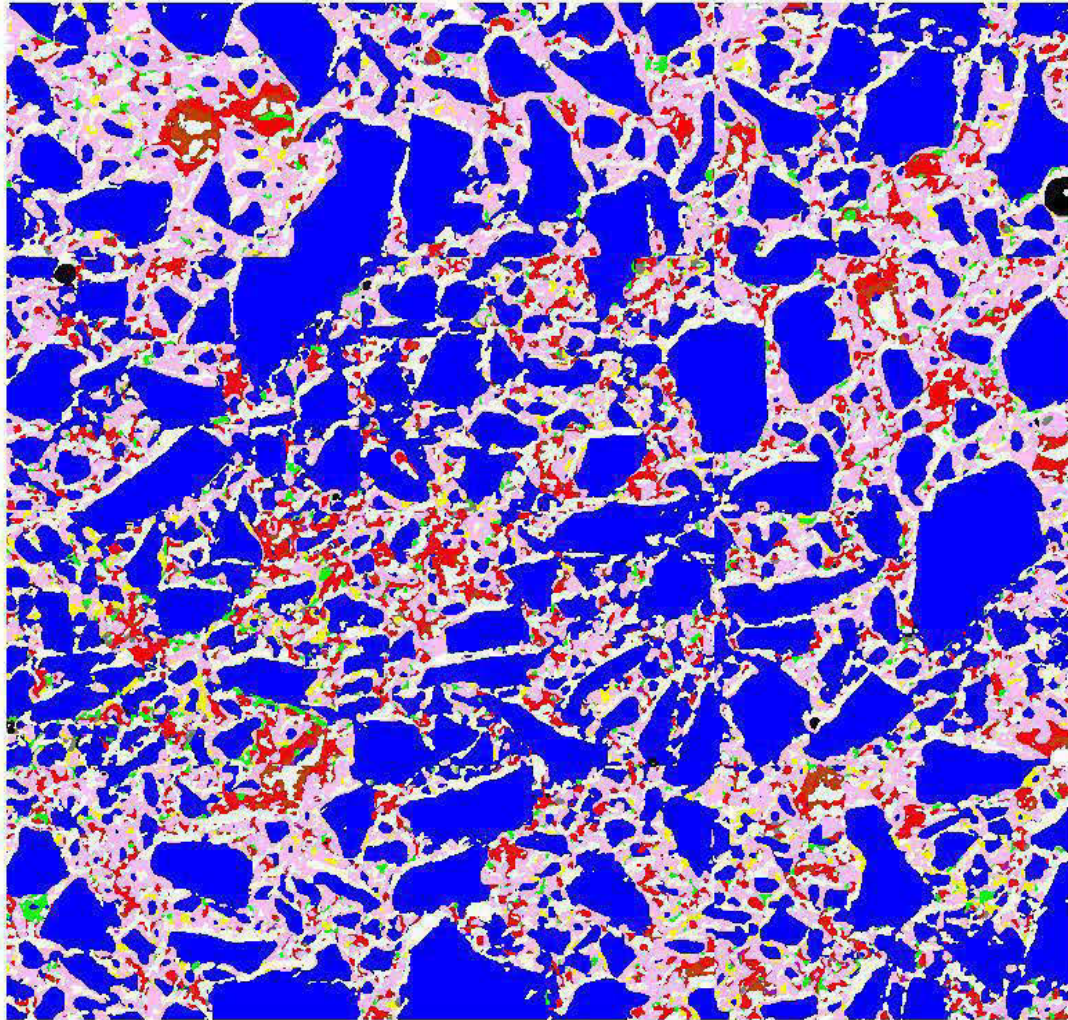
Figure 4.20, Resulting mineralogical image for T10FA-W1 specimen (colours legend is presented at Table 4.7; image width = 490 μm).

Table 4.7, Mineral phases and areas of the T10FA-W1 sample (see Figure 4.20)

Mineral phases	Colour legend			Area (%)
1- C-S-H, Portlandite, Calcite, uCS				21.0
2- Hydrogarnet, Fly ash, uCA				0.3
3- Hydrogarnet with Fe, uCAF				1.4
4- Alkalis, Fly ash				0.2
5- C-A-S-H, hydrogarnet				1.5
6- Silica				49.2
7- Gypsum, Ettringite, Monosulphate				6.7
8- Brucite, Mg minerals				0.2
9- Mg minerals with sulphur				0.8
10- Phases with sulphur and Fe or Al				0.2
11- Void space				18.4
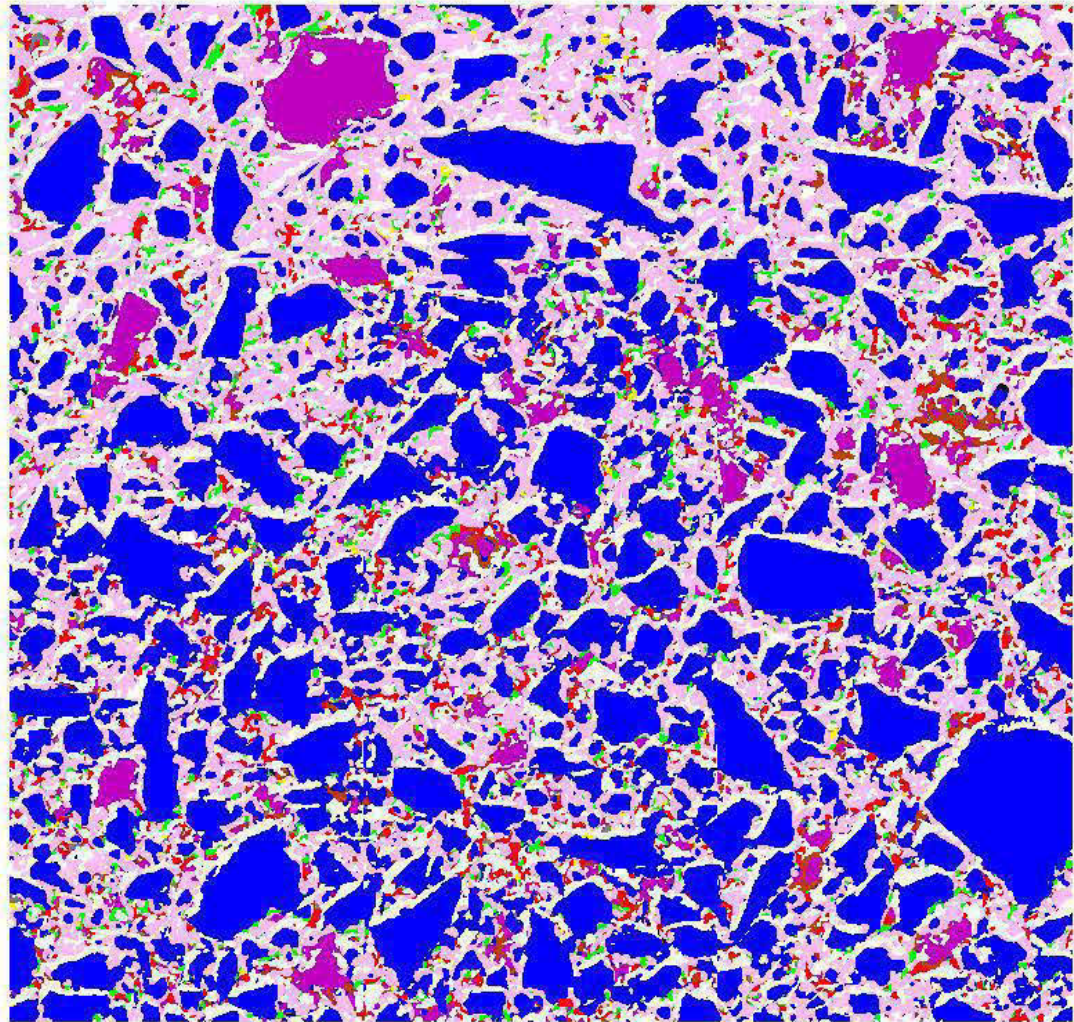
Figure 4.21, Resulting mineralogical image for T10SL-W0 specimen (colours legend is presented at Table 4.8; image width = 490 μm).

Table 4.8, Mineral phases and areas of the T10SL-W0 sample (see Figure 4.21)

Mineral phases	Colour legend			Area (%)
1- C-S-H, Portlandite, Calcite, uCS				26.7
2- Hydrogarnet, uCA				0.3
3- Hydrogarnet with Fe, uCAF				2.0
4- Alkalis				<0.1
5- C-A-S-H, hydrogarnet				0.2
6- Silica				40.6
7- Gypsum, Ettringite, Monosulphate				3.2
8- BFS				5.3
9- Mg minerals with sulphur				1.2
10- Hydrotalcite, M-S-H				0.5
11- Void space				19.9
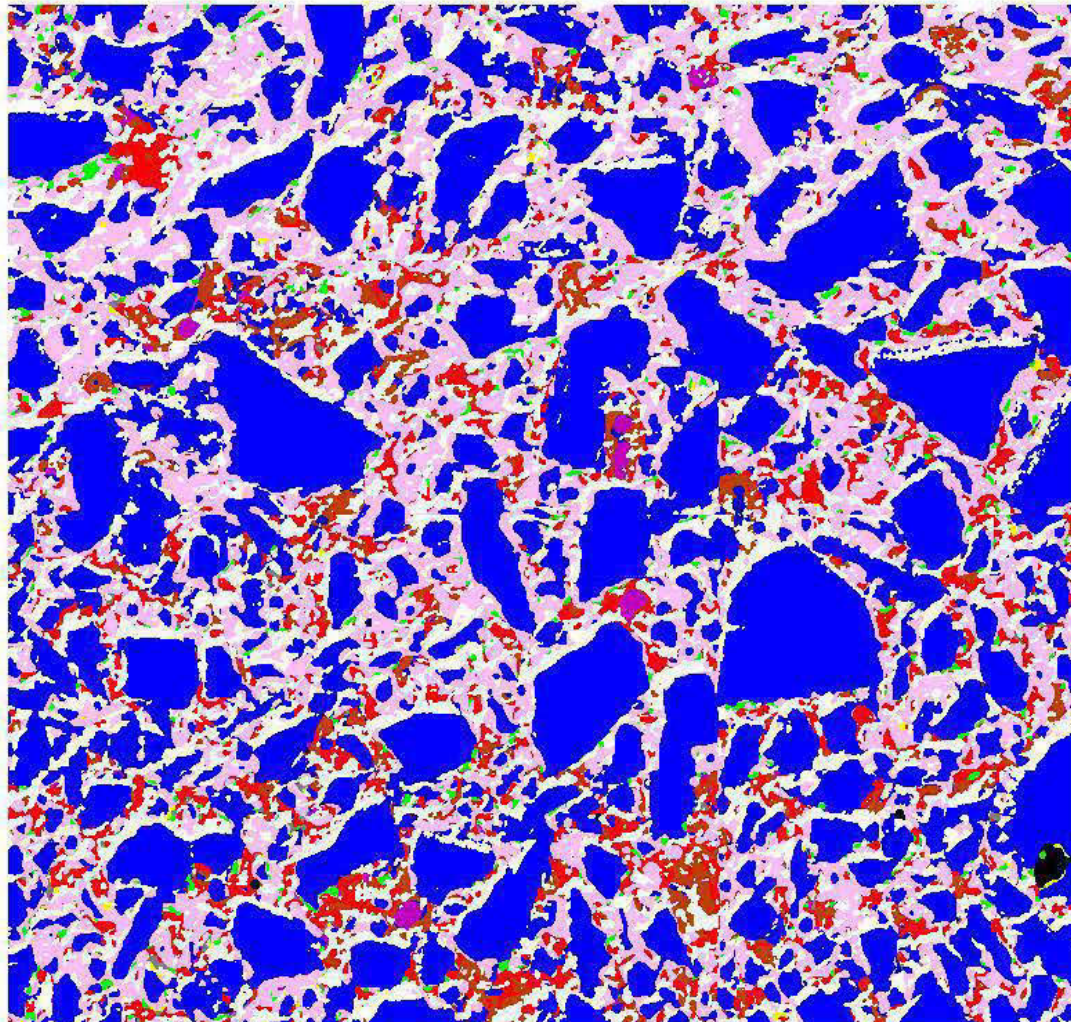
Figure 4.22, Resulting mineralogical image for T10SL-W1 specimen (colours legend is presented at Table 4.9; image width = 490 μm).

Table 4.9, Mineral phases and areas of the T10SL-W1sample (see Figure 4.22)

Mineral phases	Colour legend			Area (%)
1- C-S-H, Portlandite, Calcite, uCS				22.4
2- Hydrogarnet, uCA				0.2
3- Hydrogarnet with Fe, uCAF				1.1
4- Alkalis				0.1
5- C-A-S-H, hydrogarnet				0.2
6- Silica				45.0
7- Gypsum, Ettringite, Monosulphate				6.5
8- BFS				0.5
9- Mg minerals with sulphur				2.9
10- Hydrotalcite, M-S-H				0.5
11- Void space				20.7

4.4.3. Uniaxial compressive strength

Figure 4.23 shows the evolution of the mean UCS values after 14, 28, 90, and 180 days of curing. The strength of CPB samples increases for all samples with curing time. The minimum mean value measured is 288 kPa for T10FA-W0 at 14 days and the maximum mean value measured is 1878 kPa for T10SL-W1 at 180 days. Except for the T10-W0 specimen which acquired a significant gain of strength between 90 and 180 days, all other samples prepared with T10 or T10FA have a similar behaviour and show no water effect. T10SL samples show the highest UCS. The mixture with the sulphated water (T10SL-W1) usually has a greater strength than those with the pure water. Similar mechanical behaviour was observed on CPB samples made of the same silica and binders, but mixed with different sulphated waters (see Chapter 2). An important observation for the UCS results of the studied CPB specimens is that no strength loss related to the internal sulphate attack seems to have happened during the first 180 days of curing.
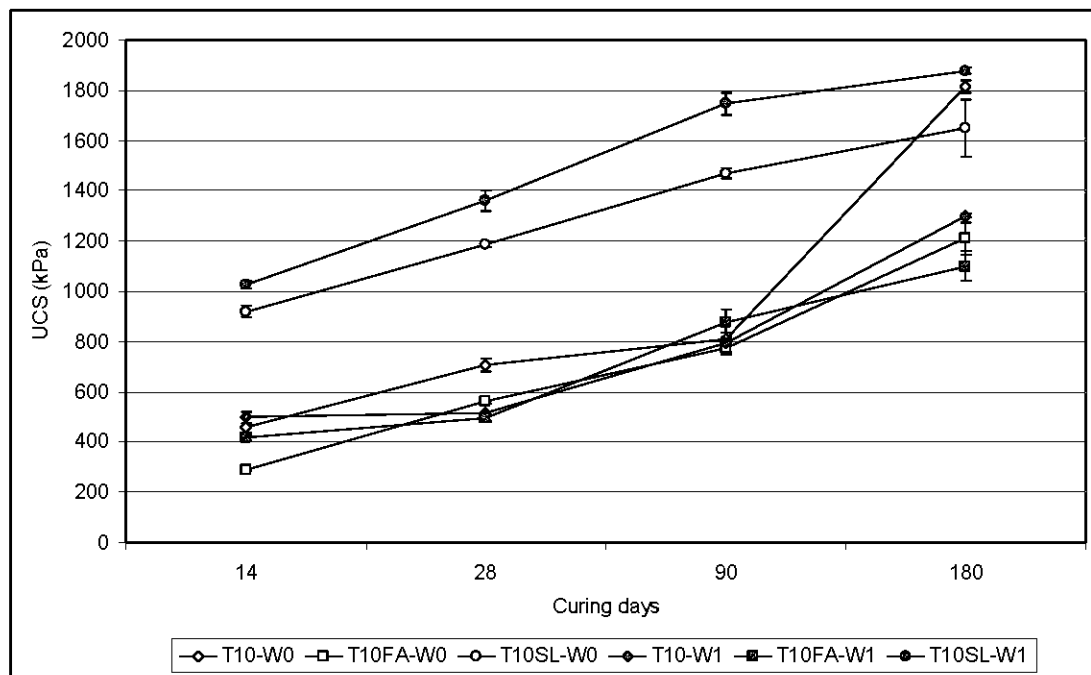
Figure 4.23, Mean UCS results for CPB samples tested at 14, 28, 90, and 180 days; error bars indicate minimum and maximum strength values.

4.5. Discussion

4.5.1. Comparison between SEM-XMAP and TGA/DSC results

In the following, a qualitative comparison between results obtained with SEM-XMAP and with the TGA/DSC methods is presented. Results from both methods seem to indicate that CPB samples made with FA, BFS, and W0 have more unhydrated binders than those made with W1. The reason for this behaviour is not fully understood but the acidity present in the W1 water (pH=3.3) could be pointed out. Abrams (1942) used mine water from coal deposits containing 8570 ppm of acidity as mixing water (see also Steinour, 1960). His results showed that these mixtures with acidic mixing water have a higher strength than the control one. Although these tests were conducted on concrete, they indicate a trend on the behaviour of acidic mixing waters in a cemented mixture. Acidic water (W1 in this study) seems to dissolve more cement in the neutralization process. This neutralization process is also indicated by the presence of portlandite in mixtures T10-W1 and T10FA-W1, meaning that pore solutions of CPB at short curing time are highly alkaline. For the T10SL binder, the products of this neutralization process increases the amount of hydrated cementitious phases and the mechanical strength of CPB samples (see Figure 4.23).

Another important concordance between SEM-XMAP and TGA/DSC results is related to the amount of sulphated minerals in the matrix. Results from SEM-XMAP indicated that the measured area for species associated with sulphur were higher in W1 specimens than in W0 specimens. TGA/DSC results presented in Section 4.2.2 indicate a more important weight loss in the 100°C-250°C region for W1 mixtures (this region can be related to C-S-H and sulphoaluminate/sulphate phases; see Table 4.3). Also, analysis of DTG profiles showed the presence of gypsum and monosulphate. In addition to TGA/DSC and SEM-XMAP methods, chemical analysis of sulphur (as sulphate) were performed using the EPA 600/2-78-054 method

(Sobek et al., 1978) for CPB samples cured for 180 days (see Table 4.10). One can see that the sulphur concentrations in samples mixed with the W1 water are higher than those for samples mixed with W0. However, this method does not provide information on the type of sulphate phase, but it indicates that sulphate minerals are present in samples.

It is however difficult to establish either the sulphated phases identified are true minerals or only a drying artefact. The latter option suggests that part of the S did not precipitate in CPB, but was still in the pore water before the drying step in an ionic form between S^{2-} and SO_4^{2-} (e.g. Appelo and Postma, 1993; Ouellet et al., 2006). The sulphate concentration in CPB interstitial water is often referred as a responsible for internal sulphate attack. In the present study, the concentration in sulphate and the geochemical conditions does not seem to be favourable to the precipitation of minerals that produce the internal sulphate attack phenomenon. In light of the results obtained with the three techniques, one can conclude that sulphated minerals are present in CPB samples and participate (to a certain degree) to the cementation of silica grains. The amount of sulphates is mainly influenced by the initial concentration in the mixing water. However, due to the limitations of the analytical methods used (all of them require a drying of the sample before testing), it is not possible to identify with certainty the sulphated minerals that precipitated in the matrix before the drying of the sample.

Table 4.10, Concentration of sulphur as sulphate in CPB samples (wt. %)

T10-W0	T10FA-W0	T10SL-W0	T10-W1	T10FA-W1	T10SL-W1
0.08	0.07	0.05	0.21	0.19	0.17

The three methods used gave complementary information, and when combined together may lead to a better understanding of the mineralogy of CPB. For example, TGA/DSC can discriminate C-S-H from portlandite and calcite and distinguish gypsum from monosulphate, which can not be done by SEM-XMAP alone. However, TGA/DSC and SEM-XMAP methods point towards the same direction regarding the remaining unhydrated binders and the amount of sulphated phases in samples. Moreover, the SEM-XMAP method allows visualizing the phase distribution in the cementitious matrix, and then gives a better idea of the mineralogical distribution in the different CPB.

4.5.2. TGA/DSC mineralogy and UCS results

The mineralogical characterization of cementious phases contained in CPB samples is a key aspect to understand the mechanical and environmental behaviour of the material. In the following, results from UCS tests are presented in relation with the mineralogy observed. The TGA/DSC analyses were performed at the same curing time as UCS tests, so a comparison can be made for these two tests. Such comparison between TGA and uniaxial compressive strength can also be found for cement base materials (Ramachandran and Beaudoin, 2001); linear relationships between UCS and the amount of portlandite estimated by TGA and the degree of hydration of cement are suggested. For the CPB samples studied, the amount of portlandite measured cannot be used as it decreases and even disappears with the curing time, contrary to the UCS results which increase with curing time. Similarly, as the w/c is high and as the amount of CO_2 has to be removed from the total weight loss to estimate de degree of hydration (e.g. Mounanga et al., 2004), the evaluation of the degree of hydration in CPB samples cannot be determined with accuracy. Nevertheless, TGA and UCS can be compared using the weight loss in the temperature zone related to C-S-H and sulphates (100°C-250°C). Figure 4.24 shows such a comparison.
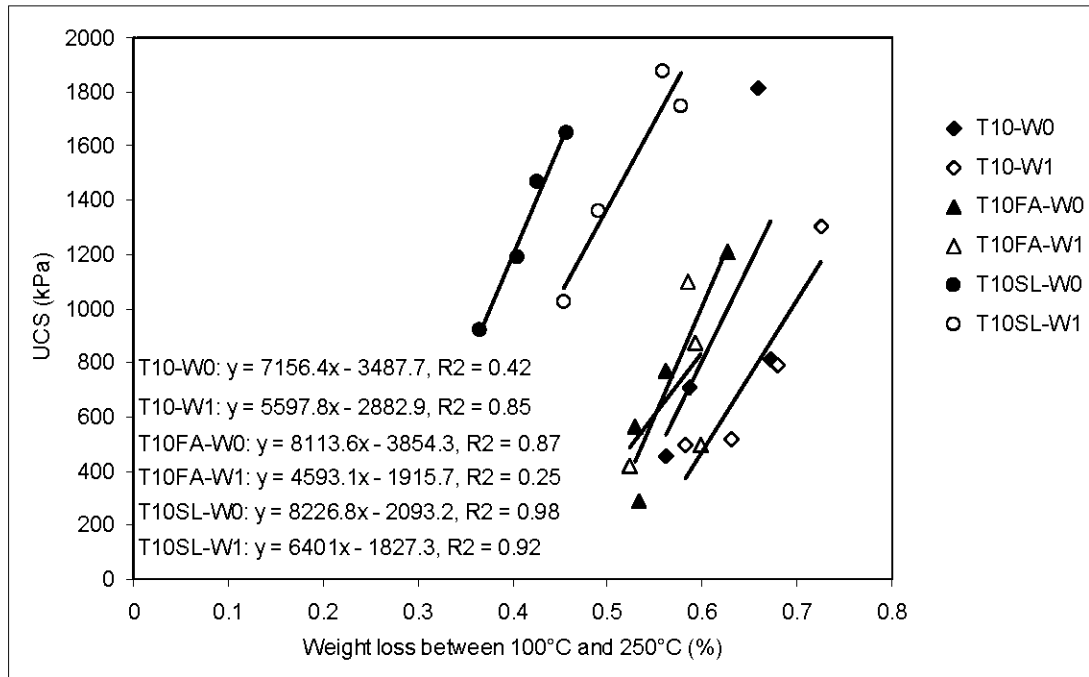
Figure 4.24, Relationships between compressive strength and TG at temperature between 100°C and 250°C.

Using these results (Figure 4.24), linear regressions are calculated to identify the trend between TG results in the region 100-250°C and UCS. For samples T10-W1, T10FA-W0, T10SL-W0, and T10SL-W1 the R^2 values are all higher than 0.85, indicating a good relationship between TG results in the selected temperature zone and UCS. The lowest R^2 are 0.25 and 0.42 for T10-W0 and T10FA-W1 respectively. These values are influenced by two points that are out of the regression curves. When these points are removed the R^2 increases to 0.82 and 0.99 for same samples. Figure 4.24 also shows that results are mainly separated into two families: the T10 and T10FA samples that lose more weight and the T10SL samples that lose less weight but get more strength. This simple comparison shows mainly that a relationship exists between weight lost associated to C-S-H and sulphoaluminate/sulphate phases and the compressive strength of the CPB samples. For instance, one can observe that slopes of regression curves are relatively similar; to the opinion of the authors this indicates a kinetic of hydration that

can be linked together for all mixtures. This aspect would need to be further investigated in the future for different CPB mixtures.

4.6. Conclusion

CPB samples made with silica powder, three binder types, and two types of water (pure water and mine process water) were characterized to investigate the influence of water quality, binder type, and curing time on the strength and on the mineralogy of cementitious phases. Silica was used as aggregate to reduce the interference of aggregate mineralogy during the characterization of the cementitious phases.

The main minerals that participate to the cementation process of the different CPB mixtures have been identified using TGA/DSC and SEM. An imaging method called SEM-XMAP was developed specifically for this study and consists in combining image X-ray dot mapping images and EDS analysis to create mineralogical maps. One advantage of this approach is the visualization of the microstructure and the mineralogy simultaneously. Both methods (TGA/DSC and SEM-XMAP) were complementary to evaluate the mineralogical differences between the CPB mixtures. Some cementitious minerals were found in all CPB samples (C-S-H, monosulphate, calcite, and complex carbonates) while others appeared or not depending on the CPB mixture (e.g. gypsum appeared only in mixtures T10-W0 and T10FA-W0; hydrotalcite appeared only in mixtures made with T10-SL). The behaviour of portlandite is also interesting. This mineral was found by TGA/DSC at early curing times and then disappeared probably due to a pozzolanic effect. Unhydrated blast furnace slag and fly ash particles were also observed by SEM-XMAP.

The study showed a significant impact of water chemistry on the mineralogy of the studied CPB. Chemical analysis revealed a higher sulphate content in CPB samples made with W1 water. Similar finding was obtained by TGA/DSC analysis and with the SEM-XMAP imaging method. Contrary to TGA/DSC that showed the presence of

sulphates (gypsum, monosulphate), SEM observations did not show significant amount of well crystallized sulphated minerals, but mostly sulphated minerals that can be identified as a drying artefact in pores. The UCS results confirm that there was little precipitation of expansive minerals containing sulphates (such as gypsum and ettringite) in the CPB samples, and no decrease of strength was observed during the 180 days of curing.

UCS results from samples mixed with W0 and W1 were in the same range as T10 and T10FA mixtures. However, the water chemistry had a more significant impact for the mixtures made of T10SL samples. The strength differences can be partly explained by T10SL binder hydration and dissolution that seems to be more influenced by the water chemistry than the other two binders. SEM-XMAP and TGA/DSC showed that W1 hydrated more easily the T10SL binder. Since W1 water was acidic, it probably dissolved more cement due to the neutralization process and contributed to increase the amount of precipitated cementitious phases. This suggests that the global chemistry (not only the SO_4^{2-} content) of the water has to be taken into account when studying the behaviour of CPB. UCS tests also correlate relatively well, for a given recipe, to the weight loss evaluated during the TDA/DSC test for temperatures between 100-250°C which are usually related to C-S-H and sulphoaluminate/sulphate minerals, meaning that these minerals are key components for the strength development in CPB.

Finally, the study showed that it is possible to characterize the mineralogy of CPB by combining different (and complementary) characterization methods and by using a mono-mineral aggregate which reduces interferences during signal measurements by SEM and TGA/DSC. However, results also raised other questions that will have to be answered, such as the effect of sulphidic tailings on the cement mineralogy and the relative impact of the mixing water and of sulphides on the internal sulphate attack of CPB. The influence of water chemistry (other than sulphate concentrations) on binder dissolution and hydration is also another aspect that deserves to be

investigated further. In that context, future works should include tests on more complex specimens including highly sulphidic tailings.

4.7. Acknowledgements

4.8. References

Abrams, D.A. (1942). Tests of impure waters for mixing concrete, Journal of American Concrete Institute, 20, 442-486.

Alarcon-Ruiz, L., Platret, G., Massieu E., Ehrlacher, A. (2005). The use of thermal analysis in assessing the effect of temperature on a cement paste, Cement and Concrete Research, 35, 3, 609-613.

Appelo, C.A.J., Postma, D. (1993). Geochemistry, groundwater and pollution, A.A. Balkema, Rotterdam Eds., 536 p.

Bai, J., Chaipanich, A., Kinuthia, J.M., O'Farrell, M., Sabir, B.B., Wild, S., Lewis, M.H. (2003). Compressive strength and hydration of wastepaper sludge ash-ground granulated blastfurnace slag blended pastes, Cement and Concrete Research, 33, 8, 1189-1202.

Belem, T., Benzaazoua, M., Bussière, B. (2000). Mechanical behaviour of cemented paste backfill, Proceedings of the 53rd Annual Conference of the Canadian Geotechnical Society, Montréal, 1, 373-380.

Belem, T., Bussière, B., Benzaazoua, M. (2001). The effect of microstructural evolution on the physical properties of paste backfill, Tailings and Mine Waste'01, Proceedings of the 8th International Conference, Fort Collins, Colorado, USA, 365-374.

Belem T., Benzaazoua, M., Bussière B., Dagenais A.-M. (2002). Effects of settlement and drainage on strength development within mine paste backfill.

Tailings and Mine Waste'02, January 27-30, Fort Collins, Colorado, Balkema, Rotterdam, 139-148.

Bénézet, JC, Benhassaine, A (2001). Contribution des populations granulométriques d'une poudre lors de la réaction pouzzolanique en pâte de chaux, Bulletin Des Laboratoires des Ponts et Chaussées, No 235, p. 59-67

Bentz, D.P., Stutzman, P.E. (1994). SEM analysis and computer modelling of hydration of Portland cement particles, Petrography of Cementitious Materials, ASTM STP 1215, 60-72.

Bentz, D.P., Stutzman, P.E., Haecker, C.J., Remond, S. (1999). SEM/x-ray imaging of cement-based materials, Microscopy Applied to Building Materials, Proceedings of 7th Euroseminar, Delft University of Technology, 457-466.

Benzaazoua, M. (1996). Caractérisation physico-chimique et minéralogique de produits miniers sulfurés en vue de la réduction de leur toxicité et de leur valorisation, Ph.D. Thesis INPL, Nancy, France, 267 p.

Benzaazoua, M., Ouellet, J., Servant, S., Newman, P., Verburg, R. (1999). Cementitious backfill with high sulfur content: physical, chemical and mineralogical characterization. Cement and Concrete Research, 29, 719-725.

Benzaazoua M., Belem, T., Jolette, D., (2000). Investigation de la stabilité chimique et son impact sur la résistance mécanique des remblais cimentés. Rapport IRSST, IRSST ed., R-260: 158p + Annexes.

Benzaazoua, M., Belem, T., Bussière, B. (2002a). Chemical factors that influence the performance of mine sulphidic paste backfill, Cement and Concrete Research, 32, 7, 1133-1144.

Benzaazoua, M., Fall. M., Ouellet, S. (2003a). Étude pluridisciplinaire visant mettre au point un outil expert pour la prédiction du comportement des remblais en pâte. IRSST Research Project 099-085, Final Report, 187 p.

Benzaazoua, M., Belem, T., Ouellet, S., Fall, M. (2003b). Utilisation du remblai en pâte comme support de terrain. Partie II : Comportement à court, à moyen et à long terme. Après-mines 2003, 5-7 Février, Nancy, France, 12 p.

Benzaazoua, M., Belem, T., Fall, M. (2004). A contribution to understand the hardening process of cemented pastefill., Minerals Enginering, 17, 141-152.

Benzaazoua, M., Fiset, J.-F., Bussière, B., Villeneuve, M., Plante, B. (2006). Sludge recycling within cemented paste backfill: Study of the mechanical and leachability properties, Minerals Engineering, 19, 5, 420-432.

Bernier, L. R., Li, M. G., Moerman, A. (1999). Effects of tailings and binder geochemistry on the physical strength of paste backfill, Sudbury'99, Mining and the environment II, Goldsack, Belzile, Yearwood and Hall Eds., Vol. 3, p. 1113-1122.

Bernier, L.R., Li, M. (2003). High temperature oxidation (heating) of sulfidic paste backfill: A mineralogical and chemical perspective, in Proceedings of Sudbury '03, Mining and the Environment III, Laurentian University, Sudbury, Ontario, 9 p.

Bertrand, V.J., Monroy, M.G. and Lawrence, R.W. (2000). Weathering characteristics of cemented paste backfill: Mineralogy and solid phase chemistry, in ICARD 2000 - Proceedings from the 5th international conference on acid rock drainage, May 21-24, Denver, Colorado, 863-876.

Brew, D.M.R., Glasser, F.P. (2005). The magnesia-silica gel phase in slag cements: alkali (K, Cs) sorption potential of synthetic gels, Cement and Concrete Research, 35, 1, 77-83.

Cayouette, J. (2003). Optimization of the paste backfill plant at Louvicourt mine, CIM Bulletin, Canadian Institute of Mining, November/December, 51-57.

Cerný, R., Totová, M., Podebradská, J., Toman, J., Drchalová, J., Rovnaníková, P. (2003). Thermal and hygric properties of Portland cement mortar after high-temperature exposure combined with compressive stress, Cement and Concrete Research, 33, 9, 1347-1355.

Dweck, J., Buchler, P.M., Vieira Coelho, A.C., Cartledge, F.K. (2000). Hydration of a Portland cement blended with calcium carbonate, Thermochimica Acta, 346, 1-2, 105-113.

Dweck, J., Ferreira da Silva, P.F., Büchler, P.M., Cartledge, F.K. (2002). Study by thermogravimetry of the evolution of ettringite phase during type II portland cement hydration, Journal of Thermal Analysis and Calorimetry, 69, 1, 179 - 186.

Fall, M., Benzaazoua, M. (2003). Modeling and simulation of paste backfill performance properties, In: Proceedings of the 56th Annual Canadian Geotechnical Conference and 4th joint IAHCNC/CGS Conference. Winnipeg, September 28–October 1, 161-169.

Fall, M., Benzaazoua, M. and Ouellet., S. (2005a). Experimental characterization of the influence of tailings fineness and density on the quality of cemented paste backfill, Minerals Engineering, 18, 1, 41-44.

Fall, M., Benzaazoua, M. (2005). Modeling the effect of sulphate on strength development of paste backfill and binder mixture optimization, Cement and Concrete Research, 35, 2, 301-314.

Fall, M., Bussière, B., Belem, T., Benzaazoua, M., Samb, S.S. (2005b). Influence of curing temperature on paste backfill properties, 58th Canadian Geotechnical and 6th Joint IAH-CNC and CGS Groundwater Specialty Conferences, Saskatoon, Canada, September 18-21, 7 p.

Feldman, R.F., Ramachandran, V.S. (1971). Differentiation of interlayer and adsorbed water in hydrated portland cement by thermal analysis, Cement and Concrete Research, 1, 6, 607-620.

Frías, M., Cabrera, J. (2001). Influence of MK on the reaction kinetics in MK/lime and MK-blended cement systems at 20°C, Cement and Concrete Research, 31, 4, 519-527.

Georgescu, M., Badanoiu, A. (1997). Hydration process in 3CaO.SiO2-silica fume mixtures, Cement and Concrete Composites, 19, 4, 295-300.

Goldstein, J.I., Romig, A.D., Newbury, D.E., Lyman, C.E., Echlin, P., Fiori, C., Joy, D.C., Lifshin, E. (1992). Scanning Electron Microscopy and X-Ray Microanalysis, 2nd ed., Plenum, New York, 820 p.

Gu, Y. (2003). Automated Scanning Electron Microscope Based Mineral Liberation Analysis: An Introduction to JKMRC/FEI Mineral Liberation Analyser, Journal of Minerals & Materials Characterization & Engineering, 2, 1, 33-41.

Hassani, F., Archibald, J. (1998). Mine backfill, CD-ROM, Canadian Institute of Mining, 263p.

Hassani, F.P., Ouellet, J., Hossein, M. (2001). Strength development in underground high-sulphate paste backfill operation, CIM Bulletin, 94, 1050, 57-62.

Kahn, H., Mano, E.S., Tassinari, M.M. (2002). Image analysis coupled with a SEM-EDS applied to the charactherization of a partially weathered Zn-Pb ore, Journal of Minerals Characterization & Engineering, 1, 1, 1-9.

Kesimal, A., Ercikdi, B. and Yilmaz, E. (2003). The effect of desliming by sedimentation on paste backfill performance, Minerals Engineering, 16, 10, 1009-1011.

Kesimal, A., Yilmaz, E., Ercikdi, B., Alp, I., Deveci, H. (2005). Effect of properties of tailings and binder on the short-and long-term strength and stability of cemented paste backfill, Materials Letters, 59, 28, 3703-3709.

Klimesch, D.S., Ray, A. (1997a). Use of the second-derivative differential thermal curve in the evaluation of cement-quartz pastes with metakaolin addition autoclaved at 180°C, Thermochimica Acta, 307, 2, 167-176.

Klimesch, D.S., Ray, A. (1997b). The use of DTA/TGA to study the effects of ground quartz with different surface areas in autoclaved cement: quartz pastes. Use of the semi-isothermal thermogravimetric technique, Thermochimica Acta, 306, 1-2, 159-165.

Klimesch, D.S., Ray, A. (1998). DTA-TGA of unstirred autoclaved metakaolin-lime-quartz slurries. The formation of hydrogarnet, Thermochimica Acta, 316, 2, 149-154.

Klimesch, D.S., Ray, A., Guerbois, J.-P., (2002). Differential scanning calorimetry evaluation of autoclaved cement based building materials made with construction and demolition waste, Thermochimica Acta, 389, 1-2, 195-198.

Knight, R.D., Klassen, R.A., Hunt, P. (2002). Mineralogy of fine-grained sediment by energy-dispersive spectrometry (EDS) image analysis – a methodology, Environmental Geology, 42, 32-40.

Kovler, K. (1998). Setting and Hardening of Gypsum-Portland Cement-Silica Fume Blends, Part 2: Early Strength, DTA, XRD, and SEM Observations, Cement and Concrete Research, 28, 4, 523-531.

Levens, R.L., Boldt, C.M.K. (1994). Environmental Impacts of Mine Waste Sandfill, Report of Investigations 9493, United States Bureau of Mines, 15 p.

Levens, R.L., Marcy, A.D., Boldt, C.M.K. (1996). Environmental Impacts of Cemented Mine Waste Backfill, RI 9599, United States Bureau of Mines, 23 p.

Mackenzie, R.C. (1972) Differential Thermal Analysis, Academic Press Inc., vol. 2, 607 p.

McCarthy, D.F. (2002). Essentials of Soil Mechanics and Foundations, Prentice Hall, 6th Edition, ISBN: 0-13030-383-6, 788 p.

Mermillod-Blondin, R. (2006). Influence des propriétés superficielles de la pyrite sur la rétention de molécules de type xanthate : Application à la désulfuration des résidus miniers, Ph. D. Thesis, École Polytechnique of Montréal, 333 p.

Mounanga, P., Khelidj, A., Loukili, A., Baroghel-Bouny, V. (2004). Predicting $Ca(OH)_2$ content and chemical shrinkage of hydrating cement pastes using analytical approach, Cement and Concrete Research, 34, 2, 255-265.

Odler, I., Abdul-Maula, S. (1984). Possibilities of quantitative determination of the AFt-(ettringite) and AFm-(monosulphate) phases in hydrated cement pastes, Cement and Concrete Research, 14, 1, 133-141.

Ouellet, J., Benzaazoua, M., Servant, S. (1998). Mechanical, mineralogical and chemical characterization of a paste backfill, Tailings and Mine Waste'98, Colorado, p. 139– 146

Ouellet, J., Hassani, F., Somot, S., Shnorhokian, S., Hossein, M. (2002). Stabilization/solidification of pyritic mill tailings by induced cementation, Tailings and Mine Waste '02 : Proceedings of the 9th International Conference, 27-30 January, 2002, Fort Collins, Colorado, Rotterdam, Balkema, 205-212.

Ouellet, S., Bussière, B., Benzaazoua, M., Aubertin, M., Fall, M., Belem, T. (2003). Sulphide Reactivity within cemented paste backfill: oxygen consumption test results. The 56th Annual Canadian Geotechnical Conference and 4th joint IAH-CNC/CGS Conference. Winnipeg, Manitoba, Canada. September 28 to October 1, 8 p.

Ouellet, S., Bussière, B., Benzaazoua, M., Aubertin, M., Belem, T. (2004) Effect of binder type and mixing water chemistry on microstructural evolution of cemented paste backfill, Proceedings of the 57th Annual Canadian Geotechnical Conference and 5th joint IAH-CNC/CGS Conference, Quebec city, Canada, October 23-27, 8 p.

Ouellet, S., Bussière, B., Mbonimpa, M., Benzaazoua, M., Aubertin, M. (2006). Reactivity and mineralogical evolution of an underground mine sulphidic cemented paste backfill, Minerals Engineering, 19, 5, 407-419.

Perkins, R.B., Palmer, C.D. (1999). Solubility of ettringite (Ca6[Al(OH)6]2(SO4)3 26H2O) at 5-75°C, Geochimica et Cosmochimica Acta, 63, 13-14, 1969-1980.

Petruk, W. (1987). The MP-SEM-IPS image analysis system, CANMET, Report 87-1E, 28 p.

Ramachandran, V.S. (1969). Applications of differential thermal analysis in cement chemistry, Chemical Pub., 308 p.

Ramachandran, V.S., Beaudoin, J.J. (2001). Handbook of Analytical Techniques in Concrete Science And Technology, National Research Council of Canada, Noyes Publications, 985 p.

Ramachandran, V.S., Paroli, R.M., Beaudoin, J.j., Delgado, A.H. (2002). Handbook of thermal analysis of construction material, Noyes Publication, William Andrew Publishing, 680 p.

Ramlochan, T., Grabinsky, M.W., Hooton, R.D. (2004). Microstructural and chemical investigations of cemented paste backfills, Tailings and Mine Waste '04, October 10-13, 2004, Vail, Colorado, 293-304.

Ray, A., Cantrill, E.R., Stevens, M.G., Aldridge, L. (1995). Use of DTA to determine the effect of mineralizers on the cement-quartz hydrothermal reactions. Part 2. Clay addition, Thermochimica Acta, 250, 1, 189-195.

Russ, J.C. (1999). The Image Processing Handbook (3rd ed.), CRC Press, Boca Raton, Florida, 771 p.

Saad Morsy, M., Abo El-Enein, S.A., Hanna, G.B. (1997). Microstructure and hydration characteristics of artificial pozzolana-cement pastes containing burnt kaolinite clay, Cement and Concrete Research, 27, 9, 1307-1312.

Santhanam, M., Cohen, M.D., Olek, J. (2003). Effects of gypsum formation on the performance of cement mortars during external sulfate attack, Cement and Concrete Research, 33, 3, 325-332.

Sha, W., O'Neill, E.A., Guo, Z. (1999). Differential scanning calorimetry study of ordinary Portland cement, Cement and Concrete Research, 29, 9, 1487-1489.

Sha, W., Pereira, G. B. (2001a). Differential scanning calorimetry study of ordinary Portland cement paste containing metakaolin and theoretical approach of metakaolin activity, Cement and Concrete Composites, 23, 6, 455-461.

Sha, W., Pereira, G. B. (2001b). Differential scanning calorimetry study of hydrated ground granulated blast-furnace slag, Cement and Concrete Research, 31, 2, 327-329.

Sharma, R.L., Pandey, S.P. (1999). Influence of mineral additives on the hydration characteristics of ordinary Portland cement, Cement and Concrete Research, 29, 9, 1525-1529.

Shaw, S., Henderson, C.M.B., Komanschek, B. U. (2000) Dehydration/ recrystallization mechanisms, energetics, and kinetics of hydrated calcium silicate minerals: an in situ TGA/DSC and synchrotron radiation SAXS/WAXS study, Chemical Geology, 167, 1-2, 141-159.

Singh, M., Garg, M. (2002). Calcium sulfate hemihydrate activated low heat sulfate resistant cement, Construction and Building Materials, 16, 3, 181-186.

Smart, R.M., Spearing, A.J.S., Harrison, A.T. (1993). The use of silicated backfill in South African gold mines, MINEFILL'93, Johannesburg, SAIMM, 289-294.

Sobek, A.A., Schuller, W.A. Freeman, J.R., Smith, R.M. (1978), Field and laboratory methods applicable to overburden and minesoils, EPA 600/2-78-054, 203 p.

Steinour, H.H. (1960). Concrete mix water – How impure can it be? Journal of the Research and Development Laboratories, PCA, 3, 3, 32-50.

Stutzman, P.E. (2004). Scanning electron microscopy imaging of hydraulic cement microstructure, Cement and Concrete Composites, 26, 8, 957-966.

TA Instruments (2004a). Thermogravimetry Analysis (TGA) Theory & Applications Training, 102 p.

TA Instruments (2004b). Differential Scanning Calorimetry (DSC) Basic Theory & Applications Training, 166 p.

TA Instruments, Determination of calcium sulfate hydrates in cement by DSC, Note TS-26, www.tainst.com, 2 p.

Taylor, H.F.W. (1990). Cement Chemistry, 475 p.

Tian, B., Cohen, M.D. (2000). Does gypsum formation during sulfate attack on concrete lead to expansion?, Cement and Concrete Research, 30, 1, 117-123.

Todor, D.N. (1976). Thermal analysis of minerals, Abacus Press, 256 p.

Ubbriaco, P., Calabrese, D. (1998). Solidification and stabilization of cement paste containing fly ash from municipal solid waste, Thermochimica Acta, 321, 1-2, 143-150.

Ubbriaco, P., Calabrese, D. (2000). Hydration Behaviour of Mixtures of Cement and Fly Ash with High Sulphate and Chloride Content, Journal of Thermal Analysis and Calorimetry, 61, 2, 615 – 623.

Ubbriaco, P., Bruno, P., Traini, A., Calabrese, D. (2001). Fly ASH Reactivity. Formation of hydrate phases, Journal of Thermal Analysis and Calorimetry, 66, 1, 293 - 305.

Vedalakshmi, R., Sundara Raj, A., Srinivasan, S., Ganesh Babu, K. (2003). Quantification of hydrated cement products of blended cements in low and medium strength concrete using TG and DTA technique, Thermochimica Acta, 407, 1-2, 49-60.

Wang, S.-D., Scrivener, K.L. (1995). Hydration products of alkali activated slag cement, Cement and Concrete Research, 25, 3, 561-571.

Wu, C., Li, Z. (2005). A simple method for predicting the spontaneous combustion potential of sulphide ores at ambient temperature, Mining Technology (Trans. Inst. Min. Metall. A), 114, 125-128.

Zhou, Q., Glasser, F.P. (2001). Thermal stability and decomposition mechanisms of ettringite at <120°C, Cement and Concrete Research, 31, 9, 1333-1339.

References for Table 4.3

1	Sha and Pereira, 2001a	19	Kovler, 1998
2	Sha and Pereira, 2001b	20	Klimesch and Ray, 1998
3	Perkins and Palmer, 1999	21	Sharma and Pandey, 1999
4	Feldman and Ramachandran, 1971	22	Shaw et al., 2000
5	Dweck et al., 2000	23	Ubbriaco and Calabrese, 2000
6	Frías and Cabrera, 2001	24	Zhou and Glasser, 2001
7	Mackenzie, 1972	25	Ubbriaco et al., 2001
8	Todor, 1976	26	Ramachandran and Beaudoin, 2001
9	Odler and Abdul-Maula, 1984	27	Singh and Garg, 2002
10	Taylor, 1990	28	Klimesch and al., 2002
11	Ray et al., 1995	29	Dweck et al., 2002
12	Wang and Scrivener, 1995	30	Ramachandran et al., 2002
13	Saad Morsy et al., 1997	31	Cerný et al., 2003
14	Georgescu and Badanoiu, 1997	32	Vedalakshmi et al., 2003
15	Sha et al., 1999	33	Santhanam et al., 2003
16	Klimesch and Ray, 1997a	34	Bai et al., 2003
17	Klimesch and Ray, 1997b	35	Alarcon-Ruiz et al., 2005
18	Ubbriaco and Calabrese, 1998	36	TA Instruments

CHAPITRE V

REACTIVITY AND MINERALOGICAL EVOLUTION OF AN UNDERGROUND MINE SULPHIDIC CEMENTED PASTE BACKFILL[7]

5. Résumé/Abstract

La réactivité d'un remblai cimenté en pâte (RCP) constitué de résidus miniers sulfureux (53% pyrite) a été étudiée dans un chantier souterrain de la mine Laronde (Québec, Canada). Des mesures de consommation d'oxygène (CO) ont été effectuées sur une période de 80 jours. Ces résultats indiquent une forte CO au début de la période d'essai (2.4 mol O_2/m²/jour en moyenne) et une baisse progressive de cette CO pour atteindre 0.2 mol O_2/m²/jour à la fin. La caractérisation physique et minéralogique de même que l'analyse de l'eau des pores du RCP permettent d'affirmer que l'atténuation de réactivité est associée au degré de saturation élevé du RCP, à un enrobement calcique des grains de pyrite et à la formation d'une couche oxydée en surface ayant une porosité plus faible que le RCP sous-jacent. Pour le RCP de la mine Laronde, l'addition de liant apparaît avoir un effet positif sur le comportement environnemental du RCP.

Mots clés : Drainage minier acide, Oxydation, Gestion des résidus miniers, Hydratation, Environnement.

The reactivity of highly sulphidic tailings (53% pyrite) used in a cemented paste backfill (CPB) was investigated at the Laronde mine (Quebec, Canada). Oxygen consumption (OC) tests were performed directly in a mine stope filled with CPB. *In situ* OC test results showed a high oxidation rate at the beginning of the testing period (mean value of 2.4 mol O_2/m²/day). However, the observed oxidation rate decreased progressively to reach a flux value of 0.2 mol O_2/m²/day after 80 days.

The physical and mineralogical characterization of the CPB and the pore water quality evolution indicated that this reduction in the oxidation rate for the Laronde CPB can be related to the high degree of saturation maintained in the material, the possible coating of the pyrite grains, and the formation of a thin oxidized layer having a lower porosity (and lower diffusion coefficient) than the bulk CPB. For the Laronde CPB, the addition of binder to the sulphidic tailings appears to have a positive environmental effect on reactive backfill environmental behaviour.

5.1. Introduction

The management of acid generating tailings is one of the most important environmental challenges for the mining industry. An interesting tailings management approach for underground mines consists of storing tailings in open stopes by using them as constituent of cemented paste backfill (CPB). CPB is prepared at the surface by mixing the total thickened mine tailings (at a pulp density usually between 75 to 85%) with binders (such as Portland cement, fly ash, blast furnace slag) and water. Mixture proportions are adjusted to achieve the required rheological and hardened strength characteristics. The CPB is usually placed in underground stopes via boreholes and pipelines. A survey conducted on 32 mines (Benzaazoua et al., 2005) showed that 44% of the surveyed underground mines in Canada, USA and Australia use CPB as backfilling technology.

Depending on the type of ore extracted at the mine, tailings used in the CPB mixture can contain sulphide minerals (such as pyrite and pyrrhotite) in a proportion varying between 1 to 70% (Goulet and Blais, 2001; Benzaazoua et al. 2003). These minerals are known to be reactive with water and oxygen to produce acidity and iron and sulphate ions (e.g. Lowson, 1982; Evangelou, 1995). Under theses conditions, sulphide oxidation reactions reduce the pH of the leachate which then increases the

solubility and concentration of various elements contained in the tailings (this phenomenon is known as Acid Mine Drainage AMD or Acid Rock Drainage ARD). The combined effect of acidity and solubilised elements can adversely affect nearby waters (surface and underground).

The use of CPB improves ground support while reducing the amount of tailings that has to be sent to surface disposal facilities. This can decrease both the environmental impact and capital expenditures of the surface tailings facility (e.g. Hassani and Archibald, 1998). However, care must be taken not to simply displace the environmental impact, from the surface to the underground. For this, one must assess if tailings are prone to contaminate underground waters. Some authors have investigated the environmental impact of sulphidic backfill material when stored in underground mines. Thomson et al. (1986) concluded that the amount of metal ions released from backfill was negligible. Levens et al. (1992; 1994; 1996) mentioned some advantages related to the utilization of CPB in underground stopes such as the increase of the neutralization potential and the retention of metal ions due to the binder addition, and the decrease of its hydraulic conductivity. Nevertheless, laboratory tests performed by Bertrand et al. (2000) on CPB showed that addition of binders was not sufficient (in the long term) to neutralize the acid generated by the oxidation of sulphide minerals contained in the studied CPB. The ability of CPB to maintain a high degree of saturation (usually greater than 90%; Benzaazoua et al., 2000; 2002; 2004b; Belem et al., 2002; Ouellet et al., 2003) over time is a key aspect to minimize environmental impacts of sulphidic CPB. Indeed, the high degree of saturation reduces oxygen migration through the CPB and consequently minimizes sulphide oxidation reaction (e.g. Elberling et al., 1994; Elberling and Damgaard, 2001; Mbonimpa et al., 2003; Ouellet et al., 2003).

Oxidation of sulphide minerals in CPB is one of the main environmental concerns since it can affect the water quality. One way to evaluate the reactivity of sulphidic wastes (in laboratory and in the field) consists of measuring the consumption rate of oxygen by sulphide minerals. This approach, called the oxygen consumption (OC)

test, was proposed by Elberling et al. (1994) and Elberling and Nicholson (1996). A few other techniques are available in order to measure (directly or indirectly) the reactivity of a sulphidic material, such as the sulphate release method (e.g. Elberling et al., 1994; Bussière et al., 2004) and the oxygen gradient method (Elberling et al., 1994; Yanful et al., 1999). Applicability of such methods is limited in the context of highly sulphidic CPB (especially for underground tests). For instance, the sulphate release method is inapplicable because Portland cement contains gypsum and the installation of oxygen ports in an underground environment (to measure oxygen concentration gradients) is difficult. The main advantages of the OC technique compared to other approaches are the rapid (quasi-instantaneous) estimation of the oxygen consumption, the relative simplicity of the technique, and its applicability to both laboratory and field conditions. Ouellet et al. (2003) performed a comparative laboratory OC study on five tailings containing different proportions of pyrite (4% to 74% wt.) and on CPB prepared with these tailings using two binders: a 50:50 mixture of Portland cement type 10 and type 50 and a 20:80 mixture of Portland cement type 10 and ground granulated blast furnace slag. Results obtained on tailings showed that the degree of saturation played a significant role on OC; for instance, for a given sulphidic waste, the OC rate was 2 orders of magnitude higher at a degree of saturation of 50% compare to that at 90%. Results on CPB indicated that over the 60-day testing period (for all types of binder), the sulphidic CPB samples oxidized only near the exposed surface; the reacting layer typically has a thickness of less than 1 mm (as was also observed by Chapman et al. (2003) on CPB containing 40% of pyrite). CPB was shown to be effective to limit oxygen diffusion into the material, due to its ability to maintain a high degree of saturation (>85%) close to the surface. The CPB containing 74% of pyrite had an OC rate of less than 1 mole $O_2/m^2/day$ at the end of the testing period (value much lower than similar sulphidic tailings without binder (e.g. Tibble and Nicholson, 1997; Bussière et al., 2004).

In this paper the authors present the results of oxygen consumption tests performed in an underground stope to evaluate the *in situ* reactivity of the Laronde mine CPB. A detailed characterization of the superficial oxidized layer and the evolution of the

CPB interstitial pore water chemistry over the testing period are also presented. The main objectives of this study were to investigate the evolving reactivity of a highly sulphidic CPB over time using OC tests, to understand the mechanisms explaining the variation of this reactivity, and ultimately to evaluate the environmental effects (and potential benefits) of incorporating sulphidic tailings into CPB. To the author's knowledge, this is the first attempt to evaluate CPB reactivity directly in an underground stope.

5.2. Materials and methodology

5.2.1. Tailings properties

Field tests were performed at the Laronde mine, Quebec, Canada, one of deepest mine in North America at a depth of 2240 metres below the surface. The daily production is approximately 7250 metric tons of ore (gold, silver, copper and zinc), resulting in a production of approximately 6150 tons of sulphidic tailings (dry mass) each day; nearly 25% of the tailings are returned underground as CPB.

Table 5.1 shows X-Ray Diffraction (XRD) analysis and ICP analysis results of the studied tailings. XRD results (see section 2.3.3.1 for XRD methodology details) show a high proportion of pyrite (53.6%) in the tailings. The other important minerals are quartz (25.7%), paragonite (6.8%), muscovite (4.6%), and albite (2.5%). The observed mineralogy is in accordance with the chemical analysis where Fe and S are the most abundant elements at 31.3% and 24.9% respectively. The high proportion of pyrite is also responsible for the high specific gravity (G_s) of 3.72 of the tailings. The volumetric grain size distribution evaluated with a Malvern Mastersizer S shows that 50% of particles have a diameter smaller than 23 μm (D_{50}). The uniformity coefficient ($C_U = D_{60}/D_{10}$) and the coefficient of curvature ($C_C = D_{30}^2/D_{60}xD_{10}$) are respectively 8.58 and 0.94. The BET multipoint surface area of the

tailings is 1.75 m²/g. According to USCS classification (e.g. McCarthy, 2002), the Laronde tailings can be classified as a non plastic silt (ML), like most of the tailings produced by hard rock mines (e.g. Aubertin et al., 2002). The tailings interstitial water was also sampled; Table 5.2 shows the ICP analysis results. Tailings water contains some metal species (e.g. 0.68 ppm of Al, 3.01 ppm of Cu and 0.16 ppm of Zn) and relatively high sulphate content (i.e. 5662 ppm; based on a stochiometric conversion assuming all sulphur ions in the sulphate form). These ions induce an electric conductivity of 7070 µS/cm. The calcium concentration in tailings water is also significant (767 ppm) and is mainly due to an ore processing technique that uses lime to increase the pH to a value of 9.6.

Table 5.1, ICP-AES analysis and XRD quantification results on tailings and CPB

ICP-AES Analysis (%)		XRD Rietveld Quantification (%)			
Element	Tailings	Minerals	Tailings	Unoxidized CPB	Oxidized CPB
Al	3.20	Albite	2.5	3.5	3.0
As	0.03	Ankerite	1.0	-	-
Ca	0.43	Calcite	0.0	0.4	7.5
Cr	0.03	Chlorite	1.8	1.4	1.4
Cu	0.10	Ettringite	0.7	2.7	0.8
Fe	31.30	Goethite	0.2	0.2	0.2
K	0.04	Gypsum	1.2	1.2	0.5
Mg	0.09	Hematite	-	2.1	2.3
Mn	0.02	Muscovite	4.6	6.9	5.9
Na	0.85	Paragonite	6.8	6.0	7.8
Pb	0.17	Pyrite	53.6	53.5	47.2
S	24.90	Quartz	25.7	22.0	22.8
Se	0.19	Siderite	-	0.1	0.6
Zn	0.69	Sphalerite	0.8	-	-

Table 5.2, ICP-AES analysis of tailings interstitial water and mixing water

Element	Tailings water (ppm)	Added mixing water (ppm)
Al	0.68	0.24
As	<0,03	<0,03
Ca	767	28
Cu	3.01	0.03
Fe	0.02	0.47
Mg	0.92	4.51
Mo	0.21	0.00
Na	338.0	2.3
K	53.5	6.6
S	1890.1	91.7
Si	0.77	2.91
Zn	0.16	0.06
pH	9.63	7.56
EhN (mV)	233.3	313.4
Cond. (µS/cm)	7070	300

5.2.2. Binder and mixing water

The studied mine stope (volume of 6600 m³) at the -2150 m level of the Laronde mine was filled in two sequences: a first one using cemented paste backfill with a binder content of 7% wt. to create a strong base in the stope and a second one using 5% wt. of binder to fill the remaining volume with cemented rock fill. The time needed to completely fill the stope was approximately one month. The binder used at the mine was a 50:50 mix of Portland cement Type 10 and Type 50 (a sulphate resisting Portland cement). The chemical quality of the mixing water is presented in Table 5.2. This water was pumped from a nearby lake. Its pH is close to neutrality and its conductivity is low, resulting from the low ions concentration in solution. The pulp density (solid percentage) of CPB was adjusted at 74% using this water.

5.2.3. Methods

5.2.3.1. Underground OC tests

When the stope was accessed, three aluminium cylinders (tapered at one end), 15 cm in diameter and 33 cm long, were inserted approximately 12 cm inside the surface of the exposed CPB (see Figure 5.1). CPB faces inside each cylinder were then trimmed to be perpendicular to the cylinder axes. The resulting oxygen chamber had a 24 cm height for each cylinder. High vacuum grease was applied all around the contact zone outside the cylinder to avoid preferential flow along the cylinder wall. Specially-designed aluminium caps allowing installation of an oxygen sensor were placed on the cylinders before each OC test.
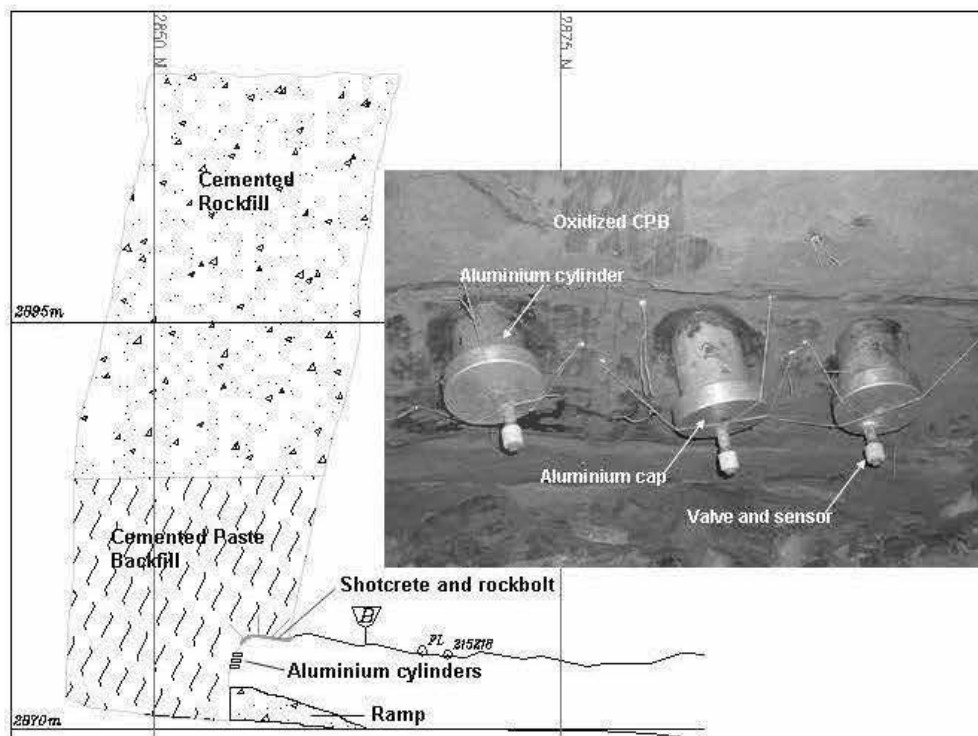
Figure 5.1, Sketch of the stope filled with CPB, and a picture (during an OC test) of the three aluminium cylinders (15 cm in diameter) inserted in CPB.

OC tests of 2-3 hours duration were performed underground in a relatively hot and humid atmosphere ($\approx$29°C and 70% RH). The OC tests were conducted each week for the first three weeks (Day 1, 7 and 14), and on Day 27, 41, 55, and 80 thereafter. Caps were removed after each test to allow oxidation of the CPB surface. Oxygen sensors manufactured by GC Industries (model GC33-200) were used to measure oxygen concentration. This sensor is made of a galvanic electrochemical cell using the Pb-PbOOH half-cell to reduce oxygen reaction (the consumption of oxygen by the sensor is considered negligible for short duration tests, see Tibble and Nicholson, 1997 for details). The voltage produced by this reaction is directly proportional to the partial pressure of oxygen in the gas phase. The sensor is accurate to a 0.1% O_2 concentration; its operating temperature is between 0 and 45°C.

5.2.3.2. Oxygen flux evaluation

The OC test consists of measuring the decrease of oxygen concentration in a sealed air chamber placed over the studied material for a short period of time. These measurements quickly provide a quasi-instantaneous sulphide oxidation rate. Examples of laboratory and field measurements with this technique can be found in the literature (e.g. Elberling et al., 1993; 1994; Nicholson et al., 1995; Elberling and Nicholson, 1996; Tibble and Nicholson, 1997; Bussière et al., 2002; 2004; Mbonimpa et al., 2002; 2003). These studies were mainly performed to evaluate oxidation rate of mine tailings without binder.

The relationship between oxygen flux (or sulphide reactivity) and the decrease in oxygen concentration in the sealed chamber is based on fundamental gas diffusion laws (here, only Fickian gas transport mechanisms are considered). Solving Fick's second law expressed with a first-order kinetic reaction term and for specified boundary conditions gives the following equation for the oxygen flux F_L (or sulphide

reactivity) under pseudo-steady state conditions (Elberling et al., 1994; Elberling and Nicholson, 1996):

$$F_L = C_0 (K_r D_e)^{\frac{1}{2}} \tag{1}$$

where K_r is the first-order reaction rate coefficient (corresponding to sulphide oxidation rate), D_e is the effective diffusion coefficient and C_0 is the initial (atmospheric) concentration of oxygen.

Fractional order dependence of sulphide oxidation on oxygen concentration has been found in literature (e.g. Li et al., 2000). For instance, Strömberg (1997) evaluated the consumption kinetic order of two sulphidic waste rock samples at 0.79 and 0.55 while Jerz and Rimstidt (2004) calculated an exponent of 0.5 for pyrite oxidation in a sealed chamber. However, based on the field results obtained by Li et al. (2000) on nearly saturated sulphidic tailings, it can be assumed that the oxygen consumption calculated using a kinetic order of 1 or 0.5 are almost similar. Thus, a first order kinetic is adopted in this study.

Solving the continuity equation (which reflects the oxygen being depleted in the head space) for the initial condition $C = C_0$ at $t = 0$, the following solution is obtained (Elberling et al., 1994; Elberling and Nicholson, 1996):

$$\ln(C/C_0) = -t (K_r D_e)^{\frac{1}{2}} (A/V) \tag{2}$$

where A and V are the area and the volume of the source reservoir respectively. The slope of the $\ln(C/C_0)$ versus time plot gives the value of $-(K_r D_e)^{\frac{1}{2}}$ when A/V is known. $-(K_r D_e)^{\frac{1}{2}}$ is substituted into Eq. (1) to evaluate the flux of oxygen at the surface, which is deemed to represent the oxygen consumption by sulphide oxidation reaction. The standard OC test applies for a small change in oxygen concentration (2 to 3% O_2) in the headspace over a one to three hour period. The change in oxygen concentration

within the pore spaces is considered insignificant during the testing period to comply with the interpretation assumption of steady state flux. More details on the interpretation method for the standard OC method are given in Elberling et al. (1994), Elberling and Nicholson (1996), and Mbonimpa et al. (2002; 2003).

5.2.3.3. Analytical methods to characterize the oxidized layer

Under its usual placement conditions, CPB can maintain a high degree of saturation over time (e.g. Belem et al., 2001; 2002; le Roux et al., 2002; Ouellet et al., 2003; Benzaazoua et al., 2004a; Godbout et al., 2004). The high water content reduces oxygen availability and consequently the oxidation of sulphide minerals contained in the CPB. Nonetheless, previous laboratory studies (Ouellet et al., 2003; Chapman et al., 2003) and *in situ* observations have shown that oxidation occurs in CPB, mainly near exposed surfaces. Therefore, a part of this study focused on the characterization of the relatively thin oxidized layer at the surface and on the comparison between the characteristics of the internal unoxidized CPB and the oxidized layer. To characterize the two materials, X-Ray Diffraction (XRD), Thermogravimetry Analysis/Differential Scanning Calorimetry (TGA/DSC), and Scanning Electron Microscopy (SEM) observations were performed.

5.2.3.3.1. X-Ray Diffraction

Tailings and CPB samples were analysed on a Bruker A.X.S. D8 Advance using a cobalt radiation source and scintillation detector. Samples were scanned over a 2-theta range of 5° - 70° with a 0.005° step size. Minerals quantification was done using the Rietveld method (Young, 1995) through the Bruker's TOPAS software. Prior to XRD, samples were grinded in alcohol using a McCrone micronizing mill to reduce crystallite sizes to approximately 10μm. Reported accuracy of the Rietveld

method is 0.2% for a simple two-phase test; the accuracy can decrease depending on the peak overlap degree of phases, on the quality of the crystallization, on the preferential orientation, and on the degree of micro-absorption of X-Rays (Raudsepp and Pani, 2003). While samples studied here were scanned overnight (using at least 10 scans of the same sample); the adopted experimental conditions induce an accuracy and detection limit of approximately 0.2% and 0.5% respectively. The interested reader can find more details on Rietveld method applied to wastes mineralogy in Raudsepp and Pani (2003).

5.2.3.3.2.   Thermogravimetry and differential scanning calorimetry

TGA/DSC tests were performed using the SDT Q600 apparatus from TA Instruments which allows simultaneous registry of weight loss and heat flow along thermal treatment of the sample. Thermal behaviours were registered in an inert nitrogen atmosphere at a rate of 20°C/min up to 1200°C with a 30 minutes delay at 50°C to remove free water from the samples. Approximately 30 mg of material was used for each test. More details on these methods are given by Todor (1976) and by Höhne et al. (2003).

5.2.3.3.3.   Scanning electron microscopy

A small sample extracted from the CPB face was cut transversally to study the oxidized layer and the unoxidized material underneath. Once that sample was dried, vacuum impregnated with low viscosity epoxy, polished and gold coated, SEM observations were performed in the secondary electron mode at high vacuum (< 0.1 Pa), using a primary voltage of 20 keV and a working distance of 15 mm. These observations provided an estimate of the oxidized depth and of the porosity of both zones. As epoxy resin fills backfill pores and as its density is less than surrounding

material, the evaluation of the porosity was performed by an image analysis technique (e.g. Lange et al., 1994; Diamond and Leeman, 1995) adapted to study CPB microstructure (see Chapter 3). Captured images were at 800x magnification with a resolution of 3.13 pixels/µm; each image covered an area of 163 µm x 117 µm. The mean porosity values presented here can be considered as the true total porosity of the material with a tolerated statistical error of less than 2% and a confidence level of 95%. In addition, Energy Dispersive X-Ray Spectrometry elemental profiles were acquired across the oxidized zone at a magnitude of 3000x to investigate the secondary mineralogy. The spatial resolution of the EDS detector is approximately 2 µm under the used conditions.

5.2.3.4. Pore water chemistry

Pore solutions of *in situ* samples were extracted after each OC test with the stainless steel die press method (e.g. Barneyback and Diamond, 1981). Such technique allows recovering interstitial water (or pore solution) from a porous material without adding water. A minimum amount of material from the oxidized layer was used (sample thickness $\leq$ 5 mm) to provide a sufficient volume of fluid ($\approx$ 40 ml). Pore solutions were collected with a 20 ml syringe and then filtered with a 0.45 µm cellulose syringe filter prior to analysis. pH and redox potential (Eh) were measured using the Benchtop pH/ISE Meter Orion model 920A with a coupling of different electrodes. An Orion Triode electrode was used for the pH and the Eh was measured with a Pt/Ag/AgCl combined electrode and then corrected for normal hydrogen electrode. Following these measurements, the extracted solutions were acidified with a 0.4% (v/v) nitric acid and total dissolved content was determined by ICP-AES technique.

The pore solution was analysed on each testing day (Day 1, 7, 14, 27, 41, 55 and 80). These chemical analyses were used to follow the evolution of some ion species (S, Zn, Ni, Cu, Fe) and to perform thermodynamic geochemical modelling. The

geochemical modelling provided the Saturation Indices (SI) of ettringite, ferrite-Ca, goethite, gypsum and hematite over the testing period. SI is defined as:

$$SI = \log(IAP/K_{sp}) \tag{3}$$

where IAP is the ion activity product and K_{sp} the solubility product constant of the solid phases. The equilibrium geochemical speciation/mass transfer balance model PHREEQC (Parkhust and Appelo, 1999) in combination with the Lawrence Livermore National Laboratory (LLNL) database were used. This computer code calculates mineral SI and suggests mineral phases that may control the pore water quality. A SI value greater than 0 signifies that IAP > K_{sp} and that the indicated mineral would precipitate under these conditions. A negative SI value means that IAP < K_{sp} and that the indicated mineral would (remain) dissolve. A SI equal to 0 indicates equilibrium conditions.

5.3. Oxygen consumption tests results

For all OC tests performed, oxygen concentration decreased significantly in the reservoir over a relative short period of 2-3 hours. Figure 5.2 (see the window on the upright) shows typical results from OC tests recorded at Day 41.
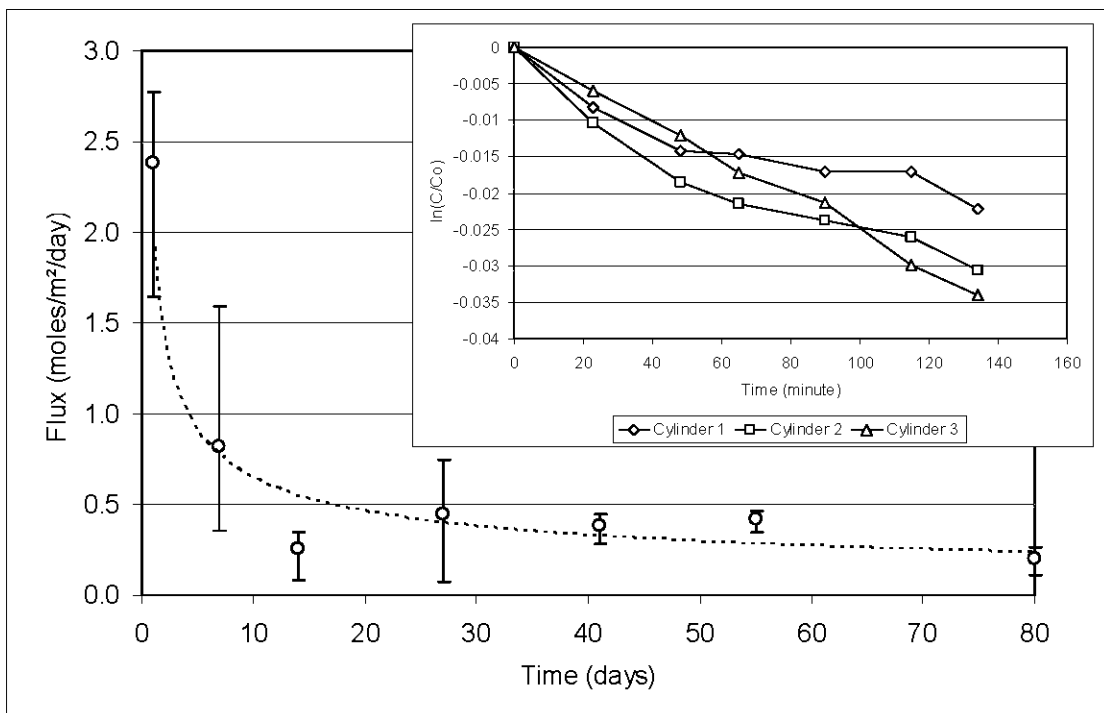
Figure 5.2, Evolution of the oxygen consumption in the field. Circles represent the mean flux and the brackets the minimum and maximum values recorded; the regression line is presented as an indicative trend. The upright figure shows an example of the oxygen concentration evolution during an OC test.

The slope values $-(K_rD_e)^{1/2}$ of the $ln(C/C_0)$ versus time plots are relatively similar for the three cylinders; they range between -1.39E-04 min^{-1} and -2.54E-04 min^{-1}. For each *in situ* OC test, the slopes were used to calculate oxygen flux (or sulphide reactivity) with Eqs. (1) and (2). Figure 5.2 presents mean oxygen flux values (circle points) for the three cylinders over the testing period; power fit regression (dashed line) is shown as an indicative trend of the oxygen consumption evolution. Brackets on each side of the mean flux show the minimum and maximum values measured.

Figure 5.2 indicates that the variability of the measurements is relatively high at the beginning. No apparent difference between the cylinders and the methodology can explain this behaviour. However, the measurements are less variable for the last 3 series of tests and the tendency is then much clearer. The CPB reactivity was relatively high during the first weeks and decreased over time. The mean oxygen flux

measured in the field during the first series of OC tests was 2.4 mol $O_2/m^2/day$; this flux decreased to approximately 0.3 mol $O_2/m^2/day$ after 14 days. The mean oxygen flux then reached an apparent steady-state, at a value between 0.2 and 0.4 mol $O_2/m^2/day$. The reactivity measurements for the three cylinders after 80 days were all under 0.3 mol $O_2/m^2/day$ with a mean value of 0.2 mol $O_2/m^2/day$.

Water content (w = mass of water over mass of solid) was measured over the testing period using field samples. The water content values ranged between 23 to 25 %, which corresponds in this case to a degree of saturation (S_r) greater than 90%. Oxygen transport in fine-grained material is generally controlled by molecular diffusion in the air phase when saturation is below 85%. For S_r values higher than 85%, the air phase is discontinuous and the amount of oxygen is limited by diffusion in water and by the maximum dissolved concentration of O_2 (Corey, 1957; Mbonimpa et al., 2003). However, as observed by Ouellet et al. (2003), the material can be locally desaturated at the surface due to exchanges with the ambient air.

5.4. Characterization of the oxidized zone

Oxidation mechanisms of pure sulphide minerals and of sulphidic mine tailings are relatively well understood (e.g. Lowson, 1982; Evangelou, 1995; Strömberg, 1997). However, oxidation of reactive tailings in the presence of hydrated cement has not been as extensively studied, and is hence poorly understood. As seen in the previous section, the studied CPB is almost fully saturated in the field. Nonetheless, local desaturation of the CPB is possible at the exposed surface and this can then induce oxidation products. At the Laronde mine, a thin oxidized layer (ochre secondary minerals) was apparent at the surface of the CPB face. This layer seemed to "protect" pyrite grains beneath from oxygen. To better understand the influence of this oxidation layer on the reactivity of fresh (unoxidized) tailings, a mineralogical characterization was performed using the different equipments and techniques presented in section 2.3.3. The pore water quality was also used to

identify probable secondary minerals precipitated in the oxidation layer through geochemical modelling.

5.4.1. SEM observations

Figure 5.3 shows a thresholded image of a CPB sample taken after 41 days at 200x magnification, where the oxidation limit was manually drawn. Based on the image resolution, the thickness of this zone is estimated to be between 200 and 400µm. Other samples were taken during the testing period and the thickness of the oxidized layer was nearly the same. 25 images were also captured at 800x magnification (163µm wide) in both the oxidized and the unoxidized zones to evaluate the porosity of the two zones using image analysis. The estimated porosity value in the oxidized zone was 21.4% ± 1.5 compared to 39.1% ± 1.7 in the fresh CPB zone. As mentioned previously, this oxidized layer seems to act as a protective layer for the subjacent material. SEM images (Figure 5.3) indicate that precipitated secondary minerals filled the initial porosity of the CPB. This in turn would tend to decrease the oxygen effective diffusion coefficient (D_e) by increasing the tortuosity, consequently limiting the ingress of oxidation in the CPB.

Another factor that could affect the reactivity of the Laronde CPB is the coating of pyrite grains by secondary minerals (e.g. Zhang and Evangelou, 1996; Holström et al. 1999; Cruz et al., 2001). A picture at 3000x magnitude in the oxidized layer can be seen in Figure 5.4. This figure shows amorphous phases filling the pores, some silicates, and an unweathered pyrite grain that is typical of other pyrite grains observed in the polished section. The EDS X-Ray profiles of calcium, sulphur, iron and silicon along the line crossing the pyrite grain are presented on the right hand side of the figure. These profiles show that sulphur seemed to be absent in the secondary mineral phases. They also reveal the presence of a coating around the pyrite grain that contains calcium (the two humps in the Ca profile outside the pyrite grain) and possibly iron and silicon. The presence of this coating means that, for the
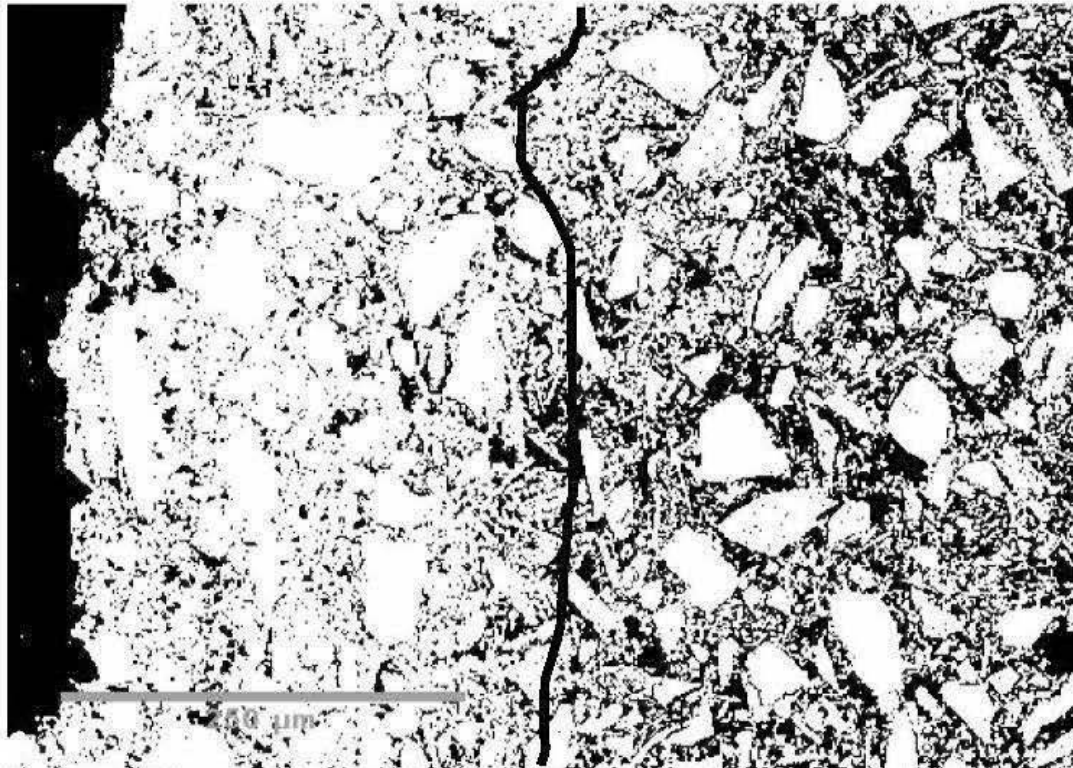
Figure 5.3, Binary image at 200x magnification (653µm x 470µm) showing the porosity in black (epoxy) and grains in white. The black line approximates the oxidation zone limit.
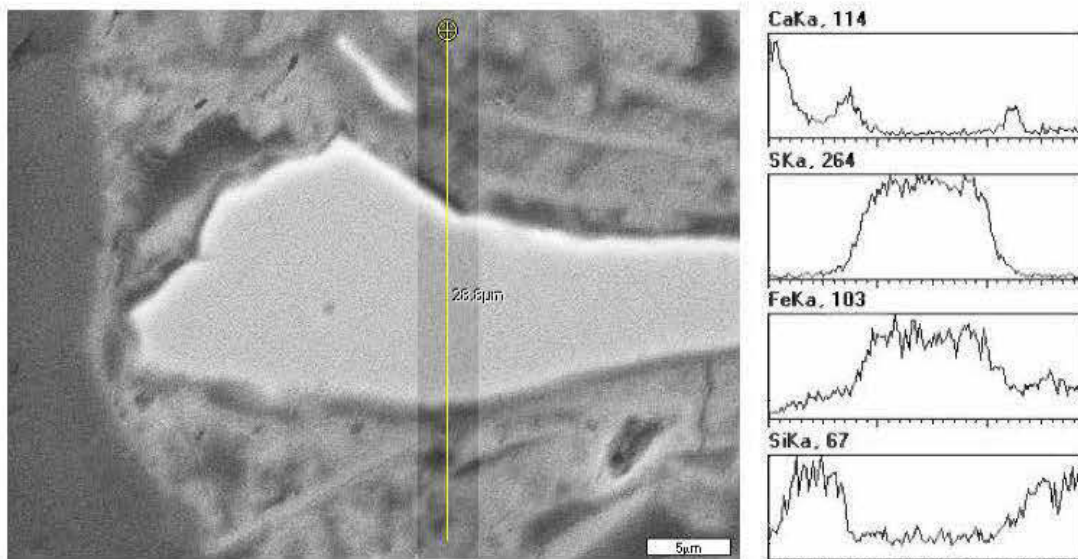
Figure 5.4, Image of the oxidized layer at 3000x magnitude and EDS spectrum of 4 elements (at the right) along the line crossing a pyrite grain.

geochemical conditions observed in the oxidized layer, some secondary minerals would precipitate. This could be armouring pyrite grains against oxygen, which eventually would reduce the reactivity of the sulphidic CPB.

5.4.2. XRD analysis

Table 5.1 shows XRD quantification results using TOPAS software (Rietveld method) for the unoxidized and the oxidized CPB. Results show that pyrite content decreased from 53% (unoxidized) to 47% (oxidized). It can be inferred that the decrease in pyrite content is mainly the result of the direct oxidation of this mineral by oxygen. This is also confirmed by ICP-AES chemistry analysis of the CPB (results not presented). Calcite, almost entirely absent in the fresh sample, increased to 7.5% in the oxidized layer. The presence of a non-negligible amount of calcite in the oxidized layer was unexpected, but it is consistent with carbonation mechanisms involving surrounding carbon dioxide. Carbonation in cement based materials is relatively well known (e.g. Taylor, 1990). Following the hydration of the main clinker phases ($3CaO \cdot SiO_2$ "C_3S" and $2CaO \cdot SiO_2$ "C_2S"), calcium-silicate-hydrate ($3CaO \cdot 2SiO_2 \cdot 3H2O$, "C-S-H", representing about 75% of the cement paste) and portlandite ($Ca(OH)_2$, "CH") are formed (see Taylor, 1990; Neville, 1981) according to the followings:

$$C_3S + H_2O \rightarrow C\text{-}S\text{-}H + CH \tag{4}$$
$$C_2S + H_2O \rightarrow C\text{-}S\text{-}H + CH \tag{5}$$

When CO_2 is freely available under favourable Eh/pH conditions, the following reactions can take place with C-S-H and CH:

$$CH \rightarrow Ca^{2+} + 2OH^- \tag{6}$$
$$CaO \cdot SiO_2(aq.) + H_2O \rightarrow Ca^{2+} + 2OH^- + CaO \cdot SiO_2(aq.) \tag{7}$$

$$CO_2 + 2OH^- \rightarrow CO_3^{2-} + H_2O \tag{8}$$

$$Ca^{2+} + CO_3^{2-} \rightarrow CaCO_3 \tag{9}$$

These precipitates can form a dense rim made largely of $CaCO_3$ on the surface of cemented material. This was already demonstrated on weathered CPB samples (Benzaazoua, 1996).

On the other hand, oxidation of pyrite produces H^+ that interact with the available cations (Blowes and Ptacek, 1994):

$$FeS_2 + 7/2O_2 + H_2O \rightarrow Fe^{2+} + 2SO_4^{2-} + 2H^+ \tag{10}$$

$$CaCO_3 + H^+ \rightarrow Ca^{2+} + HCO_3^- \tag{11}$$

$$HCO_3^- + Fe^{2+} \rightarrow FeCO_3 + H^+ \tag{12}$$
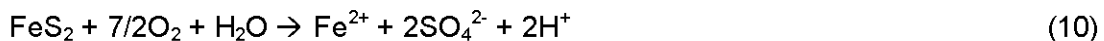
Competition between these different ions can however be quite complex, so more research is needed to better understand the processes involved. Nonetheless, XRD results indicate that calcite production dominates over siderite ($FeCO_3$) which seemed to have been produced only in small quantity in the oxidized layer (0.6%). Hematite (Fe_2O_3) appears to be present in both samples as a minor phase. The amount of sulphate minerals seems to decrease slightly in the layer; gypsum ($CaSO_4 \cdot 2H_2O$) proportion decreased from 1.2% to 0.6% and ettringite ($Ca_6Al_2(SO_4)_3(OH)_{12} \cdot 26(H_2O)$) dropped from 2.7% to 0.8%. However, gypsum and ettringite are not necessarily the results of secondary minerals formation since gypsum is a constituent of the Portland cement and ettringite is formed by the cement hydration process.

XRD analyses did not identify new secondary mineral in the oxidized layer. The inability of the XRD technique to identify clearly the presence of secondary minerals could be explained in part by the crystallographic quality of the secondary minerals precipitated; as mentioned by Bigham (1994), these minerals are often poorly crystallized or amorphous, and thus ignored by XRD analysis.

5.4.3. DTA/DSC analysis

A DTA/DSC analysis requires only 20 to 30 mg of material, and the result is not affected by crystal quality. Figure 5.5 shows DTA/DSC curves for unoxidized and oxidized CPB samples. Unoxidized CPB thermal analysis showed mainly the presence of pyrite with an important endotherm at 628°C that is characteristic of the loss of one sulphur atom from pyrite to form pyrrhotite (Todor, 1976; Mayoral et al., 2002). At approximately 1127°C, the fusion of pyrrhotite appeared with the presence of an endothermic peak and a weight loss. Calcium carbonate can be identified by a weight loss at 722°C as it loses carbon dioxide. The small endotherm having its optimum at 98°C and the small DTA hump at 125°C can be associated respectively with calcium silicate hydrate (C-S-H) gel and ettringite (Ramachandran et al., 2002). Results of DTA/DSC analysis presented on the oxidized CPB layer have been obtained on a sample taken at Day 41; another analysis was performed after 80 days and results were similar. The endothermic effect in the 100-300°C zone is related to minerals containing water. As mentioned previously, these minerals could be C-S-H gel and ettringite. Since this temperature range induced slightly more weight loses for the oxidized sample than for the unoxidized one, some other sulphate and ferrous hydroxide could be present. Endothermic effects at 587°C and 1127°C can be related to the decomposition of the remaining pyrite. Endothermic peaks at 524°C and 722°C could be due to CO_2 removal from siderite (Todor, 1976) and calcium carbonate respectively. As seen on DTA curves (and contrary to XRD results), the amount of calcium carbonate seemed to be the same in the oxidized sample and in the unoxidized one. Hematite was also a potential secondary mineral based on the DTA/DSC analysis. Indeed, a small exotherm starting at 1170°C was observed for the oxidized sample while the control unoxidized sample showed an endotherm at the same temperature. Moreover, as mentioned by Mayoral et al. (2002), the presence of hematite in a mixture with pyrite decreases the desulphuration temperature of the pyrite (which can be seen in Figure 5.5 by a shift from 628 to 587°C).
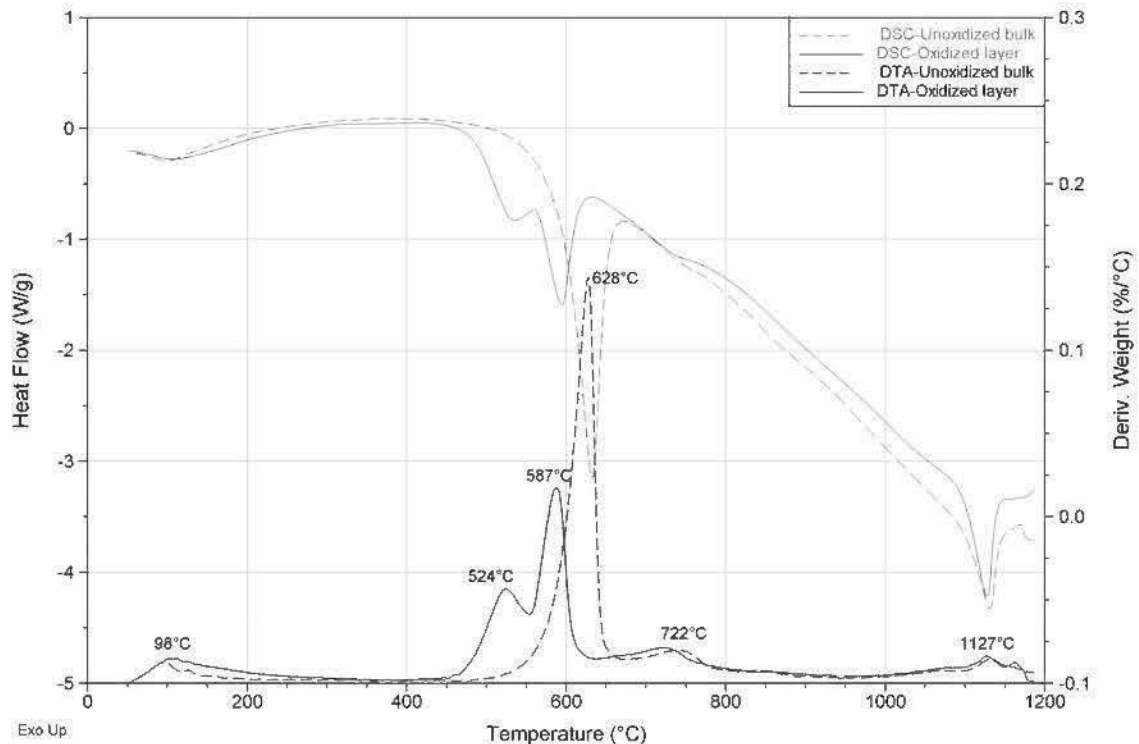
Figure 5.5, First derivative of the weight loss (DTA) and heat flow (DSC) profiles of thermal decomposition of the oxidized layer and the unoxidized CPB.

5.4.4. Pore water analysis

Figure 5.6 shows the chemical analysis of some elements and the pH of the pore solutions extracted with the stainless steel die press method. The pH value of the interstitial water ranged between 13.05 and 9.87, with a tendency to decrease with time. The pH and the chemistry of the pore solution from the fresh sample "41-internal" taken at Day 41 were similar to the ones measured at the beginning of the testing period (Day 1), indicating that no significant change occurred beneath the oxidized crust after 41 days. The pore solutions from the oxidized layer were significantly different than the ones from the unoxidized zone. The sulphur concentration reached 69 g/l in the pore water at 14 days, indicating that pyrite oxidized in the layer and that sulphur ions were in an aqueous form. According to Appelo and Postma (1993), at a pH in the range observed for the pore solutions, the

major sulphur species should be thiosulphate under a form or another between sulphide (S^{2-}) and sulphate (SO_4^{2-}). Ptacek and Blowes (2003) report the same range of soluble sulphur content in AMD, for a pH value that can become lower than one.

Figure 5.6 shows also the evolution of some metal species in the pore solutions. The concentration of zinc was 0.4 ppm at the beginning of the testing period and then decreased to less than 0.1 ppm after 7 days. Nickel concentration was always less than 0.1 ppm and copper was lower than the detection limit (0.01 ppm) almost at all time. As with other metal species, iron content was low in the pore solutions, with a maximum concentration of 0.7 ppm. Considering the high sulphur concentration, this observation suggests that iron ions precipitated in the surface layer since both elements were mainly the results from pyrite oxidation. Figure 5.6 also shows that the only time metal species were all present (in significant concentration) in the solution was on Day 41. At that time the pH was less than 10, this could indicate that solubility of metals in the CPB would increase when pH decreases.

Thermodynamic equilibrium modelling was performed, mainly to reinforce observations drawn by XRD and TGA/DSC. It also provides information about the behaviour of sulphate minerals in the bulk CPB and in the oxidized layer. Assuming that pore solutions were at equilibrium, PHREEQC Version 2.8 was used to evaluate saturation index of different minerals. Available concentrations (in mg/l) of ions obtained from CPB pore solutions were used as input data. The ionic strength of these pore solutions was high (0.2 to 1.5 molal) with three of the eight samples showing an ionic strength > 1 molal. Because PHREEQC shows some limitations when ionic strength is above 0.5 (Ptacek and Blowes, 2003), the data were also processed using Visual MINTEQ Version 2.32 (Gustafsson, 2005) with the modified Debye-Huckel option (including the B-dot term) that can address ionic strength up to 1 molal (and beyond: e.g. Bethke, 1996). The calculated results are almost similar with both programs. As PHREEQC offers more possibilities about ions selection and database availability, it has been retained for the bulk of the authors analyses.
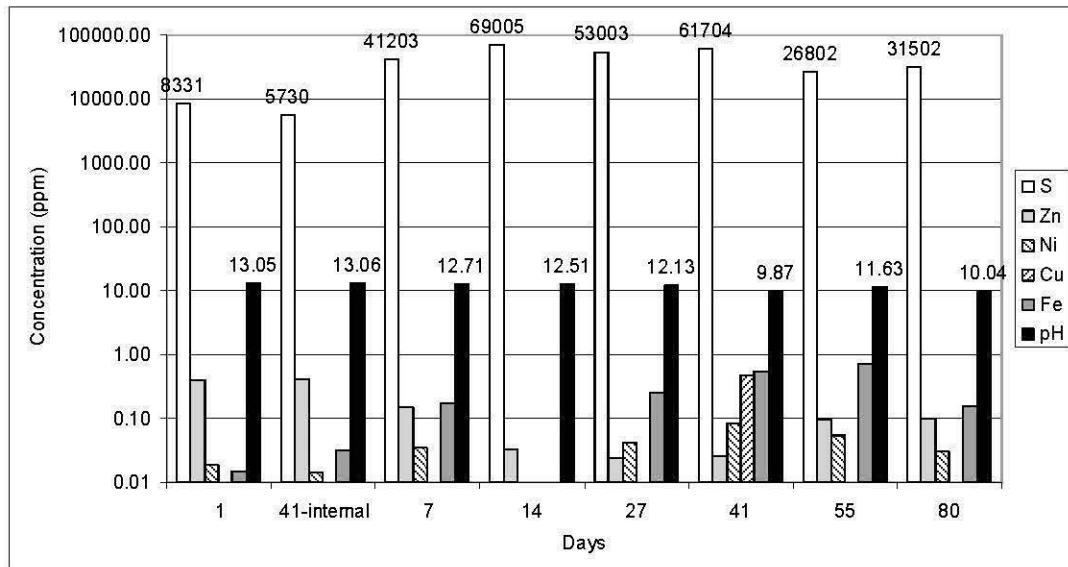
Figure 5.6, Evolution of the pH, sulphur and some metal species in the CPB pore solutions.

Figure 5.7 presents the calculated values of the evolution of the saturation index (SI) for some potential secondary minerals. As seen in this figure, ferrite-Ca, goethite and hematite were oversaturated at all time. This is in agreement with TDA/DSC results. Ettringite was slightly oversaturated at the beginning of the testing period, but became undersaturated after 14 days. Ettringite is naturally formed in a cementitious material when clinker phase $3CaO \cdot Al_2O_3$ hydrates in the presence of gypsum (e.g. Taylor, 1990). The period of time for ettringite oversaturation could correspond to the main hydration phase of cement in the CPB. Gypsum was close to equilibrium during the entire testing period; as mentioned above, this mineral participates to the formation of ettringite, but it can equally represent the only sulphate that precipitated in the oxidized layer during all the tests. TGA/DSC results on oxidized layer are in conformity with this latter assumption, as a larger mass was lost at 200°C for this sample than with the unoxidized sample. Except for gypsum, the geochemical conditions did not favour the precipitation of secondary sulphate minerals, which is again consistent with water quality and mineralogical characterization results.
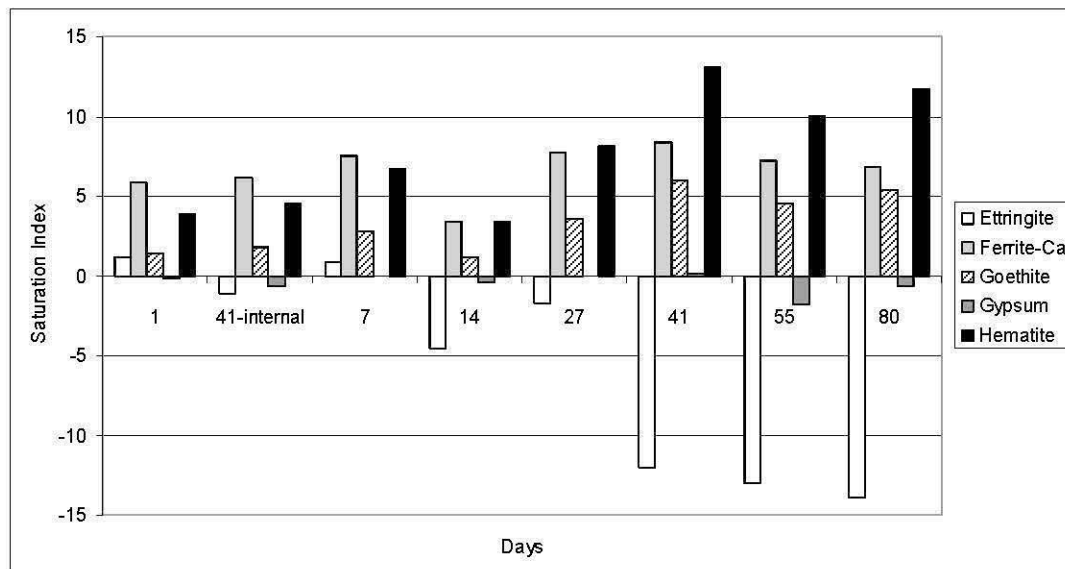
Figure 5.7, Calculated values of the saturation indices (SI) evolution of some secondary minerals over the testing period.

5.5. Discussion and conclusions

This study presented results of OC tests that were used to evaluate the reactivity of a sulphidic CPB. The tests were performed directly in an underground stope at the Laronde mine, Quebec, Canada. The *in situ* OC tests showed a high mean oxidation rate at the beginning of the testing period (2.4 mol $O_2/m^2/day$). The oxidation rate decreased progressively to reach a value near 0.3 mol $O_2/m^2/day$ after 14 days, and then stabilized between 0.2 and 0.4 mol $O_2/m^2/day$ afterward. The final mean oxygen flux was 0.2 mol $O_2/m^2/day$ after 80 testing days. This rate is significantly lower than the ones reported in literature for similar tailings without binder; typically, the oxygen flux for highly sulphidic tailings varies between 0.8 and 5.5 mol $O_2/m^2/day$ (Elberling et al., 1993, 1994; Elberling and Nicholson, 1996; Bussière et al., 1998, 2004). The higher oxidation rate measured at the beginning is attributed to the surface oxidation of the fresh CPB. The reduction of oxygen consumption with time at the Laronde mine could be due to different factors. First, the oxidation phenomenon created a thin oxidized layer (200 – 400 μm) having a lower porosity than the unoxidized CPB

due to the precipitation of secondary minerals (a porosity of 21% rather than 39% for the unoxidized CPB). This thin low porosity layer combined with the high degree of saturation of the material limits oxygen diffusion inside the material. However, it is important to note that samples used to evaluate the degree of saturation came from the bottom of the stope and consequently this behaviour is not necessarily the same elsewhere in the backfilled opening (especially near the top). Some results presented in the literature suggest that CPB is almost saturated in the field (e.g. Ouellet and Servant, 2000), but further tests are needed to confirm this and to evaluate the environmental behaviour at higher levels in the stope. Secondly, SEM images showed that the pyrite reactivity is reduced by the formation of a coating at the surface of pyrite grains. This coating appears to be made of different secondary minerals such as hematite, goethite and ferrite-Ca. Hence, the relatively low oxygen consumption by the sulphidic CPB at the end of the testing period would be due to the high degree of saturation of the CPB. Also, the oxidized layer has a lower porosity than the bulk CPB, and there is evidence of coating on pyrite grains in the thin oxidized layer. The combination of these factors limits further oxygen consumption by the CPB at the Laronde mine.

The mineralogical characterization of the CPB leads to a better understanding of the geochemical behaviour of the Laronde CPB. XRD and TGA/DSC analyses showed a decrease in the pyrite content in the oxidized layer (confirming that there is pyrite oxidation at the CPB surface) and the possible presence of siderite and hematite. However, no secondary sulphate mineral was identified by these techniques. Chemical analysis of the pore solutions extracted from the CPB revealed that Eh/pH conditions were unfavourable for sulphur ions precipitation in the oxidized layer. These results also showed that pH of the interstitial solutions decreased slightly during the project duration (from 13.05 to 10.04 over 80 days). Extrapolation of this behaviour (to pH lower than 10) could eventually bring favourable conditions for sulphate precipitation on the outer oxidized layer. Two long term scenarios can then be suggested: i) since some sulphate minerals precipitation is associated with a volume expansion, such precipitation could generate cracks at the surface of the

CPB structure and expose fresh CPB (oxygen diffusion would be increased at the surface) and; ii) a pH drop decreases the pollutant stabilization ability of the CPB and formation of AMD is possible at the exposed CPB surface. However, for the time life of a typical underground mine, these phenomena should be minor and structural stability of the CPB should not be an issue.

As a final remark, one can conclude that the binder in the Laronde sulphidic paste backfill induces a positive effect on the environmental behaviour of the tailings. This addition reduces oxygen migration and consumption through the CPB, and consequently limits the formation of acid mine drainage.

5.6. Acknowledgements

5.7. References

Appelo, C.A.J. and Postma, D. (1993). Geochemistry, groundwater and pollution, A.A. Balkema, Rotterdam Eds., 536 p.

Aubertin, M., Bussière, B. and Bernier, L. (2002). Environnement et gestion des rejets miniers, Manual on CD-ROM, Presses Internationales Polytechnique, Montreal.

Barneyback, R.S. and Diamond, S. (1981). Expression and analysis of pore fluid from hardened cement pastes and mortars. Cement and Concrete Research, 11, 279-285.

Belem, T., Benzaazoua, M., Bussière, B., Dagenais, A.-M. (2002). Effects of settlement and drainage on strength development within mine paste backfill. In: Proceedings of the Conference Tailings and Mine Waste'02, Balkema, Fort Collins, p. 139-148.

Belem, T., Bussière, B. and Benzaazoua, M. (2001). The effect of microstructural evolution on the physical properties of paste backfill, Proceedings of Tailings and Mine Waste '01, Balkema, Rotterdam, ISBN 90 5809 182 1, 365-374.

Benzaazoua, M., Bois, D., Belem, T., Gauthier, P., Ouellet, S., Fall, M. and St-Onge, J.F. (2005). Remblais souterrains, évolution des connaissances et de la pratique. 20th Colloque Contrôle de terrains, Association Minière du Québec, Val d'Or, Quebec, Canada, march 2005, 23 p.

Benzaazoua, M., Marion, P., Picquet, I., Bussière, B. (2004a). The use of pastefill as a solidification and stabilization process for the control of acid mine drainage, Minerals Engineering, 17, 233-243.

Benzaazoua M., Fall, M. and Belem, T. (2004b). A contribution to understanding the hardening process of cemented pastefill, Minerals Engineering, 17, 141–152.

Benzaazoua, M., Fall. M. and Ouellet, S. (2003). Étude pluridisciplinaire visant mettre au point un outil expert pour la prédiction du comportement des remblais en pâte. IRSST Report 099-085, 161 p.

Benzaazoua, M., Belem, T., Bussière, B. (2002). Chemical factors that influence on the performance of mine sulphidic paste backfill. Cement and Concrete Research, 32, 7, 1133–1144.

Benzaazoua, M., Belem, T., Jolette, D. (2000). Investigation de la stabilité chimique et son impact sur la résistance mécanique des remblais cimentés. IRSST Report R-260, 158 p.

Benzaazoua, M. (1996). Caractérisation physico-chimique et minéralogique de produits miniers sulfures en vue de la réduction de leur toxicité et de leur valorisation, Ph.D. Thesis, INPL, Nancy (France), 267 p.

Bertrand, V.J., Monroy, M.G. and Lawrence, R.W. (2000). Weathering characteristics od cemented paste backfill: Mineralogy and solid phase chemistry, in ICARD 2000 - Proceedings from the 5th international conference on acid rock drainage, May 21-24, 2000, Denver, Colorado, 863-876.

Bethke, C.M. (1996). Geochemical reaction modeling: concepts and applications, Oxford University Press, 397 p.

Bigham, J.M. (1994). Mineralogy of ochre deposits formed by sulfide oxidation. In: Jambor, J.L., Blowes, D.W. (Eds.), The Environmental Geochemistry of Sulfide Mine-wastes. Short Course Handbook, Vol. 22. Mineralogical Association of Canada, 103-132.

Blowes, D.W., Ptacek, C.J. (1994). Acid-neutralization mechanisms in inactive mine tailings. In: Jambor, J.L., Blowes, D.W. (Eds.), The Environmental Geochemistry of Sulfide Mine-wastes. Short Course Handbook, Vol. 22. Mineralogical Association of Canada, 271-292.

Bussière, B., Benzaazoua, M., Aubertin, M. and Mbonimpa, M. (2004). A laboratory study of covers made of low-sulphide tailings to prevent acid mine drainage, Environmental Geology, 45, 609-622.

Bussière, B., Dagenais, A.-M., Mbonimpa, M., and Aubertin, M. (2002). Modification of oxygen-consumption testing for the evaluation of oxygen barrier performance. 55th Canadian Geotechnical Conference and 3rd joint IAH-CNC and CGS Groundwater Specialty Conferences, Niagara Falls, CD, 139-146.

Bussière, B., Benzaazoua, M., Aubertin, M., Lelièvre, J., Bois, D. and Servant, S. (1998). Valorisation des résidus miniers : une approche intégrée – Phase II. Final Report submitted to the Ministère des Ressources naturelles du Québec, Canada, 198 p.

Chapman, J., Hockley, D., Sexsmith, K., Arthur, B. and Donohue, S. (2003). Testing acid generation in cemented paste backfill, in ICARD 2003 – Proceedings from 6th International Conference on Acid Rock Drainage, July 14-17, 2003, Cairns, Australia, Published by The AusIMM, P.O. Box 660, Carlton South, Victoria 3053, Australia, 863-867.

Corey, A.T. (1957). Measurement of water and air permeability in unsaturated soil, Soil Science Society of America Proceedings, 21, 1, 7-10.

Cruz, R., Méndez, B.A., Monroy, M., and Gonzalez, I. (2001). Cyclic voltametry applied to evaluate reactivity in sulfide mining residues, Applied Geochemistry, 16, 1631-1640.

Diamond, S. and Leeman, M.E. (1995). Pore size distributions in hardened cement paste by SEM image analysis, Materials Research Society Symposium Proceedings, 370, 217-226.

Elberling, B. and Damgaard, L.R. (2001). Microscale measurements of oxygen diffusion and consumption in subaqueous sulfide tailings, Geochimica and Cosmochimica Acta, 65, 12, 1897-1905.

Elberling, B. and Nicholson, R. V. (1996). Field determination of sulfide oxidation rates in mine tailings. Water Resources Research, 32 : 1773-1784.

Elberling, B., Nicholson, R.V., Reardon, E.J., and Tibble, P. (1994). Evaluation of sulphide oxidation rates: laboratory study comparing oxygen fluxes and rates of oxidation product release. Canadian Geotechnical Journal, 31: 375-383.

Elberling, B., Nicholson, R.V., and David, D.J. (1993). Field evaluation of sulphide oxidation rates, Nordic Hydrology, 24, 323-338.

Evangelou, V.P. (1995). Pyrite Oxidation and Its Control. CRC Press. 285p.

Godbout, J., Bussière, B., Aubertin, M.Belem, T. Benzaazoua, M. (2004). Évolution des propriétés de rétention d'eau des remblais miniers cimentés en pâte durant le curage, Proceedings of the 57th Annual Canadian Geotechnical Conference and 5th joint IAH-CNC/CGS Conference, Quebec city, Quebec, Canada, October 23rd to 27th, 8 p.

Goulet, C. and Blais, S. (2001). Utilisation du remblai en pâte à la mine Bouchard-Hébert, 16th Colloque en contrôle de terrain, Association minière du Québec, Val d'Or, Québec, Canada, march 2001, 21 p.

Gustafsson, J.P. (2005) Visual MINTEQ, Distributed through the Department of Land and Water Resources Engineering, Royal Institute of Technology, Sweden.

Hassani, F.P., Archibald, J. 1998. Mine Backfill, CD-ROM, CIM, 263 p.

Höhne, G., Hemminger, W. and Flammersheim, H.-J. (2003). Differential scanning calorimetry, Springer, 298 p.

Holström, H., Ljungberg, J., and Öhlander, B. (1999). Role of carbonates in mitigation of metal release from mining waste. Evidence from humidity cells tests, Environmental Geology, 37, 267-280.

Jerz, J.K. and Rimstidt, J.D. (2004). Pyrite oxidation in moist air, Geochimica et Cosmochimica Acta, 68, 4, 701-714.

Lange, D.A., Jennings, H.M. and Shah, S.P. (1994). Image analysis techniques for characterization of pore structure of cement-based materials, Cement and Concrete Research, 24, 5, 841-853.

le Roux, K., Bawden, W.F. and Grabinsky, M.W.F. (2002). Assessing the interaction between hydration rate and fill rate for cemented paste backfill (CPB). In: Proceedings of the 55th Annual Canadian Geotechnical Conference and 3th joint IAHCNC/CGS Conference. Niagara Falls, October 20–23, 427-432.

Levens, R. L. and Boldt, C. M. K. (1992). Hydrochemical impacts of mine waste backfill in underground sulfide mines, Paper in Environmental Issues and Management of Waste in Energy and Mineral Production, Proceedings: Second International Conference, ed. By R.K. Singhal, A.K. Mehrotra, K. Fytas, and J.-L. Collins, Calgary, Alberta, Canada, Sept. 1-4, 1992. A.A. Balkema, v. 2,. 891-902.

Levens, R. L. and Boldt, C. M. K. (1994). Environmental Impacts of Mine Waste Sandfill, Report of Investigations 9493, United States Bureau of Mines, 15 p.

Levens, R. L., Marcy, A. D. and Boldt, C. M. K. (1996). Environmental Impacts of Cemented Mine Waste Backfill, RI 9599, United States Bureau of Mines, 23 p.

Li, M., Catalan, L.J.J. and St-Germain, P. (2000). Rates of oxygen consumption by sulphidic tailings under shallow water covers – Field measurements and modelling. ICARD 2000 Conference Proceedings Volume II, Published by the Society for Mining, Metallurgy, and Exploration, 913-920.

Lowson, R.T. (1982). Aqueous oxidation of pyrite by molecular oxygen, Chemical Reviews, 5, 82, 461-497.

Mayoral, M. C., Izquierdo, M. T., Andrés, J. M. and Rubio, B. (2002). Mechanism of interaction of pyrite with hematite as simulation of slagging and fireside tube wastage in coal combustion, Thermochimica Acta, 390, 1-2, 103-111.

Mbonimpa, M., Aubertin, M., Aachib, M., Bussière, B. (2003). Diffusion and consumption of oxygen in unsaturated cover materials, Can. Geotech. J., 40, 916-932.

Mbonimpa, M., Aubertin, M., Dagenais, A.-M., Bussière, B., Julien, M., Kissiova, M. (2002). Interpretation of field tests to determine the oxygen diffusion and reaction rate coefficients of tailings and soil covers, 55th Canadian Geotechnical Conference and 3rd joint IAH-CNC and CGS Groundwater Specialty Conferences, Niagara Falls, CD, 147-154.

McCarthy, D.F. (2002). Essentials of Soil Mechanics and Foundations, Prentice Hall, 6th Edition, ISBN: 0-13030-383-6, 788 p.

Neville, A.M. (1981). Properties of concrete, third edition, 779 p.

Nicholson, R.V., Elberling, B., and Williams, G. (1995). A new oxygen consumption technique to provide rapid assessment of tailings reactivity in the field and the laboratory. Proceedings of the Sudubury'95 Conference, Sudbury, 999-1006.

Ouellet, S., Bussière, B., Benzaazoua, M., Aubertin, M., Belem, T. Fall, M. (2003). Sulphide reactivity within cemented paste backfill: oxygen consumption test results. In: Proceedings of the 56th Annual Canadian Geotechnical Conference and 4th joint IAHCNC/CGS Conference. Winnipeg, September 28–October 1, 8 p.

Ouellet, J. and Servant, S. (2000). In-situ mechanical characterization of a paste backfill with a self-boring pressuremeter, CIM Bulletin, 93, 1042, 110-115.

Parkhust, D.L., Appelo, C.A.J., (1999). User's Guide to PHREEQC (version 2)—A Computer Program for Speciation, Batch-reaction, One-dimensional Transport, and Inverse Geochemical Calculations. Water-Resour. Invest. Rep. 99-4259 USGS.

Ptacek, C.J. and Blowes, D.W. (2003). Geochemistry of concentrated waters at mine-waste sites. Chapter 12 in Environmental Aspects of Mine Wastes, Short course series volume 31, J.L. Jambor, D.W. Blowes and A.I.M. Ritchie Editors, Mineralogical Association of Canada, 239-260.

Ramachandran, V.S., Paroli, R.M., Beaudoin, J.J. and Delgado, A.H. (2002). Handbook of thermal analysis of construction materials, Noyes Publication, W.A. Publishing, 680 p.

Raudsepp, M. and Pani, E. (2003). Application of Rietveld analysis to environmental mineralogy, Chapter 8 in Environmental Aspects of Mine Wastes, Short course series volume 31, J.L. Jambor, D.W. Blowes and A.I.M. Ritchie Editors, Mineralogical Association of Canada, 163-180.

Strömberg, B. (1997). Weathering kinetics of sulphidic mining waste : An assessment of geochemical processes in the Aitik mining waste rock deposits, PH. D. Thesis, Royal Institute of Technology, Sweden, 73 p. + 6 articles.

Taylor, H.F.W. (1990). Cement Chemistry, 475 p.

Thomson, B. M., Longmire, P. A., Brookins, D. G. (1986). Geochemical Constraints on Underground Disposal of Uranium Mill Tailings. Applied Geochemistry, 1, 335-343.

Tibble, P.A. and Nicholson, R.V. (1997). Oxygen consumption on sulphide tailings and covers: measured rates and applications. Proceedings of the Proceedings of the 4th International Conference on Acid Rock Drainage, Vancouver, Vol. 2, 647-661.

Todor, D.N. (1976). Thermal Analysis of Minerals, Abacus Press, 256 p.

Yanful, E.K., Simms, P.H., Payant, S.C. (1999) Soil cover for controlling acid generation in mine tailings: a laboratory evaluation of the physics and geochemistry, Water, Air and Soil Pollution, 114, 347-375.

Young, R.A. (1995). The Rietveld Method, Edited by R.A.Young, Oxford University Press, 312 p.

Zhang, Y.L. and Evangelou, V.P. (1996). Influence of iron oxide forming conditions on pyrite oxidation, Soil Science, 161, 852-864.

SOMMAIRE, CONCLUSIONS ET RECOMMANDATIONS

Le remblai cimenté en pâte (RCP) est utilisé couramment pour remplir les excavations souterraines des mines en exploitation et ainsi fournir un support de terrain aux chantiers miniers. Le RCP est fabriqué à partir de résidus miniers pouvant contenir une forte proportion de sulfures de fer générateurs d'eaux acides, d'un agent de cimentation et d'eau. Grâce à ses propriétés mécaniques, le RCP améliore le taux de récupération du minerai tout en permettant de réduire les volumes de résidus miniers à entreposer en surface. Cette réduction de volume occasionne une diminution des coûts de restauration des infrastructures de surface à la fin de la vie de la mine.

Parmi les comportements évolutifs qui favorisent l'intégrité à long terme du RCP, notons le gain de résistance mécanique, la diminution de la conductivité hydraulique, l'augmentation de la rétention d'eau et de la stabilisation des contaminants et l'inhibition de l'oxydation. L'organisation du RCP à l'échelle microscopique (microstructure, proportion et structure de la porosité, minéralogie) affecte de façon directe ou indirecte l'évolution des propriétés macroscopiques du RCP. Les travaux réalisés dans le cadre de cette thèse par articles ont permis de mieux comprendre les RCP en les étudiant à l'échelle microscopique et mésoscopique à l'aide de différentes approches.

Dès le début des travaux de thèse, deux axes de recherche principaux ont été identifiés. Le premier visait une meilleure compréhension du RCP en étudiant les phénomènes fondamentaux à la base du gain de résistance mécanique, soit l'évolution de la minéralogie et son impact sur la microstructure. Le second axe visait à établir des liens entre les aspects microstructuraux préalablement étudiés et la réactivité des RCP sulfureux potentiellement générateurs d'acide.

Rétrospectivement, il est possible d'affirmer que les objectifs généraux ont été atteints. Les contributions scientifiques originales issues de ces travaux sont principalement liées à l'étude de la microstructure et de la structure des pores, ainsi que de la minéralogie des RCP. Des méthodes originales et adaptées aux RCP ont été développées pour qualifier et quantifier l'évolution du matériau dans le temps. Particulièrement, les techniques d'analyse d'image présentées, qui permettent de quantifier la structure des pores et d'estimer la nature minérale et l'organisation microstructurale des phases cimentaires des RCP, sont des contributions majeures de la thèse qui favoriseront la compréhension des comportements mécaniques et environnementaux des RCP dans un avenir proche. De surcroît, les relations établies entre la porosité, la minéralogie des RCP et la résistance en compression uniaxiale sont des moyens de lier les aspects fondamentaux de la thèse aux considérations pratiques du RCP. Par ailleurs, une contribution importante de la thèse est certainement l'étude sur la réactivité d'un RCP sulfureux en chantier; il a ainsi été possible d'établir que l'utilisation du RCP limite significativement la génération de DMA.

Les prochains paragraphes passent en revue les principales conclusions des chapitres de développement de la thèse. Pour chacun de ces chapitres (2 à 5), des recommandations afin de poursuivre les travaux de thèse sont également proposées.

Chapitre 2

Le chapitre 2 de la thèse présente une étude microstructurale des RCP en utilisant la technique du porosimètre au mercure (MIP). Ces travaux ont été effectués sur des échantillons fabriqués à partir d'une poudre de silice ayant une granulométrie similaire à celle des résidus miniers, de trois liants hydrauliques (ciment Portland de type 10 (T10), T10 additionné de 30% de cendre volante (CV) de type C et T10 additionné de 80% de laitier de haut-fourneau (LHF)) et de trois types d'eau de gâchage (une eau pure et deux eaux en provenance des usines de RCP de deux

mines). Les travaux ont montré que la technique MIP permet d'observer une évolution microstructurale des RCP étudiés, soit principalement une évolution des pores grossiers vers des pores fins avec le temps de cure. Ceci a été observé par la diminution du volume de mercure introduit dans la région du seuil d'intrusion et par une augmentation de volume à des pressions correspondant à des diamètres de pores plus fins. L'hydratation des liants utilisés et la précipitation de sulfates sont les phénomènes à la base de ces changements de propriétés. Par ailleurs, la porosité totale mesurée sur l'ensemble des échantillons par cette technique est demeurée essentiellement constante. La principale raison dégagée pour expliquer ce phénomène est associée au fort rapport eau/ciment qui ne permet pas de générer une quantité d'hydrates suffisante et ainsi résister à l'entrée du mercure sous pression dans le matériau. Il a également été possible de noter que les échantillons fabriqués avec le liant à base de laitier de haut-fourneau (LHF) montrent un comportement atypique par rapport aux deux autres liants utilisés. Les échantillons fabriqués avec le mélange T10:LHF montre la porosité la plus fine et la résistance mécanique la plus élevée. Les échantillons à base de T10 et de T10:CV présentent des propriétés microstructurales et mécaniques similaires. Un effet de la qualité de l'eau a également été noté. Pour la période d'investigation, les échantillons mélangés avec une eau sulfatée ont généralement montré une résistance mécanique plus élevée et une proportion de pores fins supérieure. La précipitation de sulfates dans les pores pourrait expliquer ces observations. Enfin, un apport original de cette partie des travaux de thèse est le développement d'une équation reliant la courbe de distribution des pores évaluée au MIP et la résistance en compression simple. Dans le contexte où l'échantillonnage en chantier est difficile et dispendieux, cette équation pourrait s'avérer un moyen utile d'estimer la résistance d'un RCP sur des petits échantillons. Après un calibrage, la relation pourrait par exemple servir à déceler des variations dans les propriétés mécaniques entre des chantiers remblayés ou à l'intérieur d'un même chantier.

Néanmoins, quelques aspects mériteraient d'être étudiés davantage afin d'approfondir les connaissances acquises et de préciser les résultats obtenus. Par

exemple, comme l'équipement de porosimétrie au mercure permet la sélection des incréments de pression lors d'un essai, il est recommandé d'augmenter la définition dans la zone de pression au seuil afin d'améliorer la précision de l'évaluation de ce paramètre ainsi que des prédictions subséquemment réalisées. Aussi, étant donné que la variabilité granulométrique n'a pas été étudiée lors de cette partie du projet, une banque d'essais MIP sur des RCP de diverses provenances pourrait être constituée. Ceci permettrait de valider l'équation proposée qui lie un résultat MIP et la résistance mécanique, et de l'adapter au besoin. Les paramètres qui régissent la non linéarité de la dépendance à la porosité pourraient être ajustés selon les incréments de pression sélectionnés et à la variabilité microstructurale des RCP.

Chapitre 3

L'étude de la porosité des RCP s'est par la suite poursuivie en utilisant le microscope électronique à balayage (MEB) et l'analyse d'image. Le but de cette étude était d'établir les bases pour la mesure par analyse d'image de certains paramètres importants de la structure des pores (porosité totale, distribution des pores et tortuosité) pour le cas particulier des RCP. Les échantillons étudiés provenaient des mêmes cylindres de RCP que ceux de l'étude MIP décrite précédemment. La porosité totale, la distribution de la taille des pores et la tortuosité telles que vues par imagerie électronique (SEM-IA) ont été investiguées à 14 et à 90 jours de cure. Les résultats ont montré que, contrairement aux résultats obtenus à l'aide du MIP, la SEM-IA permet d'observer une baisse de la porosité totale des échantillons dans le temps. Les échantillons à base de T10LHF et mélangés avec une eau contenant des sulfates montrent les plus importantes baisses de leur porosité (environ 7%). L'analyse de la distribution de la taille des pores et de la tortuosité vont dans le même sens, i.e. qu'un raffinement de la porosité s'opère dans le temps et que ce dernier augmente la constriction et la tortuosité des RCP. Les résultats font aussi ressortir une différence significative entre les courbes de distribution des pores obtenues au MIP et celles obtenues par SEM-IA. Les résultats MIP semblent être affectés par un effet de « goulot de bouteille ». Cependant, du fait

que le RCP est un matériau poreux et relativement lâche, les différences entre les deux approches sont moins marquées que pour les pâtes de ciment. Enfin, la technique utilisée pour évaluer la tortuosité (squelettisation des gorges poreuses) s'est avérée efficace pour estimer ce paramètre. Les valeurs obtenues sont semblables à d'autres tirées de la littérature sur des matériaux non-cimentés (les facteurs de tortuosité mesurés sont entre 1,60 et 2,34). Il est intéressant de noter que les résultats obtenus pour les trois paramètres décrivant la structure des pores sont cohérents avec les résultats de résistance en compression uniaxiale. En effet, les valeurs les plus élevées de résistance en compression uniaxiale ont été observées pour les échantillons ayant la plus faible porosité totale, la distribution des pores la plus fine et la tortuosité la plus élevée.

Certains aspects de la technique SEM-IA auraient toutefois besoin d'être investigués davantage. Une évaluation de la porosité totale a été appliquée avec succès au RCP de la mine Laronde (voir chapitre 5), mais il est tout de même recommandé de réaliser certains essais de calibrage avec d'autres RPC fabriqués à partir de résidus miniers réels. De plus, l'évolution de ces travaux devrait conduire vers l'utilisation de la SEM-IA pour la prédiction de la conductivité hydraulique saturée et de la courbe de rétention d'eau des RCP. Étant donné que le RCP est un matériau qui évolue dans le temps, il est difficile d'évaluer ces propriétés au laboratoire; une technique de prédiction par analyse d'image est donc envisageable et pertinente. Enfin, pour une personne voulant répéter les techniques d'analyse d'image proposées, il est important de respecter très précisément toutes les étapes et tous les réglages utilisés lors de l'étude (p. ex. grossissement, intensité du courant, mode BSE, résolution des images, logiciel d'analyse d'image, etc.). Toute variation de réglage et de traitement peut conduire à des difficultés de répétabilité et de reproductibilité des mesures.

Chapitre 4

Le chapitre 4 de la thèse porte sur la description (d'un point de vue minéralogique) de la phase solide du RCP et vise à montrer son influence sur la structure du matériau. Dans cette optique, des mélanges de RCP similaires à ceux décrits aux deux chapitres précédents ont été utilisées. Les échantillons étudiés se composaient d'une poudre de silice, des trois mêmes liants (voir ci-dessus) et de deux eaux, une eau pure et une eau ayant une teneur élevée en ions (p. ex. 21 690 ppm SO_4^{2-}) en provenance de l'épaississeur des résidus d'une mine. La revue de littérature réalisée a démontré qu'il est difficile d'identifier et de quantifier les phases cimentaires des RCP, principalement en raison de l'interférence des résidus miniers. Pour contrer ce problème, il a été décidé d'utiliser un équipement combinant la thermogravimétrie et la mesure des flux de chaleur car ces techniques permettent la quantification des phases amorphes. Ces méthodes thermiques ont aussi été appuyées par le MEB en allant toutefois plus loin que les observations qualitatives habituelles. L'analyse d'image et le développement d'un logiciel de traitement des images rayon X en mode point en provenance du MEB (SEM-XMAP) ont été introduits dans le processus d'identification minéralogique. L'utilisation de SEM-XMAP dans le contexte des RCP (faible quantité de ciment et forte proportion d'eau) a permis de cartographier la minéralogie et de visualiser la distribution des phases cimentaires dans la matrice d'un RCP. Il est à noter que dans le cas des deux méthodes choisies, le fait d'utiliser un granulat constitué d'un seul minéral (silice) a permis l'identification des phases cimentaires en limitant les interférences. Les résultats de l'étude montrent que les minéraux occasionnant la cimentation des RCP sont similaires à ceux retrouvés dans les pâtes de ciment et les mortiers, soit des silicates de calcium hydratés (C-S-H), du gypse, des monosulfates, des carbonates, des hydrogrenats et de l'hydrotalcite. La proportion de minéraux sulfatés est relativement importante, particulièrement pour les échantillons fabriqués avec l'eau provenant de l'usine de RCP. Par contre, les observations au MEB n'ont pas permis une distinction claire des minéraux sulfatés primaires et/ou secondaires et des artéfacts du séchage. Un effet pouzzolanique a aussi été noté dans les mélanges incluant des

CV et des LHF. Les analyses thermogravimétriques montrent la disparition de la portlandite avec le temps de cure et une augmentation de la proportion des minéraux pouvant être associés aux C-S-H et aux sulfates. Les observations et la quantification au MEB ont permis de mettre en évidence qu'une fraction des liants (principalement les CV et LHF) n'était pas hydratée même après 180 jours de cure. L'utilisation d'une eau sulfatée et acide semblait cependant favoriser la dissolution et l'hydratation du ciment et des ajouts minéraux. Les RCP fabriqués avec cette eau et le liant T10LHF avait une résistance mécanique supérieure aux témoins. Aucune perte de résistance mécanique ayant pu être associée à la précipitation de sulfate (attaque sulfatique) n'a été observée durant la période de 180 jours. Enfin, il est possible d'affirmer que pour les échantillons de RCP étudiés, la formation des phases cimentaires et l'apport en cohésion de certaines phases sulfatées sont responsables du gain de résistance mécanique. D'ailleurs, des relations simples ont pu être établies entre la résistance en compression uniaxiale et la perte de masse mesurée par thermogravimétrie entre 100 et 250°C.

Les principales recommandations découlant des travaux présentés au chapitre 4 sont associées à l'attaque sulfatique. La présente étude de laboratoire, qui s'est déroulée sur 180 jours, n'a pas révélé ce type de problème pour les échantillons étudiés malgré l'utilisation d'une eau contenant approximativement 22000 ppm de SO_4^{2-}. Sachant que des cas d'attaque sulfatique interne ont été observés sur des échantillons de laboratoire à un temps de cure bien en deçà de 180 jours (p. ex. Benzaazoua et al., 1999; Bernier et al., 1999; Hassani et al., 2001), il serait intéressant de pousser plus loin l'étude de l'influence des résidus sulfureux sur l'apparition du phénomène. En ce sens, il est suggéré d'étudier l'attaque sulfatique en suivant une démarche similaire à celle utilisée dans la thèse (étude porosimétrique et minéralogique) mais sur des échantillons constitués uniquement d'un sulfure de fer très réactif (p. ex. pyrrhotite). D'autre part, bien que des sulfates aient été identifiés par thermogravimétrie et par analyse chimique dans les échantillons, la présence potentielle de résidus de séchage dans les pastilles laisse perplexe quant à la nature des zones associées au soufre dans la cartographie

SEM-XMAP. En conséquence, il est recommandé de poursuivre des travaux visant à faire la lumière sur la nature réelle de ces zones. Enfin, il est à noter que les recommandations formulées ci-dessus (conclusion du chapitre 3) concernant les réglages du MEB s'appliquent aussi à la technique SEM-XMAP.

Chapitre 5

Le dernier chapitre de développement de la thèse porte sur l'évaluation de la réactivité d'un RCP sulfureux dans un chantier souterrain de la Mine Laronde, propriété de la compagnie Agnico-Eagle. Certains des outils développés et utilisés dans les chapitres précédents ont été mis à profit pour mieux comprendre le comportement environnemental du chantier remblayé. Les principaux résultats de cette étude ont montré que la consommation d'oxygène du RCP *in situ* a diminué rapidement pour se stabiliser à environ 0,2 mol O_2/m^2/jour 14 jours après l'ouverture du chantier. Ce taux d'oxydation est nettement inférieur à celui de résidus sans ciment. La diminution de la consommation d'oxygène est attribuée à la création d'une couche d'oxydation protectrice de 200 à 400 µm d'épaisseur, à une diminution de porosité dans cette couche causée par la précipitation de minéraux secondaires, au degré de saturation élevé du RCP (supérieur à 90%) et à la formation d'une couche calcique autour des grains de pyrite qui réduit leur réactivité. Les techniques d'analyse minéralogique utilisées n'ont pas permis l'identification de sulfates secondaires dans le RCP. Par contre, l'extraction sous presse de l'eau des pores a révélé de fortes concentrations en soufre et un pH de l'ordre de 10 à la fin de la période d'essai. Ainsi, malgré une proportion de sulfure d'environ 53% dans le RCP et des conditions favorables à l'oxydation, le soufre n'a pas massivement précipité sous forme de sulfate dans les 80 jours suivant l'ouverture du chantier.

Suite à cette portion de la thèse, il est suggéré de poursuivre les travaux en suivant le degré de saturation de la partie supérieure d'un RCP sulfureux en chantier. Bien que des mesures *in situ* suggèrent une saturation élevée dans cette zone (Ouellet et Servant, 2000), il serait opportun de vérifier si un comportement similaire à celui

mesuré au bas du chantier est observé. Il serait également intéressant de réaliser des essais de consommation d'oxygène dans d'autres mines ayant une minéralogie et une recette de RCP différentes.

Dernières remarques

La thèse a permis de mieux comprendre l'hydratation des liants dans les RCP et d'observer les changements microstructuraux associés. Elle a en outre permis d'observer le comportement d'un matériau ayant des propriétés se situant entre un sol cohésif et un matériau cimenté traditionnel (mortier). Les modifications internes occasionnées par la cimentation favorisent une diminution de la porosité et des changements dans la structure des pores qui contrôlent la résistance mécanique. L'analyse croisée des résultats des chapitres 2 à 4 de la thèse a également permis d'identifier une participation des sulfates présents dans l'eau de gâchage à la cohésion des RCP. Cependant, l'analyse de l'eau interstitielle des résidus ne peut pas être simplifiée à son contenu en sulfate uniquement et doit être considérée globalement quant à son implication dans les processus d'hydratation des liants. Le mélange de ciment type 10 et de laitier de haut-fourneau (T10:LHF à 20:80) se distinguait nettement des deux autres liants utilisés lors des travaux de laboratoire. La résistance mécanique obtenue avec le T10:LHF était toujours supérieure (souvent du double) et les évaluations porosimétriques indiquaient des pores plus fins. L'étude sur la minéralogie des RCP a permis d'observer que même dans le contexte des RCP (faible quantité de ciment et forte proportion d'eau), les produits de l'hydratation sont similaires à ceux rencontrés dans des mélanges ayant un rapport eau sur ciment inférieur à 0,7 (tels que les pâtes de ciment). Avec cette étude, il a aussi été possible de vérifier que l'effet pouzzolanique était présent dans les mélanges avec ajout minéral. Enfin, une des retombées importantes de cette partie du projet est le lien établi entre la microstructure et la résistance en compression.

Au niveau de l'étude sur l'oxydation des RCP réalisée en chantier, les conclusions qui doivent être retenues sont que le RPC permet de limiter l'oxydation des résidus sulfureux et qu'il améliore la stabilisation des contaminants. Sur la base des résultats de cette étude, le remblayage souterrain de résidus miniers sulfureux sous forme de RCP apparaît comme une solution environnementalement adéquate. Un prochain objectif serait de prédire le comportement environnemental des chantiers remblayés en tenant compte des propriétés du RCP, mais aussi des propriétés du massif rocheux environnant et des conditions hydrogéologiques durant et après l'exploitation du gisement. Considérant que les connaissances des propriétés microstructurales d'un matériau poreux sont essentielles pour comprendre et prédire son comportement environnemental, plusieurs thèmes développés dans la thèse pourront éventuellement être exploités. C'est le cas des analyses porosimétriques, mais aussi des essais de consommation d'oxygène qui pourraient devenir des méthodes efficaces pour évaluer la performance d'une solution de stabilisation des résidus miniers sulfureux en chantier ou ailleurs.

APPENDICE A

CIMENTS, AJOUTS MINÉRAUX ET HYDRATATION[8]

« Le principal défi de l'industrie du béton pour l'avenir est de s'intégrer dans une démarche de préservation de l'environnement (Mehta, 2001). Avec une évaluation des émissions mondiales de CO_2 établie à 7% (Malhotra, 1999), les producteurs de ciment et les compagnies utilisatrices sont maintenant confrontés à une pression environnementale favorable à une diminution des quantités de ciment utilisées en construction. Selon le type d'ajout minéraux utilisé, celui-ci peut remplacer 10 à 70% du ciment Portland ordinaire et, non seulement diminuer la quantité de ciment dans la structure, mais dans tous les cas améliorer la qualité et la durabilité des ouvrages. »

Le ciment Portland

Le ciment Portland est un mélange de pierre calcaire, d'argile (ces deux matériaux deviennent clinker après des procédés de broyage et d'anatexie) et de gypse en faible quantité. Pour diminuer la longueur des formules et équations chimiques, des abréviations sont généralement utilisées pour faire référence aux produits rencontrés (tableau A.1). Les mêmes abréviations sont occasionnellement utilisées dans la thèse. La norme CAN/CSA-A5-98 traite des cinq types de ciment Portland disponibles au Canada: le type 10 (ciment normal), le type 20 (ciment modéré), le

---

[8] La brève revue de littérature présentée dans cet appendice provient d'articles dont les travaux ont été réalisés sur des pâtes de ciment, des mortiers et des bétons. Le remblai cimenté en pâte (RCP) est un matériau ayant un comportement différent à bien des égards. Les propriétés décrites dans cet appendice ne doivent pas être considérées applicables en tout point pour un RCP.

Tableau A.1, Composition moyenne du ciment Portland et abréviations usuelles

Oxyde	Formulation	Abréviation	Proportion moyenne
Oxyde de calcium	CaO	C	63.6 %
Silice	SiO_2	S	22.7%
Alumine	Al_2O_3	A	4.7%
Oxyde de magnésium	MgO	M	3.1%
Trioxyde de soufre	SO_3	-	2.3%
Oxyde de fer	Fe_2O_3	F	1.8%
Eau	H_2O	H	-
Autres	-	-	1.8%
Composition de Bogue	Formulation	Abréviation	Proportion moyenne
Alite (clinker)	$3CaO\text{-}SiO_2$	C_3S	45.0%
Belite (clinker)	$2CaO\text{-}SiO_2$	C_2S	31.0%
Ferrite (clinker)	$4CaO\text{-}Al_2O3\text{-}Fe_2O_3$	C_4AF	5.6%
Aluminate (clinker)	$3CaO\text{-}Al_2O_3$	C_3A	9.4%
Gypse + autres	$CaS0_4\text{-}2H_2O$	-	9.0%

type 30 (ciment à haute résistance initiale), le type 40 (ciment à faible chaleur d'hydratation) et le type 50 (ciment résistant aux sulfates). Ces divers types de ciment sont obtenus en faisant varier les proportions en C_3S, C_2S, C_3A, C_4AF et gypse. La densité des ciments Portland est de l'ordre de 3.15 g/cm³ et sa surface spécifique BET de 1.3 m²/g (≈ 300 m²/kg Blaine).

Les cendres volantes

Les cendres volantes (fly ash en anglais) sont un sous-produit de la combustion du charbon dans les centrales thermiques. L'ASTM (ASTM C 618) reconnaît deux classes de cendre volante.

- La classe F, produite à partir de houille :

Les cendres de cette nature ont une phase vitreuse et des phases cristallines inertes telles que : quartz, mullite, magnétite spinel, hématite. Par exemple, Hemmings et al. (1987) rapportent qu'une cendre volante de cette classe (à haut contenu en Fer) de

l'est du Canada contient les proportions minéralogiques suivantes : 9.6% quartz, 20.4% mullite, 4.5% magnétite spinel, 5.4% hématite et 58% de verre.

- La classe C, produite à partir de lignite ou de charbon sous-bitumineux :

Les cendres de cette classe sont habituellement auto-cimentaire et ont une phase vitreuse et des phases cristallines de la même nature que les cendres de classe F, mais à celles-ci peuvent s'ajouter les minéraux suivants : anhydrite, sulfate alcalin, C_2S, C_3A, chaux (Portlandite si les cendres ont été exposées à l'humidité), melilite, merwinite, periclase, sodalite. Berry et al. (1988) rapportent qu'une cendre volante de cette classe (à faible contenu en calcium) provenant de l'ouest du Canada contient les proportions minéralogiques suivantes : 6% quartz, 14% mullite et 80% de verre.

Mehta (1989), mentionne que l'index de réactivité des cendres volantes est relatif au contenu en verre, mais peut aussi être lié à la composition chimique variable du verre entre les différentes classes (faible ou fort contenu en Ca). De façon générale, les cendres volantes de classe C contiennent plus de calcium et moins de fer et de carbone non brûlé que celles de classe F. Le tableau A.2 présente des compositions typiques de cendres volantes analysées à l'ICP (tirées du site WWW du Fly Ash Resource Center).

Les particules de cendre volante sont généralement sphériques (figure A.1) et occasionnellement creuses (figure A.2), leurs diamètres varient de moins de 1 µm à 150 µm (Malhotra, 2001). Une étude de CANMET sur 11 cendres volantes (Carette et Malhotra, 1986) montre que leurs densités varient de 1.9 à 2.53 pour les cendres à base de lignite (classe C) et de 2.22 à 2.96 pour les cendres à base de charbon bitumineux (classe F). Quant aux surfaces spécifiques, cette même étude montre que celles-ci varient de 127 à 581 m²/kg (Blaine).

Tableau A.2, Composition typique des cendres volantes (% poids)

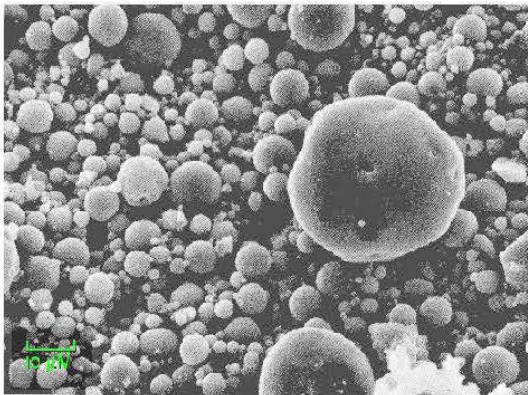|	Classe F faible-[Fe]	Classe F haute-[Fe]	Classe C haute-[Ca]	Classe C faible-[Ca]
SiO_2	46-57	42-54	25-42	46-59
Al_2O_3	18-29	16.5-24	15-21	14-22
Fe_2O_3	6-16	16-24	5-10	5-13
CaO	1.8-5.5	1.3-3.8	17-32	8-16
MgO	0.7-2.1	0.3-1.2	4-12.5	3.2-4.9
K_2O	1.9-2.8	2.1-2.7	0.3-1.6	0.6-1.1
Na_2O	0.2-1.1	0.2-0.9	0.8-6.0	1.3-4.2
SO_3	0.4-2.9	0.5-1.8	0.4-5.0	0.4-2.5
LOI	0.6-4.8	1.2-5.0	0.1-1.0	0.1-2.3
TiO_2	1-2	1-1.5	<1	<1

Figure A.1, Image SEM de cendre volante (tirée du site WWW du Fly Ash Resource Center).
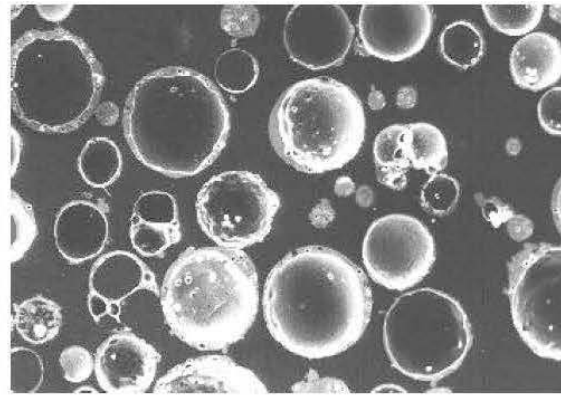
Figure A.2, Particules de cendre volante cénosphériques (tirée du site WWW du Fly Ash Resource Center).

Les laitiers de haut-fourneau

Le laitier de haut-fourneau (LHF) est un sous-produit de la sidérurgie. Lorsqu'il est refroidi rapidement et finement moulu, il développe une capacité à s'associer à l'eau. Ainsi, plusieurs laitiers sont des matériaux cimentaires jusqu'à un certain degré (Malhotra, 2001). Il est dénoté divers types de laitiers : refroidis à l'air, dilatés, granulés et expansés. Le tableau A.3 présente la composition chimique typique d'un LHF.

Tableau A.3, Composition chimique (% poids) d'un laitier de haut-fourneau.
(tirée de Saric-Coric et Aïtcin, 2001)

SiO_2	Al_2O_3	Fe_2O_3	CaO	MgO	K_2O	Na_2O	SO_3	LOI
36.78	10.3	0.7	36.5	12.6	0.44	0.37	0.24	0

En termes de proportion dans les bétons, il est habituel de retrouver des proportions de l'ordre de 25 à 50% en poids en remplacement du ciment. La densité des laitiers est de l'ordre de 2.85 à 2.95 g/cm³. Ceci confère une augmentation de volume de la pâte de ciment sur la base d'un remplacement par poids d'un ciment Portland. Les laitiers maintenant disponibles au Canada et aux États-Unis ont des surfaces spécifiques de plus de 450 m²/kg (Blaine).

L'hydratation des ciments et la structure des C-H-S

Le phénomène dit «de la prise du ciment» fait interagir le ciment et l'eau dans un processus complexe d'organisation structurale et de durcissement. En premier lieu, les fractions silicatées (C_3S, C_2S) forment, une fois combinées à l'eau, les C-S-H (silicate de calcium hydraté). Le C_3S et le C_2S constituent environ 75 % du ciment. Lors de l'hydratation, ils dégagent tous deux de la chaleur à des niveaux différents et leurs vitesses de réaction sont différentes. En effet, le C_3S réagit plus rapidement que le C_2S et il dégage plus de chaleur. La chaleur d'hydratation peut se définir comme la quantité de chaleur dégagée lors d'une hydratation complète à une température donnée (Neville, 1981). Cette chaleur dépend de la composition chimique du ciment, soit des C_3S, C_2S, C_3A et C_4AF. En lisant la partie «Heat of Hydratation of Cement» du livre de Neville (1981), il est possible de dégager des propriétés physiques reliées à la chaleur d'hydratation :

- La chaleur totale d'hydratation est très près de la somme des chaleurs d'hydratation des composés du ciment séparés. Woods et al. (1933) ont déduit une relation reliant la chaleur d'hydratation du ciment et les différents composés:
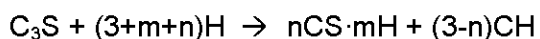
Chaleur d'hydratation d'un gramme de ciment (J/g) = $136[C_3S]$ + $62[C_2S]$ + $200[C_3A]$ + $30[C_4AF]$ (les termes entre crochets représentent le pourcentage poids des composés respectifs).

- Le dégagement de chaleur est fonction de la proportion de chacun des composés (surtout C_3A et C_3S). Plus on augmente la quantité de C_3A et/ou C_3S, plus la chaleur dégagée augmente.

- La vitesse de libération de la chaleur est aussi fonction de la finesse des grains de ciment. Ceci n'affecte cependant pas la quantité de chaleur dégagée.

- Le rapport influence la vitesse et la quantité totale de chaleur dégagée.

- Enfin, plus la température à laquelle l'hydratation se fait est élevée, plus la chaleur dégagée et plus la vitesse de la réaction augmentent.

D'autre part, les C_3S et C_2S régissent le comportement de la pâte de ciment. Ils donnent la résistance au ciment et sont responsables du durcissement. Le C_3S influence surtout la prise initiale et le durcissement à court terme, alors que le C_2S serait tenu responsable de la résistance à long terme. Enfin, il faut noter que la réaction d'hydratation libère de la chaux hydratée ou portlandite ($Ca(OH)_2$ ou CH).

La réaction du C_3A avec l'eau est très rapide. Elle contribue à la résistance de la pâte, mais peut aussi causer une prise éclair (flash set) si elle n'est pas contrôlée. C'est pour pallier à ce problème que le gypse est ajouté au clinker. Le rôle du gypse est alors d'enrober les particules de C_3A (en formant des sulfoaluminates de calcium hydratés par des réactions complexes) et de permettre une hydratation plus lente de ce composé. Un surplus de gypse peut cependant réagir avec le C_3A résiduel après la prise et, par expansion lors de la formation des sulfoaluminates, causer une fissuration et des pertes de résistance. Les prochaines lignes résument les réactions d'hydratation du ciment (tiré de Hewlett, 1998).
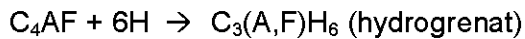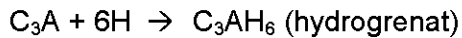
Pour le C_3S:

C_3S + $(3+m+n)H$ → $nCS \cdot mH$ + $(3-n)CH$

Pour le C_2S:

$C_2S + H \rightarrow C-S-H + CH$

Pour les C_3A et C_4AF (sans gypse):

$C_3A + 6H \rightarrow C_3AH_6$ (hydrogrenat)

$C_4AF + 6H \rightarrow C_3(A,F)H_6$ (hydrogrenat)

Pour les C_3A et C_4AF (en présence de gypse, $S'=SO_4$):

$C_3A + 3CS'H_2 + 26H \rightarrow C_6AS'_3H_{32}$ (ettringite) et aussi $C_4AS'H_{12}$, C_4AH_{19} (processus similaire pour le C_4AF, incorporation de Fe dans la structure des minéraux).

Lorsque du C_3A demeure présent après la formation de l'ettringite, il peut y avoir transformation en monosulfate :

$C_6AS'_3H_{32} + 2C_3A + 4H \rightarrow 3C_4AS'H_{12}$ (monosulfate).
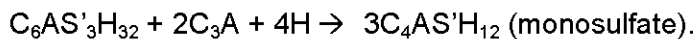
En présence d'ajout minéral tel que la cendre volante ou le laitier de haut-fourneau, les produits de l'hydratation ne changent pas tellement et sont toujours majoritairement représentés par les C-S-H (Taylor, 1990). On peut cependant noter que la réaction pouzzolanique fera réagir la chaux pour former des C-S-H additionnels ayant cependant un rapport Ca/Si inférieur aux C-S-H issus des clinkers. Des minéraux comme la stratlingite et l'hydrogrenat sont des phases rencontrées en présence de cendre volante ayant une forte proportion de calcium (Taylor, 1990). Si le laitier de haut-fourneau est l'ajout minéral utilisé, l'hydrotalcite peut devenir un produit de l'hydratation, tout comme un silicate de magnésium hydraté (M-S-H; Brew et Glasser, 2005). De façon générale, le temps de prise est augmenté, à température constante, lors de l'introduction de CV ou de LHF dans un mélange cimentaire.

La description physique de l'hydratation d'un clinker slicaté ou du ciment Portland peut être explicitée en quatre étapes (e.g. Troxell et al., 1968):

1. Activité chimique intense au contact de l'eau et du ciment, activité qui dure quelques minutes.

2. Activité chimique faible et peu de chaleur dégagée (période dormante), dure entre 1.5 heure et 4 heures.

3. Reprise de l'activité chimique et du dégagement de chaleur, c'est le début de la prise (création de liens chimiques).

4. Diminution graduelle de l'activité chimique et de la chaleur d'hydratation, c'est la période de durcissement, elle dure plus d'un an.

La figure A.3, résume ces étapes.

De ces quatre étapes, la période dormante (étape 2) est particulièrement intéressante. C'est en effet lors de cette période de relative inactivité qu'un béton est transportable sans qu'il y ait prise. C'est aussi lors de cette même période qu'agissent les superplastifiants, les durcisseurs, les retardants, etc. L'hypothèse proposée par Skalny et Young (1980) explique le phénomène de la période dormante par la présence d'une couche quasi imperméable autour des particules de ciment, empêchant momentanément le passage d'ions OH^- et Ca^{2+} et donc la formation des C-S-H (figure A.4).

L'autre phénomène physique auquel il est opportun de s'attarder, est la contraction Le Chatelier. Cette contraction induit un volume des produits de l'hydratation plus faible que le volume initial du ciment et de l'eau réunis, dans un rapport d'environ 8% (voir Neville, 1981). L'hydratation du ciment crée donc des vides à l'intérieur de la pâte de ciment, vides qui peuvent expliquer une part des déformations liées au retrait de la pâte de ciment dans les premières heures de l'hydratation (Regourd,1982).
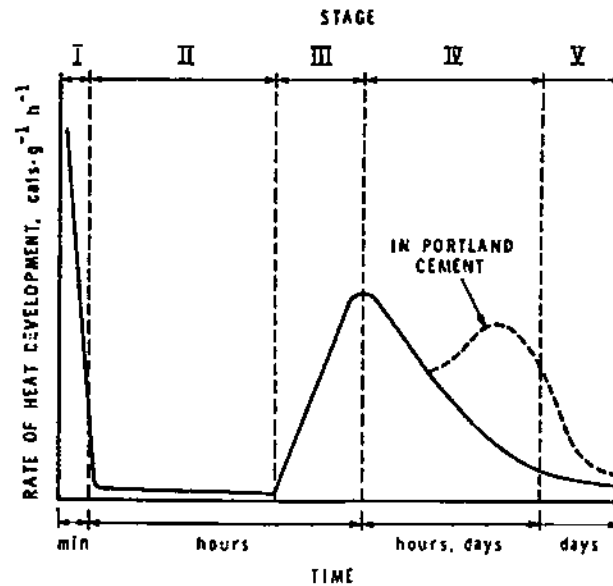
Figure A.3, Relation entre le temps d'hydratation et la chaleur dégagée, mesurée en conduction calorimétrique (trait plein = C3S, pointillé = ciment Portland, tirée de Ramachandran et Beaudoin, 2001).
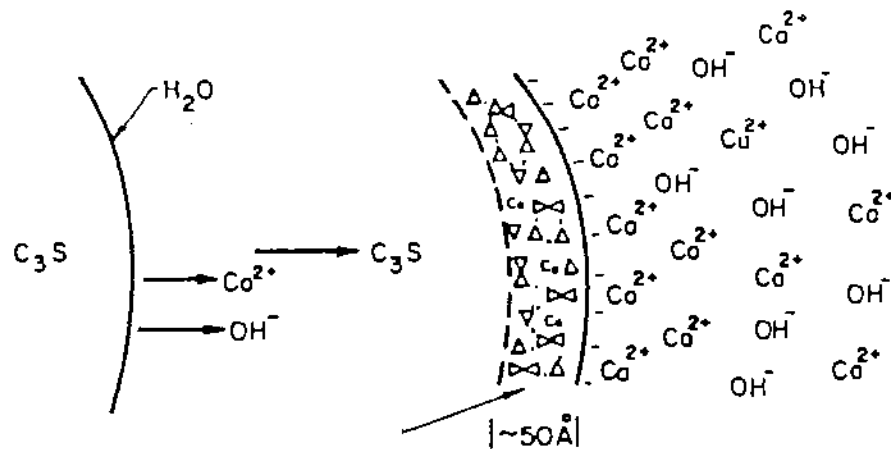
Figure A.4, Schéma des réactions initiales d'hydratation de C3S. (tirée de Regourd, 1982).

Comme il a déjà été mentionné, les C-S-H sont principalement responsables de la résistance d'une pâte de ciment. Cette résistance est évidemment associée à la nature des liens chimiques. Pour les C-S-H, ces liens se partagent en trois, à savoir majoritairement hydrogènes et covalents, mais aussi de Van der Waals. Il semble,

par ailleurs, que ces liens se modifient avec le temps. En effet, des études de Diamond (1981), portées sur la forme des C-S-H montrent des changements de structure avec le temps. Diamond dégage ainsi quatre types de C-S-H:

Les hydrates qui se forment dans l'espace disponible au début de l'hydratation :
I = Tubulaire (jeune)
II = En nid d'abeilles

Les hydrates tardifs :
III = En plaquettes empilées
IV = Compact (mature)

La portlandite libérée par la réaction d'hydratation se forme initialement en cristaux hexagonaux de l'ordre de 10µm, pour adopter une forme massive par la suite. Cette chaux a un potentiel chimique très élevé et peut constituer jusqu'à 26% par volume (Beaudoin et al., 2001) d'un mélange à base de ciment Portland, sous forme de portlandite.

La porosité d'une pâte de ciment est répartie en deux: la porosité de gel et la porosité capillaire. La porosité de gel (ou porosité de l'ensemble des hydrates) se définit comme l'espace contenant l'eau adsorbée sur les surfaces des microcristaux. Les pores de gel sont très petits (de l'ordre de 1.5 à 2.0 nm d'épaisseur) et traduisent une conductivité hydraulique d'environ 10^{-15} m/s. Les pores de gel occupent environ 28% de l'espace de l'ensemble des hydrates. Contrairement à ces derniers, les pores capillaires sont 10000 fois plus grands avec une épaisseur d'environ 0.1 µm. Les pores capillaires représentent les espaces entre les grains de ciment qui n'ont pas encore été remplis par les hydrates. Ainsi, si la pâte de ciment est conservée à l'humidité et que l'hydratation se fait convenablement, la porosité tend à diminuer et le réseau de pores capillaires devient discontinu. Cependant, un rapport e/c trop élevé favorise une grande porosité initiale continue, et le réseau

capillaire ne pourra se dissocier. Le tableau 4 montre le temps de cure humide nécessaire pour rendre le réseau de pores discontinu, et ce, selon le rapport e/c.

Dans le processus d'hydratation du ciment, l'eau se lie, soit chimiquement, soit physiquement, à l'intérieur des hydrates. L'eau ainsi liée au C-S-H est identifiée sous trois types (Sierra, 1980):

- Eau Hydroxylique: c'est toute l'eau combinée chimiquement, elle est très fortement ancrée aux atomes de Ca et Si des C-S-H. Cette eau est considérée comme non-évaporable.
- Eau Interfeuillet: eau retenue physiquement par des ponts hydrogènes, cette eau a un très faible degré de liberté, mais elle est néanmoins considérée comme évaporable.
- Eau Interlamellaire: c'est une eau adsorbée sur les parois des C-S-H et retenue par des forces de surface (forces de Van der Waals et des liaisons hydrogène). Cette eau est évaporable.

L'eau résiduelle au processus d'hydratation se retrouve dans les pores capillaires, cette eau est évidemment évaporable.

Tableau 4, Temps nécessaire de cure humide pour dissocier la porosité
(tiré de Powers et al., 1959)

Rapport eau/ciment	0.4	0.45	0.5	0.6	0.7	> 0.7
Temps	3 jours	7 jours	14 jours	6 mois	1 an	impossible

Références

Beaudoin, J.J. Catinaud, S., Marchand, J. (2001). Volume stability of calcium hydroxide in aggressive solutions, Cement and Concrete Research, 31, 2, 149-151.

Berry, Hemmings, Cornelius (1988). Speciation in Size and Density Fractionated Fly Ash. The Influence of HCL Leaching on the Glassy constituents of a High-Ca Fly Ash, Materials Research Society Symposia Proceedings, Fly Ash and Coal Conversion by-Products: Characterization, Utilization and Disposal, Vol.113

Brew, D.M.R., Glasser, F.P. (2005). The magnesia-silica gel phase in slag cements: alkali (K, Cs) sorption potential of synthetic gels, Cement and Concrete Research, 35, 1, 77-83.

Carette, C. G., Malhotra, V. M. (1986). Characterization of Canadian fly ashes and their relative performance in concrete. Energy, Mines and Resources Canada, Ottawa, ON, CANMET Report 86-6E.

Diamond, S. (1981). Cement pastes rheology and evolution of properties and structure, in: Proceedings of the 7th International Congress on the Chemistry of Cement, Editions Septima, Paris.

Hemmings, Berry, Cornelius, Sheetz (1987). Speciation in Size and Density Fractionated Fly Ash. Characterization of a Low-Calcium, High-Iron Fly Ash, Materials Research Society Symposia Proceedings, Fly Ash and Coal Conversion By-Products: Characterization, Utilization and Disposal, Vol. 86.

Hewlett, P.C. (1998) Lea's chemistry of cement and concrete, 4th ed., 1053 p.

Mehta, P. K. (1989), Pozzolanic and cimentitious by-products in concrete – another look. Proceedings, 3rd CANMET/ACI International Conference on the Use of Fly Ash, Silica Fume, Slag, and Other Mineral By-products in Concrete, Trondheim, Norway, June 18-23, 1989. Edited by V.M. Malhotra. American Concrete Institute, Detroit, MI, Special Publication SP-114, Vol. 1, 1-43.

Mehta, P. K. (2001), Growth with sustainability – A great challenge confronting the concrete industry, Symposium P.-C. Aïtsin sur l'évolution de la technologie du béton, American Concrete Institute Section du Québec et de l'est de l'Ontario, 89-98.

Malhotra, V. M. (1999). Making concrete greener with fly ash, Concrete International, 21, 5, 61-66.

Malhotra, V. M. (2001), High-Performance – High-Volume Fly Ash Concrete for Sustainability, Symposium P.-C. Aïtsin sur l'évolution de la technologie du béton, American Concrete Institute Section du Québec et de l'est de l'Ontario, 19-74.

Neville, A.M., (1981). Properties of concrete, third edition, 779 p.

Powers, T.C., Copeland, L.E., Mann, H.M. (1959). Capillary continuity or discontinuity in cement pastes, Journal of the Portland cement association, Research and development laboratories, I, 2.

Ramachandran, V.S., Beaudoin, J.J. (2001). Handbook of Analytical Techniques in Concrete Science And Technology, National Research Council of Canada, Noyes Publications, 985 p.

Regourd, M. (1982). Microstructures et propriétés des ciments, mortiers et bétons, Ciments, Bétons, Platres, Chaux, 734-1/82, Publication CERILH 272, 41-48

Saric-Coric, M., Aïtcin, P.C. (2001). La résistance à l'écaillage des ciments composes au laitier, ACI, Progrès dans le domaine du béton 2001, 4 décembre, 11 p.

Sierra, R. (1980). Répartition des différentes formes d'eau dans la structure des pâtes pures de C3S et de ciment Portland, Paris, vol. 3, 4, 201-206.

Skalny, J.P., Young, J.F. (1980). Mechanisms of Portland cement hydration, Principal report, Paris, 2, 2, 123-128.

Taylor, H.F.W. (1990). Cement Chemistry, Academic Press Ltd., 475 p.

Troxell, G.E., Davis, H.E., Kelly, J.W. (1968). Composition and properties of concrete, 2nd edition, McGraw-Hill book company.

Woods, H., Steinour, H.H., Starke, H.R. (1933). Heat evolved by cement in relation to strength, New York, Engng. News Rec., 431-433.

APPENDICE B

EFFECT OF BINDER TYPE AND MIXING WATER CHEMISTRY
ON MICROSTRUCTURAL EVOLUTION OF CEMENTED PASTE BACKFILL[9]

RÉSUMÉ

Des essais au porosimètre au mercure (PHg) ont été effectués sur 54 échantillons de pâte de ciment (PC) (e/c = 0.33) et de remblais en pâte cimentés (RPC) (e/c = 7). Les échantillons étudiés étaient constitués de trois liants (CP type 10, CP 10-cendre volante, CP type 10-laitier de haut-fourneau) et de trois eaux ayant chacune une teneur en sulfate différente (≈ nulle, 4613, 7549 ppm). L'étude au PHg des pâtes de ciment a permis de rehausser les différences microstructurales entre les 3 ciments et d'identifier les principaux paramètres d'influence de l'évolution microstructurale et ce, avant la réalisation des essais sur les remblais cimentés en pâte. Les résultats obtenus sur les RPC montrent que malgré une porosité totale constante, il y a une diminution de la taille des pores avec la cure. Le raffinement des pores est plus important avec le ciment au laitier, ce qui pourrait expliquer en partie les meilleures résistances mécaniques obtenues. Par ailleurs, la présence de sulfate dans l'eau de gâchage a un effet positif sur le raffinement des pores et le gain de résistance mécanique. Les essais ont montré qu'il existe un lien direct entre l'UCS et la finesse des pores, et que le PHg est un outil efficace pour investiguer la microstructure des RPC.

ABSTRACT

Mercury intrusion porosimetry (MIP) tests were performed on 54 hardened cement paste (CP) (w/c = 0.33) and cemented paste backfill (CPB) (w/c = 7) samples. Three

[9] Ouellet, S., Bussière, B., Benzaazoua, M., Aubertin, M., Belem, T. (2004) Effect of binder type and mixing water chemistry on microstructural evolution of cemented paste backfill, Proceedings of the 57th Annual Canadian Geotechnical Conference and 5th joint IAH-CNC/CGS Conference, Quebec, Quebec, Canada, October 23rd to 27th, 8 p.

binders (PC type 10, PC T10-fly ash, PC T10-blast furnace slag) and three waters containing different sulphate proportions ($\approx$ 0, 4613, 7549 ppm) were used in the specimen preparation process. Cement paste study showed microstructural differences between binders and to identify the main influence factors of the microstructural evolution before the porosimetry tests performed on cemented paste backfill samples. MIP results on CPB indicate that despite a constant total porosity, pore size diameter decreased with curing time. Pore refinement was more important with the slag binder, which would explain higher mechanical strength with this binder. Moreover, the effect of sulphate ions in mixing water was positive on pore refinement and on strength evolution. Tests showed a direct relationship between mechanical strength and pores refinement; and that MIP technique is an efficient tool to evaluate microstructure of CPB.

INTRODUCTION

Every year the mining industry produces a large amount of mill tailings. A part of the generated tailings can be stored in underground mines as a cemented paste backfill (CPB) to stabilize open stopes (e.g. Hassani and Archibald, 1998; Benzaazoua et al., 1999; Aubertin et al., 2002). CPB is a composite material made of a mixture of thickened tailings (at a pulp density between 75 to 85%), binders (such as Portland cement, fly ash, blast furnace slag or a combination) and water. The main benefits of underground paste backfill include a higher strength and lower operating costs (in most cases) compared to hydraulic fills (Hassani and Archibald, 1998). Moreover, the use of paste backfill reduces the amount of tailings that have to be sent to surface disposal facilities. This reduction decreases both the environmental impact and capital expenditures of the tailings facility. Because the mining industry in Canada and around the world increasingly uses CPB, a better knowledge of their microstructural characteristics and of the main influence factors affecting microstructure and strength (water quality and quantity; type and percentage of binder, grain size distribution and mineralogy of tailings, etc.) is needed to get a global understanding of such material.

Over the past few years, a few authors investigated the microstructure of CPB. Mitchell and Wong (1982) showed a relationship between porosity, cement content, and pulp density. They showed that the porosity of the backfill decreased when the cement content was increased from 4 to 12 %, and that thickening tailings (removing water) was one of the main parameters to reduce total porosity. Keren and Kajnian (1983) incorporated the porosity parameter in a study on the water percolation rate through hydraulic fills. Benzaazoua et al. (2000) and Belem et al. (2001) used mercury intrusion porosimetry (MIP) tests to investigate the porosity of CPB. Their results showed that the total CPB porosity was very close to that of an agglomerated tailings. Belem et al. (2001) also showed that the addition of binder (5%wt) reduces pore size significantly, which reduces the saturated hydraulic conductivity and increases the water retention properties of the CPB. Finally, le Roux (2004) performed different tests including mercury intrusion porosimetry to evaluate and compare the microstructure of in situ and laboratory prepared CPB. MIP results showed that field and laboratory samples have a similar pore size distribution.

This paper presents a comparative study of the microstructural evolution using mercury intrusion porosimetry (MIP) technique for different cement pastes (CP) and cement paste backfills (CPB) at different curing times. Cement paste mixtures (binder and water only) were prepared to enhance the cementitious effects and to isolate interactions between the water and the binder. The mixtures studied were made from three typical binders used in the mining industry (at 5%wt) and three types of water containing different typical sulphate concentrations. It is a common practice in the mining industry to use recycled water in the CPB preparation. Depending on the ore and the mineralurgical process at the mine, this water can contain sulphate ions that play a role in the hydration process of binders, and can precipitate in the paste and possibly generate cracks and loss of strength (Subauste and Odler, 2002). To complete the study, uniaxial compressive strength (UCS) tests were performed on samples to show the link between porosity evolution and mechanical strength.

MATERIALS AND METHODS

Materials and samples preparation

Both CPB and CP were prepared in small batches in a 20 litres bucket and mixed for at least 5 minutes with a ½ inch electric drill using a paint mixer bit. The three binders used were a CAN3-A5-M77 PC type 10 cement (T10) (100%), a mix of 20% PC T10 and 80% blast furnace slag (T10SL), and a mix of 70% PC T10 and 30% fly ash (T10FA). Table B.1 presents the chemistry of binders (ICP-AES analysis) and some physical properties. The PC T10 binder showed a typical chemistry for this type of cement (Neville, 1981) and the calculated Bogue's composition is 64.4% for C_3S, 6.6% for C_2S, 8.7% for C_3A and 7.4% for C_4AF. According to ASTM C618-00 standard, the studied fly ash can be classified as a class C with a cumulative value for SiO_2, Al_2O_3 and Fe_2O_3 less than 70% and a SO_3 content less than 5%. BF slag met the recommendation of Malhotra (2001) to prevent sulphate attack with an Al_2O_3 percentage less than 11%. BF slag shows also the highest BET specific surface with a value of 21 380 cm²/g indicating that the size of particles was the finest of all binders. The specific surfaces of the other two binders are 12 764 and 8 697 cm²/g for OPC T10 and Fly ash respectively.

The mixtures used three different types of water: the first one was deionised by filtration (named W0), the second one was a mine water sampled at a backfill plant which contained a sulphate concentration of 4613 ppm (named W1), and the last one was also a mine water sampled at the backfill plant of a second mine which had a sulphate concentration of 7549 ppm (named W2). One can see in Table B.2 that the calcium content of mine waters are relatively high (803 and 1790 ppm for W1 and W2 respectively). These high concentrations are mainly due to the ore processing techniques that use lime in the process to increase the pH. Alkali concentrations are relatively high but only the W1 water exceeded the recommended maximum concentration of 500 ppm Na_2O equivalent from ASTM-C94 standard with

a value of 1266.2 ppm Na_2Oeq. The W2 water had a Na_2Oeq. concentration of 187.7 ppm. The pH varied for the different waters between 4.57 to 9.62. Mine waters were filtered to remove suspended particles before analysis and mixing. For all CPB mixtures ground silica from BEI Pecal was used to simulate tailings. The silica contains 99.76% SiO_2 and has a grain size distribution (evaluated with a laser Mastersizer from Malvern Instruments) close to the average of 11 mine tailings (coming from the province of Quebec and northern Ontario) with a percentage passing 80 μm of approximately 80% and a percentage of particles less than 2 μm of about 10% (Figure B.1). The uniformity coefficient ($C_U = D_{60}/D_{10}$) and the coefficient of curvature ($C_C = D_{30}^2/D_{60}\text{-}D_{10}$) are respectively 16.5 and 3.4. According to USCS classification the silica material can be classified as a non plastic silt (ML).

Table B.1. Chemical composition of binders (ICP analysis)

	OPC T10 (%wt)	Fly ash (%wt)	BF Slag (%wt)
SiO_2	19.25	44.93	36.37
Al_2O_3	4.82	17.67	10.28
Fe_2O_3	2.42	6.09	0.51
CaO	60.59	15.39	31.34
MgO	2.19	2.95	11.18
K_2O	0.81	0.65	0.48
Na_2O	2.10	7.41	2.01
SO_3	3.92	1.90	3.20
D_r	3.12	2.53	2.91
SS BET (cm²/g)	12764	8697	21380

Table B.2. Chemical composition of waters (ICP analysis)

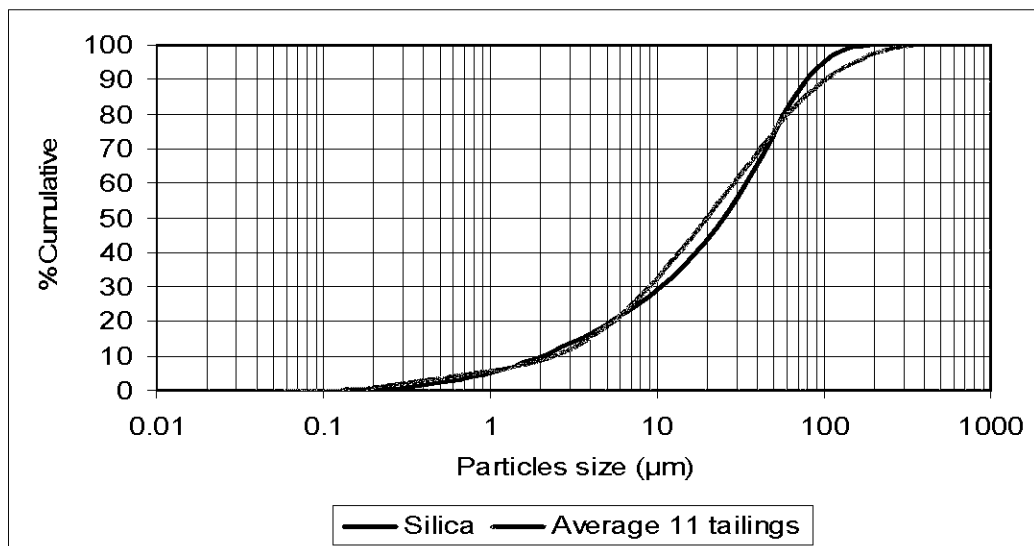|	W0 (ppm)	W1 (ppm)	W2 (ppm)
Al	0.03	1.06	0.29
Ca	0.02	803.00	1790.00
Cu	<0.01	0.59	0.21
Fe	0.05	0.04	1.01
K	0.14	41.40	48.00
Mg	0.01	1.00	1.71
Na	<0.2	915.00	111.00
Si	3.78	0.82	0.50
Zn	<0.02	0.08	0.53
SO_4^{2-}	0.36	4613.22	7548.91
pH	6.09	9.62	4.57
EhN	435.8	243.7	361.1
Cond. (µS/cm)	2	5950	3740

Figure B.1, Particles size distribution of silica.

A total of 108 CPB and CP cylinders of 10 cm long and 5 cm in diameter were cured at room temperature and at a relative humidity greater than 75%. The binder proportion for the CPB was 5% by weight of dry silica. Water to cement ratios were 7 for the CPB mixtures (representing a water to solid ratio of 0.33) and 0.33 for the CP samples. Two cylinders of each mixture were cast to evaluate the uniaxial compressive strength (UCS) after 14, 43 and 92 curing days using a MTS 10/GL

press with a 50kN capacity. After the UCS test was performed, a fraction of each cylinder was sampled (about 20 g) for the microstructural characterization.

Drying of the samples was performed by a combination of freeze drying and oven drying. Samples were first cut in small cubes of about 1 cm³ each and immersed for more than 5 minutes in liquid nitrogen. Samples were then dried for a period of 24 hours at 7 miliTorr and -50°C in a Virtis Ultra 35 Super XL freeze dryer. Immersion in liquid nitrogen allows solidifying rapidly the internal water in microcrystals of ice. The second step in the vacuum freeze dryer directly sublimates the ice without returning to a liquid phase. Another period of 24 hours in an oven at 45°C completed the drying; according to Kjellsen (1996) this should complete the drying without generating cracks. After the drying steps, all CP and CPB samples were maintained in a desiccator to avoid rehydration. Freeze drying technique, as the one used in this study, is considered a gentle drying technique that has been applied for many years on cement pastes (Gallé, 2001; Kjellsen, 1996) and on clayey soils (Hueckel et al., 1997; Simms and .Yanful, 2001). Trying to keep the microstructure of a cement material as close as possible to the original microstructure is important. Oven drying at a too high temperature can cause cracks (Gallé, 2001) and remove water physically adsorbed and/or chemically attached on some hydrated minerals (Ramachandran and Beaudoin, 2001).

Mercury intrusion porosimetry

Mercury intrusion porosimetry (MIP) is based on the capillary law governing the penetration of a liquid into pores (Ramachandran and Beaudoin, 2001). For the case of a non-wetting liquid like mercury and a material with cylindrical pores, this law is expressed by the Washburn equation (e.g. :

$$D = -(1/P)\ 4\gamma cos\varphi, \qquad (1)$$

where D is pore diameter, P the applied pressure, γ the surface tension and φ the contact angle.

According to MIP test theory, when a pressure is applied to a porous media surrounded by mercury, the mercury should fill the pores of a diameter equal to the pressure applied in respect to Washburn relation. The main limitation of the MIP test is related to the ink bottle effect. Because mercury must pass through the narrowest pores connecting the pore network, MIP cannot provide a true pore size distribution (Cook and Hover, 1999). Many papers were written on the evaluation of cement paste porosity by MIP technique. Winslow and Diamond (1970) studied parameters influencing MIP and defined the parameter named "threshold diameter" that corresponds to the diameter, according to Washburn's equation, where the maximum of mercury fills the sample. The significance of this parameter was explained by the authors to be the minimum diameter of pores which are geometrically continuous throughout the cement paste sample. Later, Diamond (2000) concluded that the MIP misallocated the sizes of almost all of the volume of pores in hydrated cementitious materials. However, he mentioned that the MIP was a technique with a good repeatability and when used on a comparative basis was able to give valid information on permeability, ions transport and total porosity in cement systems. Other authors (Cook and Hover, 1999; Wild, 2001; Chatterji, 2001; Gallé, 2003) added that monitoring the threshold diameter evolution over the curing time is a useful technique that reflects the pore refinement within the cement paste. Based on the available literature it can be said that MIP is a reliable qualitative test to evaluate the microstructure evolution of cemented materials if the limitations of the technique are taken into account.

In this study MIP tests were performed on CP and CPB samples after each curing period. The equipment used is an Autopore III 9420 from Micromeritics that can generate a maximum pressure of 414 MPa and evaluate a theoretical pore diameter of 0.003 µm. The contact angle and surface tension assumed for all tests were respectively 130° and 485 dynes/cm. Depending on the average porosity, the

samples were cut in small cubes between 0.6 and 3 grams to reach the manufacturer recommendation of mercury stem volume between 25 and 90%.

MIP RESULTS AND ANALYSIS

Cemented paste backfill is a material with a low cement content and a high water/cement ratio. Usually about 5% of binder by weight of dry tailings is added and a water/cement ratio of 7 is used. In these conditions it is difficult to isolate and study the cementitious matrix. Keeping in mind that the evolution of the CPB over time is controlled by the binder, mixtures of cement paste (binder and water only) were prepared to enhance the cementitious effects and to allow the observation of the water and binder behaviour on the microstructure of CPB. In addition, because literature on cement paste is abundant, the tests on CP samples were used to validate the research protocol and MIP results.

Cement pastes

Figures B.2 to B.7 present MIP pore size distribution of CP mixed with waters W0 and W2 (results using W1 water are not shown here but exhibit the same behaviour). In these graphs, the sum of porosity for each increment of pressure corresponds to the CP total porosity. Table B.3 and B.4 present respectively the total porosity and the threshold diameter for all CP mixtures. Let's recall that the threshold diameter corresponds to the pore diameter where the highest rate of mercury intrusion occurs in the CP.
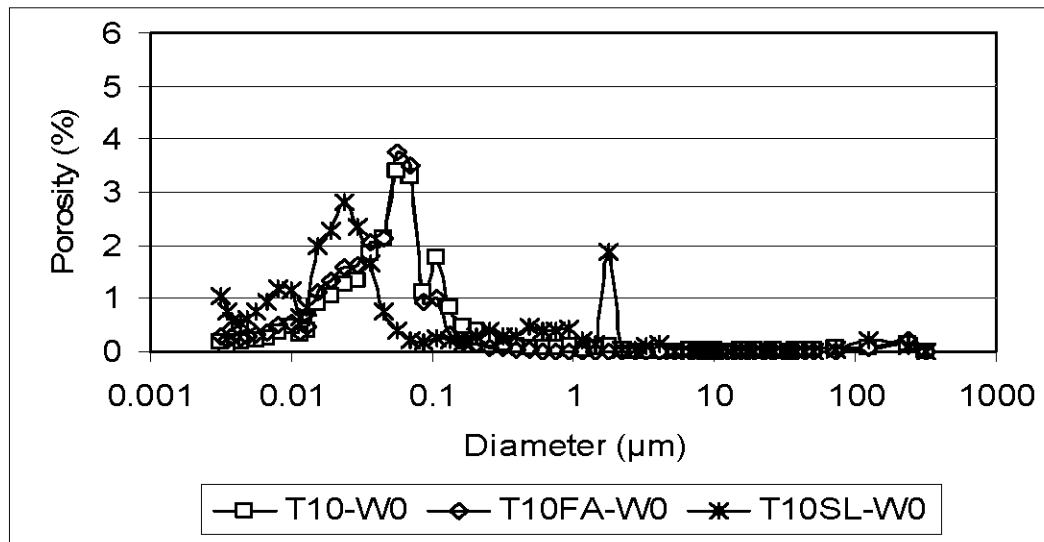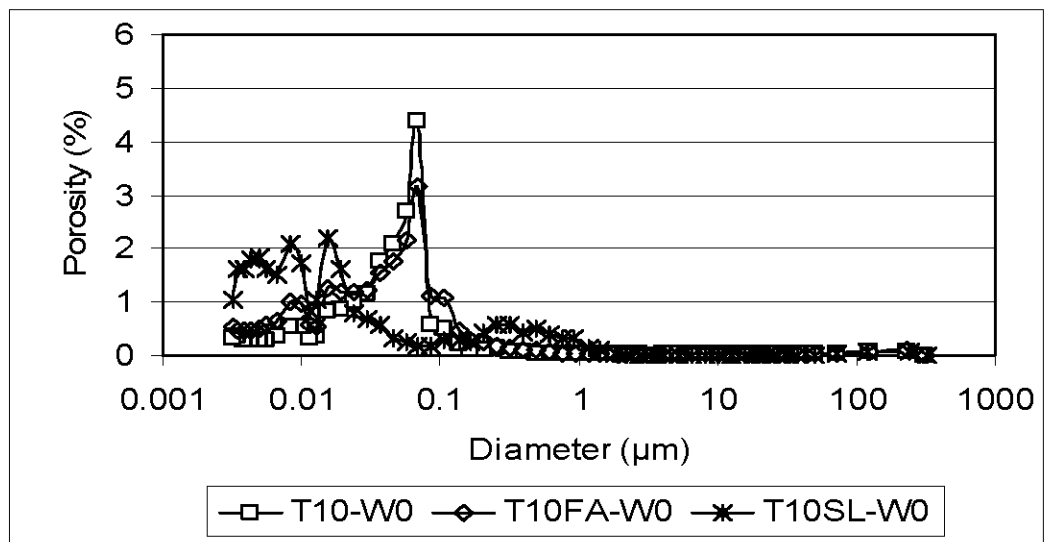
Figure B.2, MIP results at 14 days with W0 water.

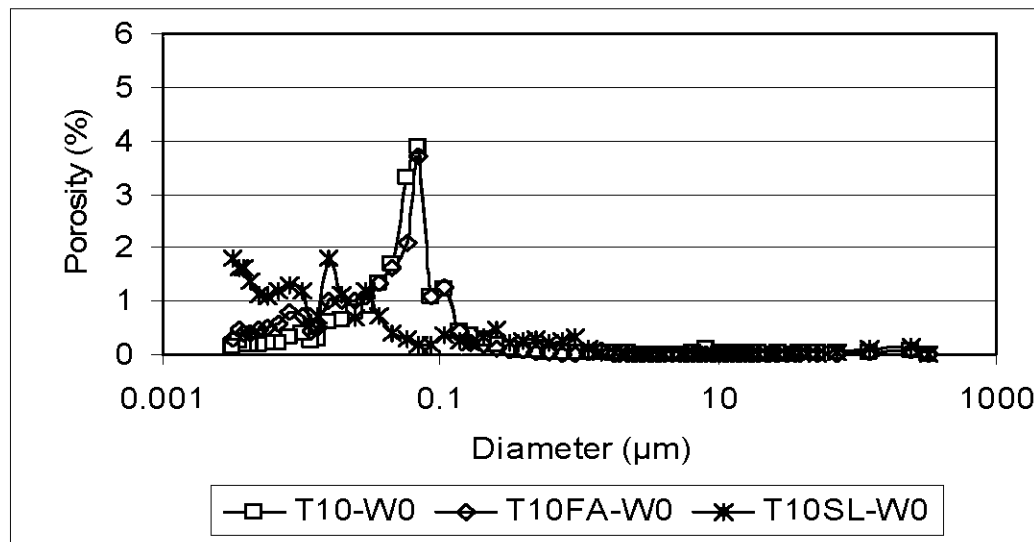Figure B.3, MIP results at 43 days with W0 water.

Figure B.4, MIP results at 92 days with W0 water.

Effect of binders

Figures B.2 to B.4 show that CP samples with T10SL binder exhibit a different behaviour than the CP samples using T10 and T10FA. First, the position of the highest mercury intrusion (threshold diameter) is at the left side of the graph (smaller pore size), compared with the other two. This means that pastes using T10SL need more pressure to be intruded by the mercury, indicating a finer porosity. Another particularity of T10SL CP samples is the small intrusion at a diameter near 1 µm. This may well imply that these pastes have two families of pores: a small one near 1 µm and another (the main one) usually below 0.1 µm. CP mixtures with T10 and T10FA binders show similar intrusion behaviour and seem to have similar microstructures. CP mixtures using the T10SL binder show significant changes of threshold diameter. For these samples, the threshold diameter drops by about one half from 14 to 92 days (Table B.4), while it stays relatively unchanged for CP using T10 and T10FA.
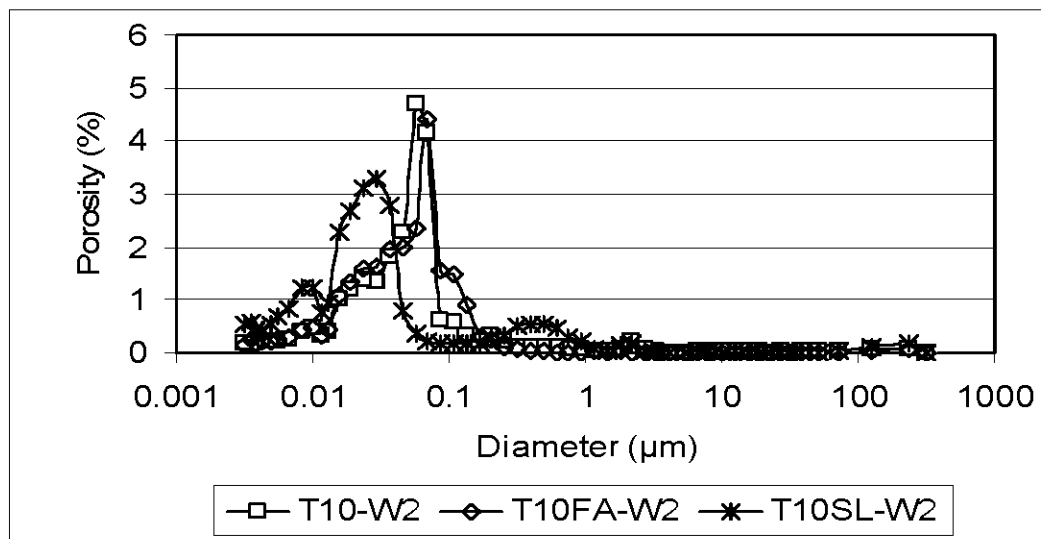
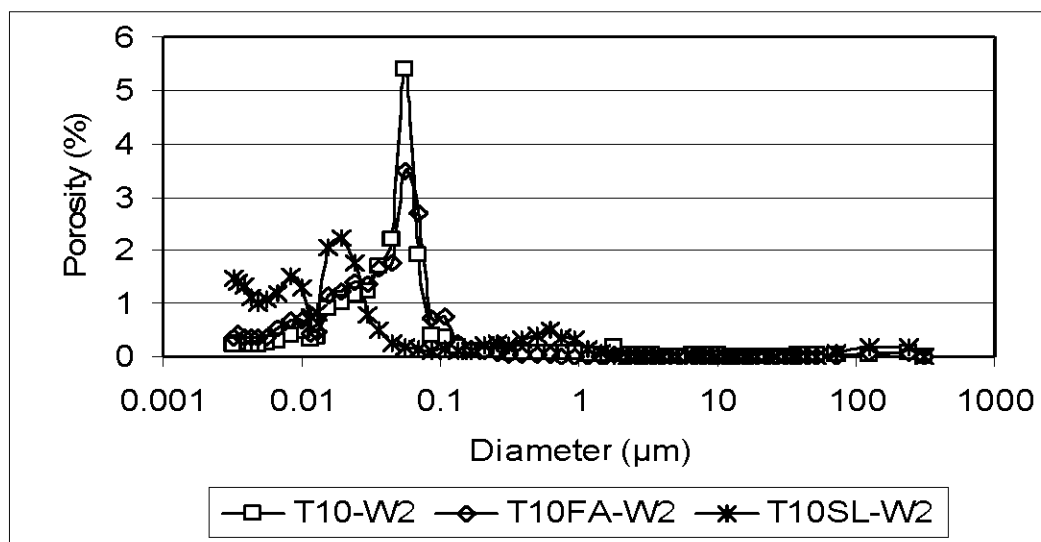Figure B.5, MIP results at 14 days with W2 water.

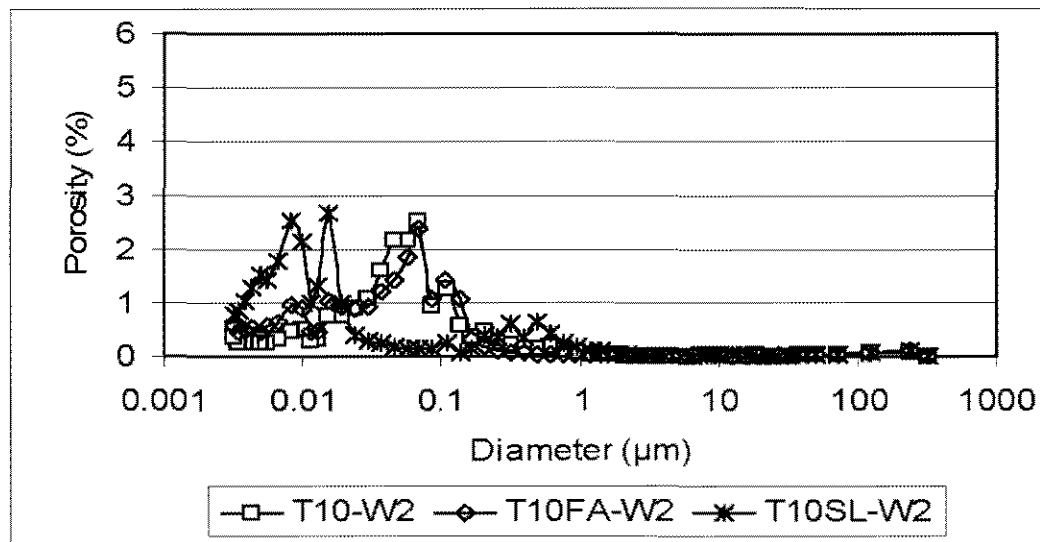Figure B.6, MIP results at 43 days with W2 water.

Figure B.7, MIP results at 92 days with W2 water.

Table B.3, CP's total MIP porosity (%)

	14 days	43 days	92 days
W0-T10	23.87	21.09	20.07
W0-T10FA	24.40	24.49	22.38
W0-T10SL	28.33	28.59	23.99
W1-T10	23.39	20.88	18.24
W1-T10FA	25.45	23.10	23.01
W1-T10SL	26.73	25.96	24.17
W2-T10	24.31	20.78	20.37
W2-T10FA	24.67	22.50	21.89
W2-T10SL	28.52	24.74	25.03

Table B.4, Paste's threshold diameters (μm)

	14 days	43 days	92 days
W0-T10	0.0565	0.0698	0.0698
W0-T10FA	0.0565	0.0697	0.0698
W0-T10SL	0.0237	0.0155	0.0154
W1-T10	0.0697	0.0566	0.0454
W1-T10FA	0.0697	0.0566	0.0565
W1-T10SL	0.0237	0.0191	0.0082
W2-T10	0.0565	0.0565	0.0697
W2-T10FA	0.0699	0.0565	0.0696
W2-T10SL	0.0294	0.0191	0.0155

Another interesting aspect of T10SL pastes is that at all curing times, the total porosity is higher than that of the other pastes, even if the pore size distribution is finer. To illustrate the differences within pastes, Figure B.8 shows the sum of pores ≤ 0.01 µm (corresponding to an intrusion pressure of 137 MPa and higher). This sum corresponds to the porosity associated to each increment of pressure for pore size less or equal to 0.01 µm. The difference between binders is highlighted in this figure. Mixtures with T10SL binder show a higher proportion (more than 50% after 92 days), but the mixtures with T10FA binder show a difference with T10 samples (between 21 and 25% for T10FA vs 11 to 14% for T10). This difference could be produced by a late hydration of FA particles and a pozzolanic effect.
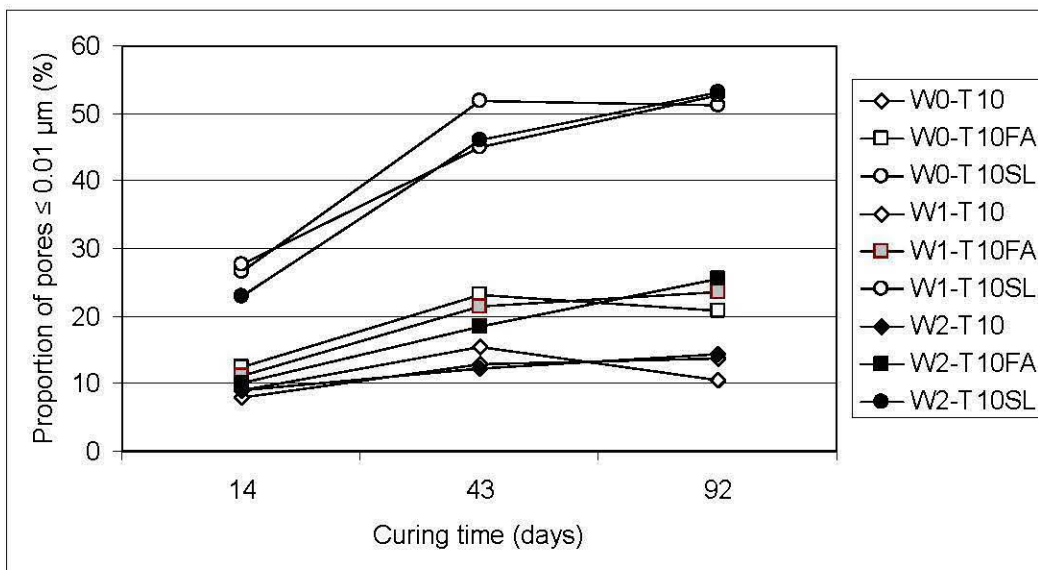

Figure B.8, Evolution of porosity ≤ 0.01 µm (137 MPa).

Effect of curing time

All CP samples show a slight decrease of the total porosity with the curing period (Table B.3). Figures B.2 to B.4 present an increase in the porosity under 0.01 µm with curing time for all binders. The same behaviour is observed in Figures B.5 to B.7 (CP with W2 water). Results presented in Figure B.7 (MIP results at 92 days with

W2 water) show a clear difference in the maximum intrusion values, which are all below 3% porosity. This means that there is a better distribution of the pore size in the matrix (on the finer side), with fewer large size families.

Effect of mixing water quality

Figure B.8 also shows the influence of water quality. For the curing time of 43 days and 92 days, the percentage of pores corresponding to a diameter ≤0.01 µm decreases or stays the same for samples with W0 water, but continues to rise slowly for mixtures containing sulphated water. This could indicate the precipitation of sulphated minerals in the mid to large size pores, contributing to an increase in the number of pores under 0.01 µm.

Cemented paste backfills

MIP tests on CP samples highlighted the influence of some factors (binder type, water type, curing time) on MIP porosity results. Other tests on CPB samples have been preformed to evaluate if observations on CP samples are still valid for CPB samples.

Figures B.9 to B.14 show the evolution of MIP porosity of CPB samples while Tables B.5 and 6 present respectively the total MIP porosity and the threshold diameter evolution. The comparison between Figures B.9 to B.14 and Figures B.2 to B.7 shows that the main differences between CP and CPB results are the height of the maximum mercury intrusions, which are much more important for CPB mixtures (about 10% for CPB compared to about 4% for CP), and the position of the maximum intrusion diameter, of approximately 1 µm for all CPB curves (compared to less than 0.1 µm for CP samples).
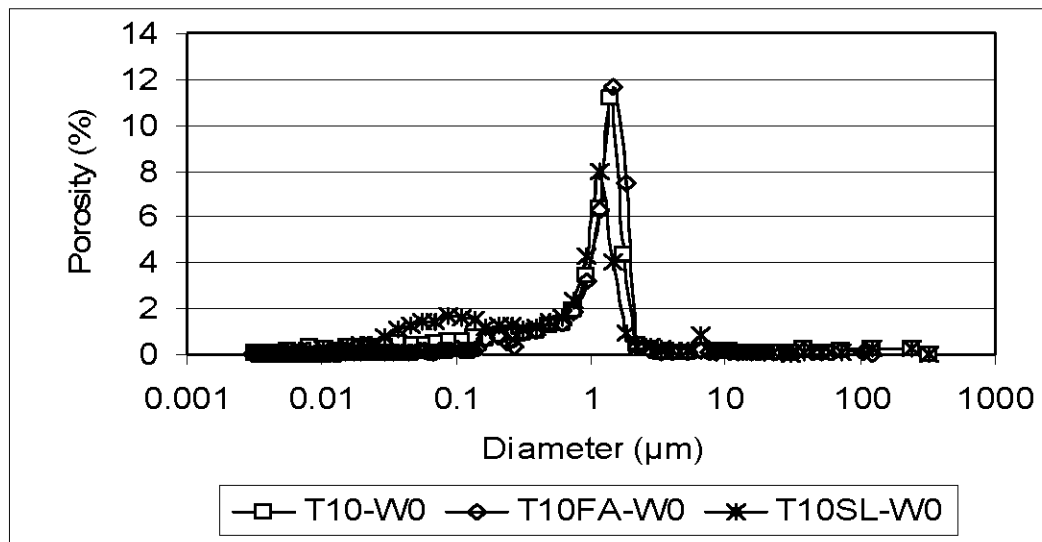
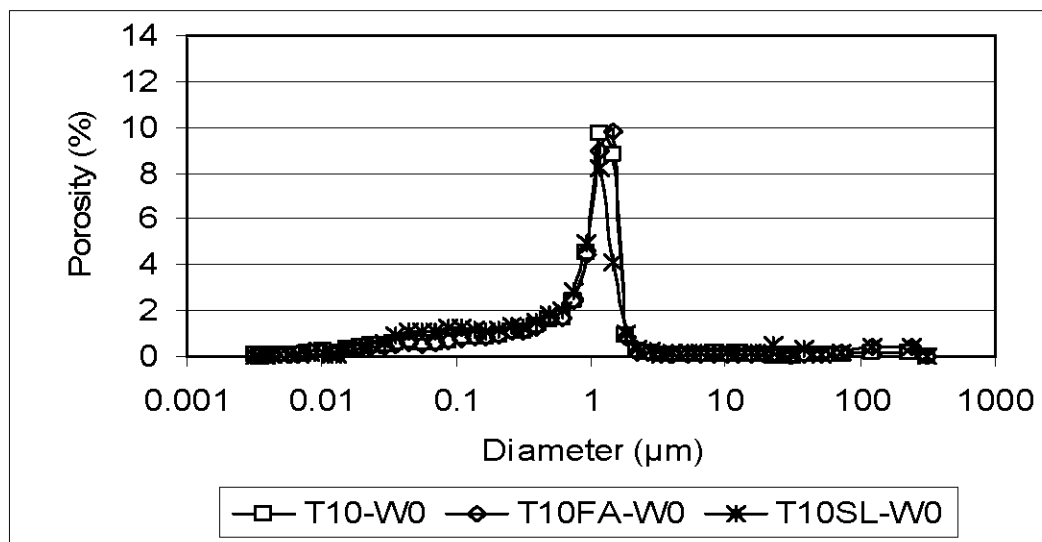Figure B.9, MIP results at 14 days with W0 water.

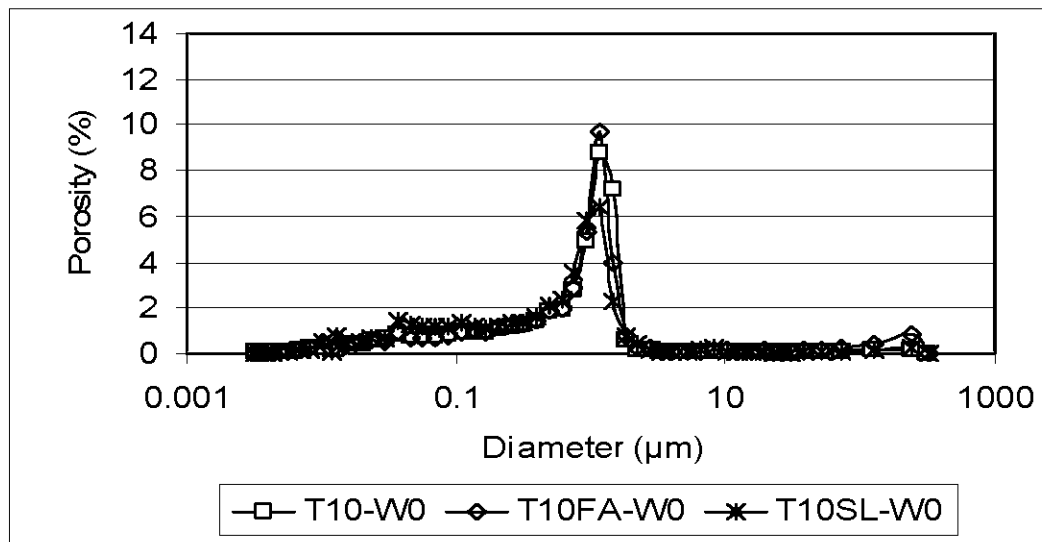Figure B.10, MIP results at 43 days with W0 water.

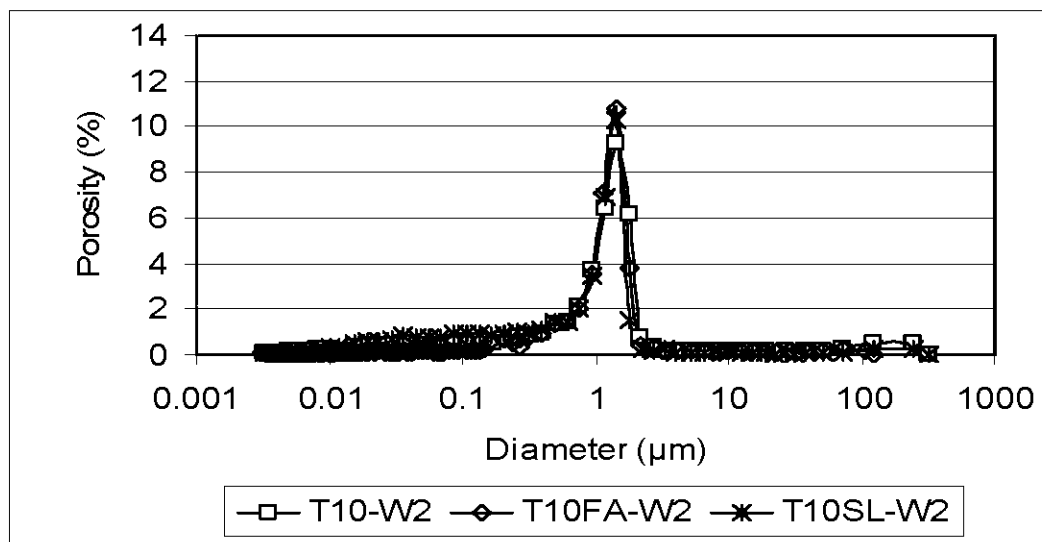Figure B.11, MIP results at 92 days with W0 water.

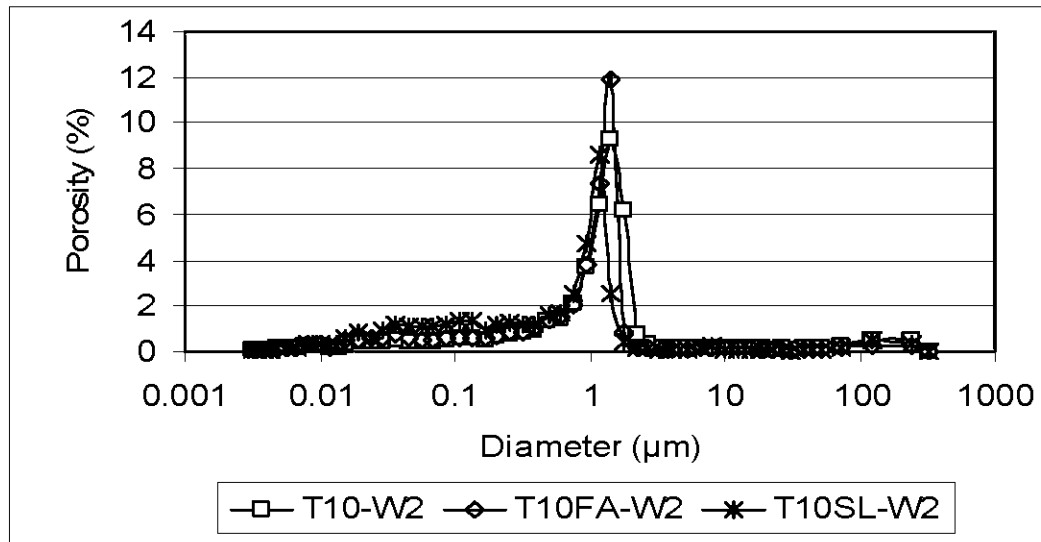Figure B.12, MIP results at 14 days with W2 water.

Figure B.13, MIP results at 43 days with W2 water.
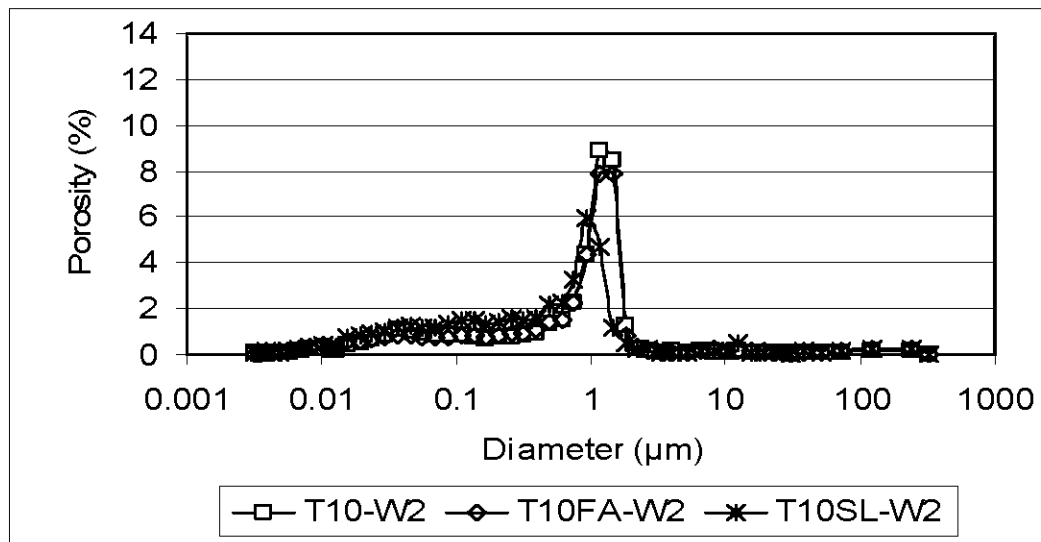

Figure B.14, MIP results at 92 days with W2 water.

Effect of binders

As observed for CP mixtures, Figures B.9 to B.14 shows that results for CPB mixtures with T10SL binder are different than the ones for the other two binders. For

example, Figure B.9 shows that the curves with T10 and T10FA binders have a similar shape; there is only one peak of intrusion at 1 µm and the maximum intrusion takes about 12% of the total porosity. For CPB samples using T10SL binder, the position of the maximum peak is at the left of the other two, being lower at a value of approximately 8% of total porosity. Nevertheless, similar to the CP results, samples using T10SL binder developed a larger proportion of finer porosity than other samples with T10 and T10FA.

Effect of curing time

For similar total porosity of CPB samples (Table B.5), a significant decrease in the height of the main intrusion peaks and a movement of the pore size distribution to the left with the curing time is observed, indicating a refinement of the porosity. On Figures B.9 to B.11, which show the evolution of MIP porosity for the mixtures using the W0 water, the proportion of the porosity at the maximum rate of intrusion drops from a value of 12% at 14 days to a value lower than 10% after 92 days for T10 and T10FA samples, and from 8% to a value near 6% for the mixture with the T10SL binder. Since the total porosity measured by the MIP technique is unchanged even after a curing time of 92 days, pores of CPB samples become finer with curing time. Another effect of curing time is the decrease of the threshold diameter (Table B.6). For T10 and T10FA samples, the threshold diameter moves from about 1.43 µm to about 1.17 µm. This indicates that as these CPB samples evolve, the pores are finer and the pressure to apply to significantly intrude the matrix with mercury increases. The same trend is observed for T10SL samples with water W2; threshold diameters of T10SL samples using W0 and W1 waters remain constant over 92 days.

Effect of mixing water quality

The behaviour of mixtures made with W2 water is similar to the ones with W0 water (see Figures B.12 to B.14). The pore refinement effect is more apparent at a curing time of 92 days with W2 water. Only the mixture using the T10SL binder and the W2 water has a threshold diameter lower than 1 μm with a value of 0.93 μm at 92 days. A combination of the behaviour of the T10SL binder and a potential precipitation of sulphated minerals in the pores could explain the decrease in bigger pore proportion and the increase of finer pore proportion.

Table B.5, CPB's total MIP porosity (%)

	14 days	43 days	92 days
W0-T10	43.99	44.70	44.91
W0-T10FA	45.80	44.85	45.79
W0-T10SL	45.18	45.95	45.03
W1-T10	44.52	43.59	44.94
W1-T10FA	44.16	44.04	44.26
W1-T10SL	44.82	44.34	43.88
W2-T10	44.94	43.80	44.41
W2-T10FA	44.73	43.67	43.63
W2-T10SL	44.52	43.96	45.06

Table B.6, CPB's threshold diameters (μm)

	14 days	43 days	92 days
W0-T10	1.4189	1.1729	1.1718
W0-T10FA	1.4378	1.4375	1.165
W0-T10SL	1.1666	1.1653	1.1622
W1-T10	1.4326	1.1716	1.1717
W1-T10FA	1.434	1.1661	1.1663
W1-T10SL	1.1633	1.1647	1.1658
W2-T10	1.4345	1.4387	1.1732
W2-T10FA	1.4348	1.4409	1.1679
W2-T10SL	1.4418	1.1632	0.9283

Figure B.15 shows the sum of the porosity with a MIP pore diameter under 0.1 µm at all curing times. Although the results presented are less significant than those for CP mixtures (see Figure B.8), it is still the mixture using the T10SL binder and the W2 water that shows the more important proportion of pores under 0.1 µm at all curing times. Moreover, sulphated water seems to have a beneficial effect on the reduction of the pore size. Except for CPB samples using T10SL and W0 water, all other samples using sulphated water show a higher percentage of small pores than the equivalent control samples using W0 water.
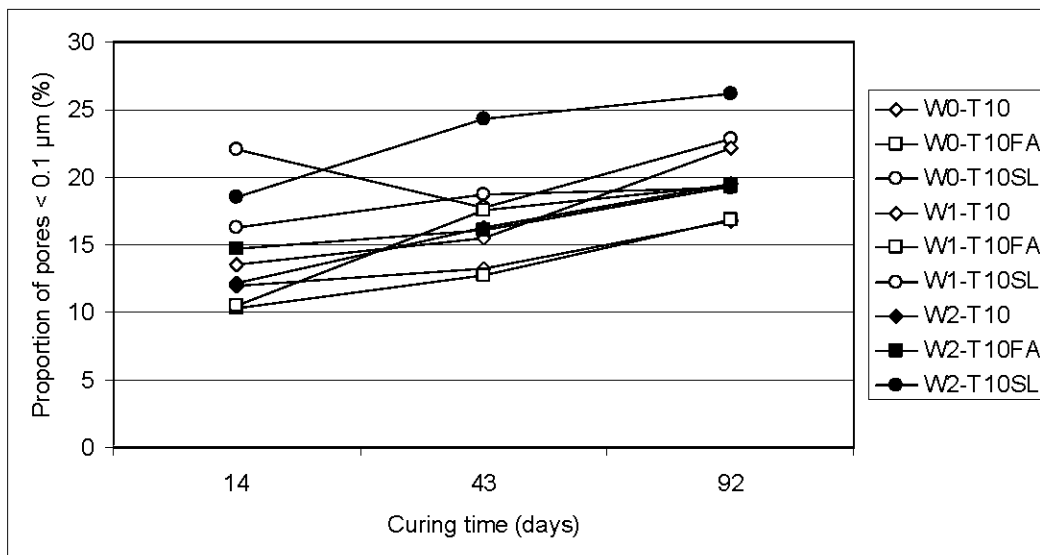

Figure B.15, Proportion of pores lower than 0.1µm.

MIP porosity vs uniaxial compressive strength

Another important aspect of the microstructural behaviour of CPB is the strength development (represented in this study by UCS results). Figure B.16 shows the UCS results for CPB samples at the three same curing times (14, 43 and 92 days). Once again as for the MIP tests, the mixtures using the T10 and the T10FA binders have similar behaviour. For these CPB, the UCS typically ranges from 280 kPa at 14 days to about 800 to 1000 kPa at 92 days for the three water types. The strength of mixtures with T10SL binder is higher than those of the other two binders for all samples at all curing times. The highest value is 1822 kPa with water W2 at 92 days, which is in concordance with MIP results that showed a finer porosity for this CPB mixture. Water effects are also present in UCS results. In almost all cases, the sulphated waters gave a better strength than the clean water (W0), supporting the hypothesis that precipitation of sulphate minerals contribute significantly to strength development (Benzaazoua et al., 2004).
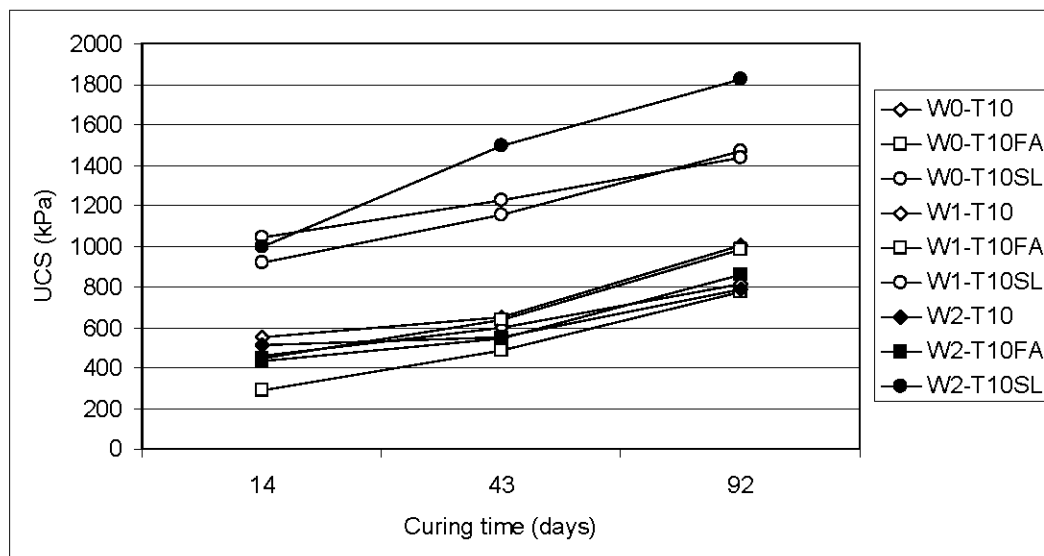

Figure B.16, UCS results for CPB samples.

To relate the mechanical strength to the porosity, Figure B.17 presents a graph of UCS results against the sum of pore size less than 0.1 µm. The squares represent all results using the T10SL binder and circles represent all results with T10 and T10FA binders (since the study showed that their behaviours are similar). Note that the grey square is not included in the line equation for T10SL binder. According to this graph, the UCS shows a linear relationship (see Figure B.17 for equations) with the proportion of pores less than 0.1 µm and an implicit refinement of pores with the curing time. As the finer pores proportion increases, the UCS increases. For the same proportion of pores < 0.1 µm, the UCS is greater for CPB samples made from T10SL binder. For both relationships, the coefficients of determination are higher than 0.8.

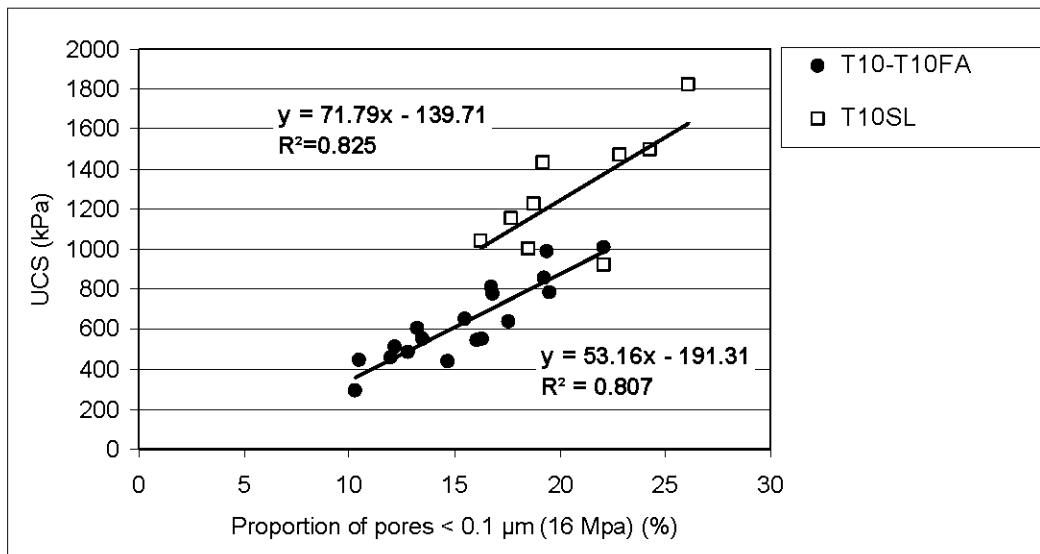Figure B.17, UCS results against proportion of pores size less than 0.1 µm.

SUMMARY AND CONCLUSION

This paper showed porosity evolution measured by mercury intrusion porosimetry on cement paste samples and cement paste backfill samples made with ground silica. Three binders were tested: a type 10 Portland cement alone (T10), a mix 20:80 of type 10 Portland cement and blast furnace slag (T10SL) and a mix 70:30 of type 10 Portland cement and fly ashT10FA. Three different types of water were used in the preparation of the mixtures: a deionised water and two waters coming from two mine backfill plants and containing 4613 and 7549 ppm SO_4^{2-}. The following conclusions can be drawn from this study:

For cement pastes:
- MIP study showed clearly the influence of the binder on the MIP porosity, especially with pore size calculated to be less than 0.01µm.
- MIP total porosity showed a slight decrease with time for all mixtures and threshold diameter that remained relatively constant for T10 and T10FA binders while it decreased with T10SL mixtures.
- T10SL binder gave finer pores at all curing times compared to pastes with T10 and T10FA binders.
- MIP porosity curves using T10 and T10FA binders were similar for the different curing times and for the different waters.
- Over the curing period of 92 days, waters (W1 and W2) containing sulphate ions up to a value of 7549 ppm induces a finer pore size distribution.
- CP mixtures enhance the impact of ingredients on MIP porosity; the influence factors on CP samples were also observed on CPB samples but to a lesser extent due to the higher w/c ratio.

For cement paste backfills:
- MIP technique allowed comparing porosity evolution for different CPB mixtures.

- Total porosity remained around 44% at all curing times and the threshold diameter decreased with time for all mixtures, indicating a low decrease of pore size.

- For all curing periods and for the studied waters, the sulphated water contributed to the refinement of the porosity and the increase of UCS.

- T10SL binder showed a larger proportion of pore size finer than 0.1 µm and the higher UCS values.

- Microstructural and strength evolution of T10 and T10FA mixtures were similar; replacement of T10 binder by at least 30% of FA could be a good economic opportunity.

- Despite the constant total porosity, MIP results showed that an evolution of pore size finer than 0.1 µm is correlated with UCS evolution.

ACKNOWLEDGEMENTS

REFERENCES

Aubertin M, Bussière B, and Bernier L. (2002). Environnement et gestion des résidus miniers. CD, Les Éditions de l'École Polytechnique de Montréal, Montreal, Canada.

Belem, T., Bussière, B. and Benzaazoua, M. (2001). The effect of microstructural evolution on the physical properties of paste backfill, Proceedings of Tailings and Mine Waste '01, Balkema, Rotterdam, ISBN 90 5809 182 1, 365-374.

Benzaazoua, M., Ouellet, J., Servant, S., Newman, P. and Verburg, R. (1999). Cementitious backfill with high sulfur content Physical, chemical, and mineralogical characterization, Cement and Concrete Research, 29, 5, 719-725.

Benzaazoua, M., Belem, T. and Jolette, D. (2000). Investigation de la stabilité chimique et son impact sur la qualité des remblais miniers cimentés, Rapport IRSST R-260, ISBN 2-551-20431-3, 158 p.

Benzaazoua, M., Fall, M. and Belem, T. (2004). A contribution to understanding the hardening process of cemented pastefill, Minerals Engineering, 17, 2, 141-152.

Chatterji, S. (2001). A discussion of the paper "Mercury porosimetry--an inappropriate method for the measurement of pore size distributions in cement-based materials" by S. Diamond, Cement and Concrete Research, 31, 11, 1657-1658.

Cook, R.A. and Hover, K.C. (1999). Mercury porosimetry of hardened cement pastes, Cement and Concrete Research, 29, 6, 933-943.

Diamond, S. (2000). Mercury porosimetry: An inappropriate method for the measurement of pore size distributions in cement-based materials, Cement and Concrete Research, 30, 10, 1517-1525.

Gallé, C. (2001) Effect of drying on cement-based materials pore structure as identified by mercury intrusion porosimetry: A comparative study between oven-, vacuum-, and freeze-drying, Cement and Concrete Research, 31, 10, 1467-1477.

Gallé, C. (2003). Reply to the discussion by S. Diamond of the paper "Effect of drying on cement-based materials pore structure as identified by mercury intrusion porosimetry: a comparative study between oven-, vacuum- and freeze-drying", Cement and Concrete Research, 33, 1, 171-172.

Hassani, F. and Archibald, J. (1998). Mine backfill CD-ROM, 263 p.

Hueckel, T., Kaczmarek, M. and Caramuscio P. (1997). Theoretical assessment of fabric and permeability changes in clays affected by organic contaminants, Canadian Geotechnical Journal, 34, 588-603.

Keren, L. and Kajnian, S. (1983). Influence of tailings particles on physical and mechanical properties of fill, Proceedings of the International Symposium on Mining with Backfill, Lulea, 7-9 June, 21-29.

Kjellsen, K.O. (1996). Heat curing and post-heat curing regimes of high-performance concrete: influence on microstructure and C-S-H composition, Cement and Concrete Research, 26, 2, 295-307.

le Roux, K-A (2004). In situ properties and liquefaction potential of cepented paste backfill, Ph. D. thesis to be published, University of Toronto, 183 p.

Malhotra, V.M. (2001). High-performance high-volume fly ash concrete for sustainability, Proceedings of the P.-C. Aïtcin symposium on the evolution of concrete technology, American Concrete Institute, A. Tagnit-Hamou, K.H. Khayat and R. Gagné Eds., 19-74.

Mitchell, R.J. and Wong, B.C. (1982). Behaviour of cemented tailings sands, Can. Geotech. J., 19, 289-295.

Neville, A.M. (1981). Properties of concrete, third edition, 779 p.

Ramachandran, V.S. and Beaudoin, J.J. (2001). Handbook of Analytical Techniques in Concrete Science And Technology, National Research Council of Canada, Noyes Publications, 985 p.

Simms P.H. and Yanful E.K. (2001). Measurement and estimation of pore shrinkage and pore distribution in a clayey till during soil-water characteristic curve tests, Canadian Geotechnical Journal, 38, 741-754.

Subauste, J.C. & Odler, I. (2002). Stresses generated in expansive reactions of cementitious systems, Cement and Concrete Research, 32, 1, 117-122

Winslow, D.N. and Diamond, S. (1970). A mercury porosimetry study of the evolution of porosity in portland cement. Journal of Materials, 5, 3, 564-585.

Wild, S. (2001). A discussion of the paper "Mercury porosimetry--an inappropriate method for the measurement of pore size distributions in cement-based materials" by S. Diamond, Cement and Concrete Research, 31, 11, 1653-1654.

APPENDICE C

SULPHIDE REACTIVITY WITHIN CEMENTED PASTE BACKFILL: OXYGEN CONSUMPTION TEST RESULTS[10]

RÉSUMÉ

Des essais de consommation d'oxygène ont été effectués sur 5 rejets de concentrateur sulfureux préparés au laboratoire dont les proportions en poids de pyrite sont approximativement de 4, 12, 22, 34 et 74%. Les essais ont été effectués à différents degrés de saturation. D'autres essais de consommation d'oxygène ont été effectués sur des cylindres de remblai en pâte cimentés fabriqués à partir de ces mêmes rejets. Les résultats de consommation d'oxygène sur les rejets de concentrateur montrent que la réactivité des résidus est une fonction de la quantité de pyrite et du degré de saturation. Quant aux essais sur les échantillons de remblai en pâte, ceux-ci ont montré que la réactivité des échantillons semble aussi une fonction de du type de liant utilisé, et que la réactivité du mélange n'augmente plus après 28 jours de cure. En comparant les résultats des essais de consommation d'oxygène sur des rejets de concentrateur incorporés ou non dans un remblai en pâte, on s'aperçoit que les échantillons de remblai en pâte sont beaucoup moins réactifs que les rejets de concentrateurs sans liant qui ont un degré de saturation inférieur à 70%. Cependant, à saturation plus élevée, les rejets de concentrateur ont une réactivité similaire ou inférieure au remblai en pâte. Les résultats de cette étude préliminaire confirment que la technologie du remblai en pâte cimenté est une approche intéressante pour réduire la réactivité de rejets de concentrateur sulfureux stockés en surface.

---

[10] Ouellet, S., Bussière, B., Benzaazoua, M., Aubertin, M., Fall, M., Belem, T. (2003). Sulphide Reactivity within cemented paste backfill: oxygen consumption test results. The 56th Annual Canadian Geotechnical Conference and 4th joint IAH-CNC/CGS Conference. Winnipeg, Manitoba, Canada. September 28 to October 1, 8 p.

ABSTRACT

Oxygen consumption tests were performed on 5 manufactured laboratory tailings containing approximately 4, 12, 22, 34 and 74% wt. of pyrite at different degree of saturation, and on the same tailings when incorporated into cemented paste backfill (CPB). Oxygen consumption results showed that tailings reactivity depends on pyrite content and degree of saturation. For CPB samples, oxygen consumption seems to be related also to type of binder. The results showed that the reactivity of a given paste backfill recipe does not significantly increase after 28 days of curing time. Comparing the oxygen consumption results of sulphide tailings and the corresponding paste backfill samples indicate that CPB samples are less reactive than the non-cemented manufactured tailings at degrees of water saturation less than 70%. However, at higher degrees of saturation, the oxygen consumption results of the manufactured tailings were similar and even less than for the CPB samples. The results of this preliminary study demonstrate that CPB technology is a viable means to reduce the reactivity of sulphide tailings in surface disposal areas.

INTRODUCTION

Sulphide minerals such as pyrite and pyrrhotite oxidize in the presence of water and oxygen to generate sulphuric acid. The oxidation of the reactive (sulphide) minerals reduces the pH of the leachate, and this increases the solubility and concentration of various elements, including metals derived from the host rocks. The combined effect of acidity and solubilized elements increases the toxicity of the effluent, which can adversely affect nearby ecosystems. Sulphide oxidation mechanisms have been studied by many authors (e.g. Lowson, 1982; Nicholson et al., 1988; Elberling et al., 1993; Stromberg, 1997; Elberling et Damgaard, 2001; Aubertin et al., 2002; Rimstidt et Vaughan, 2003) and are still an important research topic. The global chemical oxidation reaction of pyrite can be expressed, in a simplified manner, by the following equation:

$$FeS_2 + 3.5O_2 + H_2O = Fe^{2+} + 2H^+ + 2SO_4^{2-} \qquad (1)$$
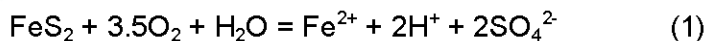
Mining operations have developed different strategies to make certain that acid mine drainage (AMD) does not significantly affect the environment. The main methods are chemical or biological treatment of water, construction of impermeable or low diffusion covers, and underwater tailings disposal (MEND, 2001; Aubertin et al., 2002). Even if these strategies are efficient to control the AMD production, they make site reclamation more difficult upon mine closure. This is why alternative approaches are being developed to improve tailings management during the mine operation, and to facilitate rehabilitation of the site afterward.

Cemented paste backfill (CPB) is one of these alternative approaches. This method can be used to place tailings underground to stabilize open stopes (e.g. Hassani and Archibald, 1998; Benzaazoua et al., 1999; Belem et al., 2000). When used as underground backfill material, paste backfill is a composite material made of a mixture of mine tailings (at a solid percentage between 75 to 85%), binders (such as ordinary Portland cement, fly ash, blast furnace slag or a combination of these) and water. The main benefits of underground paste backfill are a higher backfill strength and lower operating costs (in most cases) compared to hydraulic fills (Hassani and Archibald, 1998). Moreover, the use of paste backfill reduces the amount of tailings that have to be sent to surface disposal facilities. This reduction decreases both the environmental impact and capital expenditures for the tailings facility.

Paste backfill has also been proposed as a new method of surface tailings disposal (e.g. Cincilla et al., 1997; Grabinsky et al., 2002). The main advantages of this approach come from the small amount of free water at the surface, which reduces the size of water-retaining structures, less particles segregation (more homogeneous materials), and improved tailings hydro-geotechnical properties which are then more stable. Moreover, the addition of hydraulic binder in the surface paste backfill increases its strength, durability, and acid neutralisation potential. Cementation can also stabilise contaminants in the paste backfill matrix (Benzaazoua, 1996; Benzaazoua et al. 2002). But despite these advantages, there are still considerable uncertainties on the environmental behaviour of paste backfill.

Some authors have investigated the environmental impact of backfill material when used in underground mines. Thomson et al. (1986) concluded that the metal ions released from backfill were negligible. Levens et al. (1992, 1994, 1996) mentioned the following advantage to the utilization of CPB in underground stopes: i) the neutralization potential is higher, ii) there is a reduction of oxidation by decreasing the exposed surface area of sulphide minerals and the limitation of air diffusion prior to flooding, and iii) it lowers hydraulic conductivity of CPB that allows it to retain metal ions. However, to the knowledge of the authors, there has been little quantitative study on the environmental behaviour of paste backfill. In this paper, the authors present the results of a preliminary laboratory study to evaluate the reactivity of different sulphide tailings by oxygen consumption (OC) tests. The tests were done on fresh tailings at different degree of saturation and on tailings incorporated into CPB (two type of cements were tested in the CPB). The main objective of this study was to evaluate the environmental benefits of incorporating sulphide tailings into CPB.

MATERIALS AND METHODS

Mill tailings sampling and preparation

Sampling was done at the Louvicourt mine, Val-d'Or, Quebec, in the summer of 2002. The tailings were flooded in 40 gallon barrels to protect them from atmospheric oxidation. From these tailings, 5 tailings with 5 different pyrite contents were made by desulphurization of the original tailings with a laboratory flotation bench (Benzaazoua et al., 2003). After flotation, each manufactured tailings was also kept under water until the the paste backfill mixture was made. Table C.1 shows the mineralogical composition of the feeding tailings by X-ray diffraction (XRD) analysis. Table C.2 shows the composition of the 5 manufactured tailings following ICP-AES

analysis. The main physical properties of the manufactured tailings are presented in Table C.3 while Figure C.1 shows their different grain size distributions.
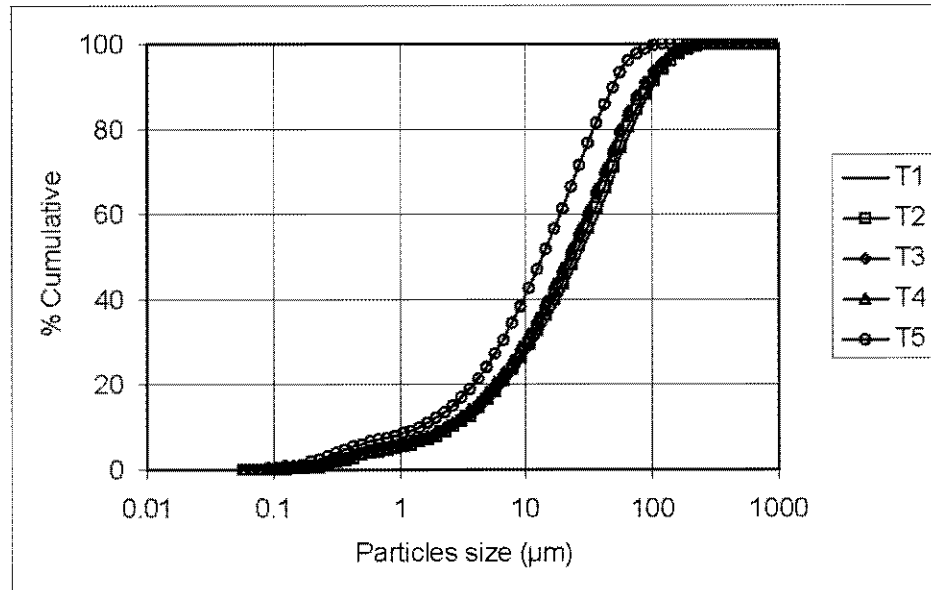

Figure C.1, Particles size distribution of 5 tailings.

Table C.1, Tailings X-ray diffraction measurements

Minerals	XRD (%wt)	Minerals	XRD (%wt)
Quartz	25	Chalcopyrite	-
Chlorite	26	Sphalerite	-
Mica	5	Galena	-
Pyrite	18	Arsenopyrite	-
Dolomite	6	Pyrrhotite	-
Magnesite	7	Goethite	-
Apatite	4	Magnétite	-
Feldspar	3	Total	94

Table C.2, Prepared tailings ICP analysis

	Feed (%wt)	T1 (%wt)	T2 (%wt)	T3 (%wt)	T4 (%wt)	T5 (%wt)
K	0.67	0.39	0.34	0.29	0.25	0.13
Al	4.55	5.08	4.79	4.20	3.50	1.67
Ca	1.27	1.45	1.34	1.19	1.02	0.38
Cu	0.06	0.05	0.07	0.09	0.11	0.19
Fe	19.50	12.50	15.30	20.90	26.10	47.50
Mg	1.67	4.03	3.71	3.30	2.74	1.11
Mn	0.14	0.18	0.16	0.14	0.12	0.05
Na	0.66	0.71	0.71	0.55	0.46	0.34
S	13.80	2.33	6.12	11.70	18.10	39.50
Zn	0.21	0.06	0.07	0.11	0.14	0.22
Total	42.53	26.78	32.61	42.47	52.54	91.09

Table C.3, Physical properties of prepared tailings

	Feed	T1	T2	T3	T4	T5
G_s	3.40	2.95	3.07	3.20	3.38	4.21
D_{10} (µm)	2.3	2.8	2.6	2.5	2.3	1.4
D_{30} (µm)	8.3	11.6	10.7	10.4	9.5	6.5
D_{50} (µm)	17.1	26.3	24.1	22.5	21.1	13.5
D_{90} (µm)	72.0	102.7	97.1	84.9	85.5	48.5
C_u	10.2	12.9	12.9	12.5	12.9	12.9
C_c	3.2	4.0	3.7	3.8	3.3	2.5

In Table C.1, one can see that the main sulphide mineral in the feeding tailings is pyrite (approximately 18%wt) while the gangue minerals are mainly quartz and chlorite. Table C.2 shows that the 5 manufactured tailings, labelled T1 to T5, contain 2.3, 6.1, 11.7, 18.1 and 39.5%wt of sulphur, respectively, which corresponds to pyrite percentages of approximately 4, 12, 22, 34 and 74%wt. Particle size distributions presented in Figure C.1 show that the five tailings have relatively similar grain size distributions. T5 (corresponding to the flotation sulphide concentrate) seems to be finer grained than the other manufactured tailings due to a high proportion of pyrite.

Cemented paste mould preparation

Ten different CPB mixtures were made with the manufactured tailings. Each manufactured tailings were mixed with 2 different binders at proportions of 4.5%wt: a 50:50 mix of CAN3-A5-M77 type 10 and type 50 cements (T10/T50) and a 20:80 mix of CAN3-A5-M77 type 10 cement and conforming ASTM C989-99 ground granulated blast-furnace slag (T10/SL). Tap water from Rouyn-Noranda was added to the resultant paste mixtures to adjust the slump to 17.5 cm ($\pm$ 0.5). All of the moulds were 10 cm in diameter and 20 cm long. Samples were cured at room temperature and at a relative humidity of greater than 60%. Table C.4 gives a summary of mixture characteristics in terms of specific gravity (G_s), water/cement ratio (W/C), water content and solid percentage. W/C and water content decrease from T1 to T5 because there is more binder added to denser tailings, and because total water content is similar in all of the mixtures. For the same reason, the solids percentage rises from 75% for CPB with tailings T1 to more than 80% for T5 mixtures.

Table C.4, Characteristics of the studied paste backfill

	G_s	W/C	Water content (%)	Solids (%)
T1-T10/T50	2.91	7.8	32.9	75.3
T1-T10/SL	2.93	8.0	33.7	74.8
T2-T10/T50	2.99	7.7	31.9	75.8
T2-T10/SL	3.01	7.7	31.9	75.8
T3-T10/T50	3.12	7.5	31.0	76.3
T3-T10/SL	3.15	7.4	31.6	76.0
T4-T10/T50	3.28	7.2	28.8	77.6
T4-T10/SL	3.30	7.2	29.8	77.1
T5-T10/T50	3.98	6.0	23.5	81.0
T5-T10/SL	3.99	6.0	24.9	80.1

Oxygen consumption tests

Elberling et al. (1994) and Elberling and Nicholson (1996) proposed an approach called the oxygen consumption (OC) method to evaluate the oxidation rate of sulphide mine wastes. Basically, the concept of the OC test is to measure the decrease of oxygen concentration in a sealed air chamber which is placed over the reactive materials for a short period of time. The decrease in oxygen concentration is due to oxygen diffusion and pyrite oxidation. The corresponding oxidation rate can be calculated by using the oxygen depletion rate and the stoechiometry of the pyrite oxidation reaction (first-order reaction rate for pyrite oxidation). These measurements provide a rapid indication of the oxidation rate. The main assumptions of this approach are that steady state conditions ($\delta C/\delta t=0$; C is the concentration of oxygen) exist before the beginning of measurements and that it is maintained for the duration of the test. To respect this criteria, Elberling et al. (1994) recommended that the test duration be about 3 to 5 hours duration, with a decrease in oxygen concentration during the test less than about 3% O_2 in the chamber. Examples of laboratory and field measurements with this technique can be found in the literature (e.g. Elberling et al., 1994; Nicholson et al., 1995; Elberling and Nicholson, 1996; Tibble and Nicholson, 1997; Bussière et al., 2002).

Most of the OC tests performed in this study did not meet the criterion proposed by Elberling et al. (1994) in terms of oxygen depletion (less than 3 %) during the 3 hour test. Therefore, the results will be presented in terms of oxygen consumption in the chamber (cumulative mass of oxygen consumed per unit area) with respect to time. These results can not be taken as pyrite reaction rates, but they can be used on a relative basis to compare the reactivity of the different materials (tailings and paste backfill).

OC tests were performed on the CPB and the raw tailings to evaluate the oxygen consumption of both materials. An oxygen chamber approximately 2 cm high was dug into the top of the cylinder after the first 14 days curing time in the CPB moulds.

Also, special mould caps were designed to permit oxygen concentration measurements (see Figure C.2). The type of oxygen sensor used for this study was a GC33-200 manufactured by GC Industries. The sensor is a galvanic electrochemical cell using the Pb-PbOOH half-cell to reduce oxygen (the consumption of oxygen by the sensor is considered negligible for that period of time, see Tibble and Nicholson, 1997). The voltage produced by this reaction is directly proportional to the partial pressure of oxygen in the gas phase. The sensor is accurate to a 0.1% O_2 concentration. OC tests on CPB cylinders were performed for durations of 3 to 5 hours and after each tests the moulds were returned to the fog room. For the 5 manufactured tailings, the tests were performed in the same conditions as the CPB moulds but in a glass jar with known volumes of dry tailings and water. Therefore, it was possible to calculate the water saturation (S_r) and many tests were done to link S_r and oxygen decay.

Figure C.2, Oxygen-consumption setup for the CPB samples.

RESULTS

OC tests on manufactured tailings

Figures C.3 to C.7 present the oxygen consumption results for all manufactured tailings at different degrees of saturation (S_r). Values were calculated on the basis of cumulative oxygen consumed in the chamber in millimol of oxygen per unit area.

Figure C.3 presents the oxygen consumption data for the manufactured tailings T1, which contain approximately 4% pyrite, at 3 different S_r values: 47%, 70% and 90%. At a S_r of 47%, the cumulative oxygen consumed in the isolated chamber is less than 50 mmol/m^2 after 230 minutes. Figure C.3 also shows that the consumption of oxygen after 3 hours increases as S_r decreases. This is due to the increase of the effective diffusion coefficient D_e when the material contains less water (e.g. Elberling et al., 1994; Aachib et al., 2002; Mbonimpa et al., 2002). The results obtained for manufactured tailings T2 (approximately 12% pyrite) are presented in Figure C.4. They are similar to those of tailings T1, with a slight increase in terms of oxygen consumption. At a S_r value of 48%, 81 mmol O_2/m^2 were consumed in the chamber after 240 minutes. Figures C.5 and C.6 present the results for manufactured tailings T3 and T4 which contain approximately 22% and 34% of pyrite, respectively. The results show that these two tailings are more reactive than the manufactured tailings T1 and T2, especially when the saturation degrees are below 75%. For example, after 230 minutes, the cumulative oxygen mass per unit area consumed in the chamber of T3 tailings is 215 mmol/m^2 (for a S_r value of 46%) while the consumed oxygen in the chamber of manufactured tailings T4 at a S_r value of 45 % is 302 mmol/m^2 after 215 minutes.
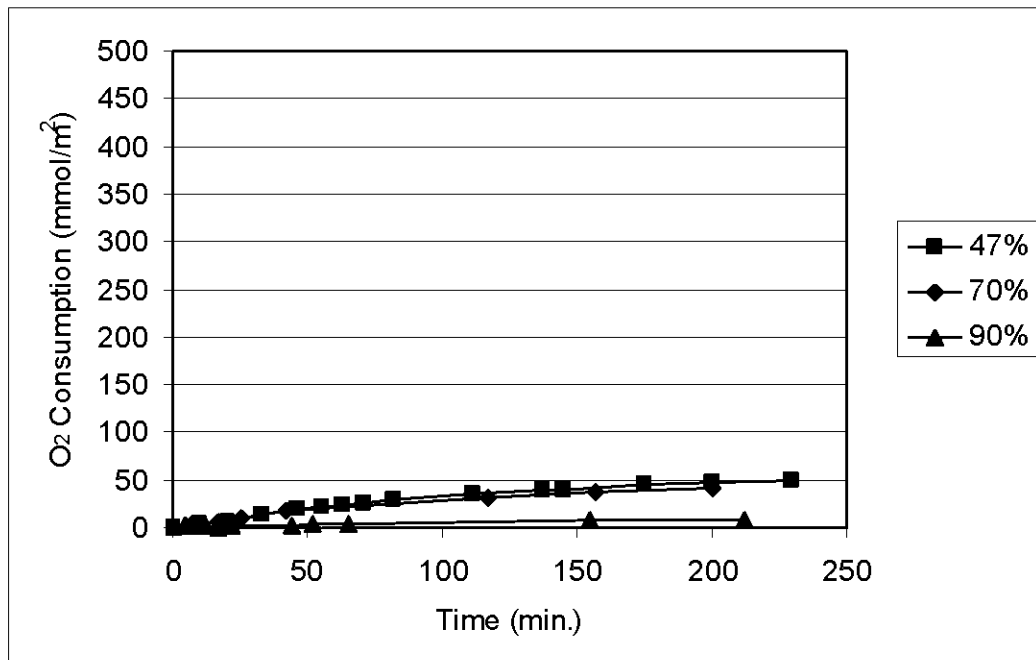
Figure C.3, Oxygen consumption of manufactured tailings T1 at 3 degree of saturation: 47%, 70% and 90%.
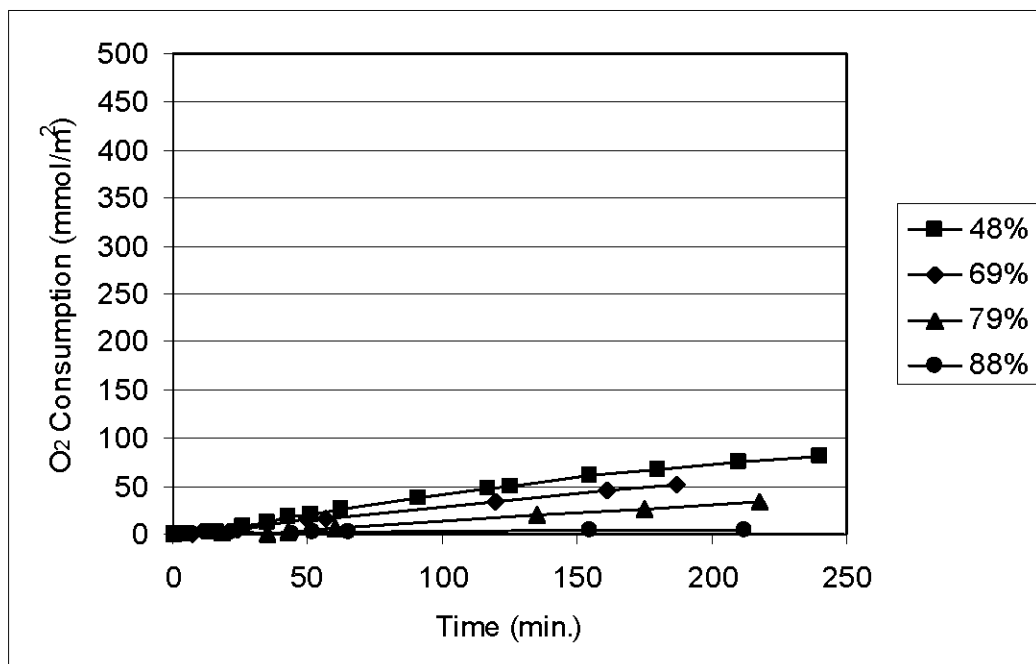

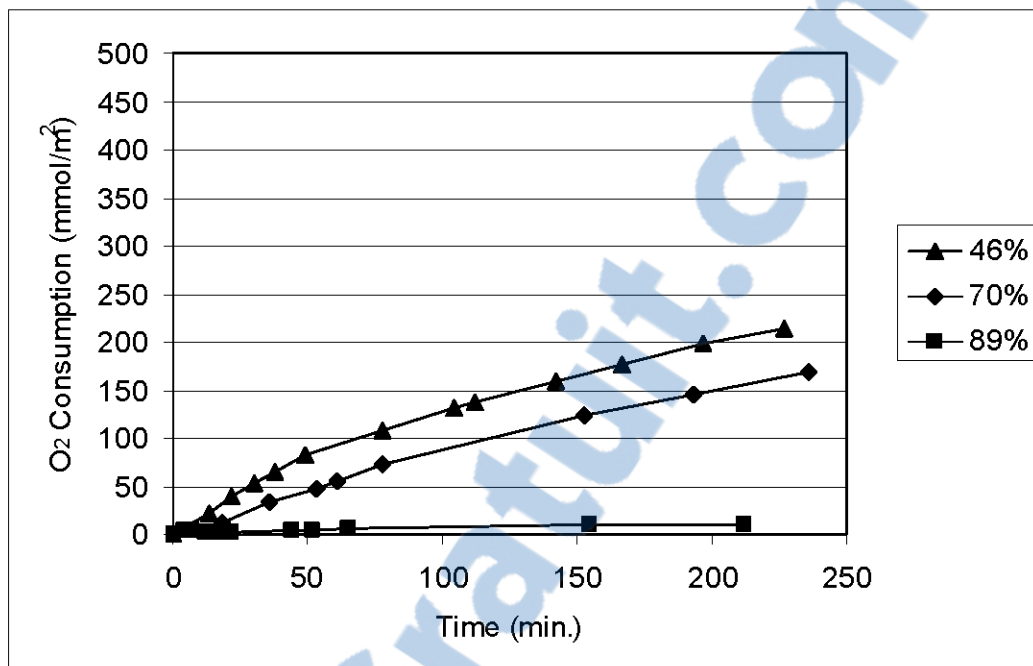Figure C.4, Oxygen consumption of manufactured tailings T2 at 4 degree of saturation: 48%, 69%, 79% and 88%.

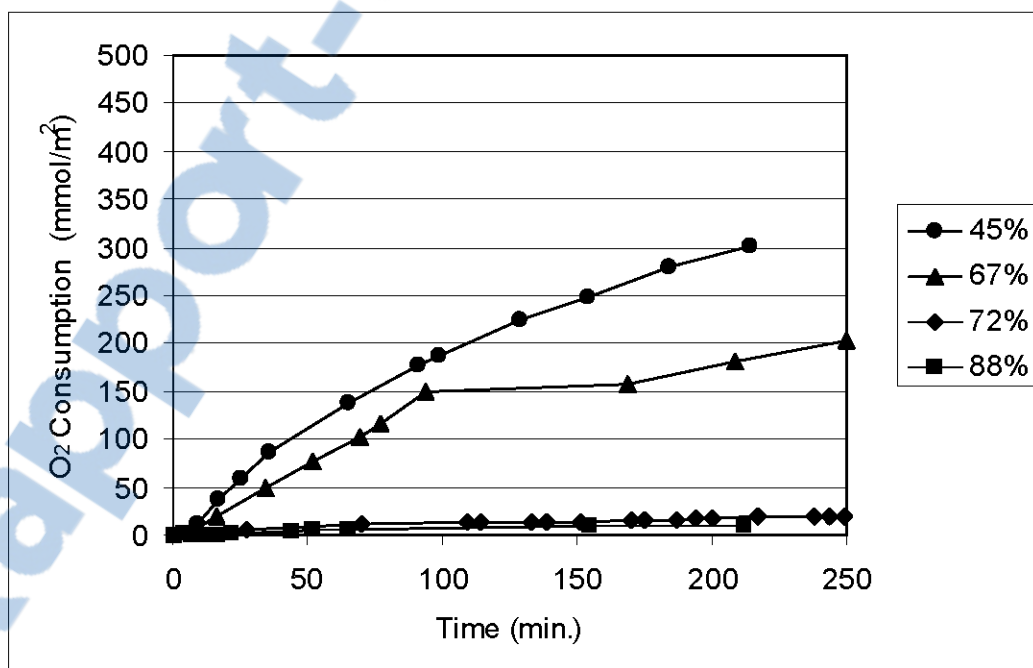Figure C.5, Oxygen consumption of manufactured tailings T3 at 3 degree of saturation: 46%, 70% and 89%.

Figure C.6, Oxygen consumption of manufactured tailings T4 at 4 degree of saturation: 45%, 67%, 72% and 88%.

Tailings T5, which contains approximately 74% pyrite, were tested over a wide range of saturation levels: S_r varied from 37% to 99% (see Figure C.7). The consumption of oxygen increases as the degree of saturation decreases. At a S_r value of 40%, the consumption is very fast with 260 mmol O_2/m^2 consumed after 80 minutes.
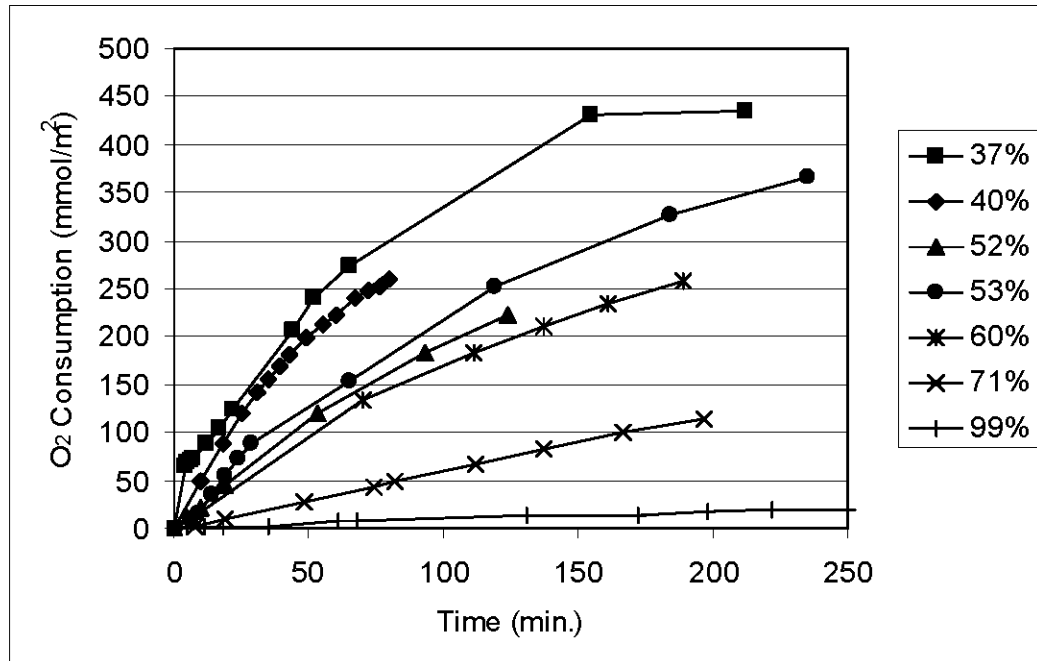
Figure C.7, Oxygen consumption of manufactured tailings T5 at 7 degree of saturation: 37%, 40%, 52%, 53%, 60%, 71% and 99%.

According to Figures C.3 to C.7, it's clear that the reactivity of sulphide tailings is strongly dependent on the proportion of sulphide minerals (pyrite, in this case) and on the degree of saturation with similar particle sizes for all of the tailings samples (except T5 which is a bit finer grained). In all the cases studied, for S_r values greater than 88%, oxygen consumption was very low. This observation is in agreement with literature (e.g. Delleur, 1999) that usually stipulates that the air porosity of a material is disconnected for S_r values greater than 80 to 85%. When the air porosity is disconnected, the oxygen must diffuse through water filled pores which reduces the effective diffusion coefficient D_e of the material and consequently, the oxygen flux through the material (e.g. Aachib et al., 2002).

OC tests on cemented paste backfill

Figures C.8 to C.11 present oxygen consumption over time for the different paste backfill mixtures at 4 different curing times: 14, 28, 45 and 60 days. Like the manufactured tailings data, all of the results on those graphs were calculated on the basis of the oxygen consumption in the chamber in millimol of oxygen per square meter. OC tests were done on the samples at their natural degree of saturation which was between 90 and 100%, depending on the curing times.

Figure C.8 shows the oxygen consumption data after curing for 14 days. For all of the cylinders, oxygen consumption is low. For example, CPB T5 (made of manufactured tailings T5 which contain 74% pyrite) with T10/T50 binder shows an oxygen consumption of 23 mmol/m^2 after 240 minutes. There is no obvious correlation between the pyrite percentage or binder type and oxygen consumption for this curing time.

The results after 28 days of curing in the fog room are presented in Figure C.9. One can see that the oxygen consumption is greater than after 14 days. As the pyrite percentage increases, the reactivity expressed in terms of oxygen depletion becomes greater. For example, the oxygen loss after 200 minutes for manufactured tailings, T1 (4% pyrite) with T10/SL binder is 59 mmol O_2/m^2 compared to approximately 100 mmol/m^2 for manufactured tailings T4 (34% pyrite) with the same binder.

Figures C.10 and C.11 present data for 45 days and 60 days of curing time, respectively. The results show that the reactivity of the CPB samples is usually less, for these curing times, than that after 28 days.
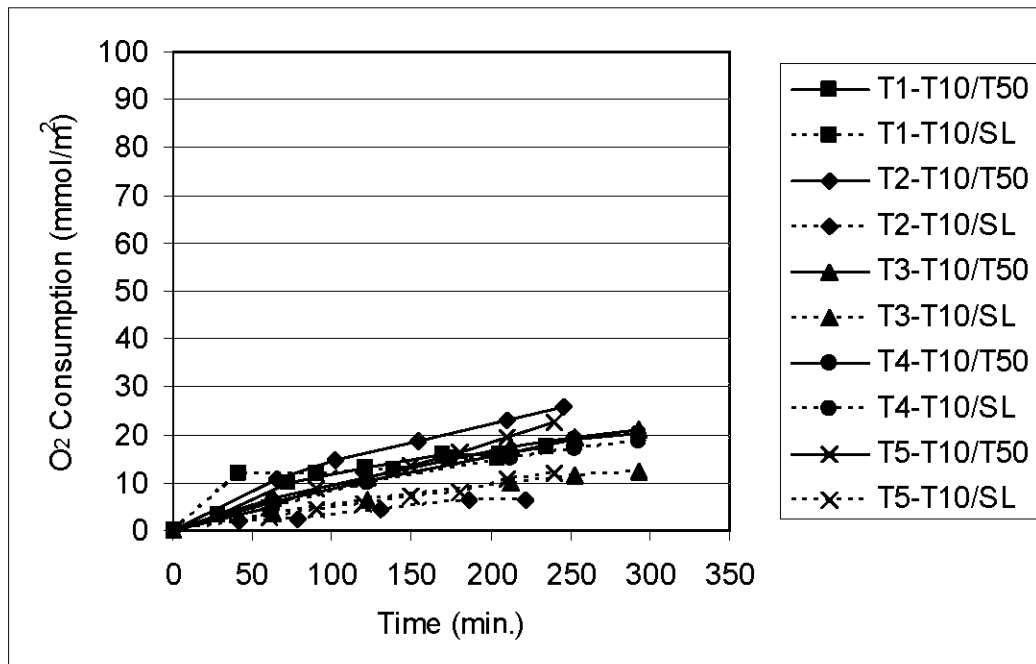
Figure C.8, Consumption of CPB cylinders after a curing period of 14 days.
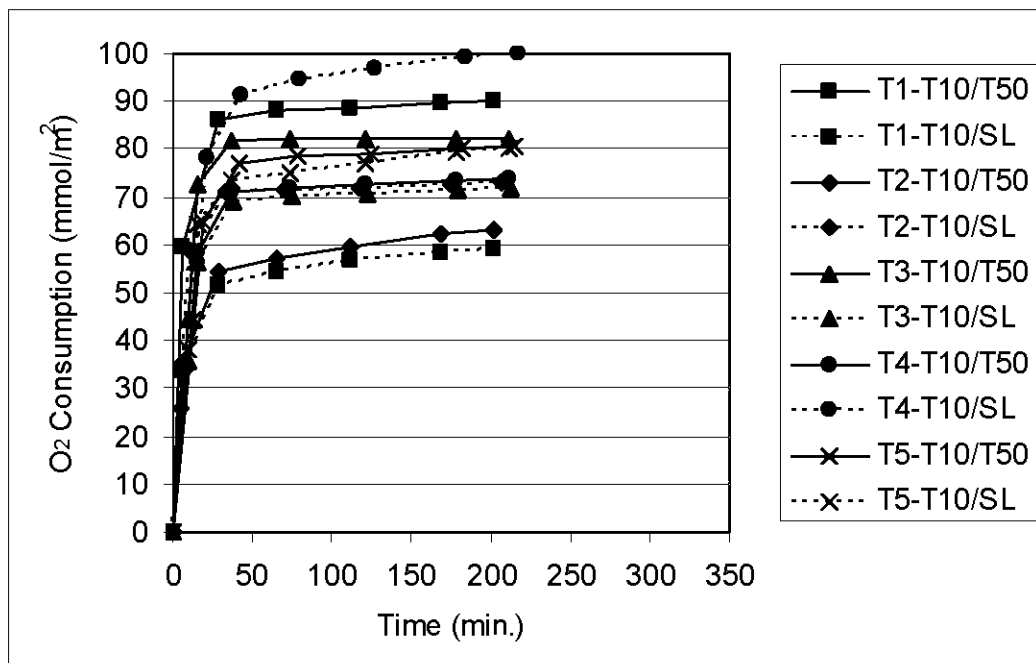

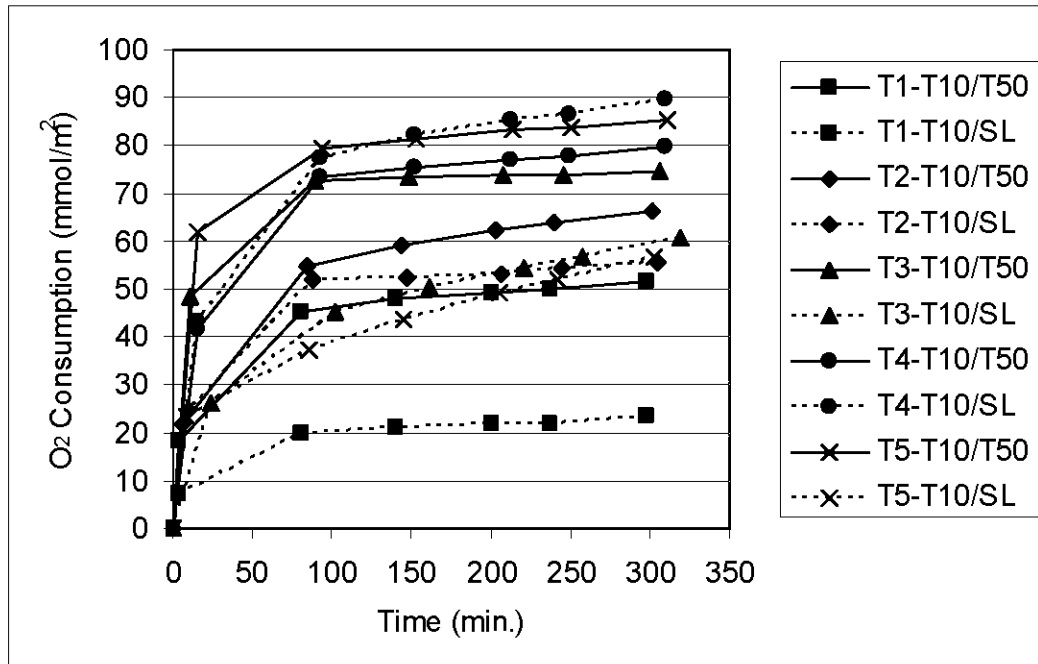Figure C.9, Consumption of CPB cylinders after a curing period of 28 days.

Figure C.10, Consumption of CPB cylinders after a curing period of 45 days.
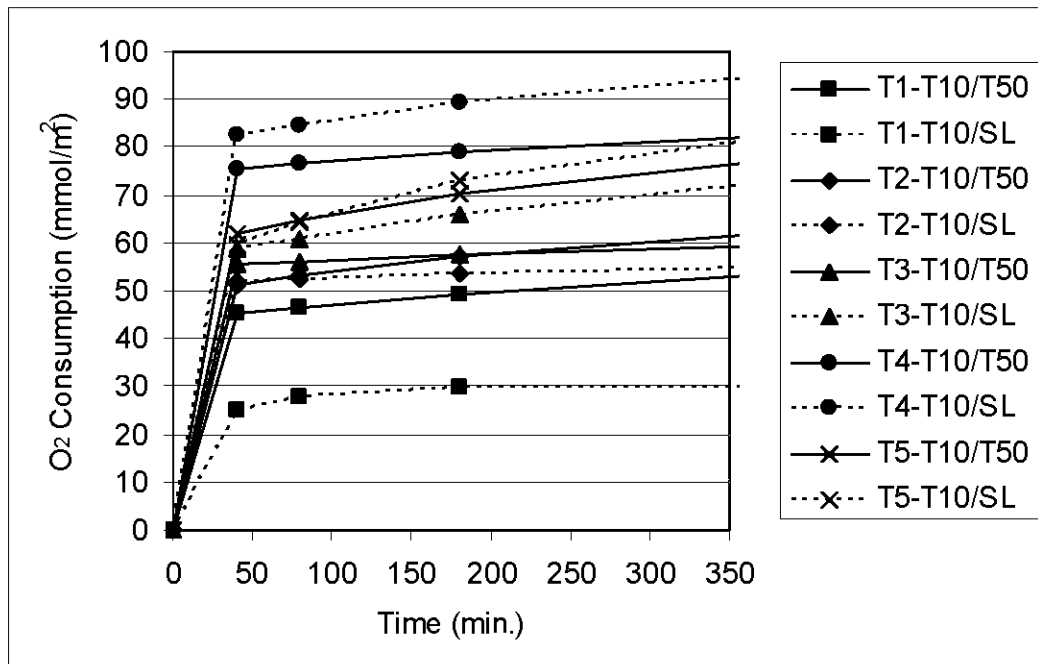

Figure C.11, Consumption of CPB cylinders after a curing period of 60 days.

For example, the percentage of oxygen consumption in the chamber of CPB samples made of manufactured tailings, T1 were approximately 22 and 49 mmol O_2/m^2 after 45 days for the binders T10/SL and T10/T50, respectively, compared to 59 and 90 mmol O_2/m^2 after 28 days.

RESULTS ANALYSIS

Oxygen consumption (OC) tests on the five manufactured tailings showed that oxygen consumption increases as the pyrite proportion increases. Nevertheless, even with tailings with almost 75% of pyrite, the oxygen consumption can be limited to low values when the degree of saturation is high. This is due to the reduction of the effective oxygen diffusion coefficient D_e with the increase of the degree of saturation. This coefficient is related to the flux of oxygen through a material; the mathematical relationships between D_e and oxygen flux are represented by Fick's first and second laws (e.g. Nicholson et al., 1989; Aachib et al., 2002; Mbonimpa et al., 2002).

As for tailings oxygen consumption results, it seems that the reactivity of CPB cylinders is a function of the pyrite percentage; the oxygen consumption increases with the pyrite percentage. The results also showed that the reactivity of a given mixture does not increase (and even decrease in some cases) after 28 days of curing time. One can also see in Figures C.8 to C.11 that the binder T10/SL is generally more efficient than the T10/T50 binder in reducing the reactivity of the CPB samples. This can be explained by the differences in term of density of cementitious matrix obtained by using these two types of binders. Table C.5 shows the differential percentages between remaining oxygen in the chambers of the T10/SL samples and the T10/T50 samples after 180 minutes of consumption (mmol O_2 T10/SL – mmol O_2 T10/T50). On 20 differential percentages, oxygen consumption is higher (negative values in Table C.5) for T10/SL binder 14 times.

The lower reactivity usually observed for CPB made of T10/SL can be partially explained by a better cement hydration in the paste backfill made with this binder. Uniaxial compressive strength testing on the CPB samples used in this study (not shown here because of space constraints, see Benzaazoua et al. 2003) showed that, for all of the samples at all of the curing times, the strength development is improved with the T10/SL binder. A higher compressive strength is attained with better hydration with more rigid cement minerals and less porosity. Therefore, the microstructural quality of the paste is a good indicator of its environmental behavior.

Figure C.12 shows all of the oxygen consumption results for the manufactured tailings T1 to T5 versus degree of saturation, and data from CPB after 60 days of curing in the fog room. All of the data in that figure are for test durations of 180 minutes. Degrees of saturation of CPB samples were evaluated at the end of the test, after 60 days of curing. The S_r values of these samples were between 90 to 97%. Figure C.12 shows that the CPB samples are less reactive than the corresponding manufactured tailings (without binder) at levels of saturation S_r less than 70 % ($S_r < 70\%$ are frequently found in tailings pond exposed to atmospheric conditions; e.g. Vick, 1983; Aubertin et al. 1999). Considering that a CPB has lower hydraulic conductivity and higher water retention than tailings due to binder hydration (e.g. Belem et al., 2001), this indicates that the reactivity of tailings would be significantly reduced by incorporating them into the CPB (the tailings remain at a higher degrees of saturation which will reduce oxygen consumption).

Table C.5, Differences between oxygen loss for the two binders at the end of the oxygen consumption tests (mmol O_2 T10/SL – mmol O_2 T10/T50)

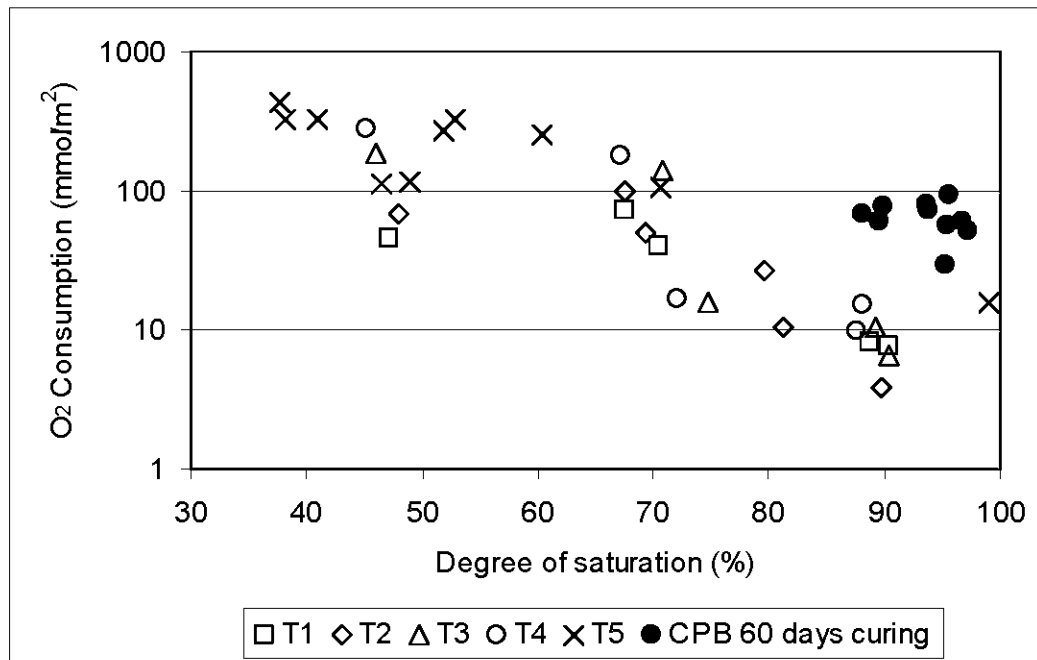|	14 days	28 days	45 days	60 days
T1-T10/SL	-1.4	-31.1	-27.2	-19.7
T2-T10/SL	-15.6	10.3	-8.2	-3.6
T3-T10/SL	-6.5	-10.6	-21.8	8.5
T4-T10/SL	-1.1	25.8	7.4	10.3
T5-T10/SL	-8.5	-0.5	-35.3	2.7

Figure C.12, Oxygen consumption data after 180 minutes for manufactured tailings T1 to T5 and 60 days of curing CPB samples versus degree of saturation.

However, oxygen consumption between 30 to 92 mmol/m^2 of O_2 are measured in the chamber of the CPB samples as compared to values between 4 and 16 for the corresponding manufactured tailings at similar degree of saturation (see Figure C.12). This phenomenon could be explained by a local desaturation at the top of the CPB cylinders. Figure C.13 shows a picture of the top portion of T5-T10/T50 CPB sample. One can see a desaturated zone of less than 1 mm (this was not clear in the manufactured tailings samples). This desaturated zone at the top was too small to evaluate the saturation level accurately, but it appears that the CPB reactivity is controlled by this zone. No oxidation evidence is observed in the bulk sample due to the ability of the CPB to maintain a high degree of saturation (higher than 90 % in the internal zone). These observations mean that the oxidation in the CPB would be located near the top and, in the long term, the acid generating potential of the tailings incorporated into the CPB would be less.

Figure C.13, Pieces of T5-T10/T50 CPB showing a thin desaturated zone (less than 1 mm) at the top.

SUMMARY AND CONCLUSION

After desulphurization of the tailings from the Louvicourt mine, Quebec, 5 laboratory manufactured tailings containing approximately 4, 12, 22, 34 and 74%wt of pyrite were used to make cemented paste backfill (CPB) samples. CPB cylinders were mixed with 4.5% of 2 types of binder: 50:50 Portland type-10 and type-50 cements and 20:80 Portland type-10 cement and ground granulated blast-furnace slag. Tap water was also added to adjust the slump of the pastes to 17.5 cm ± 0.5. Oxygen consumption testing was done on the 5 tailings at different degrees of saturation. The results showed that the oxygen consumption of tailings was a function of the amount of pyrite and degree of saturation. Oxygen-consumption testing was also done on the CPB samples for different curing times. As with the tailings oxygen consumption results, the reactivity of CPB cylinders is a function of the pyrite percentage; the oxygen consumption increases with the pyrite percentage. The

binder type has a definite impact on the oxygen consumption. In this study, CPB made of T10/SL is generally more able to reduce the reactivity of the tailings incorporated into it. The results also showed that CPB samples are much less reactive than the corresponding manufactured tailings (without binder) at degrees of saturation less than 70 %. The weathering observed on the samples was restricted to the top of the CPB samples.

Considering that the hydraulic conductivity is reduced by binder hydration and that the water retention properties are increased (Belem et al., 2001), CPB should be an viable approach to reduce the reactivity of sulphide tailings disposed at the surface. However, more research is necessary to confirm this hypothesis. Over the coming months, the authors and collaborators will concentrate their efforts on understanding of mineralogical evolution in a CPB, and the impact of this evolution on the geotechnical and environmental properties of cemented paste backfill.

ACKNOWLEDGEMENTS

REFERENCES

Aachib M, Aubertin M, and Mbonimpa M. 2002. Laboratory measurements and predictive equations for gas diffusion coefficient of unsaturated soils, Ground and Water: Theory to Practice, Proceedings of the 55th Canadian Geotechnical Conference, Niagara Falls, Ontario, Canada, October 20-23 2003, 163-171.

Aubertin M, Bussière B, and Bernier L. 2002. Environnement et gestion des résidus miniers. CD, Les Éditions de l'École Polytechnique de Montréal, Montreal, Canada.

Aubertin M, Bussière B, Joanes A-M, Monzon M, Gagnon D, Barbera J-M, Bédard C, Chapuis RP, and Bernier L 1999. Projet sur les barrières sèches construites à partir de résidus miniers, Phase II: essais en place. MEND Report 2.22.2c, CANMET, Ottawa, Canada.

Belem, T., Bussière, B., and Benzaazoua, M. 2001. The effect of microstructural evolution on the physical properties of paste Backfill, Tailings and Mine Waste 2001 Balkema, Rotterdam, ISBN 90 5809 182 1, 365-374.

Belem, T., Benzaazoua, M., and Bussière, B. 2000. Mechanical behaviour of cemented paste backfill, 53rd Annual Conference Of The Canadian Geotechnical Society, Montreal, Vol. 1, ISBN 0-920505-15-5, 373-380.

Benzaazoua, M. 1996. Caractérisation physico-chimique et minéralogique de produits miniers sulfures en vue de la réduction de leur toxicité et de leur valorisation, Ph.D. Thesis INPL, Nancy, France, 267 pp.

Benzaazoua, M., Belem, T., and Bussière, B. 2002. Chemical factors that influence the performance of mine sulphidic paste backfill, Cement and Concrete Research, 32, 7, 1133-1144.

Benzaazoua, M., Fall, M., and Ouellet, S. 2003. Étude pluridisciplinaire visant à mettre au point un outil expert pour la prédiction du comportement des remblais en pâte. Final Report, Contract IRSST no 099-085. (To be published).

Bussière, B., Dagenais, A.-M., Mbonimpa, M., and Aubertin, M. 2002. Modification of oxygen-consumption testing for the evaluation of oxygen barrier performance. 55th Canadian Geotechnical Conference and 3rd joint IAH-CNC and CGS Groundwater Specialty Conferences, Niagara Falls, CD, 139-146.

Cincilla, W.A., Landriault, D.A., and Verburg, R. 1997. Application of paste technology to surface disposal of mineral wastes, Proceedings of 4th International Conference on Tailings and Mine Waste '97, Fort Collins, Colorado, 13-16 January 1997, 343-356.

Delleur, J.W. 1999. The Handbook of Groundwater Engineering. CRC Press, New York, 992 pp.

Elberling, B., Nicholson, R.V., and David, D.J. 1993. Field evaluation of sulphide oxidation rates, Nordic Hydrology, 24, 323-338.

Elberling, B., Nicholson, R.V., Reardon, E.J., and Tibble, P. 1994. Evaluation of sulphide oxidation rates: laboratory study comparing oxygen fluxes and rates of oxidation product release. Canadian Geotechnical Journal, 31: 375-383.

Elberling, B. and Nicholson, R. V. 1996. Field determination of sulfide oxidation rates in mine tailings. Water Resources Research, 32 : 1773-1784.

Elberling, B. and Damgaard, L.R. 2001. Microscale measurements of oxygen diffusion and consumption in subaqueous sulfide tailings, Geochimica et Cosmochimica Acta, 65, 12, 1897-1905.

Grabinsky, M.W., Theriault, J., and Welch, D. 2002. An overview of paste and thickened tailings disposal on surface, Symposium 2002 sur l'environnement et les mines, Rouyn-Noranda, 3-5 novembre, 8 pp.

Hassani, F., and Archibald, J. 1998. Mine backfill, CD-ROM 263p.

Levens, R.L. and Boldt, C.M. K. 1992. Hydrochemical impacts of mine waste backfill in underground sulfide mines, Paper in Environmental Issues and Management of Waste in Energy and Mineral Production. Proceedings: Second International Conference, ed. by R. K. Singhal, A. K. Mehrotra, K. Fytas, and J.-L. Collins (Calgary, AB, Sept. 1-4, 1992). Balkema, vol. 2, pp. 891-902.

Levens, R.L. and Boldt, C.M. K. 1994. Environmental Impacts of Mine Waste Sandfill, Report of Investigations 9493, United States Bureau of Mines, 15 pp.

Levens, R.L., Marcy, A.D., and Boldt, C.M.K. 1996. Environmental Impacts of Cemented Mine Waste Backfill, RI 9599, United States Bureau of Mines, 23 pp.

Lowson, R.T. 1982. Aqueous oxidation of pyrite by molecular oxygen, Chemical Reviews, 5, 82, 461-497.

Mbonimpa, M., Aubertin, M., Dagenais, A.-M., Bussière, B., Julien, M., and Kissiova, M. 2002. Interpretation of fields tests to determine the oxygen diffusion and reaction rate coefficients of tailings and soil covers, Ground and Water: Theory to Practice, Proceedings of the 55th Canadian Geotechnical Conference, Niagara Falls, Ontario, Canada, October 20-23 2003, 147-154.

MEND Secretariat CANMET. 2001. MEND Manual, Report 5.4.2, Volumes 1 — Summary, Volume 2 — Sampling and Analysis, Volume 3 — Prediction, Volume 4 — Prevention and Control, Volume 5—Treatment, Volume 6 — Monitoring.

Nicholson, R.V., Elberling, B., and Williams, G. 1995. A new oxygen consumption technique to provide rapid assessment of tailings reactivity in the field and the laboratory. Proceedings of the Sudubury'95 Conference, Sudbury, 999-1006.

Nicholson, R.V., Gillham, R.W., Cherry, J.A., and Reardon, E.J. 1989. Reduction of acid generation in mine tailings through the use of moisture-retaining cover layers as oxygen barriers. Canadian Geotechnical Journal, 26: 1-8.

Nicholson, R.V., Gillham, R.W., and Cherry, J.A. 1988. Pyrite oxidation kinetics in carbonate-buffered solution: 1. Experimental kinetics. Geochemica et Cosmochimica Acta, 52: 1077-1085.

Rimstidt, D.J. and Vaughan, D.J. 2003. Pyrite oxidation: a state-of-the-art assessment of the reaction mechanism, Geochimica et Cosmochimica Acta, 67, 5, 873-880.

Strömberg, B. 1997. Weathering kinetics of sulphidic mining waste : An assessment of geochemical processes in the Aitik mining waste rock deposits, Thèse de doctorat, Royal Institute of Technology, Sweden, 73 p. + 6 articles.

Thomson, B.M., Longmire, P.A., and Brookins, D.G. 1986. Geochemical Constraints on Underground Disposal of Uranium Mill Tailings. Appl. Geochem., 1, 335-343.

Tibble, P.A. and Nicholson, R.V. 1997. Oxygen consumption on sulphide tailings and covers: measured rates and applications. Proceedings of the Proceedings of the 4th International Conference on Acid Rock Drainage, Vancouver, Vol. 2, 647-661

Vick, S.G. 1983. Planning, Design, and Analysis of Tailings Dams. John Wiley and Sons.

APPENDICE D

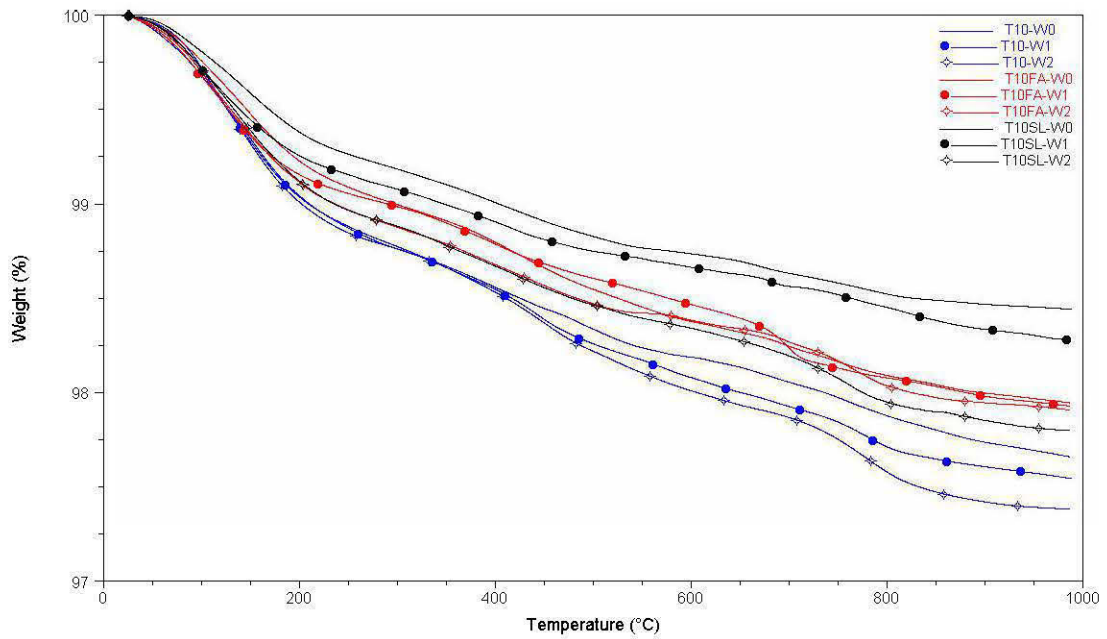# THERMOGRAVIMÉTRIE ET FLUX DE CHALEUR

Figure D.1, Perte de masse (TG) des échantillons de CPB à 92 jours (échantillons référés aux chapitres 2 et 3).
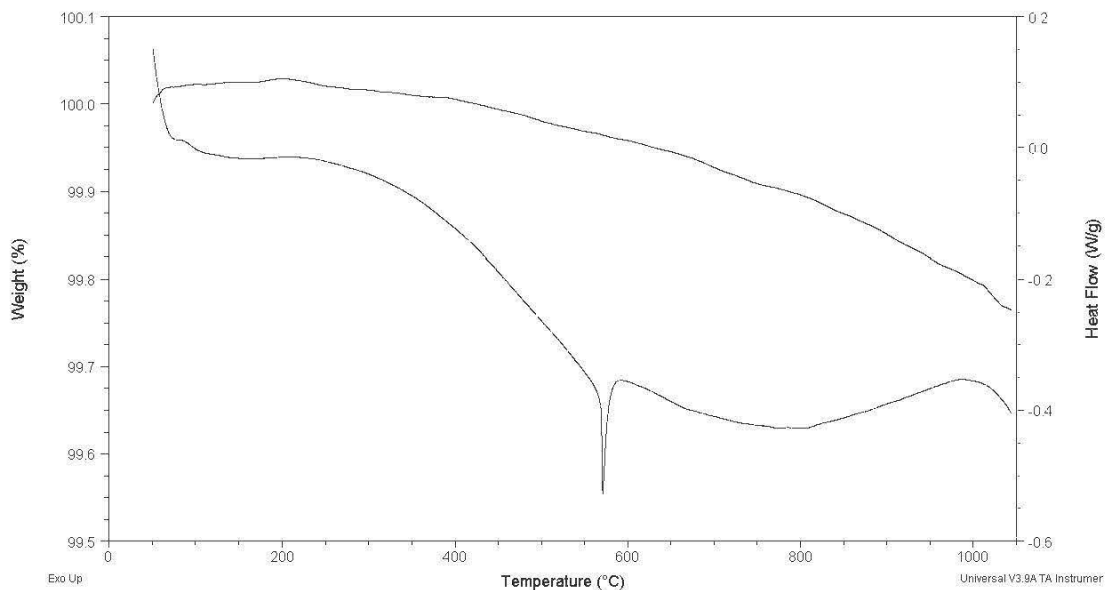
Figure D.2, Perte de masse (TG) et mesure des échanges de flux de chaleur (DSC) pour la poudre de silice.
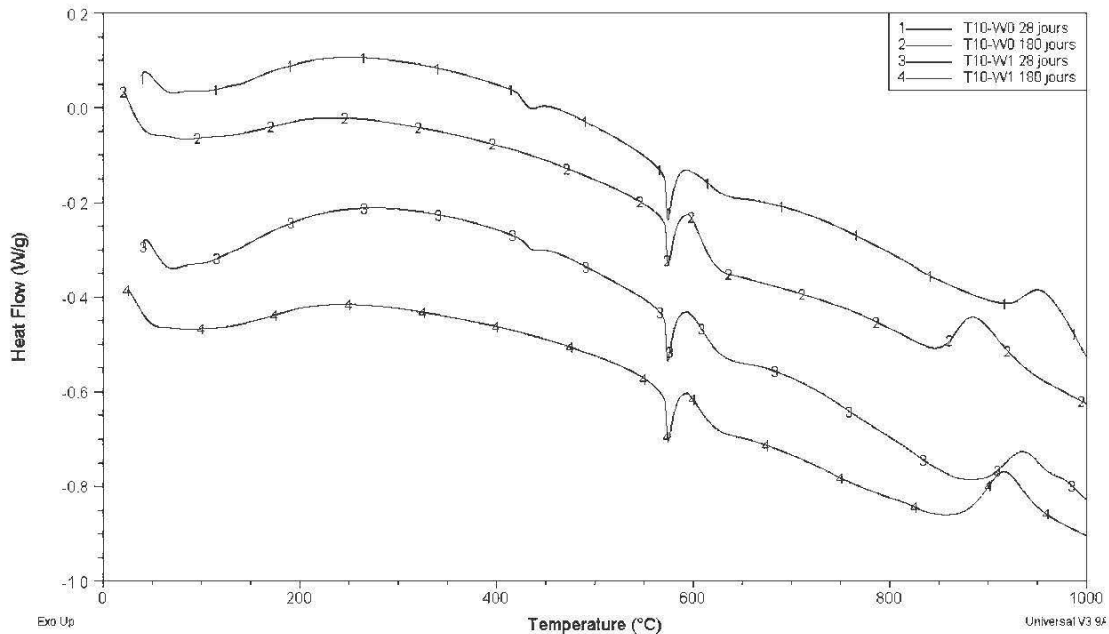

Figure D.3, Mesure des échanges de flux de chaleur (DSC) pour les échantillons T10-W0 et T10-W1 à 28 et 180 jours de cure.
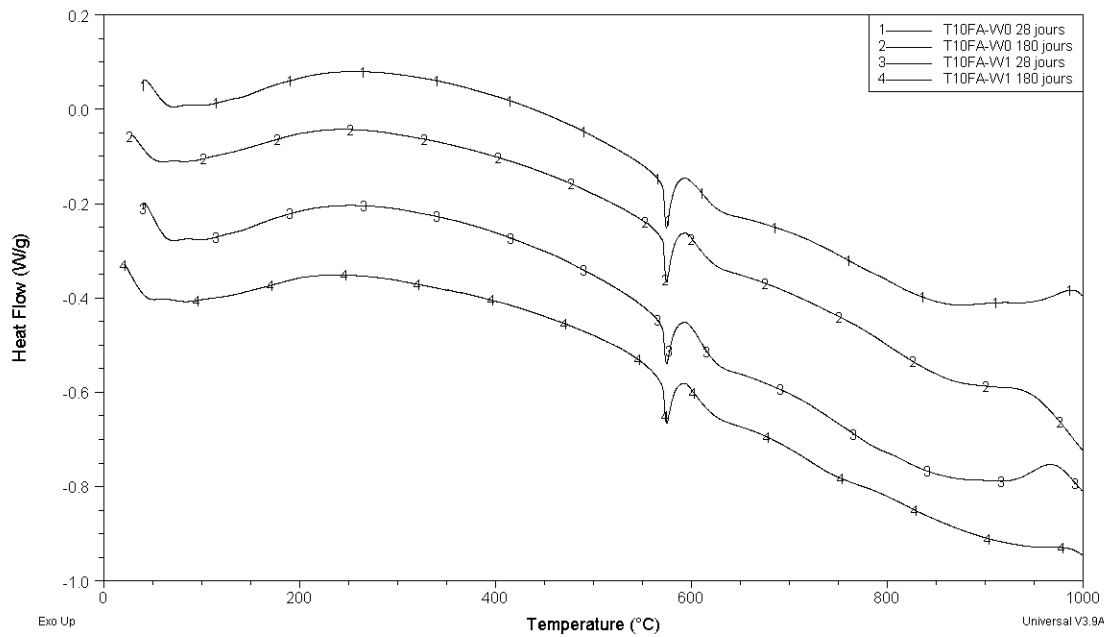
Figure D.4, Mesure des échanges de flux de chaleur (DSC) pour les échantillons T10FA-W0 et T10FA-W1 à 28 et 180 jours de cure.
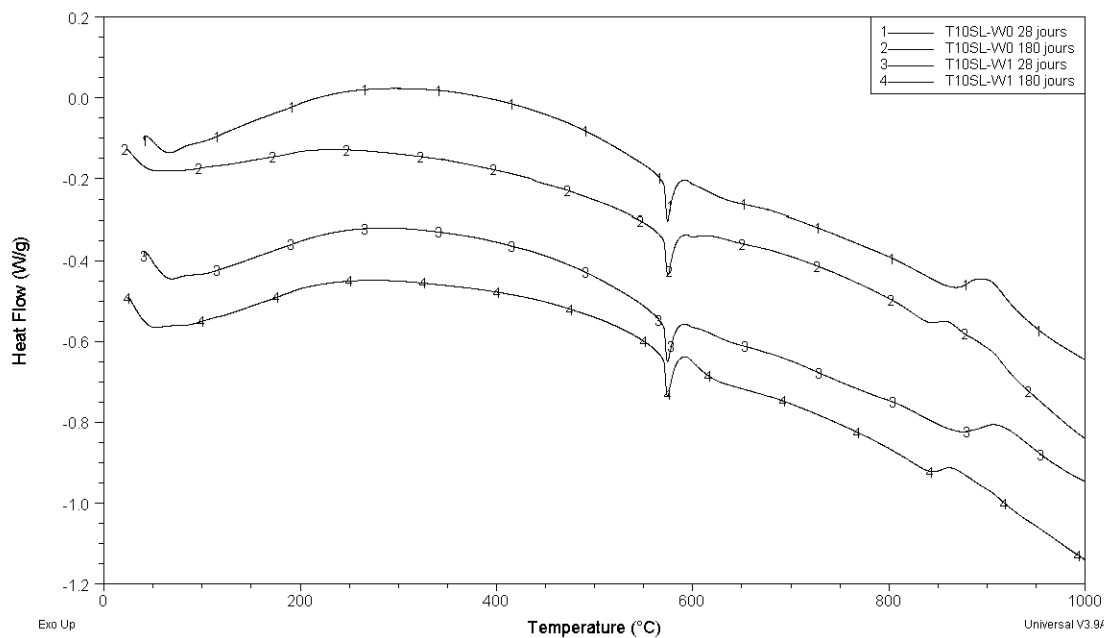

Figure D.5, Mesure des échanges de flux de chaleur (DSC) pour les échantillons T10SL-W0 et T10SL-W1 à 28 et 180 jours de cure.
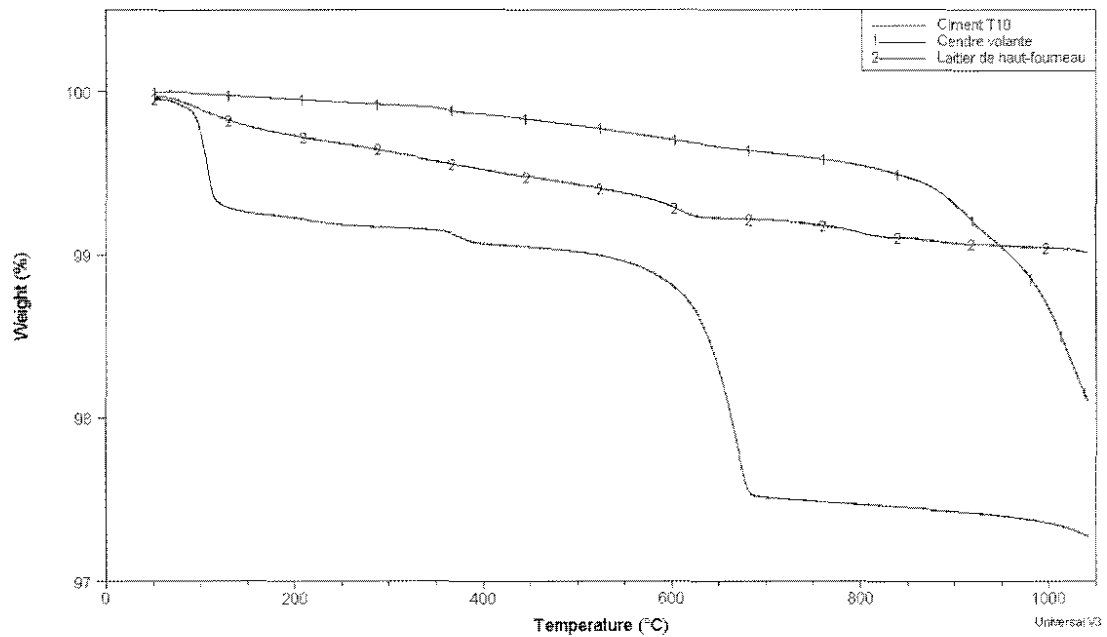
Figure D.6, Perte de masse (TG) pour le ciment T10, la cendre volante et le laitier de haut-fourneau.
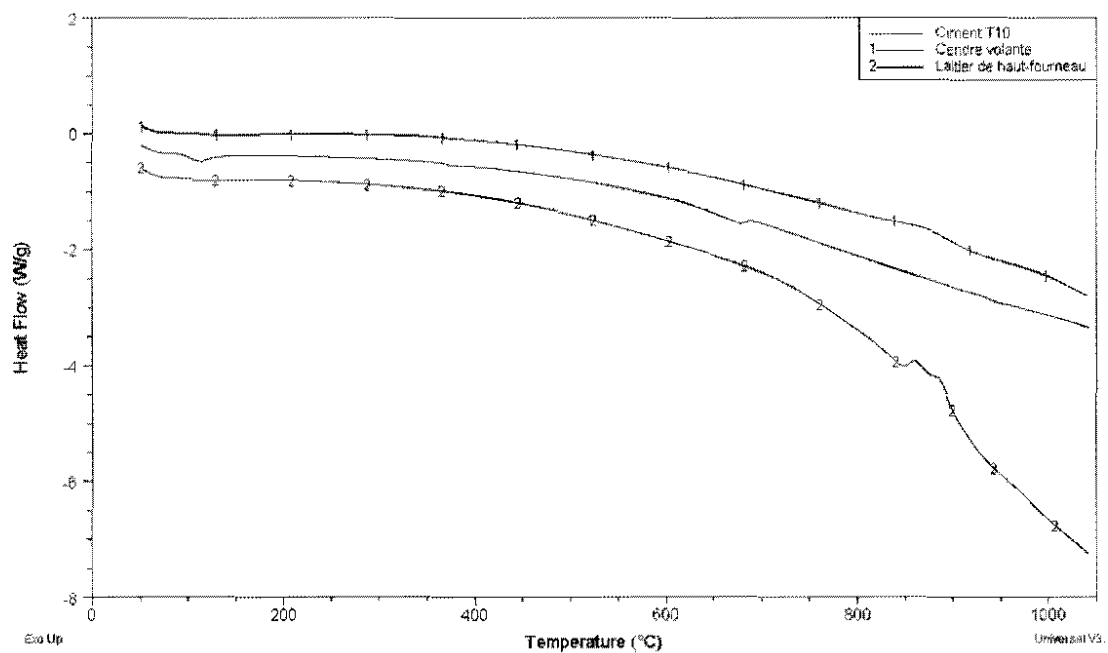

Figure D.7, Mesure des échanges de flux de chaleur (DSC) pour le ciment T10, la cendre volante et le laitier de haut-fourneau.

APPENDICE E

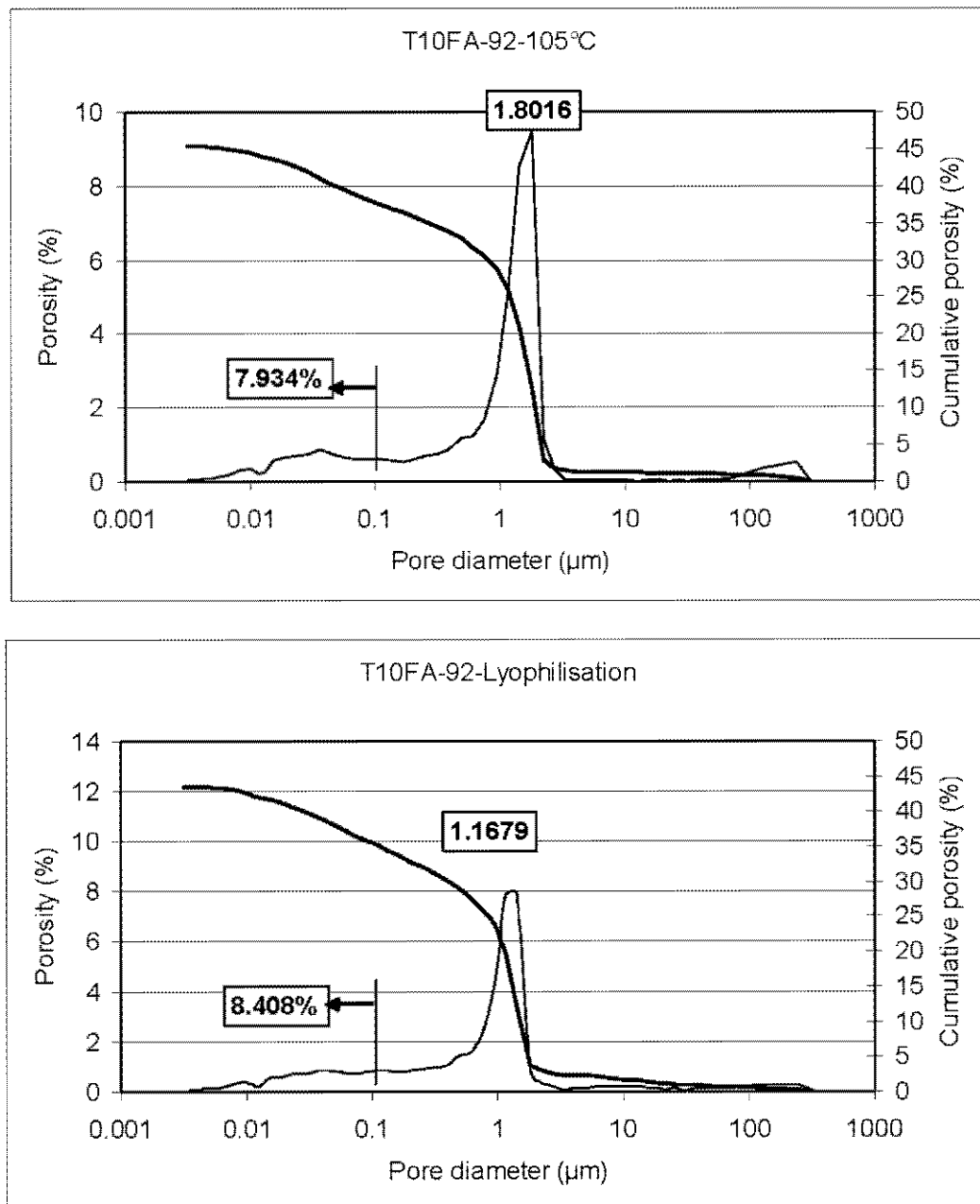**ESSAIS DE POROSIMÉTRIE AU MERCURE SUPPLÉMENTAIRES**

Figure E.1, Tests de séchage (étuve à 105°C versus lyophilisation) sur des échantillons de remblai à base de ciment de type 10 et de cendre volante à 92 jours de cure.
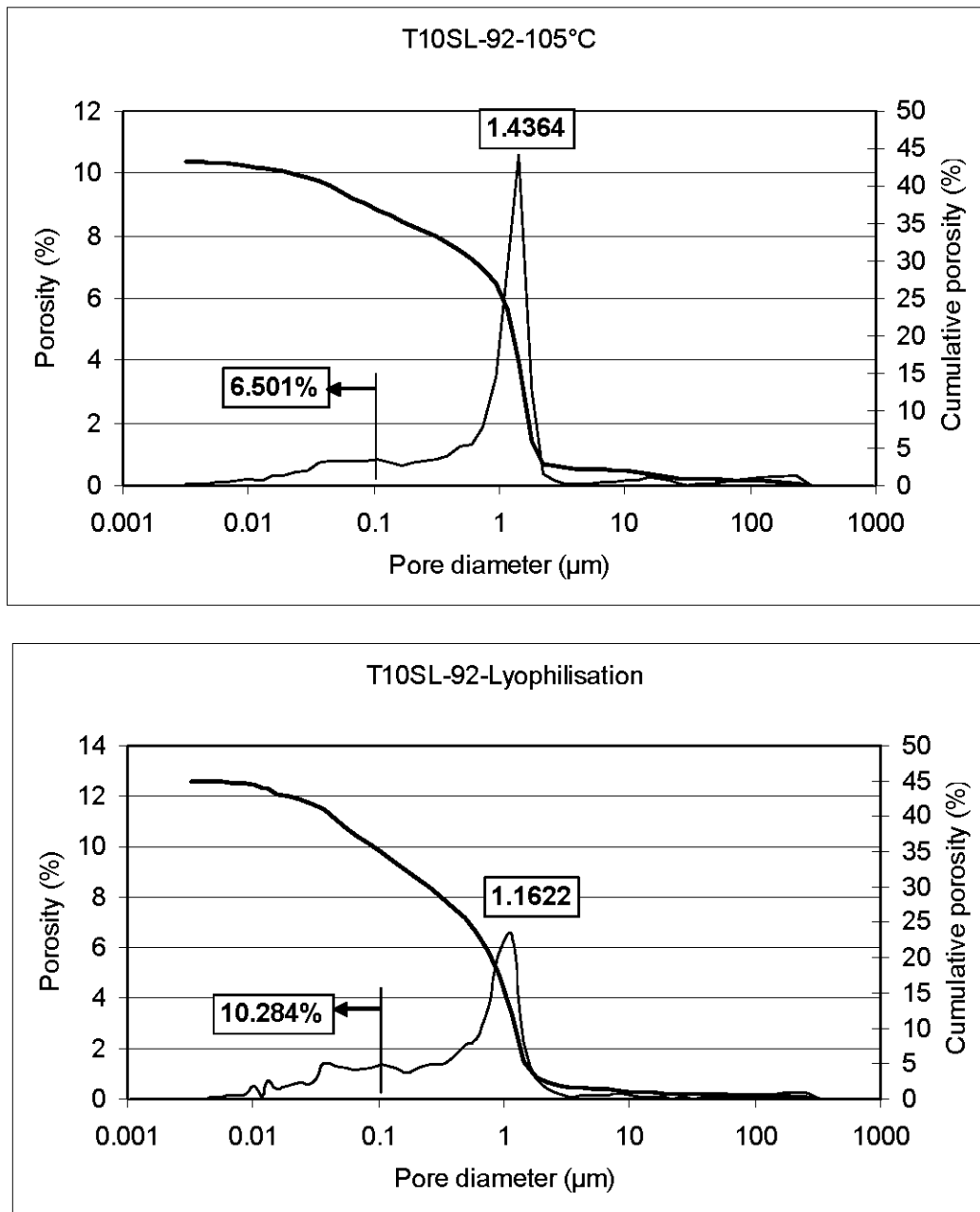
Figure E.2, Tests de séchage (étuve à 105°C versus lyophilisation) sur des échantillons de remblai à base de ciment de type 10 et de laitier de haut-fourneau à 92 jours de cure.
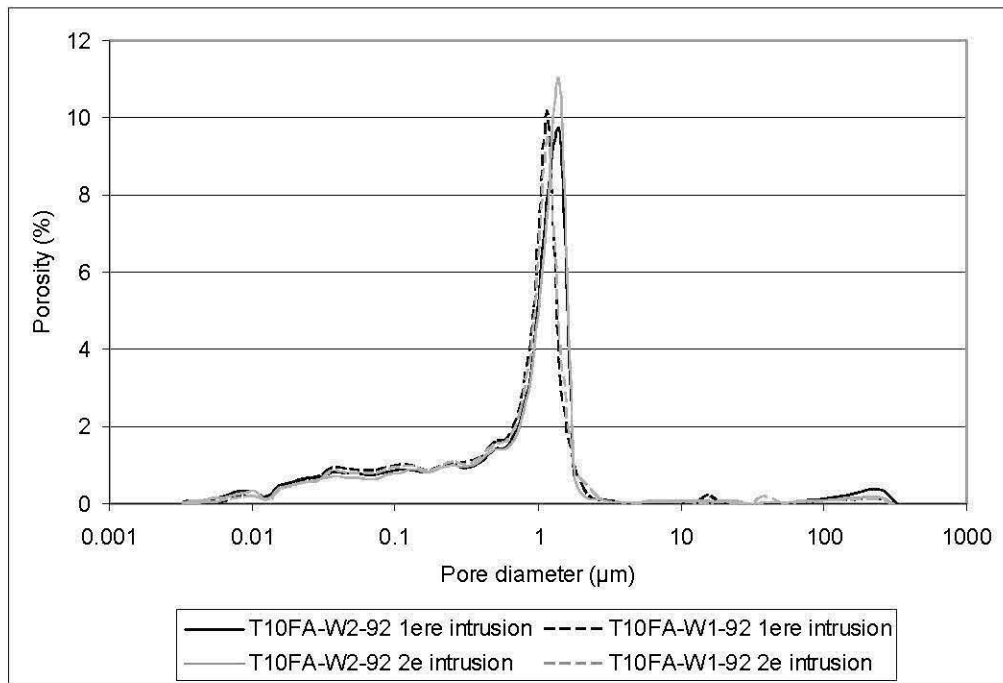
Figure E.3, Essais de porosimétrie au mercure doubles sur les échantillons T10FA-W1 et T10FA-W2 à 92 jours de cure. Avant le deuxième essai, les échantillons ont été séchés pendant 7 jours à 90°C et à environ 3 kPa.
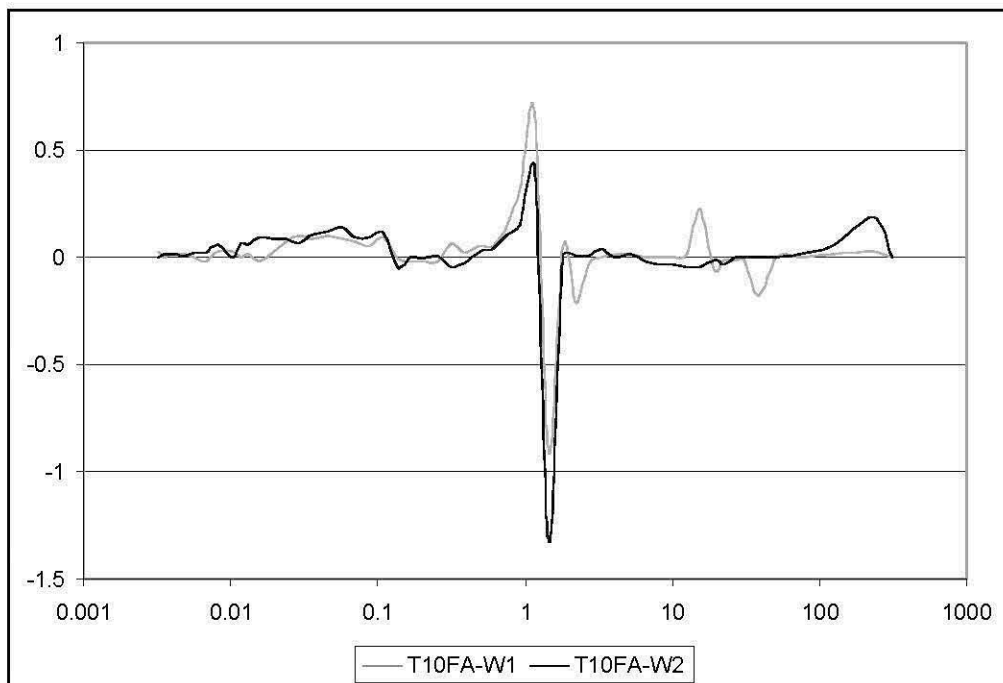

Figure E.4, Différentiel de porosité entre les deux essais MIP de la figure E.3.

APPENDICE F

**IMAGES DE LA CALIBRATION DE LA TECHNIQUE SEM-XMAP
SUR DES PASTILLES DE CALCITE ET DE SPHALÉRITE.**

Lors de la période de développement de la technique SEM-XMAP plusieurs tests ont été réalisés avant d'arriver à une solution satisfaisante. Parmi ces tests, certains l'ont été avec des minéraux ou des combinaisons minéralogiques relativement simples dont la chimie, la diffraction aux rayons X et la granulométrie étaient préalablement connues (voir Mermillod-Blondin, 2006). Les pastilles réalisées avec ces minéraux l'ont été dans les mêmes conditions que celles décrites au chapitre 4 de la thèse. Notez que les couleurs des images rayon-X en mode points présentées dans cette appendice ont été inversées (noir→blanc) pour améliorer l'aspect visuel. Les figures F.1 à F.7 sont dédiées à la pastille de calcite alors que les figures F.8 à F.17 traitent de la pastille de sphalérite.
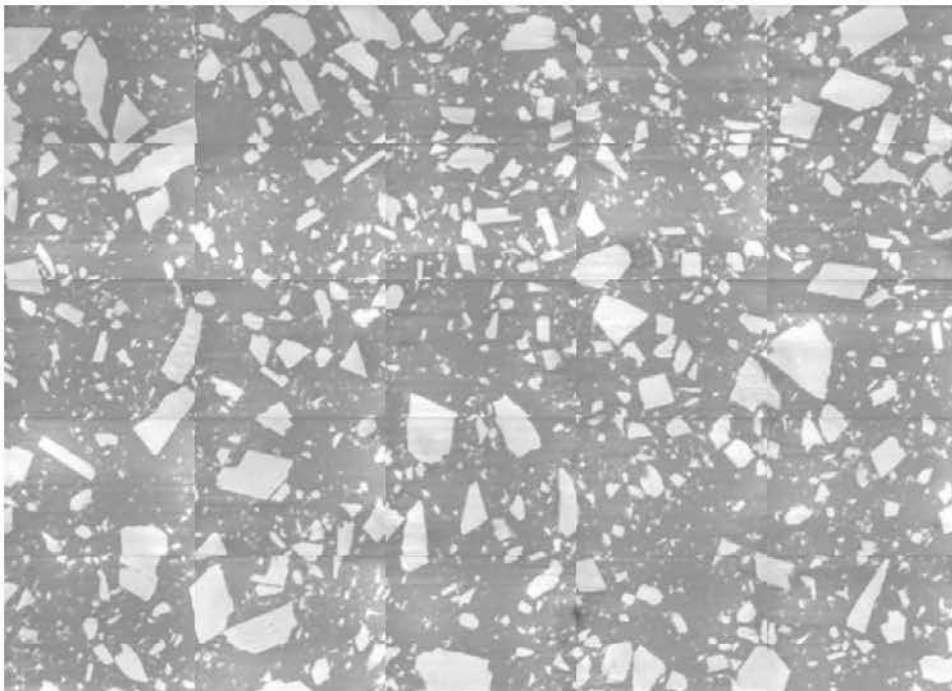
Figure F.1, Mosaïque des images BSE capturées avec la pastille de calcite.

Figure F.2, Image X du Calcium.

Figure F.3, Image X du Magnésium.

Figure F.4, Image X du Silicium.
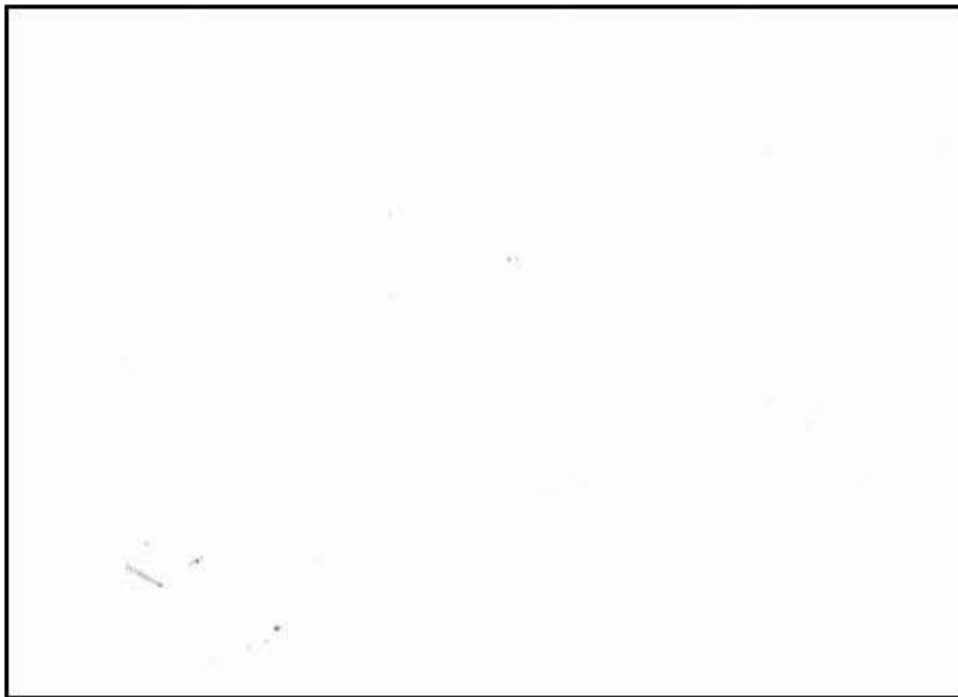
Figure F.5, Image X de l'Aluminium.
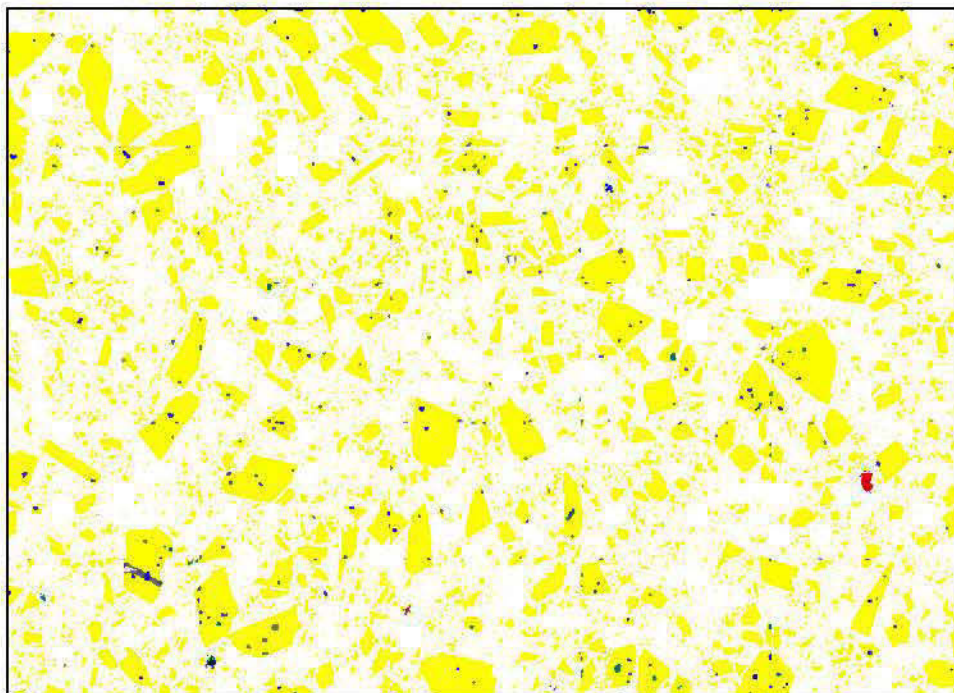
Figure F.6, Image SEM-XMAP sur la pastille de calcite.

Si	Ca	Al	Na	MgSi
		SiAl		SiMg

CaSi	CaMg	CaAl	SiMgCa	CaAlSi
SiCa	MgCa	AlCa	SiCaMg	CaSiAl
		CaNa	MgSiCa	AlCaSi
		NaCa	CaSiMg	
			CaMgSi	

Figure F.7, Légende des couleurs de la figure F.6.
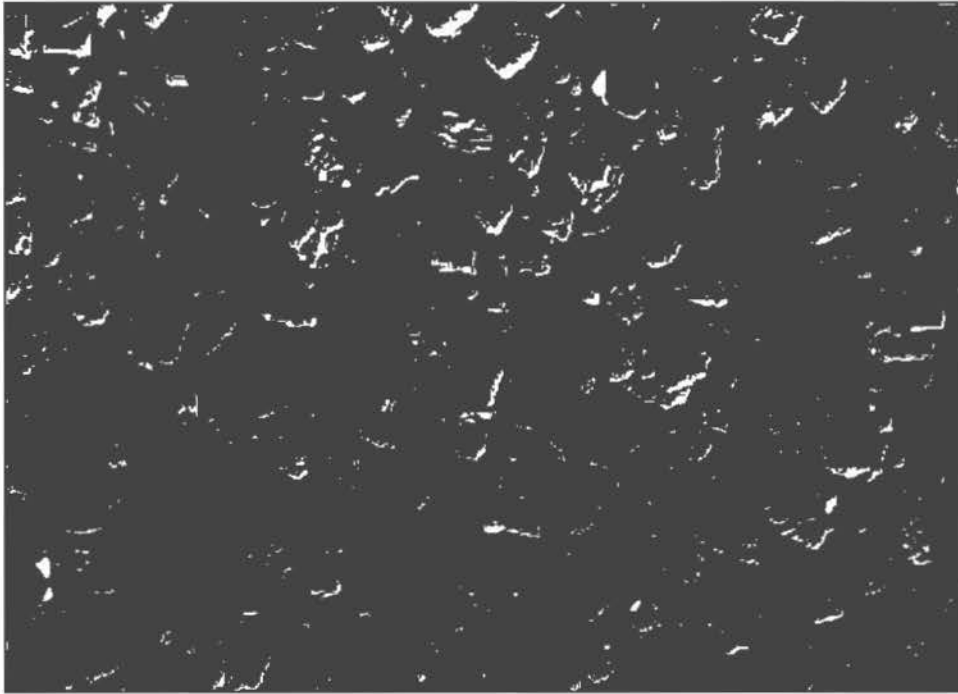
Figure F.8, Mosaïque des images BSE capturées avec la pastille de sphalérite.
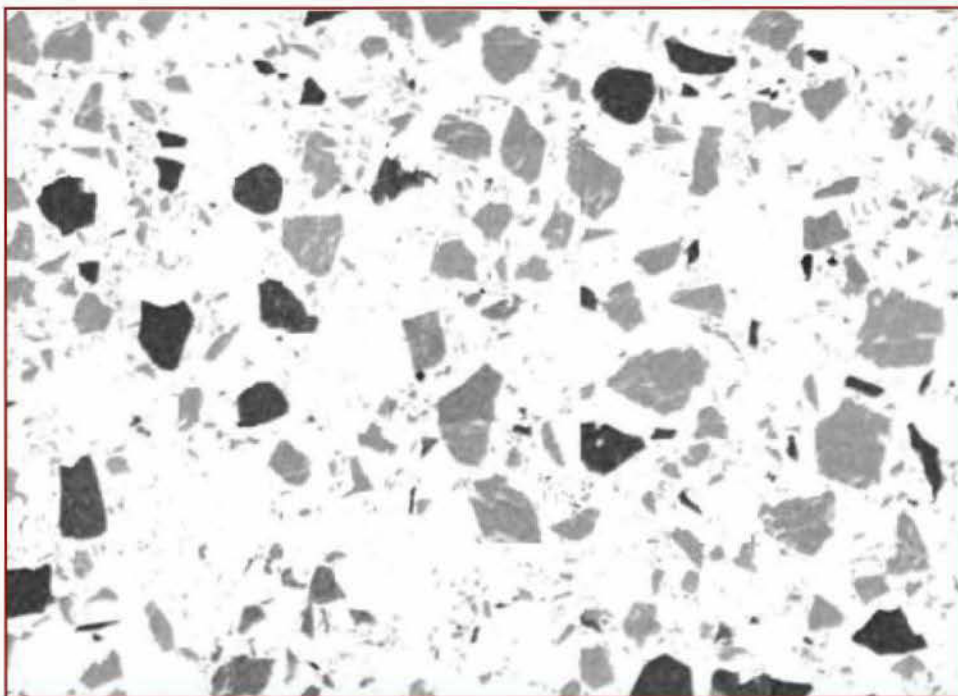
Figure F.9, Image X du Soufre.
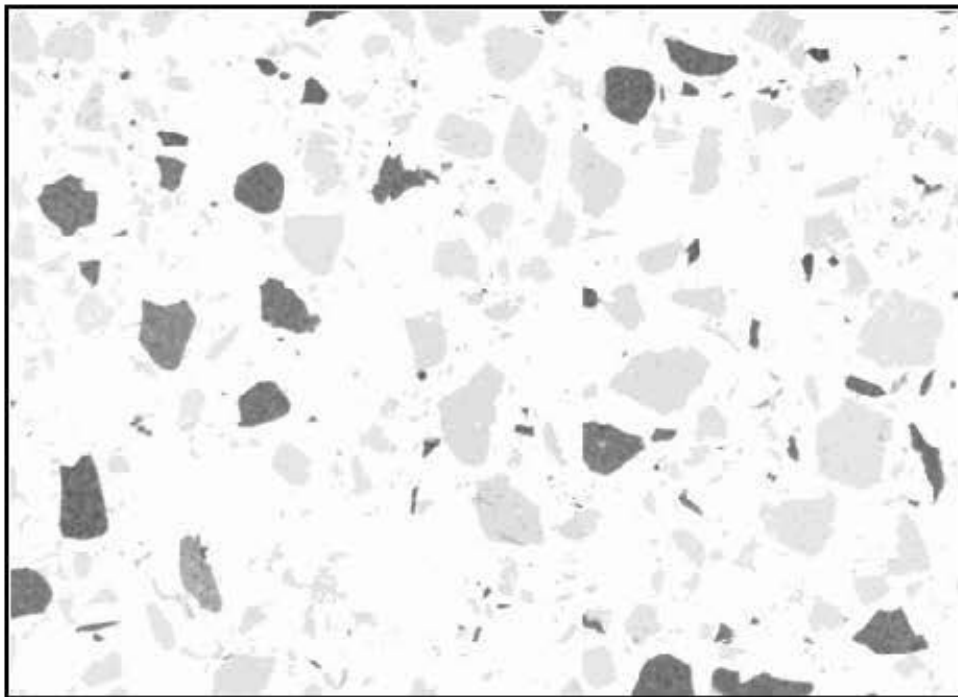
Figure F.10, Image X du Fer.
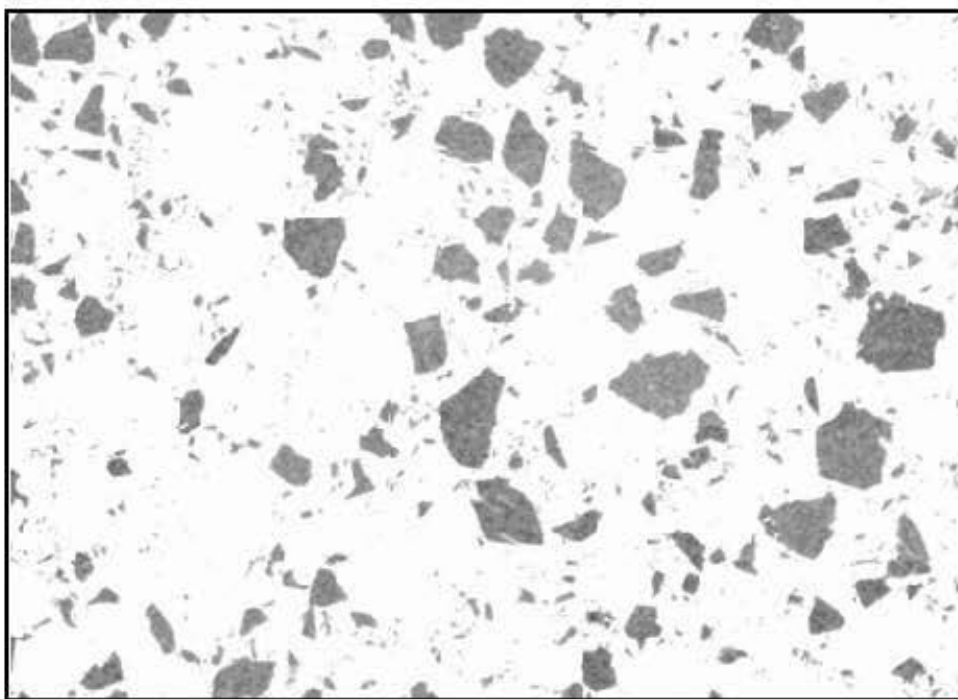
Figure F.11, Image X du Zinc.
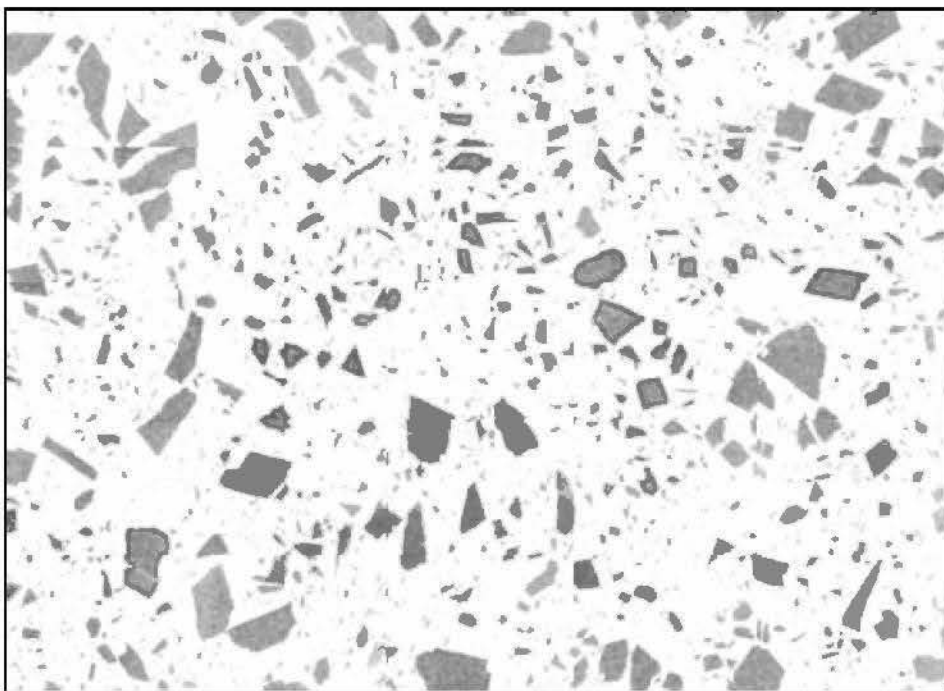
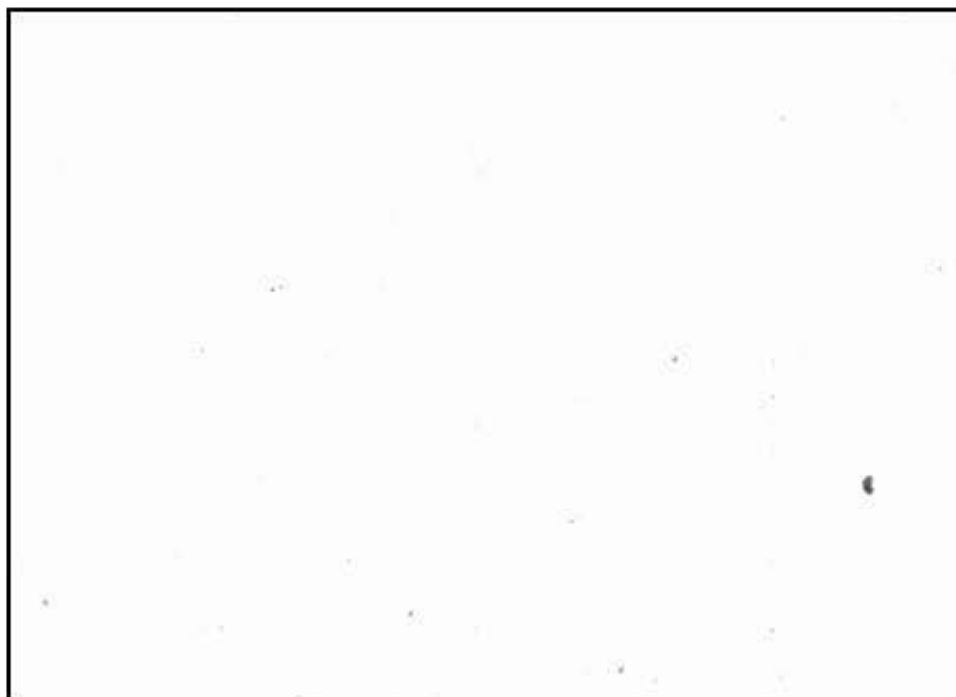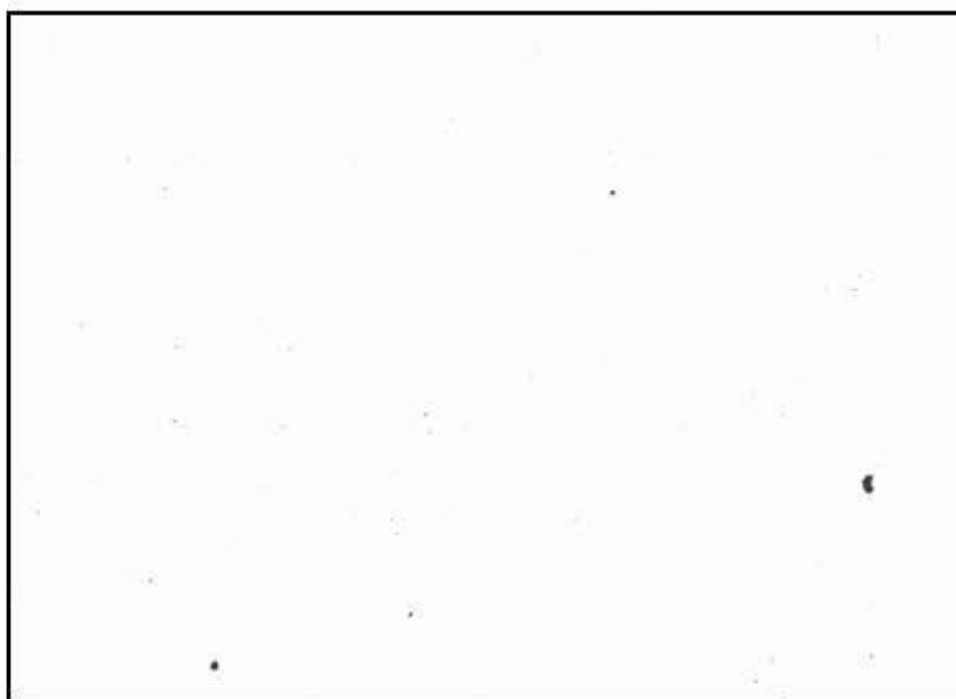Figure F.12, Image X de l'Aluminium.

Figure F.13, Image X du Calcium.
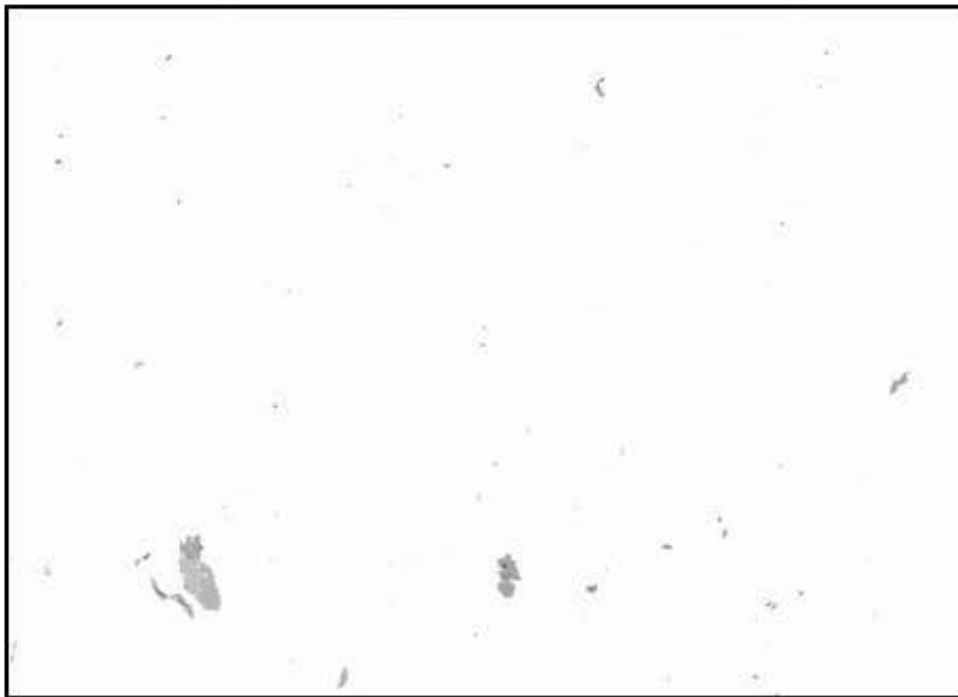
Figure F.14, Image X du Magnésium.
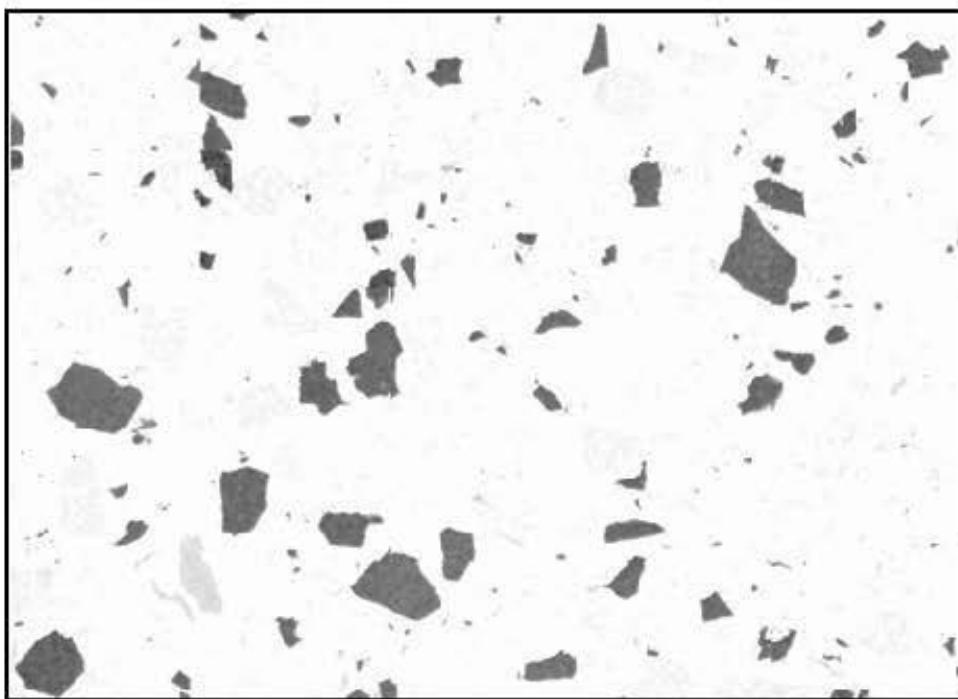
Figure F.15, Image X du Silicium.
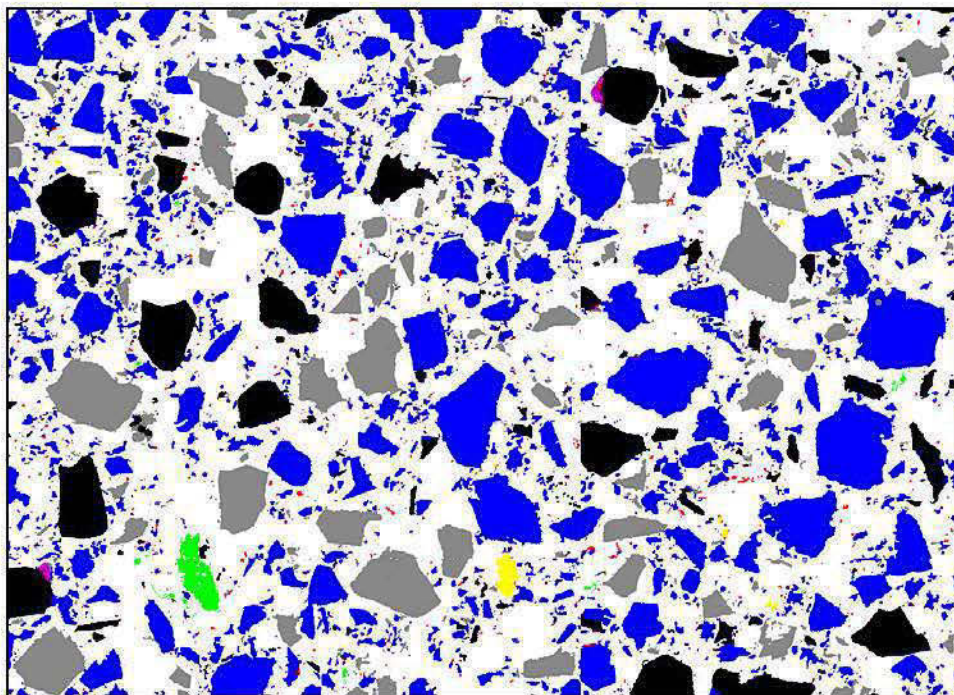
Figure F.16, Image SEM-XMAP sur la pastille de sphalérite.

AlMgFeS	S	SiS	SFe	SZn
AlMgSiF	CaS	SSi	FeS	ZnS
AlFeMgS		SiAl		ZnSi
FeAlMgS		Si		Zn
FeMgAlS				FeZn

SMg	CaMg			
SAl	MgCa			

Figure F.17, Légende des couleurs de la figure F.16.

RÉFÉRENCES

Amaratunga, L.M., Hein, G.G. (1997). Development of high strength total tailings paste fill using fine sulphide mill tailings, Proceedings of 29th annual meeting of the canadian mineral processors, CIM, Ottawa, Canada, 293-305.

Amaratunga, L.M., Yaschyshyn, D.N. (1997), Development of a high modulus paste fill using fine gold mill tailings, Geotechnical and Geological Engineering, 15, 205–219

Annor, A.B. (1999). A study of the characteristics and behaviour of composite backfill material, Ph. D. Thesis, McGill University, Montreal, Canada, 394 p.

Atkins, R.J., Hay, D. et Robertson, J. (1997). Shallow water cover design methodology and field verification. Proceedings of the 4th International Conference on Acid Rock Drainage, Vancouver, 211-228.

Aubertin, M., Chapuis, R.P., Aachib, M., Bussière, B., Ricard, J-F., Tremblay, L. (1995). Évaluation en laboratoire de barrières sèches construites à partir de résidus miniers. Mine Environment Neutral Drainage (MEND), Report 2.22.2a, Secretariat CANMET, Ottawa, Ont.

Aubertin, M., Bussière, B., Bernier, L. (2002). Environnement et gestion des rejets miniers, Manual on CD-ROM, Presses Internationales Polytechnique, Montreal.

Aubertin M., Li L., Arnoldi S., Belem T., Bussière B., Benzaazoua M., Simon R. (2003). Interaction between backfill and rock mass in narrow stopes. in Proceedings on the Panamerican Conference on Soil Mechanics and Geotechnical Engineering and 39th U.S. Rock Mechanics Symposium (12th : June 22-25, 2003 : MIT, Cambridge, Massachusetts), Boston, Mass., Verlag Gückauf GmbH (VGE), Essen, , vol. 1, 1157-1164.

Audry, S., Blanc, G., Schafer, J. (2005). The impact of sulphide oxidation on dissolved metal (Cd, Zn, Cu, Cr, Co, Ni, U) inputs into the Lot-Garonne fluvial system (France), Applied Geochemistry, 20, 5, 919-931.

Belem, T., Benzaazoua, M., Bussière, B. (2000). Mechanical behaviour of cemented paste backfill, Proceedings of the 53rd Annual Conference of the Canadian Geotechnical Society, Montréal, 1, 373-380.

Belem, T., Bussière, B., Benzaazoua, M. (2001). The effect of microstructural evolution on the physical properties of paste backfill, Tailings and Mine Waste'01, Proceedings of the 8th International Conference, Fort Collins, Colorado, USA, 365-374.

Belem T., Benzaazoua, M. (2003) Utilisation du remblai en pâte comme support de terrain. Partie I : de sa fabrication à sa mise en place sous terre. Après-mines 2003, 5-7 Février, Nancy, France, 12 p.

Belem T., Harvey A., Simon R., Aubertin M. (2004). Measurement and prediction of internal stresses in an underground opening during its filling with cemented fill. in 5th International Symposium on Ground Support in Mining & Underground

Construction, (5th : September 28-30, 2004 : Perth, Australia), Villaescusa, E., Potvin, Y. (éds), London, Taylor & Francis, 619-630.

Benzaazoua, M. (1996). Caractérisation physico-chimique et minéralogique de produits miniers sulfurés en vue de la réduction de leur toxicité et de leur valorisation, Ph.D. Thesis INPL, Nancy, France, 267 p.

Benzaazoua M., Ouellet, J., Servat, S., Newman, P. and Verburg, R. (1999). Cementitious backfill with high sulfur content: physical, chemical and mineralogical characterization. Cement and Concrete Research, 29, 719-725.

Benzaazoua M., Belem, T., Jolette, D., (2000). Investigation de la stabilité chimique et son impact sur la résistance mécanique des remblais cimentés. Rapport IRSST, IRSST ed., R-260: 158p + Annexes.

Benzaazoua, M., Belem, T., Bussière, B. (2002a). Chemical factors that influence the performance of mine sulphidic paste backfill, Cement and Concrete Research, 32, 7, 1133-1144.

Benzaazoua, M., Belem, T., Bussière, B. (2002b). Propriétés hydrogéochimiques des remblais en pâte : impact sur le remblayage souterrain et l'entreposage en surface, Journée NEDEM 2000, Sherbrooke, Canada, 12 p.

Benzaazoua, M., Fall. M., Ouellet, S. (2003a). Étude pluridisciplinaire visant mettre au point un outil expert pour la prédiction du comportement des remblais en pâte. IRSST Research Project 099-085, Final Report, 187 p.

Benzaazoua, M., Belem, T., Ouellet, S., Fall, M. (2003b). Utilisation du remblai en pâte comme support de terrain. Partie II : Comportement à court, à moyen et à long terme. Après-mines 2003, 5-7 Février, Nancy, France, 12 p.

Benzaazoua, M., Belem, T., Fall, M. (2004a). A contribution to understand the hardening process of cemented pastefill., Minerals Enginering, 17, 141-152.

Benzaazoua, M., Fall. M., Ouellet, S. (2004b). Étude pluridisciplinaire visant à mettre au point un outil expert pour la prédiction du comportement des remblais en pâte Rapport IRSST R-390, 21 p.

Benzaazoua, M., Marion, P., Picquet, I., Bussière, B. (2004c). The use of pastefill as a solidification and stabilization process for the control of acid mine drainage. Minerals Engineering, 17-2, 233-243.

Benzaazoua, M., Bois, D., Belem, T., Gauthier, P., Ouellet, S., Fall, M. and St-Onge, J.-F. (2005a). Remblais souterrains, évolution des connaissances et de la pratique. 20th Colloque Contrôle de terrains, Association Minière du Québec, Val d'Or, Quebec, Canada, march 2005, 23 p.

Benzaazoua, M., Bussière, B., Ouellet, S., Godbout, J., Fiset, J.-F., Fall, M., Aubertin, M., Belem, T. (2005b). Contribution à l'évaluation du comportement environnemental des remblais miniers cimentés en pâte, Symposium 2005 Mines and the Environment, Rouyn-Noranda, Canada, May 15-18, 15 p.

Benzaazoua, M., Fiset, J.-F., Bussière, B., Villeneuve, M., Plante, B. (2006). Sludge recycling within cemented paste backfill: Study of the mechanical and leachability properties, Minerals Engineering, 19, 5, 420-432.

Bernier, L.R., Li, M.G., Moerman, A. (1999). Effects of tailings and binder geochemistry on the physical strength of paste backfill, Sudbury'99, Mining and the environment II, Goldsack, Belzile, Yearwood and Hall Eds., Vol. 3, p. 1113-1122.

Bernier, L.R., Li, M. (2003). High temperature oxidation (heating) of sulfidic paste backfill: A mineralogical and chemical perspective, in Proceedings of Sudbury '03, Mining and the Environment III, Laurentian University, Sudbury, Ontario, 9 p.

Bertrand, V.J., Monroy, M.G. and Lawrence, R.W. (2000). Weathering characteristics of cemented paste backfill: Mineralogy and solid phase chemistry, in ICARD 2000 - Proceedings from the 5th international conference on acid rock drainage, May 21-24, Denver, Colorado, 863-876.

Brackebusch, F.W. (1994). Basics of paste backfill systems, Mining Engineering, 1175-1178.

Brake, S., Connors, K., Romberger, S. (2001). A river runs through it: impact of acid mine drainage on the geochemistry of West Little Sugar Creek pre- and post-reclamation at the Green Valley coal mine, Indiana, USA, Environmental Geology, 40, 11 - 12, 1471 - 1481.

Brookins, D.G., Thomson, B.M., Longmire, P.A. (1982). Early Diagenesis of Uranium Mine Stope Backfill. Paper in Uranium Mill Tailings Management, Proceedings of the Fifth Symposium (Ft. Collins, CO, 1982). Civil Eng. Dep., CO State Univ., 27-37.

Bussière, B., Benzaazoua, M., Aubertin, M., Mbonimpa, M. (2004). A laboratory study of covers made of low-sulphide tailings to prevent acid mine drainage, Environmental Geology, 45, 5, 609 – 622.

Bussière, B. (2006). Colloquium 2004: hydro-geotechnical properties of mine tailings and novel surface disposal approaches to minimize environmental impacts, Canadian Geotechnical Journal, submitted.

Cayouette, J. (2003). Optimization of the paste backfill plant at Louvicourt mine, CIM Bulletin, Canadian Institute of Mining, November/December, 51-57.

Chapman, J., Hockley, D., Sexsmith, K., Arthur, B. and Donohue, S. (2003). Testing acid generation in cemented paste backfill, in ICARD 2003 – Proceedings from 6th International Conference on Acid Rock Drainage, July 14-17, 2003, Cairns, Australia, Published by The AusIMM, P.O. Box 660, Carlton South, Victoria 3053, Australia, 863-867.

Dagenais, A.-M. (2005). Techniques de contrôle du DMA basées sur les effets capillaires, Ph. D. Thesis, École Polytechnique de Montréal, Montréal, Canada, 394 p.

DeSouza, E., DeGagné, D., Archibald, J.F. (2001). Minefill Applications, Practices and Trends in Canadian Mines. Proceedings of the 7th International Symposium on Mining with Backfill, Society for Mining, Metallurgy, and Exploration, 311-319.

Doepker, R.D., O'Conner, W.K. (1990a). Column Leach Study I: Heavy Metal Dissolution Characteristics from Selected Copper Mine Tailings. Paper in 5th Billings Symposium on Disturbed Land Rehabilitation, Reclamation Research Unit, MT State Univ., Bozeman, MT, Publ. No. 9003, 1, 27-40.

Doepker, R.D., O'Conner, W.K. (1990b). Column Leach Study II: Heavy Metal Dissolution Characteristics from Selected Lead-Zinc Mine Tailings. Column Leach Study II: Heavy Metal Dissolution Characteristics from Selected Lead-Zinc Mine Tailings. Chapter 9 in Mining and Mineral Processing Wastes: Proceedings of the Western Regional Symposium on Mining and Mineral

Processing Wastes, ed. by F. M. Doyle (Berkeley, CA, May 30-June 1, 1990). Soc. Min. Eng., 69-80.

Doepker, R.D., Drake, P.L. (1990). Laboratory Study of Submerged Metal-Mine Tailings 1: Effect of Solid-Liquid Contact Time and Aeration on Contaminant Concentrations. Trans. of SME, 288, 1826-1830.

Doepker, R.D. Drake, P.L. (1991). Laboratory Study of Submerged Metal-Mine Tailings 3: Factors Influencing the Dissolution of Metals. Paper in Proceedings, 2nd International Conference on the Abatement of Acidic Drainage (Montreal, PQ, Sept. 16-18,

Doepker, R. D. (1991a). Column Leach Study IV: Factors Affecting the Dissolution of Metals from Sulfitic Mine Tailings. Paper in Proceedings, 2nd International Conference on the Abatement of Acidic Drainage (Montreal, Sept. 16-18). Centre de Recherches Minerales, Quebec, PQ, 1, 115-138.

Doepker, R. D. (1991b). Enhanced Heavy Metal Mobilization From Unsaturated Mine Tailings. Trans. of SME, 288, 1801-1805.

Douglas, E., Malhotra, V.M. (1989). Ground granulated blast-furnace slag for cemented mine backfill: production and evaluation, CIM Bulletin, 82, 929, 27-36.

Doye, I., Duchesne, J. (2003). Neutralisation of acid mine drainage with alkaline industrial residues: laboratory investigation using batch-leaching tests, Applied Geochemistry, 18, 8, 1197-1213.

Duchesne, J, Reardon, E.J. (1999). Lime Treatment of Fly Ash: Characterization of Leachate Composition and Solid/Water Reactions. Waste Management, 19, 221-231.

Dullien, F.A.L. (1992). Porous media: fluid transport and pore structure, 2nd ed., Academic Press, 574 p.

Elberling, B., Nicholson, R.V., Reardon, E.J., Tibble, P. (1994). Evaluation of sulphide oxidation rates: laboratory study comparing oxygen fluxes and rates of oxidation product release. Canadian Geotechnical Journal, 31, 375-383.

Elberling, B., Schippers, A., Sand, W. (2000). Bacterial and chemical oxidation of tailings at low temperatures, Journal of Contaminant Hydrology, 41 225–238.

Elberling, B., Damgaard, L.R. (2001). Microscale measurements of oxygen diffusion and consumption in subaqueous sulfide tailings, Geochimica et Cosmochimica Acta, 65, 12, 1897-1905.

Elberling, B., Balić-Žunić, T., Edsberg, A. (2003). Spatial variations and controls of acid mine drainage generation, Environmental Geology, 43, 7, 806 – 813.

Evangelou, V.P. (1995). Pyrite Oxidation and Its Control. CRC Press. 285p.

Fall, M., Benzaazoua, M. (2003). Modeling and simulation of paste backfill performance properties, In: Proceedings of the 56th Annual Canadian Geotechnical Conference and 4th joint IAHCNC/CGS Conference. Winnipeg, September 28–October 1, 161-169.

Fall, M., Benzaazoua, M. and Ouellet., S. (2005a). Experimental characterization of the influence of tailings fineness and density on the quality of cemented paste backfill, Minerals Engineering, 18, 1, 41-44.

Fall, M., Benzaazoua, M. (2005). Modeling the effect of sulphate on strength development of paste backfill and binder mixture optimization, Cement and Concrete Research, 35, 2, 301-314.

Fall, M., Bussière, B., Belem, T., Benzaazoua, M., Samb, S.S. (2005b). Influence of curing temperature on paste backfill properties, 58th Canadian Geotechnical and 6th Joint IAH-CNC and CGS Groundwater Specialty Conferences, Saskatoon, Canada, September 18-21, 7 p.

Frau, F. (2000). The formation-dissolution-precipitation cycle of melanterite at the abandoned pyrite mine of Genna Luas in Sardinia, Italy: environmental implications, Mineralogical Magazine, 64, 6, 995-1006.

Gauthier, P. (2004). Valorisation des liants et des rejets industrielles dans les remblais miniers. Mémoire de DESS, Université du Québec en Abitibi Témiscamingue, 146 p.

Godbout, J. (2005). Évolution des propriétés hydriques des remblais miniers cimentés en pâte durant le curage, M. Sc. A. Thesis, École Polytechnique de Montréal, Montréal, Canada, 190 p.

Grice, A. (1998). Underground mining with backfill, The 2nd Annual Summit – Mine Tailings Disposal Systems, Brisbane, Australia, 6 p.

Hassani, F., Bois D., (1992). Economic and technical feasibility for backfill design in Quebec underground mines. Final report 1/2, Canada-Quebec Mineral Development Agreement, Research & Development in Quebec Mines. Contract no. EADM 1989-1992, File no. 71226002.

Hassani, F., Hossein, M., Newman, P. Bois D., (1994). Comparison of surface and underground disposal of tailings waste, CIM Bulletin, 87, 976, 58-65.

Hassani, F., Archibald, J. (1998). Mine backfill, CD-ROM, Canadian Institute of Mining, 263p.

Hassani, F., Fotoohi, K., Doucet, C. (1998). Paste backfill performance in a narrow vein gold mine, CIM/CMMI/MIGA, Montreal, 15 p.

Hassani, F.P., Ouellet, J., Hossein, M. (2001). Strength development in underground high-sulphate paste backfill operation, CIM Bulletin, 94, 1050, 57-62.

Holmes, P.R., Crundwell, F.K. (2000). The kinetics of the oxidation of pyrite by ferric ions and dissolved oxygen: An electrochemical study. Geochemica and Cosmochimica Acta, 64, 263–274.

Jambor, J.L. (2003). Mine waste mineralogy and mineralogical perspectives of acid-base accounting. Chapter 6 in Environmental Aspects of Mine Wastes, Short course series volume 31, J.L. Jambor, D.W. Blowes and A.I.M. Ritchie Editors, Mineralogical Association of Canada, 117-145.

James M., Li L., Aubertin M. (2004). Evaluation of the earth pressures in backfilled stopes using limit equilibrium analysis. in Proceedings of the 57th Annual Canadian Geotechnical Conference and 5th Joint IAH-CNC-CGS Conference (57th : October 24-27, 2004 : Quebec, Canada), Session 6F, 33-40.

Janzen, M.P., Nicholson, R.V., Scharer, J.M. (2000). Pyrrhotite reaction kinetics Reaction rates for oxidation by oxygen, ferric iron and for nonoxidative dissolution, Geochimica et Cosmochimica Acta, 64, 1511–1522.

Jerz, J.K. and Rimstidt, J.D. (2004). Pyrite oxidation in moist air, Geochimica et Cosmochimica Acta, 68, 4, 701-714.

Jones, D.R., Li, H.Y., Waite, T.D. et Fenton, B. (2001). Hydrochemical and geotechnical properties of cemented uranium paste tailings. Tailings and mine waste '01, Balkema, Rotterdam, 401-409.

Kesimal, A., Ercikdi, B. and Yilmaz, E. (2003). The effect of desliming by sedimentation on paste backfill performance, Minerals Engineering, 16, 10, 1009-1011.

Kesimal, A., Yilmaz, E., Ercikdi, B. (2004). Evaluation of paste backfill mixtures consisting of sulphide-rich mill tailings and varying cement contents, Cement and Concrete Research, 34, 10, 1817-1822.

Kesimal, A., Yilmaz, E., Ercikdi, B., Alp, I., Deveci, H. (2005). Effect of properties of tailings and binder on the short-and long-term strength and stability of cemented paste backfill, Materials Letters, 59, 28, 3703-3709.

Kleinmann, R.L.P., Crerar, D.A., Pacelli, R.R. (1981). Biogeochemistry of acid mine drainage and a method to control acid formation, Mining Engineering, March 1981, 300-304

Lamos, A.W., Clark, I.H. (1989). The influence of material composition and sample geometry on the strength, Innovation in Mining backfill technology, Hassani et al. eds., Rotterdam, ISBN 9061919851, 89-94.

Landriault, D. (1995). Paste backfill Mix design for Canadian Underground Hard Rock Mining. 97th Annual General Meeting of CIM. Rock Mechanics and Strata Control Session. Halifax, Nova Scotia, May 14-18, 229-238.

Landriault, D.A., Brown, R.E., Counter, D.B. (2001). Paste backfill study for deep mining at Kidd Creek, CIM, Montréal, 14 p.

Landriault, D., Johnson, J.M., Palkovits, F. (2005). Thickened tailings and paste technology: The future of industrial waste disposal, SME Annual Meeting, Salt Lake City, 10 p.

Lee, C.H. (2003). Assessment of contamination load on water, soil and sediment affected by the Kongjujeil mine drainage, Republic of Korea, Environmental Geology, 44, 5, 501 – 515.

le Roux, K. (2004). In Situ Properties and Liquefaction Potential of Cemented Paste Backfill. Ph.D. Thesis, University of Toronto, Canada, 271 p.

le Roux, K., Bawden, W.F., Grabinsky, M.F. (2005). Field properties of cemented paste backfill at the Golden Giant mine, Mining Technology (Trans. Inst. Min. Metall. A), 114, 65-80.

Levens, R.L., Boldt, C.M.K. (1994). Environmental Impacts of Mine Waste Sandfill, Report of Investigations 9493, United States Bureau of Mines, 15 p.

Levens, R.L., Marcy, A.D., Boldt, C.M.K. (1996). Environmental Impacts of Cemented Mine Waste Backfill, RI 9599, United States Bureau of Mines, 23 p.

Li L., Aubertin M., Simon R., Bussière B., Belem T. (2003). Modeling arching effects in narrow backfilled stopes with FLAC. in FLAC and Numerical Modeling in Geomechanics: Proceedings of 3rd International FLAC Symposium (3rd, October 22-24, 2003 : Sudbury, Canada), Rotterdam, A.A. Balkema, 211-219.

Li, L. and Aubertin , M. (2003). A general relationship between porosity and uniaxial strength of engineering materials, Can. J. Civ. Eng., 30, 4, 644-658.

Li L., Aubertin M., Belem T., Simon R., James M., Bussière B. (2004). A 3D analytical solution for evaluating earth pressures in vertical backfilled stopes. in Proceedings of the 57th Annual Canadian Geotechnical Conference and 5th Joint IAH-CNC-CGS Conference (57th : October 24-27, 2004 : Quebec, Canada), Session 6F, 41-48.

Li, M., Aubé, B. et St-Arnaud, L. (1997). Considerations in the use of shallow water covers for decomissioning reactive tailings. Proceedings of the 4th International Conference on Acid Rock Drainage, Vancouver, 117-130.

Liping, L. (1997). Solidification and strengthening of mine tailings using a high-water rapid-setting cement, Master Thesis, Technical University of Nova-Scotia, Halifax, Canada, 148 p.

Lowson, R.T. (1982). Aqueous oxidation of pyrite by molecular oxygen. Chem. Rev., 82, 461-497.

Malhotra, V.M., Carino, N.J. (1991). CRC Handbook on Nondestructive Testing of Concrete, CRC Press, 343 p.

Manca, P.P., Massacci, G. et Rossi, G. (1983). Mill tailings and various binder mistures for cemented backfill : Analysis of properties related to mining problems, Proceedings of the international symposium on mining with backfill, Lulea, 7-9 june 1983, 39-47.

Ministère du Développement durable, de l'Environnement et des Parcs « MDDEP » (2005). Directive 019 sur l'industrie minière, Direction des politiques de l'eau, Service des eaux industrielles, ENV/2005/0120, 101 p.

Mitchell, R.J., Wong, B.C. (1982). Behaviour of cemented tailings sands, Can. Geotech. J., 19, 289-295.

Mermillod-Blondin, R. (2006). Influence des propriétés superficielles de la pyrite sur la rétention de molécules de type xanthate : Application à la désulfuration des résidus miniers, Ph. D. Thesis, École Polytechnique of Montréal, 333 p.

Moncur, M., Ptacek, C.J., Blowes, D.W., Jambor, J.L. (2003). Fate and Transport of Metals from an Abandoned Tailings Impoundment after 70 Years of Sulfide Oxidation, in Proceedings of Sudbury '03, Mining and the Environment III, Laurentian University, Sudbury, Ontario, 10 p.

Moses, C.O., Nordstrom, D.K., Herman, J.S., Mills, A.L. (1987). Aqueous pyrite oxidation by dissolved oxygen and ferric iron, Geochimica et Cosmochimica Acta, 51 1561–1571.

Nicholson, R.V. (1994). Iron-sulfide oxidation mechanisms: Laboratory studies, In: Jambor, J.L., Blowes, D.W. (Eds.), The Environmental Geochemistry of Sulfide Mine-wastes. Short Course Handbook, Vol. 22. Mineralogical Association of Canada, 163-183.

Nicholson, R.V., Gillham, R.W., Reardon, E.J. (1988). Pyrite oxidation in carbonate-buffered solution: 1. Experimental kinetics, Geochimica et Cosmochimica Acta, 52, 5, 1077-1085.

Nicholson, R.V. (1994). Iron-sulfide oxidation mechanisms: Loratory studies. In: Jambor, J.L., Blowes, D.W. (Eds.), The Environmental Geochemistry of Sulfide Mine-wastes. Short Course Handbook, Vol. 22. Mineralogical Association of Canada, 163-183.

Nicholson, R.V., Scharer, J.M. (1994). Laboratory studies of pyrrhotite oxidation kinetics, in Environmental Geochemistry of Sulfide Oxidation, C.N. Alpers and D.W. Blowes eds., American Chemical Society, p. 14-30.

Nordstrom, D.K., Alpers, C.N. (1999). Geochemistry of acid mine drainage, in The Environemental Geochemistry of Mineral Deposits, G.S. Plumlee and M.J. Logsdon eds., Vol. 6A, p. 133-160.

Nordstrom, D.K., Alpers, C.N., Ptacek, C.J., Blowes, D.W. (2000). Negative pH and Extremely Acidic Mine Waters from Iron Mountain, California, Environ. Sci. Technol., 34, 2, 254 -258.

Ouellet, J., Benzaazoua, M., Servant, S. (1998). Mechanical, mineralogical and chemical characterization of a paste backfill, Tailings and Mine Waste'98, Colorado, 139-146

Ouellet, J., Servant, S. (2000). In-situ mechanical characterization of a paste backfill with a self-boring pressuremeter, CIM Bulletin, 93, 1042, 110-115.

Ouellet, J., Hassani, F., Somot, S., Shnorhokian, S., Hossein, M. (2002). Stabilization/solidification of pyritic mill tailings by induced cementation, Tailings and Mine Waste '02 : Proceedings of the 9th International Conference, 27-30 January, 2002, Fort Collins, Colorado, Rotterdam, Balkema, 205-212.

Ouellet, S., Bussière, B., Benzaazoua, M., Aubertin, M., Fall, M., Belem, T. (2003). Sulphide Reactivity within cemented paste backfill: oxygen consumption test results. The 56th Annual Canadian Geotechnical Conference and 4th joint IAH-CNC/CGS Conference. Winnipeg, Manitoba, Canada. September 28 to October 1, 8 p.

Ouellet, S., Bussière, B., Benzaazoua, M., Aubertin, M., Belem, T. (2004) Effect of binder type and mixing water chemistry on microstructural evolution of cemented paste backfill, Proceedings of the 57th Annual Canadian Geotechnical Conference and 5th joint IAH-CNC/CGS Conference, Quebec city, Canada, October 23-27, 8 p.

Paynter, J.T. , Dodd, J.C. (1997). The Design, Commissioning and Operation of the Golden Giant Paste Backfill Plant. Proceedings of the 29th annual meeting of the Canadian Mineral Processors (Division of the CIM), Ottawa, Ontario, 21-23 January, 382-403.

Potvin, Y., Fourie, A. (2005). Paste fill in Australia, Symposium 2005 Mines and the Environment, Rouyn-Noranda, Canada, May 15-18, 16 p.

Ptacek, C.J., Blowes, D.W. (2003). Geochemistry of concentrated waters at mine-waste sites. Chapter 12 in Environmental Aspects of Mine Wastes, Short course series volume 31, J.L. Jambor, D.W. Blowes and A.I.M. Ritchie Editors, Mineralogical Association of Canada, 239-260.

Ramlochan, T., Grabinsky, M.W., Hooton, R.D. (2004). Microstructural and chemical investigations of cemented paste backfills, Tailings and Mine Waste '04, October 10-13, 2004, Vail, Colorado, 293-304.

Rimstidt, J.D., Vaughan, D.J. (2003). Pyrite oxidation: A state-of-the-art assessment of the reaction mechanism, Geochimica et Cosmochimica Acta, 67, 873–880.

Rzhevsky, V., Novik, G. (1971). The physics of rocks. MIR Publisher, Moscow.

Sánchez España, J., López Pamo, E., Santofimia, E., Aduvire, O., Reyes, J., Barettino, D. (2005). Acid mine drainage in the Iberian Pyrite Belt (Odiel river watershed, Huelva, SW Spain): Geochemistry, mineralogy and environmental implications, Applied Geochemistry, 20, 7, 1320-1356.

Smart, R.M., Spearing, A.J.S., Harrison, A.T. (1993). The use of silicated backfill in South African gold mines, MINEFILL'93, Johannesburg, SAIMM, 289-294.

Thomas, E.G., Nantel, L.H., Notley, K.R. (1979). Fill technology in underground metlliferous mines, International Academic Services Limited, 293 p.

Thomas, E.G. (1983). Characteristics of cemented deslimed mill tailing fill prepared from finely ground tailing. Proceedings of the International Symposium on Mining with Backfill, Lulea, 59-65.

Thomson, B.M., Longmire, P.A., Brookins, D.G. (1986). Geochemical Constraints on Underground Disposal of Uranium Mill Tailings. Appl. Geochem., 1, 335-343.

Tremblay, G.A., Hogan, C.M., Gardiner, E.J. (2003). Mine Environment Neutral Drainage (MEND) Initiative, in ICARD 2003 – Proceedings from 6th International Conference on Acid Rock Drainage, July 14-17, 2003, Cairns, Australia, Published by The AusIMM, P.O. Box 660, Carlton South, Victoria 3053, Australia, 5-8.

USEPA, Office of ground water and drinking water (1999). The Class V Underground Injection Control Study, Volume 10, Mining, Sand, or Other Backfill Wells, EPA/816-R-99-014j, 72 p.

Verburg, R., Johnson, B., Fordham, M., Logsdon, M. (2003). A rapid and cost-effective method for bench screening of geochemical performance and disposal options for high-sulfide tailings, in ICARD 2003 – Proceedings from 6th International Conference on Acid Rock Drainage, July 14-17, 2003, Cairns, Australia, Published by The AusIMM, P.O. Box 660, Carlton South, Victoria 3053, Australia, 739-749.

Williams, T. M., Smith, B. (2000). Hydrochemical characterization of acute acid mine drainage at Iron Duke mine, Mazowe, Zimbabwe, Environmental Geology, 39, 3 - 4, 272 – 278.

Zagury, G. J., Neculita, C. M., Bussière, B. (2005). Passive biological treatment of acid mine drainage: challenges of the 21st century, Symposium 2005 Mines and the Environment, Rouyn-Noranda, Canada, May 15-18, 22 p.